CHAPTER 2:

SOLUTE RELATIONSHIPS IN GROUNDWATERS FROM THE CULEBRA DOLOMITE AND RELATED ROCKS IN THE WASTE ISOLATION PILOT PLANT AREA, SOUTHEASTERN NEW MEXICO

Malcolm D. Siegel and Karen L. Robinson
Sandia National Laboratories

Jonathan Myers
International Technology Corporation

ABSTRACT

This chapter summarizes solute concentrations in waters of the Culebra member of the Rustler Formation. The solute relationships are used to delineate hydrochemical facies, to compare flow directions suggested by water chemistry with those indicated by modern hydrologic potentials, and to formulate a hypothesis for the chemical evolution of the Culebra groundwaters. Descriptions of waters from the Magenta dolomite, Rustler/ Salado contact zone, the Dewey Lake Red Beds, and the Bell Canyon Formation are also included.

Four hydrochemical facies have been delineated in the Culebra. Zone A contains saline (about 3.0 m) NaCl brine and is found in the eastern third of the study area, roughly coincident with the region of low transmissivity and the occurrence of halite in several units of the Rustler Formation. Zone B contains a dilute Ca-SO_4-rich water (I <0.1 m) in the southern part of the study area and is coincident with a zone of high transmissivity where halite is absent from the Rustler. Zone C contains waters of variable composition and ionic strengths (0.3 to 1.6 m); it extends from the central part of the Waste Isolation Pilot Plant (WIPP) Site (four-mile zone), where halite is present in the unnamed member of the

Rustler, to the eastern side of Nash Draw where no Rustler halite has been found. Zone D contains WIPP-27 and WIPP-29 and is defined on the basis of anomalously high salinities (3-6 m) and K/Na ratios (0.2), probably related to contamination from potash refining operations in the area.

Three factors were extracted by R-mode principal component analysis of major and minor solute data. The first factor is dominated by Na, K, Mg, Br, and Cl. The second most important factor also has a strong Na-Cl influence, but is dominated by Ca, bicarbonate alkalinity, and Sr. It is likely that these two factors represent addition of solutes by the dissolution of halite, gypsum/anhydrite, and carbonates. A third factor showed the interelement correlations independent of effects attributable to halite dissolution. This factor contains two groups of inversely correlated elements: Mg, bicarbonate alkalinity, and SiO_2 form one group; and pH, B, and Li form another group. This pattern of element associations might reflect ion exchange, silicate hydrolysis, and carbonate diagenesis.

Saturation indices for minerals commonly observed in the Ochoan Series were calculated with the PHRQPITZ code, which uses the Pitzer model for ion interactions. All water samples are saturated with respect to gypsum. Dolomite and calcite saturation indices generally indicate apparent supersaturation with respect to the carbonates. The Mg/Ca ratios indicate that the degree of supersaturation increases with ionic strength. Potential sources of error in the carbonate data include uncertainties in the pH measurements, loss of CO_2 gas from the samples during collection, and uncertainties in the values of the free energy of dolomite used to calculate the saturation indices. All waters are undersaturated with respect to halite, and, with the exception of the Culebra waters from WIPP-29, all samples are undersaturated with respect to anhydrite.

This study confirms earlier observations that solute distribution patterns are not consistent with steady-state hydrologic flow over long (>10,000 year) time periods. Zone B, a facies with low salinity and element ratios inconsistent with halite dissolution, lies downgradient from more saline water in Zone C.

A model for the chemical evolution of water in the Culebra suggests that as water flowed through the aquifer, it increased in salinity as it dissolved halite, carbonates, and sulfates. Theoretical calculations show that the increase in salinity caused by the dissolution of halite changes the solubilities of carbonates and sulfates; solubilities increase up to 3 molal ionic strength and then decrease. Addition of magnesium by dissolution of carnallite and/or polyhalite and suppression of dolomite precipitation are consistent with the observed Mg/Ca ratios.

CONTENTS

CONTENTS (Continued)

CONTENTS (Continued)

FIGURES

FIGURES (Continued)

FIGURES (Continued)

TABLES

CHAPTER 2.0

2.1 INTRODUCTION

2.1.1 Objectives

This chapter provides a synthesis of solute concentration data available in late 1987 and proposes hypotheses concerning the origin of solutes in groundwaters in the Culebra dolomite of the Rustler Formation. Spatial trends in the concentrations of major solutes in the study area are used to define hydrochemical facies. These facies are then compared to the modern groundwater flow system to determine if flow directions indicated by modern hydraulic head potentials and transmissivities are consistent with flow directions suggested by solute concentrations.

Where relevant, data from the Magenta dolomite, Dewey Lake Red Beds, Rustler/Salado contact zone, and the Bell Canyon Formation are included in this chapter. Data and discussion of the redox potential and isotope geochemistry of Rustler and Dewey Lake groundwaters and a discussion of the mineralogy of the Culebra are found in other chapters of this report.

This synthesis is not intended to be taken as a final comprehensive model of the solute chemistry in the Rustler. Instead, it is a summary of current ideas that may indicate the framework within which some future data collection and modeling activities will be carried out.

2.1.2 Study Area and Stratigraphy

Figure 2-1 shows the region of interest for this study, the locations of wells discussed in this chapter, and the site boundary (sometimes called the four-mile zone or the WIPP Site).

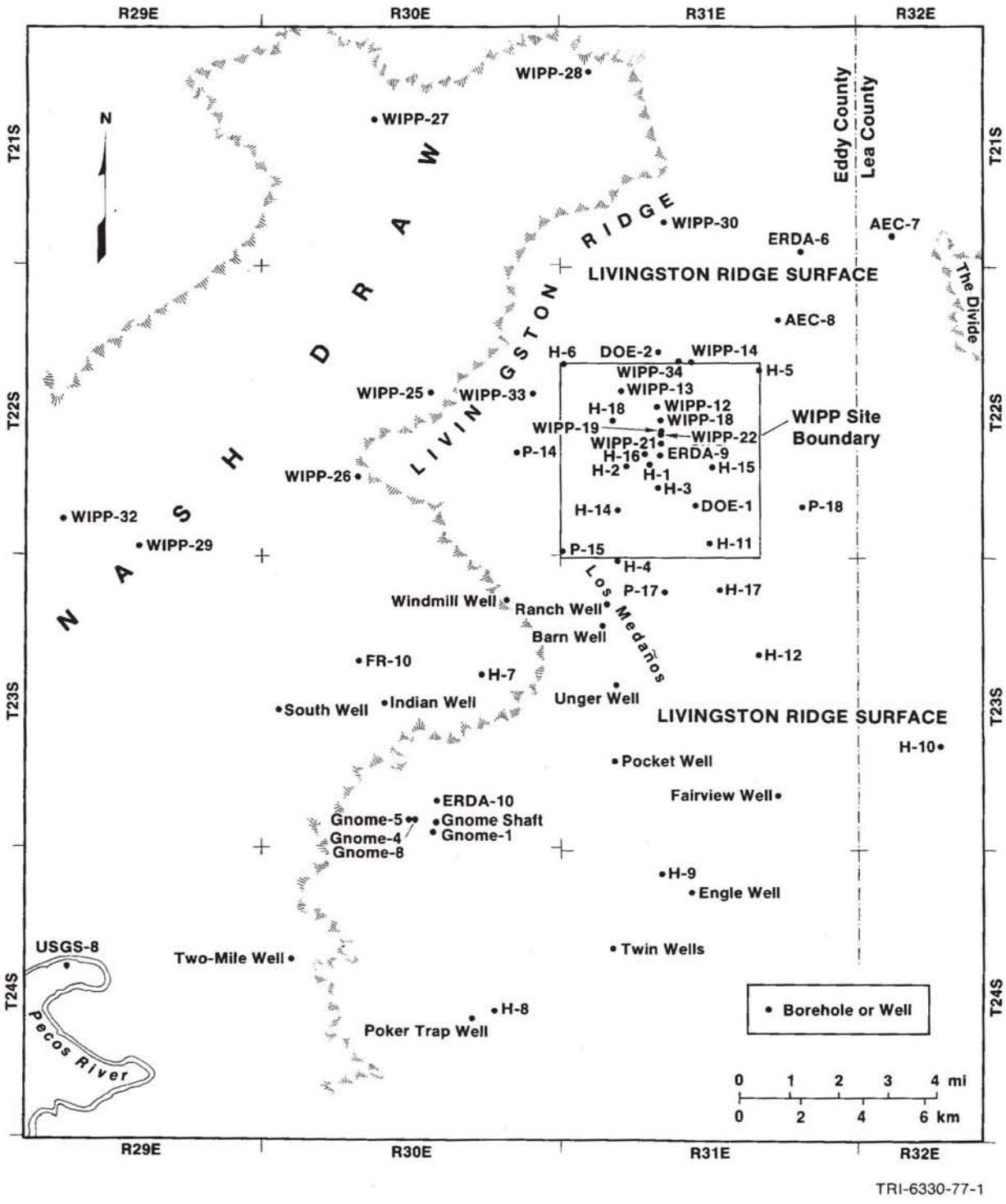

Figure 2-1. Map showing locations of wells in the study area.

The stratigraphy has been well documented (Siegel and Lambert, Chapter 1; Lappin, 1988, and references cited therein) and is not repeated here. In descending order, the units of interest here are the Dewey Lake Red Beds, the Rustler Formation (which contains the Forty-niner, Magenta dolomite, Tamarisk, Culebra dolomite, and unnamed lower members), the Salado Formation, the Castile Formation, and the Bell Canyon Formation.

2.1.3 Previous Work

Mercer (1983) provided a summary of geohydrologic and hydrochemical data from the Los Medaños area. The study area included 800 square miles surrounding the WIPP Site. Mercer (1983) summarized the results of previous US Geological Survey (USGS) studies and compiled analyses of major and minor solutes and radiochemical data from the Culebra, Magenta, and Rustler/Salado contact zone collected from 1976 to 1980. Although Mercer did not define any hydrochemical facies zones in the Culebra, he did show a line to the east of which the sum of the potassium plus magnesium concentrations was greater than 100 milliequivalents per liter (Figure 19 of Mercer, 1983). This line approximated the dividing line between regions of higher transmissivity to the west and lower transmissivity to the east. In addition, it coincided roughly with "a line to the east of which halite is present in the Rustler Formation below the Culebra and to the west of which the halite beds have been removed by dissolution" (p. 63, Mercer, 1983). Listings of other relevant reports and sources of data published before 1983 can be found in this report and in Ramey (1985) discussed below.

Ramey (1985) recast the Culebra chemical data from Mercer's report in terms of hydrochemical facies and calculated saturation indices for minerals commonly observed in evaporite deposits. He defined three hydrochemical-facies zones in the Culebra. Ramey's Zone A comprised the eastern quarter of the four-mile zone (Figure 2-1) and extended to the eastern edge of the current study area. It was characterized by a saline (total dissolved solids [TDS] >60,000 mg/L) Na-Cl brine with considerable amounts of Mg and K. Ramey's Zone B lay to the south of the four-mile zone and contained fresher (TDS <3,500 mg/L) Ca-SO_4 waters. Ramey's Zone C included the western three-fourths of the

four-mile zone and extended to Nash Draw to the west. Waters in this zone contained Na and Cl as their predominant constituents and showed a wide range of salinities (9,000 mg/L <TDS <240,000 mg/L).

Ramey observed that the water chemistries in the Culebra did not support the hydrologic flow path proposed by Gonzalez (1983) and Barr et al. (1983). According to these workers, water flows southeast from the center of the site and then westward to Malaga Bend. This would mean that water along the flow path changes from a saline Na-Cl brine to a dilute Ca-SO_4 solution along the flow path. No plausible geochemical process has been identified that would cause this transformation in a hydrologically confined aquifer.

For the Culebra samples, Ramey calculated saturation indices for halite (NaCl), anhydrite ($CaSO_4$), gypsum ($CaSO_4 \cdot 2H_2O$), calcite ($CaCO_3$), and dolomite ($CaMg(CO_3)_2$) with the WATEQFC computer code. He found that all Culebra samples were undersaturated with respect to halite and concluded that waters from all parts of the study area had the potential to dissolve additional salt. His calculations indicated that all Culebra waters except those from H-4, H-5, and P-18 were saturated with respect to gypsum, and that, with the exception of WIPP-27 and WIPP-29 to the west, all waters were undersaturated with respect to anhydrite. Saturation indices for carbonates indicated areas of undersaturation and areas of apparent supersaturation.

Ramey suggested that the saturation indices for the saline (>0.5 molal) waters were in error because the WATEQFC code uses an inadequate model for activity coefficients. The code uses the extended Debye-Huckel equation (misidentified by Ramey as the Davies equation) to calculate activity coefficients. The constants used to calculate the activity coefficients by this equation were obtained from mean salt data over a range of approximately 0-3 molar ionic strength (Truesdell and Jones, 1974). Plummer and Parkhurst (1985) provide evidence that this equation accurately estimates the saturation indices of halite, calcite, gypsum, and dolomite in natural waters with ionic strengths of up to 2 molal. However, Møller et al. (1985) and Wolery et al. (1985) show that calculations of solubility

of gypsum in simple Ca-Na-SO_4-Cl-H_2O solutions with this equation do not reproduce experimental data satisfactorily. The accuracy of this equation for other minor solutes is generally considered to be poor at moderate to high ionic strengths (>0.2 m) (Phillips et al., 1988).

Meijer et al. (1987) examined the consistency of densities and chemical compositions of water samples collected from the Culebra between 1976 and 1984. They calculated saturation indices for several minerals using a critically-evaluated thermochemical data base and the PHREEQE computer code with a WATEQ-Debye-Huckel equation. They claimed that their calculational method was accurate at ionic strengths up to 3.0 molal (TDS of about 100,000 mg/L), and they suggested that their results were qualitatively similar to those reported by Ramey (1985). Meijer et al. also calculated densities from the chemical analyses and compared them to densities measured in the field. Based on their calculations, they concluded that 11 of the 22 water samples used by Ramey (1985) were not representative Culebra formation waters.

2.2 MAJOR, MINOR, AND TRACE SOLUTE DATA

2.2.1 Sources of Data

For this work we considered major-, minor-, and trace-solute data from water samples collected by several different agencies and analyzed in different laboratories from 1976 to 1987. Data were obtained from the following sources:

- Sandia National Laboratories (SNL). Samples collected by several different agencies were analyzed by United Nuclear Corporation (UNC) Geotech (formerly Bendix Field Engineering Corporation), Grand Junction, CO. The data, as well as details of methods of sample collection and analytical techniques, are reported in Robinson (1988).

- USGS. Samples collected by the USGS were analyzed by the USGS Central Laboratories (Branch of Analytical Services, Water Resource Division) and reported by Mercer (1983) and Mercer and Orr (1979).

- International Technology (IT) Corporation. Samples collected for the Water Quality Sampling Program (WQSP) were analyzed by the IT Analytical Services (ITAS) laboratory, Murraysville, NJ. The data are given in a series of annual reports (Uhland and Randall, 1986; Uhland, et al., 1987; Randall et al., 1988; and Lyon, 1989).

- New Mexico Environmental Evaluation Group (EEG). The New Mexico Bureau of Mines & Mineral Resources (NMBM&MR) analyzed samples from the WQSP for the EEG (personal communication from Chapman in Robinson, 1988).

Table 2-1 summarizes the different data sets that were consulted in this work.

2.2.2 Criteria Used to Evaluate Chemical Data

In some cases, large differences exist between the chemical compositions reported by different laboratories for the same water sample or by the same laboratory for different samples from the same well. Data from UNC, ITAS, the NMBM&MR, and the USGS laboratories collected from 1976 to 1987 were reviewed, and the critical evaluation procedure of Robinson (1988) was used to select those data considered to be most reliable at the time most of the studies in this chapter were being done (late 1987).

Samples, obtained after a lengthy pumping test, have proved to be more reliable than those obtained by bailing or swabbing (Robinson, 1988). During a pumping test, samples can be periodically collected and analyzed for selected parameters in the field. These samples ("serial" samples) are collected at regular intervals until the measured parameters reach a constant value (the "steady-state" value). At this time, "final" samples are collected

Table 2-1. Sources of Solute Data

Collection Dates	Program or Collector[1]	Labs[2]	References
1976-1980	USGS	USGS	Mercer and Orr, 1979; Mercer, 1983
1980-1981	Sandia	UNC	Lambert and Robinson, 1984; Robinson, 1988
1983-1984	HGC	UNC	Robinson, 1988
1985-1987	WQSP	ITAS, UNC, NMBM&MR	Uhland and Randall, 1986; Uhland et al., 1987; Randall et al., 1988; Robinson, 1988; SNL, unpublished data from UNC

1. USGS = United States Geological Survey
   WQSP = Water Quality Sampling Program
   HGC = Hydro Geo Chem, Inc., Tucson, AZ (a SNL subcontractor)
2. ITAS = IT Analytical Services, Murraysville, PA
   NMBM&MR = New Mexico Bureau of Mines & Mineral Resources, Socorro, NM
   UNC = UNC Geotech (formerly Bendix Field Engineering Corp.), Grand Junction, CO
   USGS = United States Geological Survey, Central Laboratory

for analysis in various laboratories. For some parameters, such as chloride, the steady-state value is considered representative of the unperturbed groundwater; for other parameters, such as iron, the steady-state value often does not represent the actual concentration in the in-situ groundwater (Robinson, 1988).

During a pumping test, if the concentrations of chloride and divalent cations (calcium plus magnesium) reach steady-state, then the samples are considered representative with respect to concentrations of the major solutes (Cl, SO_4, Ca, Mg, Na, and K) and certain minor and trace elements (Br, F, I, B, Li, and Sr). This assumption is based on the observation that at some wells, the same concentrations have been observed in samples collected several years apart using the serial sampling method. However, a steady-state value for a parameter such as iron does not necessarily mean that the sample is not contaminated. For

example, in some wells, the steady-state value for iron varied as the pumping rate changed, suggesting that a process such as corrosion of the well casing was controlling the concentration of iron in the sampled water (Uhland et al., 1987; Robinson, 1988).

We assume that samples are representative of a given location if samples of the same composition have been collected during several different sampling periods several years apart. However, this assumption may not always be valid. Even if reproducible samples (that is, samples with the same solute concentrations) are collected from a well during more than one sampling episode, the samples may still not be representative of unperturbed groundwater. The steady-state concentrations observed during serial-sampling and analyses may actually represent transient conditions. Thus, for example, samples with apparently anomalous solute chemistries such as the Culebra groundwater from P-14 (as discussed in subsequent sections of this chapter) may be extensively contaminated.

2.2.3 Results of Evaluation of Data from Culebra Samples

2.2.3.1 Major, Minor, and Trace Solute Data

Table 2-2 summarizes the data from the Rustler Formation, the Dewey Lake Red Beds, and the Bell Canyon Formation. The sources in Table 2-1 were consulted for data to estimate the ranges of solute concentrations observed at the wells and to calculate average values for use in element ratio contours described in Section 2.3.1. Analyses reported by UNC Geotech were used in the saturation index calculations and principal component analysis (PCA) discussed in Sections 2.3.4 and 2.3.3, respectively.

Uncertainties in the data are related to several sources including analytical techniques, sampling techniques (contamination introduced by the sampling apparatus or loss of solutes during sampling), and contamination of waters at depth or in the well. The last source of uncertainty is sometimes indicated by a change in the water chemistry over a period of several years.

Table 2-2. Concentrations of Solutes[1] in Groundwaters from the Rustler Formation, Dewey Lake Red Beds, and Bell Canyon Formation
Part A: Major Solutes, pCO_2, and pH

Well(s)	Date[2]	Lab[3]	Zone[4]	Na (mg/L)	K (mg/L)	Ca (mg/L)	Mg (mg/L)	Cl^- (mg/L)	SO_4^{2-} (mg/L)	Alkalinity[5] as HCO_3^- (mg/L)	pCO_2[6]	pH[5]
DOE-1	04/85	UNC	CuA	45800	1100	1730	1610	73600	7350	45	-2.60	7.1
DOE-1	[2]	*avg*	CuA	*46000*	*1100*	*1700*	*1600*	*75000*	*7400*			
DOE-1	[2]	rng	CuA	45000-46000	[1]	[1]	[1]	73000-77000	[1]	45-46		7.1
DOE-2	03/85	UNC	CuC	18400	410	1960	1060	34600	3950	67	-2.33	7.0
DOE-2	[2]	*avg*	CuC	*18000*	*420*	*1900*	*1000*	*33000*	*3700*			
DOE-2	[2]	rng	CuC	17000-19000	410-420	1900-2000	900-1100	32000-35000	3400-4000	[1]		[1]
H-2A	04/86	UNC	CuC	3570	93.5	743	167	5310	2980	57	-3.38	8.0
H-3B3	06/84	UNC	CuC	17400	495	1550	829	29500	5130		-2.83	7.4
H-3B3	02/85	UNC	CuC	18000	425	1470	783	30300	4820	52	-2.86	7.4
H-3B2, H-3B3	[4]	*avg*	CuC	*18000*	*440*	*1400*	*760*	*29000*	*4800*			
H-3B2, H-3B3	[4]	rng	CuC	17000-19000	360-500	1200-1600	690-830	27000-31000	4600-5200	50-52		7.4
H-4B	05/81	UNC	CuC	6080	215	700	455	7980	6230	71	-3.35	8.0
H-4C	08/84	UNC	CuC	6150	222	698	505	7950	5700	75	-3.11	7.8
H-4B	07/85	UNC	CuC	5850	210	691	427	7480	5520	69	-3.04	7.7
H-4B, H-4C	[4]	*avg*	CuC	*6000*	*220*	*690*	*450*	*7700*	*5700*			
H-4B, H-4C	[4]	rng	CuC	5800-6200	180-260	690-700	400-510	7400-8000	5500-6300	68-75		7.6-8.0
H-5B	06/81	UNC	CuA	52400	1290	1710	2140	89500	7360	80	-3.21	7.9
H-5C	10/81	UNC	CuA	52300	1300	1720	2150	89500	7570	86	-3.17	7.9
H-5B	08/85	UNC	CuA	54100	1350	1700	2170	85400	7840	50	-2.86	7.4
H-5B, H-5C	[4]	*avg*	CuA	*53000*	*1300*	*1700*	*2200*	*87000*	*7600*			
H-5B, H-5C	[4]	rng	CuA	52000-55000	1200-1400	1700-1800	2100-2200	84000-90000	7300-7900			

Table 2-2. Concentrations of Solutes[1] in Groundwaters from the Rustler Formation, Dewey Lake Red Beds, and Bell Canyon Formation
Part A: Major Solutes, pCO_2, and pH (Continued)

Well(s)	Date[2]	Lab[3]	Zone[4]	Na (mg/L)	K (mg/L)	Ca (mg/L)	Mg (mg/L)	Cl^- (mg/L)	SO_4^{2-} (mg/L)	Alkalinity[5] as HCO_3^- (mg/L)	pCO_2[6]	pH[5]
H-6B	05/81	UNC	CuC	18600	450	2150	1080	33000	3980	96	-2.16	7.0
H-6B	09/85	UNC	CuC	18000	375	2040	1040	32300	3570	94	-2.07	6.9
H-6B	[3]	*avg*	CuC	*18000*	*420*	*2000*	*1100*	*33000*	*3600*			
H-6B	[3]	rng	CuC	17000-19000	370-450	1900-2200	1000-1200	32000-34000	3300-4000	90-96		6.9-7.2
H-7B1	03/86	UNC	CuB	207	7.0	587	130	320	1850	120	-2.20	7.3
H-7B1	[3]	*avg*	CuB	*210*	*7.0*	*570*	*130*	*320*	*1800*			
H-7B1	[3]	rng	CuB	200-210	7.0	540-590	130	300-350	1700-1900	120		7.3-7.4
H-8B	01/86	UNC	CuB	55.1	3.83	548	157	30.5	1950	96	-2.70	7.3
H-8B	[2]	*avg*	CuB	*54*	*3.9*	*540*	*170*	*32*	*1800*			
H-8B	[2]	rng	CuB	51-56	3.7-4.1	520-550	150-180	30-33	1600-2000	93-96		7.2-7.3
H-9B	11/85	UNC	CuB	146	6.85	590	137	194	1900	110	-2.43	7.4
H-9B	[2]	*avg*	CuB	*150*	*7.2*	*580*	*150*	*190*	*1800*			
H-9B	[2]	rng	CuB	140-150	6.8-7.6	560-620	130-170	170-200	1700-1900	110		7.3-7.4
H-11B3	06/85	UNC	CuA	40400	943	1700	1320	65900	7180	54	-2.63	7.2
H-11B3	[2]	*avg*	CuA	*39000*	*940*	*1600*	*1300*	*66000*	*7200*			
H-11B3	[2]	rng	CuA	37000-41000	[1]	1500-1700	1300-1400	65000-67000	[1]	54-55		7.2-7.3
H-12	08/85	UNC	CuA	49200	1270	1760	1980	79000	7210	53	-2.61	7.2
H-12	[2]	*avg*	CuA	*50000*	*1300*	*1800*	*2000*	*80000*	*7200*			
H-12	[2]	rng	CuA	49000-51000	[1]	1700-1900	1900-2000	78000-80000	[1]	53-62		7.2

Table 2-2. Concentrations of Solutes[1] in Groundwaters from the Rustler Formation, Dewey Lake Red Beds, and Bell Canyon Formation
Part A: Major Solutes, pCO_2, and pH (Continued)

Well(s)	Date[2]	Lab[3]	Zone[4]	Na (mg/L)	K (mg/L)	Ca (mg/L)	Mg (mg/L)	Cl^- (mg/L)	SO_4^{2-} (mg/L)	Alkalinity[5] as HCO_3^- (mg/L)	pCO_2[6]	pH[5]
P-14	02/86	UNC	CuC	4360	37.9	3520	840	14500	1590	110	-1.81	6.8
P-14	[2]	*avg*	CuC	*4100*	*41*	*3700*	*800*	*14000*	*1600*			
P-14	[2]	rng	CuC	3700-4400	37-45	3500-3900	760-840	13000-15000	1500-1700	100-110		6.8-6.9
P-17	03/86	UNC	CuC	28300	782	1620	1460	48200	6020	64	-2.90	7.5
P-17	[2]	*avg*	CuC	*28000*	*820*	*1600*	*1500*	*49000*	*6000*			
P-17	[2]	rng	CuC	28000-29000	780-880	1500-1700	1400-1600	48000-51000	5900-6100	61-64		7.5
WIPP-13	02/87	*avg*	CuC	*19000*	*340*	-	-	*36000*	*4500*	*~120*		*~6.6*
WIPP-25	08/80	UNC	CuC	3160	73.5	905	260	5250	2500	210	-1.69	6.9
WIPP-25	08/80	*avg*	CuC	*3200*	*74*	*900*	*260*	*5200*	*2500*			
WIPP-25	08/80	rng	CuC	[1]	[1]	[1]	[1]	5200-5300	[1]	[1]		[1]
WIPP-25	02/86	UNC	CuC	3180	102	1140	315	6320	2380	130		7.2
WIPP-25	02/86	*avg*	CuC	*3300*	*100*	*1100*	*330*	*6200*	*2400*			
WIPP-25	02/86	rng	CuC	3100-3400	100-110	1100-1200	310-340	6200-6400	2300-2400	[1]		[1]
WIPP-26	08/80	UNC	CuC	3620	170	1240	355	7200	2480	140	-1.86	6.9
WIPP-26	08/80	*avg*	CuC	*3600*	*170*	*1200*	*360*	*7000*	*2500*			
WIPP-26	08/80	rng	CuC	[1]	[1]	[1]	[1]	6900-7200	[1]	[1]		6.9

Table 2-2. Concentrations of Solutes[1] in Groundwaters from the Rustler Formation, Dewey Lake Red Beds, and Bell Canyon Formation
Part A: Major Solutes, pCO_2, and pH (Continued)

Well(s)	Date[2]	Lab[3]	Zone[4]	Na (mg/L)	K (mg/L)	Ca (mg/L)	Mg (mg/L)	Cl^- (mg/L)	SO_4^{2-} (mg/L)	Alkalinity[5] as HCO_3^- (mg/L)	pCO_2[6]	pH[5]
WIPP-26	11/85	UNC	CuC	4220	343	1340	380	8770	2420	120	-2.14	7.1
WIPP-26	11/85	*avg*	CuC	*4100*	*350*	*1300*	*390*	*8600*	*2400*			
WIPP-26	11/85	rng	CuC	3800-4300	340-360	1200-1400	370-430	8400-8800	2300-2500	[1]		[1]
WIPP-27	09/80	UNC	CuD	39200	8060	3210	1900	78500	3830	120	-1.33	6.4
WIPP-27	[2]	*avg*	CuD	*39000*	*8100*	*3200*	*2000*	*78000*	*3900*			
WIPP-27	[2]	rng	CuD	39000-40000	[1]	3100-3300	1900-2000	77000-79000	3800-3900	[1]		6.4
WIPP-28	09/80	UNC	CuC	15200	485	1180	555	24800	4380		-.076	6.5
WIPP-28	09/80	*avg*	CuC	*15000*	*480*	*1200*	*560*	*24000*	*4400*			
WIPP-28	09/80	rng	CuC	[1]	[1]	[1]	[1]	24000-25000	[1]			
WIPP-29	08/80	UNC	CuD	71400	15600	950	5480	138000	14000	210	-0.87	6.1
WIPP-29	08/80	*avg*	CuD	*71000*	*16000*	*880*	*5600*	*140000*	*14000*			
WIPP-29	08/80	rng	CuD	[1]	[1]	810-950	5400-5700	130000-140000	13000-14000	[1]		6.1
WIPP-29	12/85	UNC	CuD	94900	23300	413	6500	179000	20000	160	-0.75	5.9
WIPP-29	12/85	*avg*	CuD	*92000*	*22000*	*410*	*6400*	*180000*	*18000*			
WIPP-29	12/85	rng	CuD	90000-95000	20000-24000	[1]	6300-6500	179000-180000	17000-20000	[1]		[1]
WIPP-30	09/80	UNC	CuC	8570	255	1140	460	14600	4120	40 HCO_3^- & 17 CO_3^{2-}	-4.41	8.8
WIPP-30	09/80	*avg*	CuC	*8600*	*260*	*1100*	*460*	*15000*	*4100*			
WIPP-30	09/80	rng	CuC	[1]	[1]	[1]	[1]	14000-15000	[1]	[1]		[1]

Table 2-2. Concentrations of Solutes[1] in Groundwaters from the Rustler Formation, Dewey Lake Red Beds, and Bell Canyon Formation
Part A: Major Solutes, pCO_2, and pH (Continued)

Well(s)	Date[2]	Lab[3]	Zone[4]	Na (mg/L)	K (mg/L)	Ca (mg/L)	Mg (mg/L)	Cl^- (mg/L)	SO_4^{2-} (mg/L)	Alkalinity[5] as HCO_3^- (mg/L)[5]	pCO_2[6]	pH[5]
Engle	03/85	UNC	CuB	200	5.60	588	152	231	1990	110	-2.44	7.4
Engle	03/85	*avg*	CuB	*190*	*5.5*	*580*	*140*	*230*	*1900*			
Engle	03/85	rng	CuB	180-200	5.4-5.6	570-590	130-160	220-240	1800-2000	[1]		[1]
H-3B1	07/85	UNC	Mag	1520	34.5	1000	292	3360	2310	47		8.0
H-3B1	[3]	rng	Mag	1500-1600	34-36	1000	270-300	3300-3400	2200-2400	45-47		7.7-8.0
H-4C	11/86	UNC	Mag	7110	85.1	651	411	8460	7100	70		8.4
H-4C	[2]	rng	Mag	7100-7300	85-99	610-660	390-420	8400-8500	[1]	70-85		8.1-8.4
H-5C	10/86	UNC	Mag	1480	33.6	550	173	1070	3620	56		8.0
H-5C	10/86	rng	Mag	1400-1500	[1]	[1]	170-190	1000-1100	[1]	[1]		[1]
H-6C	10/86	UNC	Mag	642	16.6	546	160	428	2700	51		7.7
H-6C	10/86	rng	Mag	[1]	[1]	[1]	160-170	420-430	2400-2700	[1]		[1]
WIPP-25	09/80	UNC	Mag	2910	71.5	905	260	5250	2490	180		6.9
WIPP-27	09/80	UNC	Mag	43200	8090	3660	2100	85200	3410	210		6.4
WIPP-25	07/80	UNC	R/S	123000	3330	560	3260	192000	12400	130		7.4
WIPP-26	07/80	UNC	R/S	68600	1200	1420	1660	108000	7480	270		7.7

Table 2-2. Concentrations of Solutes[1] in Groundwaters from the Rustler Formation, Dewey Lake Red Beds, and Bell Canyon Formation
Part A: Major Solutes, pCO_2, and pH (Continued)

Well(s)	Date[2]	Lab[3]	Zone[4]	Na (mg/L)	K (mg/L)	Ca (mg/L)	Mg (mg/L)	Cl^- (mg/L)	SO_4^{2-} (mg/L)	Alkalinity[5] as HCO_3^- (mg/L)	pCO_2[6]	pH[5]
WIPP-28	07/80	UNC	R/S	97100	4300	605	3400	155000	16700	170		7.0
WIPP-29	07/80	UNC	R/S	36100	1480	1080	2320	58000	12000	200		7.2
WIPP-30	07/80	UNC	R/S	121000	2180	955	2770	192000	7390	620		7.5
Ranch	06/86	UNC	DL	200	4.0	420	202	418	1100	220		7.0
Ranch	06/86	rng	DL	180-200	3.6-4.0	[1]	190-210	390-420	920-1100	[1]		[1]
Twin-Pasture	01/86	UNC	DL	25.4	3.85	80.4	22.5	44.1	75.1	230		7.8
Twin-Pasture	01/86	rng	DL	24-26	3.7-4.3	80-81	22-25	44-47	70-76	[1]		[1]
DOE-2	07/85	UNC	BC	49600	885	5910	1330	89700	2020	48		6.8
DOE-2	07/85	rng	BC	[1]	[1]	[1]	[1]	89000-90000	[1]	(lab)		[1]

Table 2-2. Concentrations of Solutes[1] in Groundwaters from the Rustler Formation, Dewey Lake Red Beds, and Bell Canyon Formation
Part B: Minor and Trace Solutes, TDS, and Ionic Strength

Well(s)	Date[2]	Lab[3]	Zone[4]	TDS[7] (mg/L)	IS[6] (molal)	Br^- (mg/L)	F^- (mg/L)	I^- (mg/L)	B (mg/L)	Li (mg/L)	Sr (mg/L)	Silica as SiO_2 (mg/L)[2]	Fe (mg/L)	Mn (mg/L)
DOE-1	04/85	UNC	CuA	131200	2.53	56			37	0.64	26	8.4	0.28	
DOE-1	[2]	*avg*	CuA			*60*	*1.2*		*36*	*0.64*	*21*			
DOE-1	[2]	rng	CuA			56-	1.0-		35-	[1]	16-	8-		
						64	1.7		37		26	24		
DOE-2	03/85	UNC	CuC	60400	1.19	34	1.7	0.22	16	0.47	38	17	0.036	0.30
DOE-2	[2]	*avg*	CuC			*35*	*1.6*	*0.22*	*18*	*0.47*	*29*			
DOE-2	[2]	rng	CuC			34-	1.2-	[1]	14-	[1]	22-	17-		
						36	2.2		24		38	24		
H-2A	04/86	UNC	CuC	12900	0.27	5.6	2.2	0.081	10	0.22	9.5	13	1.1	0.055
H-3B3	06/84	UNC	CuC	55000	1.08	29	2.1	0.13	30	0.53	23	9.8	0.57	0.13
H-3B3	02/85	UNC	CuC	55800	1.08	26	1.9	0.14	26	0.40	30	11	0.20	0.12
H-3B2, H-3B3	[4]	*avg*	CuC			*31*	*1.8*	*0.14*	*28*	*0.41*	*25*			
H-3B2, H-3B3	[4]	rng	CuC			26-	1.5-	0.13-	21-	0.30-	23-	9-		
						39	2.1	0.14	34	0.53	30	20		
H-4B	05/81	UNC	CuC	21700	0.46	42			18	0.39	14	11		
H-4C	08/84	UNC	CuC	21200	0.45	48	2.1	0.23	20	0.49	18	13	2.2	0.20
H-4B	07/85	UNC	CuC	20200	0.42	43	2.7		14	0.40	14	14	0.32	0.11
H-4B, H-4C	[4]	*avg*	CuC			*44*	*2.2*	*0.23*	*18*	*0.42*	*15*			
H-4B, H-4C	[4]	rng	CuC			43-	1.7-	[1]	14-	0.39-	13-	11-		
						48	2.7		23	0.49	18	30		
H-5B	06/81	UNC	CuA	154400	2.99	62			33	0.77	32	6.2		
H-5C	10/81	UNC	CuA	154500	3.00	64			35	0.77	31	5.8		
H-5B	08/85	UNC	CuA	152600	2.97	49	2.0	0.19	34	0.81	29	7.1	2.9	0.29
H-5B, H-5C	[4]	*avg*	CuA			*58*	*1.3*	*0.19*	*33*	*0.78*	*31*			
H-5B, H-5C	[4]	rng	CuA			49-	0.8-	[1]	29-	0.77-	29-	5-		
						64	2.0		35	0.81	32	36		

Table 2-2. Concentrations of Solutes[1] in Groundwaters from the Rustler Formation, Dewey Lake Red Beds, and Bell Canyon Formation
Part B: Minor and Trace Solutes, TDS, and Ionic Strength (Continued)

Well(s)	Date[2]	Lab[3]	Zone[4]	TDS[7] (mg/L)	IS[6] (molal)	Br^- (mg/L)	F^- (mg/L)	I^- (mg/L)	B (mg/L)	Li (mg/L)	Sr (mg/L)	Silica as SiO_2 (mg/L)[2]	Fe (mg/L)	Mn (mg/L)
H-6B	05/81	UNC	CuC	59300	1.18	34			11	0.44	32	20		
H-6B	09/85	UNC	CuC	57400	1.13	34	1.9	0.096	10	0.45	30	18	0.094	0.13
H-6B	[3]	*avg*	CuC			*34*	*1.6*	*0.096*	*9.5*	*0.44*	*28*			
H-6B	[3]	rng	CuC			34-35	1.3-1.9	[1]	7-11	0.44-0.45	24-32	18-43		
H-7B1	03/86	UNC	CuB	3220	0.089	0.57	1.5	0.052	0.76	0.10	8.5	47	0.056	0.050
H-7B1	[3]	*avg*	CuB			*0.57*	*1.4*	*0.052*	*0.77*	*0.11*	*7.7*			
H-7B1	[3]	rng	CuB			[1]	1.2-1.5	[1]	0.74-0.80	0.10-0.12	5.8-8.7	47-92		
H-8B	01/86	UNC	CuB	2830	0.083	0.085	2.5	0.14	0.48	0.12	6.9	29	0.036	0.021
H-8B	[2]	*avg*	CuB			*0.085*	*2.4*	*0.14*	*0.49*	*0.12*	*6.7*			
H-8B	[2]	rng	CuB			[1]	2.1-2.5	[1]	0.48-0.50	0.12	5.9-7.4	29-56		
H-9B	11/85	UNC	CuB	3080	0.087	0.24	3.3	0.11	0.63	0.18	7.5	27	0.032	0.015
H-9B	[2]	*avg*	CuB			*0.24*	*3.0*	*0.11*	*0.66*	*0.18*	*7.2*			
H-9B	[2]	rng	CuB			[1]	2.6-3.3	[1]	0.63-0.70	0.17-0.18	7.0-7.5	27-39		
H-11B3	06/85	UNC	CuA	117400	2.23	47			32	0.62	25		0.14	0.22
H-11B3	[2]	*avg*	CuA			*48*	*1.3*		*31*	*0.50*	*20*			
H-11B3	[2]	rng	CuA			47-48	1.0-1.6		30-32	0.38-0.62	18-25	25-32		
H-12	08/85	UNC	CuA	140500	2.72	76			39	1.2	31	7.2	0.22	0.087
H-12	[2]	*avg*	CuA			*76*	*1.5*		*38*	*0.85*	*29*			
H-12	[2]	rng	CuA			76-77	1.1-2.3		35-39	0.61-1.2	18-38	7-96		
P-14	02/86	UNC	CuC	24900	0.58	72	1.7	0.42	0.72	0.28	51	30	2.0	0.18
P-14	[2]	*avg*	CuC			*72*	*1.5*	*0.42*	*0.72*	*0.28*	*50*			
P-14	[2]	rng	CuC			[1]	1.2-1.7	[1]	[1]	[1]	48-51	30-69		

Table 2-2. Concentrations of Solutes[1] in Groundwaters from the Rustler Formation, Dewey Lake Red Beds, and Bell Canyon Formation
Part B: Minor and Trace Solutes, TDS, and Ionic Strength (Continued)

Well(s)	Date[2]	Lab[3]	Zone[4]	TDS[7] (mg/L)	IS[6] (molal)	Br^- (mg/L)	F^- (mg/L)	I^- (mg/L)	B (mg/L)	Li (mg/L)	Sr (mg/L)	Silica as SiO_2 (mg/L)[2]	Fe (mg/L)	Mn (mg/L)
P-17	03/86	**UNC**	CuC	86500	1.67	**72**	**1.9**	**0.18**	**38**	**0.87**	**29**	**8.5**	**4.0**	**0.87**
P-17	[2]	*avg*	CuC			*70*	*1.6*	*0.18*	*35*	*0.87*	*31*			
P-17	[2]	rng	CuC			69-72	1.2-1.9	[1]	32-38	[1]	28-36	0-8.5		
WIPP-13	02/87	*avg*	CuC			*39*	*1.4*		*11*	*0.35*	*25*			
WIPP-25	08/80	**UNC**	CuC	12100	0.26	**2.6**			**1.5**	**0.20**	**12**	**34**		
WIPP-25	08/80	*avg*	CuC			*2.6*			*1.5*	*0.20*	*12*			
WIPP-25	08/80	rng	CuC			[1]			[1]	[1]	[1]	[1]		
WIPP-25	02/86	**UNC**	CuC	13600		**3.4**	**1.7**	**0.042**	**1.7**	**0.22**	**17**	**33**	**0.50**	**0.11**
WIPP-25	02/86	*avg*	CuC			*3.8*	*1.6*	*0.042*	*1.7*	*0.22*	*17*			
WIPP-25	02/86	rng	CuC			3.4-4.2	1.6-1.7	[1]	1.7	[1]	[1]	33-67		
WIPP-26	08/80	**UNC**	CuC	15100	0.33	**3.2**			**1.4**	**0.24**	**17**	**33**		
WIPP-26	08/80	*avg*	CuC			*3.2*			*1.4*	*0.24*	*17*			
WIPP-26	08/80	rng	CuC			[1]			[1]	[1]	[1]	[1]		
WIPP-26	11/85	**UNC**	CuC	17600	0.37	**3.9**	**1.7**	**0.070**	**1.6**	**0.23**	**20**	**35**	**0.026**	**<0.01**
WIPP-26	11/85	*avg*	CuC			*3.9*	*1.5*	*0.070*	*1.6*	*0.23*	*18*			
WIPP-26	11/85	rng	CuC			[1]	1.3-1.7	[1]	[1]	[1]	17-20	35-65		
WIPP-27	09/80	**UNC**	CuD	134700	2.57	**28**			**2.3**	**0.33**	**51**	**23**		
WIPP-27	[2]	*avg*	CuD			*28*			*2.1*	*0.33*	*51*			
WIPP-27	[2]	rng	CuD			[1]			1.9-2.3	[1]	[1]	13-23		

Table 2-2. Concentrations of Solutes[1] in Groundwaters from the Rustler Formation, Dewey Lake Red Beds, and Bell Canyon Formation
Part B: Minor and Trace Solutes, TDS, and Ionic Strength (Continued)

Well(s)	Date[2]	Lab[3]	Zone[4]	TDS[7] (mg/L)	IS[6] (molal)	Br^- (mg/L)	F^- (mg/L)	I^- (mg/L)	B (mg/L)	Li (mg/L)	Sr (mg/L)	Silica as SiO_2 (mg/L)[2]	Fe (mg/L)	Mn (mg/L)
WIPP-28	09/80	UNC	CuC	46600	0.90	7.2			5.8	0.30	16	36		
WIPP-28	09/80	*avg*	CuC			*7.2*			*5.8*	*0.30*	*16*			
WIPP-28	09/80	rng	CuC			[1]			[1]	[1]	[1]	[1]		
WIPP-29	08/80	UNC	CuD	245400	4.91	45			4.4	0.78	29	22		
WIPP-29	08/80	*avg*	CuD			*45*			*4.4*	*0.78*	*29*			
WIPP-29	08/80	rng	CuD			[1]			[1]	[1]	[1]	[1]		
WIPP-29	12/85	UNC	CuD	324100	6.57	61	4.6	0.38	5.2	0.70	13	15	1.1	1.7
WIPP-29	12/85	*avg*	CuD			*61*		*0.38*	*5.5*	*0.70*	*11*			
WIPP-29	12/85	rng	CuD			[1]	0.9-4.6	[1]	5.2-5.8	[1]	9-13	15-110		
WIPP-30	09/80	UNC	CuC	29100	0.58	10			6.1	0.27	18	6.5		
WIPP-30	09/80	*avg*	CuC			*10*			*6.1*	*0.27*	*18*			
WIPP-30	09/80	rng	CuC			[1]			[1]	[1]	[1]	[1]		
Engle	03/85	UNC	CuB	3270	0.09	0.27	2.8	0.12	0.97	0.17	8.4	29	0.59	0.060
Engle	03/85	*avg*	CuB			*0.27*	*2.8*	*0.12*	*0.87*	*0.17*	*7.7*			
Engle	03/85	rng	CuB			[1]	2.8-2.9	[1]	0.77-0.97	[1]	7.0-8.5	29-54		
H-3B1	07/85	UNC	Mag	8560		5.8	2.4	1.2	2.0	0.32	17	10	0.11	0.028
H-3B1	[3]	rng	Mag			5.8-6.0	1.8-2.6	1.2-2.0	2.0-4.5	0.32	13-18	10-26		

Table 2-2. Concentrations of Solutes[1] in Groundwaters from the Rustler Formation, Dewey Lake Red Beds, and Bell Canyon Formation
Part B: Minor and Trace Solutes, TDS, and Ionic Strength (Continued)

Well(s)	Date[2]	Lab[3]	Zone[4]	TDS[7] (mg/L)	IS[6] (molal)	Br^- (mg/L)	F^- (mg/L)	I^- (mg/L)	B (mg/L)	Li (mg/L)	Sr (mg/L)	Silica as SiO_2 (mg/L)[2]	Fe (mg/L)	Mn (mg/L)
H-4C	11/86	UNC	Mag	23900		5.9	2.4	0.31	12	0.46	12	9.1	0.71	0.29
H-4C	[2]	rng	Mag			5.9-7.5	2.2-2.6	[1]	11-12	0.41-0.46	12-14	9-26		
H-5C	10/86	UNC	Mag	6980		0.93	2.5	0.31	11	0.20	10	11	1.5	0.020
H-5C	10/86	rng	Mag			[1]	2.5	[1]	10-11	0.20	8-10	11-26		
H-6C	10/86	UNC	Mag	4540		2.3	1.5	0.086	2.2	0.21	9.8	11	0.26	0.010
H-6C	10/86	rng	Mag			1.0-2.3	1.5-1.7	[1]	2.2-2.4	0.19-0.21	7.1-9.8	11-28		
WIPP-25	09/80	UNC	Mag	11900		2.5			1.5	0.20	12	33		
WIPP-27	09/80	UNC	Mag	145700		28			2.3	0.34	59	30		
WIPP-25	07/80	UNC	R/S	334400		51			41	1.6	11	4.0		
WIPP-26	07/80	UNC	R/S	188400		19			32	1.2	27	6.2		
WIPP-28	07/80	UNC	R/S	277100		29			46	1.8	12	7.8		
WIPP-29	07/80	UNC	R/S	111000		12			20	1.3	21	15		
WIPP-30	07/80	UNC	R/S	325900		78			82	0.72	18	5.5		
Ranch	06/86	UNC	DL	2520		2.3	0.82	0.13	0.10	0.12	5.9	52	0.024	<0.01
Ranch	06/86	rng	DL			2.3	0.8-1.0	[1]	0.10-0.19	[1]	3.2-5.9	52-86		

Table 2-2. Concentrations of Solutes[1] in Groundwaters from the Rustler Formation, Dewey Lake Red Beds, and Bell Canyon Formation
Part B: Minor and Trace Solutes, TDS, and Ionic Strength (Continued)

Well(s)	Date[2]	Lab[3]	Zone[4]	TDS[7] (mg/L)	IS[6] (molal)	Br^- (mg/L)	F^- (mg/L)	I^- (mg/L)	B (mg/L)	Li (mg/L)	Sr (mg/L)	Silica as SiO_2 (mg/L)[2]	Fe (mg/L)	Mn (mg/L)
Twin-Pasture	01/86	UNC	DL	401		0.17	0.58	<0.01	0.13	<0.05	1.1	47	<0.01	<0.01
Twin-Pasture	01/86	rng	DL			[1]	0.5-1.4	[1]	0.13-0.16	[1]	0.6-1.1	47-90		
DOE-2	07/85	UNC	BC	149500		250	1.1	6.4	54	5.8	150	2.5	11	28
DOE-2	07/85	rng	BC			[1]	0.4-1.4	6.4-7.9	54-61	2.8-5.8	150-300	2-30		

1. Solute values from various laboratories have been rounded as follows.
   - Na, K, Ca, Mg, Cl^-, SO_4^{2-} from UNC : 3 significant figures
   - all other solutes from UNC, all "avg" values, all alkalinity values : 2 sig. figs.
   - all minimum "rng" values : down to 2 sig. figs.
   - all maximum "rng" values : up to 2 sig. figs.
   - all TDS : to nearest 100 mg/L or to 3 sig. figs. (for TDS<10000)
   - all pH values : to 0.1 pH unit
   - all pCO_2 values : to 0.01 unit
   - all ionic-strength values : to 0.01 molal

2. The date on which samples were collected. In the "date" column, a number in square brackets indicates that values in the same row are averages or ranges of data for samples collected on that number of dates.

3. avg: average of one or more values from one or more laboratories. These values were used to calculate element ratios and generate contour plots. Values are shown in *italics*.
   rng: range of values from one or more laboratories. The values give crude estimates of the uncertainties associated with the data. A single value means that all values were identical. A "[1]" means that only one reliable value was available (and is listed in the UNC row).

Table 2-2. Concentrations of Solutes[1] in Groundwaters from the Rustler Formation, Dewey Lake Red Beds, and Bell Canyon Formation
Part B: Minor and Trace Solutes, TDS, and Ionic Strength (Continued)

UNC: UNC Geotech (formerly, Bendix Field Engineering Corp.), Grand Junction, CO. These data were used in calculations of saturation indices, in factor-analysis calculations, and to generate Piper diagrams. Values are emboldened.

4. The stratigraphic zone and, within the Culebra, the hydrochemical facies (as defined in this work).
   CuA, CuB, CuC, CuD: Culebra dolomite, hydrochemical facies -- Zone A, Zone B, Zone C, Zone D, respectively.
   Mag: Magenta Dolomite
   R/S: Rustler/Salado contact zone
   DL : Dewey Lake Red Beds
   BC : Bell Canyon Formation

5. Alkalinity values and pH values were measured in the field when the samples were collected. (Exception: alkalinity in the DOE-2 Bell Canyon sample was measured in the laboratory.)

6. pCO_2 and ionic strength (IS) were calculated using PHRQPITZ. See the text for details.

7. Concentration of TDS, calculated by summing the concentrations of major solutes.

When available, samples from the WQSP were used in this study. Many of the WQSP samples have been analyzed by up to three different laboratories, and the results are amenable to interlaboratory comparisons. In general, most of the major, minor, and trace solute data from UNC Geotech are considered reliable and are used as reference values. Similarly, most of the data from the NMBM&MR are acceptable. Some of the ITAS data from Round 1 of the WQSP are suspect, based on poor charge balance and lack of agreement with the other laboratories. However, the ITAS data from Rounds 2 and 3 of the WQSP seem to be generally acceptable. Some of the USGS (Central Labs) data, especially some potassium analyses, are also suspect.

The evaluation of minor and trace solute data is preliminary, and the values are not considered as reliable as those for the major elements. For some minor and trace solutes, none of the available data is considered reliable at this time. For example, as discussed above, iron concentrations may be controlled by pipe corrosion; other minor or trace elements that may adsorb onto colloids, such as manganese, are also suspect. Although the silica data are considered in some detail in this work, the silica concentrations may be affected by precipitation of a colloidal Fe-Si floc after sample collection.

Table 2-3 identifies wells in which concentrations of major solutes in Culebra groundwaters have changed during the sampling period (1976 to 1987) and wells from which the samples are otherwise suspect. Changes in the Culebra-water composition at WIPP-29 appear to be related to contamination from nearby potash-refining operations. The causes for the changes in the water chemistry at the other wells are not understood at this time.

2.2.3.2 Alkalinity, pH, and pCO_2

There are several potential sources of error associated with characterization of the carbonate systems of these waters. These sources include loss of CO_2 gas during sample collection, inaccurate pH measurements due to the high ionic strengths of the brines, and inaccuracies in the alkalinity measurements.

Table 2-3. Wells in Which Culebra Groundwater Compositions Have Changed with Time or for Which Compositions Are Otherwise Suspect

Hydropad or Well	Remarks
DOE-2	Alkalinity was 67 mg/L HCO_3^- in 3/85 (WQSP round 1) and was 150 mg/L HCO_3^- in 8/86 (WQSP round 2). The increase occurred because the hole was acidized in 1985 (Saulnier et al., 1987).
H-2	Na and Cl are changing with time, although the other major solutes have remained fairly constant. Field chloride values did not reach steady-state during round 1 of the WQSP, and the chloride value measured during round 2 was lower yet. This change in NaCl is not understood at this time. The representativeness of all samples from the Culebra at H-2 is questioned.
H-5	The alkalinity at H-5B was 80 mg/L HCO_3^- in 6/81 and at H-5C was 86 mg/L in 10/81. In 8/85 (WQSP round 1), the alkalinity at H-5B had decreased to 50 mg/L and it remained the same in 5/86 (WQSP round 2). The decrease is thought to be due to the purging of contaminants.
WIPP-25	Between 8/80 (Sandia sampling program) and 2/86 (WQSP round 1) the concentrations of several solutes, notably Ca and Cl (and to a lesser extent Na and Mg), increased significantly. Between 2/86 (WQSP round 1) and 4/87 (WQSP round 2), these concentrations did not change. Also, between 8/80 and 2/86 the alkalinity decreased from 210 to 130 mg/L HCO_3^-; it remained at 130 mg/L in 4/87. The change in major solutes is not understood at this time. The decrease in alkalinity is probably due to the purging of contaminants.

Table 2-3. Wells in Which Culebra Groundwater Compositions Have Changed with Time or for Which Compositions Are Otherwise Suspect (Continued)

Hydropad or Well	Remarks
WIPP-26	Between 8/80 (Sandia sampling program) and 11/85 (WQSP round 1), the concentrations of several solutes, notably Na, K, and Cl (and to a lesser extent Ca and Mg), increased significantly. Between 11/85 (WQSP round 1) and 4/87 (WQSP round 2), the values of the solutes decreased to concentrations similar to or lower than those observed in 1980. Also, between 8/80 and 11/85 the alkalinity decreased slightly from 140 to 120 mg/L HCO_3^-; it was 110 mg/L in 4/87 (not significantly different from the 11/85 value). The changes in major solutes are not understood at this time. The slight decrease in alkalinity may be due to the purging of contaminants.
WIPP-27	Although WIPP-27 was sampled only in 1980 (by both the USGS and Sandia), the solute relationships indicate that potash-mining activities have affected the groundwater quality at this location. Thus, there is no reason to believe that the 1980 samples are representative of unperturbed native groundwater at this location.
WIPP-28	WIPP-28 was sampled in 9/80 by Sandia. Although the samples are considered representative with respect to most solutes, the alkalinity value measured in the field is <u>not</u> considered representative. During a four-day pumping test, the alkalinity values decreased slowly but steadily; alkalinity had <u>not</u> reached a steady-state value when final samples were collected and the test was terminated. Therefore, the final alkalinity value of 350 mg/L HCO_3^- is considered an upper limit.

Table 2-3. Wells in Which Culebra Groundwater Compositions Have Changed with Time or for Which Compositions Are Otherwise Suspect (Continued)

Hydropad or Well	Remarks
WIPP-29	Between 8/80 (Sandia sampling program) and 12/85 (WQSP round 1), the concentrations of several solutes, notably Na, K, Cl, and SO_4, increased and the concentration of Ca decreased significantly. Between 12/85 (WQSP round 1) and 3/87 (WQSP round 2), the values of the solutes changed again. Also, between 8/80 and 12/85 the alkalinity decreased from 210 to 160 mg/L HCO_3^-; it remained at 160 mg/L in 3/87. The changes in major solutes are attributed to potash-refining activities in the area. The decrease in alkalinity is probably due to the purging of contaminants.

Loss of CO_2 Gas

Effervescence of the water samples during collection has been commonly observed and recorded in field notes from various water sampling programs listed in Table 2-1. The effervescence may be due to the loss of CO_2 gas in response to changes in the confining pressure and temperature experienced by the water sample during collection, or it may be due to the release of air introduced into the sample during pumping. If the former process is responsible, then the field pH measurements and calculated pCO_2 values may be in error, as discussed in Section 2.3.4.4. Unfortunately, because the presence or absence of effervescence was not always recorded in the field notes, no assessment of the ubiquitousness or importance of this effect can be made at this time.

Inaccurate pH Measurements

The accuracy and precision of pH measurements, independent of the effect of CO_2 loss, cannot be assessed at this time because there are insufficient data. The pH is a measure of the activity of a single ion, H^+; individual pH values only have meaning in a relative sense with reference to a particular activity scale. Problems associated with the interpretation of pH in saline waters have been summarized by workers interested in the measurement of pH in seawater (Plummer and Sundquist, 1982; Plummer et al., 1988; Bates, 1975; Bates and Culberson, 1977). Potential sources of error include liquid junction potential effects and inconsistencies among the activity scales of the buffer solutions, measured pH, and aqueous chemical speciation model.

Inaccurate Alkalinity Measurements

For the groundwaters discussed in this chapter, alkalinity (the ability of a solution to neutralize a standard acid) is assumed to be due only to bicarbonate and carbonate. The low concentrations of boron, silica, and organic carbon in these waters (cf. Table 2-2; Myers et al., Chapter 6) suggest that errors due to the contribution of noncarbonate species to the total alkalinity are probably not appreciable in these waters. However, this assumption is not correct for all waters of interest to the WIPP Project, such as certain intergranular fluids in the Salado Formation or some brines from the Castile Formation.

Although the accuracy cannot be estimated, the precision of the (bi)carbonate alkalinity determinations is probably plus or minus several mg/L HCO_3^- at the 95% confidence level. The loss of CO_2 will not affect the alkalinity appreciably. Field measurements of alkalinity are generally made within several minutes of sample collection and are used as reference values. Results of alkalinity measurements made in laboratories are very close to field values, suggesting little change over periods of weeks to months.

The Culebra groundwater in several wells, however, may have been contaminated with modern organic carbon during the drilling process (cf. Lambert, Chapter 5). These organics were apparently metabolized by bacteria, leading to high alkalinities. For example, the samples from H-5 collected in 1981 were contaminated with modern carbon (Lambert, 1987); by 1985, the alkalinity had dropped by a factor of two. At WIPP-25, the alkalinity was 170 mg/L HCO_3^- in 1980 and dropped to 110 mg/L HCO_3^- by 1986. Thus, even if a measurement is accurate, it may represent a transient value due to recent contamination. If carbon-isotope data are not available, or if the available carbon-isotope data cannot be used to conclusively identify contamination, multiple sets of serial samples must be collected over several years to determine if transient effects are present.

The accuracy of measurements of parameters in the carbonate system is of particular concern for a nuclear-waste repository associated with a dolomite aquifer. Values for the pH, carbonate alkalinity, and pCO_2 are used in calculations of saturation indices of dolomite ($CaMg(CO_3)_2$) and calcite ($CaCO_3$) and in calculations of the speciation of actinides such as americium, neptunium, and plutonium for which carbonate complexation may be important (Bidoglio et al., 1985; Bidoglio et al., 1987; Tien et al., 1985). For this reason, the significance of the uncertainties in the pH measurements is discussed in Section 2.3.4.4.

2.3 SOLUTE RELATIONSHIPS IN WATERS IN THE RUSTLER FORMATION AND RELATED ROCKS

2.3.1 Spatial Distributions of Solutes in Culebra Groundwaters

2.3.1.1 Introduction

The spatial distributions of selected elements and elemental ratios in Culebra groundwaters have been examined to understand the geochemical and hydrologic processes occurring within the unit. Average concentrations for 13 solutes and element ratios for several pairs of solutes in water samples from the Culebra in 21 wells were calculated as

described below. The spatial distributions of eight solutes and four element ratios were contoured.

The sets of data examined were described in Section 2.2. The solutes considered were calcium, magnesium, sodium, potassium, chloride, sulfate, bromide, fluoride, iodide, boron, lithium, strontium, and silica. Samples from Well H-2A were excluded from consideration because the representativeness of those samples is questioned (see Table 2-3). Other samples of questionable quality (for example, from WIPP-25 and WIPP-26) were included because changes at those wells have been less drastic.

The average values given in Table 2-2 were calculated using the laboratory (UNC, ITAS, NMBM&MR, and USGS) and field data that the authors considered reliable at the time these spatial-distribution studies were being completed (late 1987). Because more recent WQSP data may indicate that some values rejected as outliers are, in fact, reasonable (within acceptable analytical variation), or that some values that appeared reasonable are, in fact, in error, these average values should not be viewed as "recommended" or even "best available" values. Because the silica results from the UNC and ITAS laboratories differed widely, average concentrations for silica were not calculated; rather, the ITAS data were used for the contouring study. Element ratios for several solute pairs--Na/Cl, K/Na, Mg/Ca, and Cl/Br--were calculated using the average values from Table 2-2.

The spatial distributions of the elements and element ratios were contoured on base maps of the WIPP area using the SURFER software package developed by Golden Software, Inc. The contours are produced in a two-stage process. First, a regularly spaced grid is created from the irregularly spaced input data. Then, the file containing the regularly spaced interpolated values is used as input to the contouring routine. Adjustable parameters include grid size, radius of influence, method of interpolation, smoothing factor, and contour interval. The plots presented below employ a kriging technique to generate the regularly spaced grid (Golden Software, Inc., 1987).

Twenty-one wells were part of this investigation. Data from WIPP-29 and in some cases WIPP-27 were not included in contours drawn in Figures 2-2 through 2-12. Figures 2-13 through 2-16 include the data from WIPP-27 and WIPP-29 and are drawn on a coarser contour interval. In Figures 2-2 to 2-16, the concentration (or ratio) at each well is also given; the concentrations are the "average" values given in Table 2-2. The location of the four-mile zone is indicated for reference. Because the location of each contour is influenced by several data points, there may be discrepancies between the placement of contour lines and the concentrations at some well locations. Descriptions of the spatial distributions of the major solutes, Na/Cl ratios, Cl/Br ratios, silica concentrations, the apparent anomalies at P-14, and the apparent anomalies at WIPP-27 and WIPP-29 are discussed below. Because the concentrations of several solutes (B, Li, F) and the element ratios of several solute pairs (Sr/Ca, several trace-solute/Cl pairs) were either uniform over the site or varied randomly, these solutes and element ratios are not discussed in this section.

2.3.1.2 Major Solutes

Regional variations in the concentrations of major solutes have been plotted in Figures 2-2, 2-3, and 2-4, which show contours of the distributions of Na, K, and Mg, respectively. This pattern is also representative of the distributions of Cl, TDS, and fluid density. The patterns show lower concentrations of these dissolved constituents in the southern and southwestern areas (H-7B, H-8B, H-9B, and Engle) compared to higher concentrations in the northern and eastern parts of the study area. Within the four-mile zone, the concentrations of the solutes decrease from east to west. The distribution of Mg/Ca weight ratios (Figure 2-5) shows a similar pattern; the ratio increases from approximately 0.3 in the south and west to a value of 1.3 in the eastern part of the region.

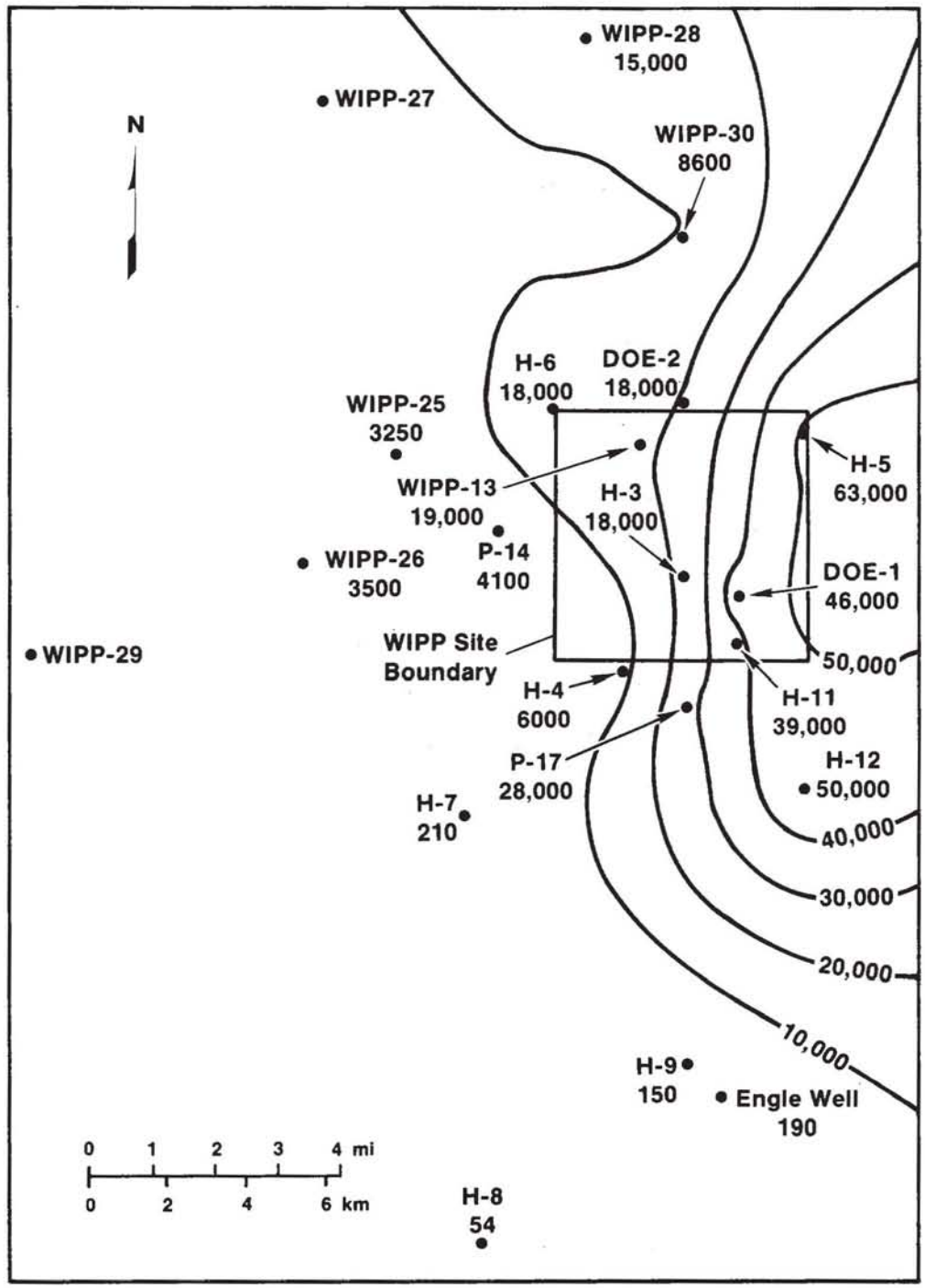

Figure 2-2. Contour plot of sodium concentrations (mg/L) in Culebra groundwaters.

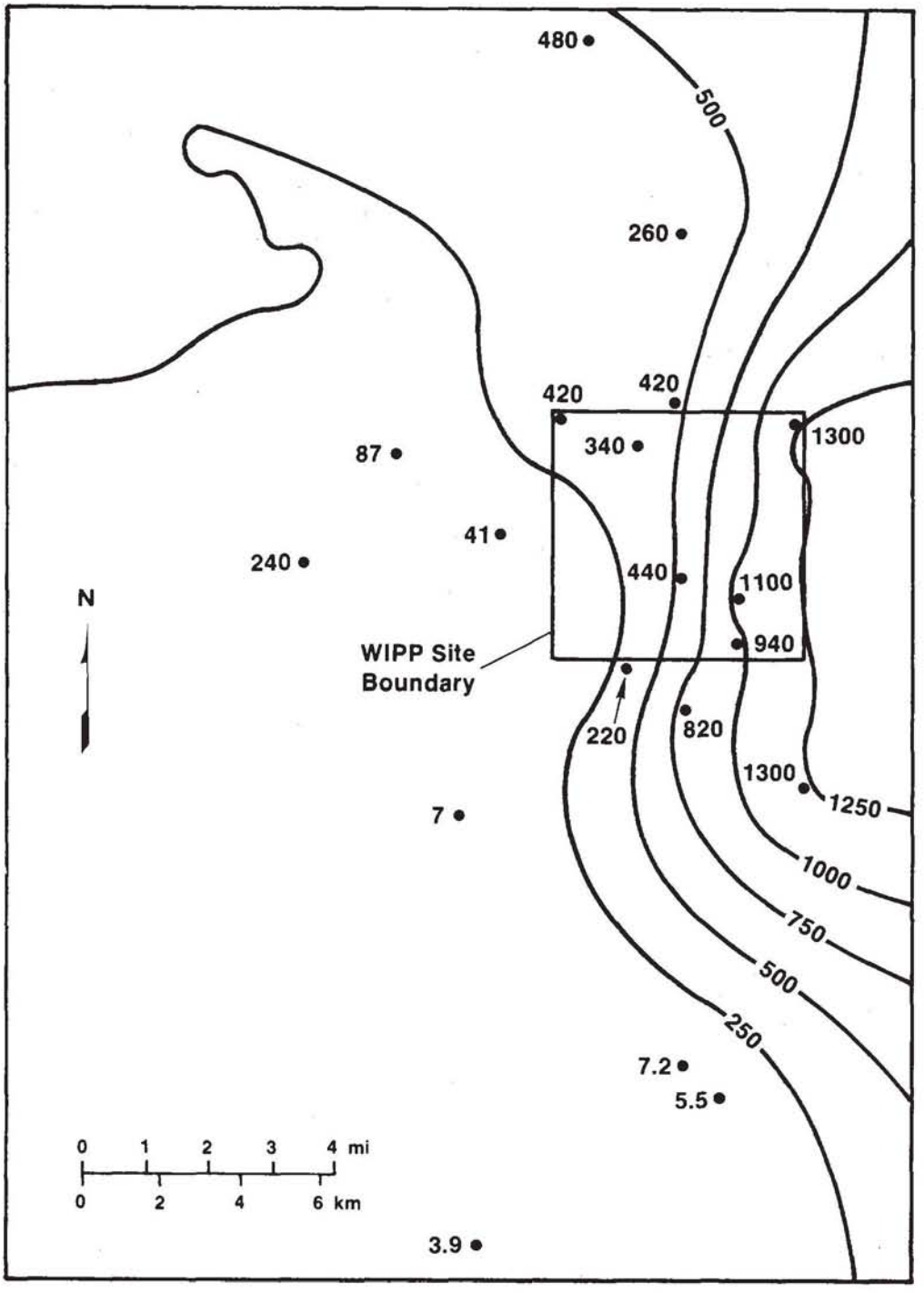

Figure 2-3. Contour plot of potassium concentrations (mg/L) in Culebra groundwaters.

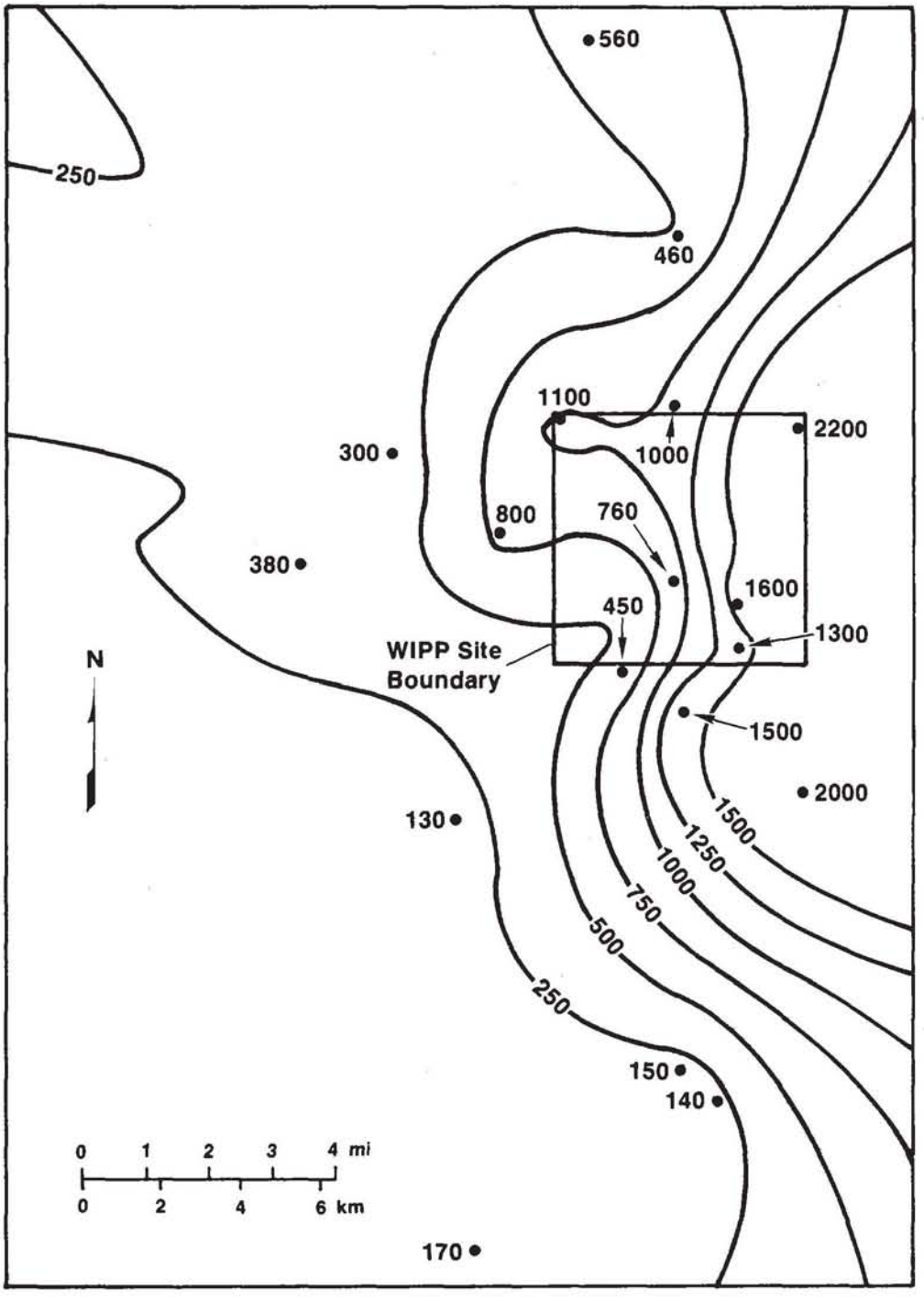

Figure 2-4. Contour plot of magnesium concentrations (mg/L) in Culebra groundwaters.

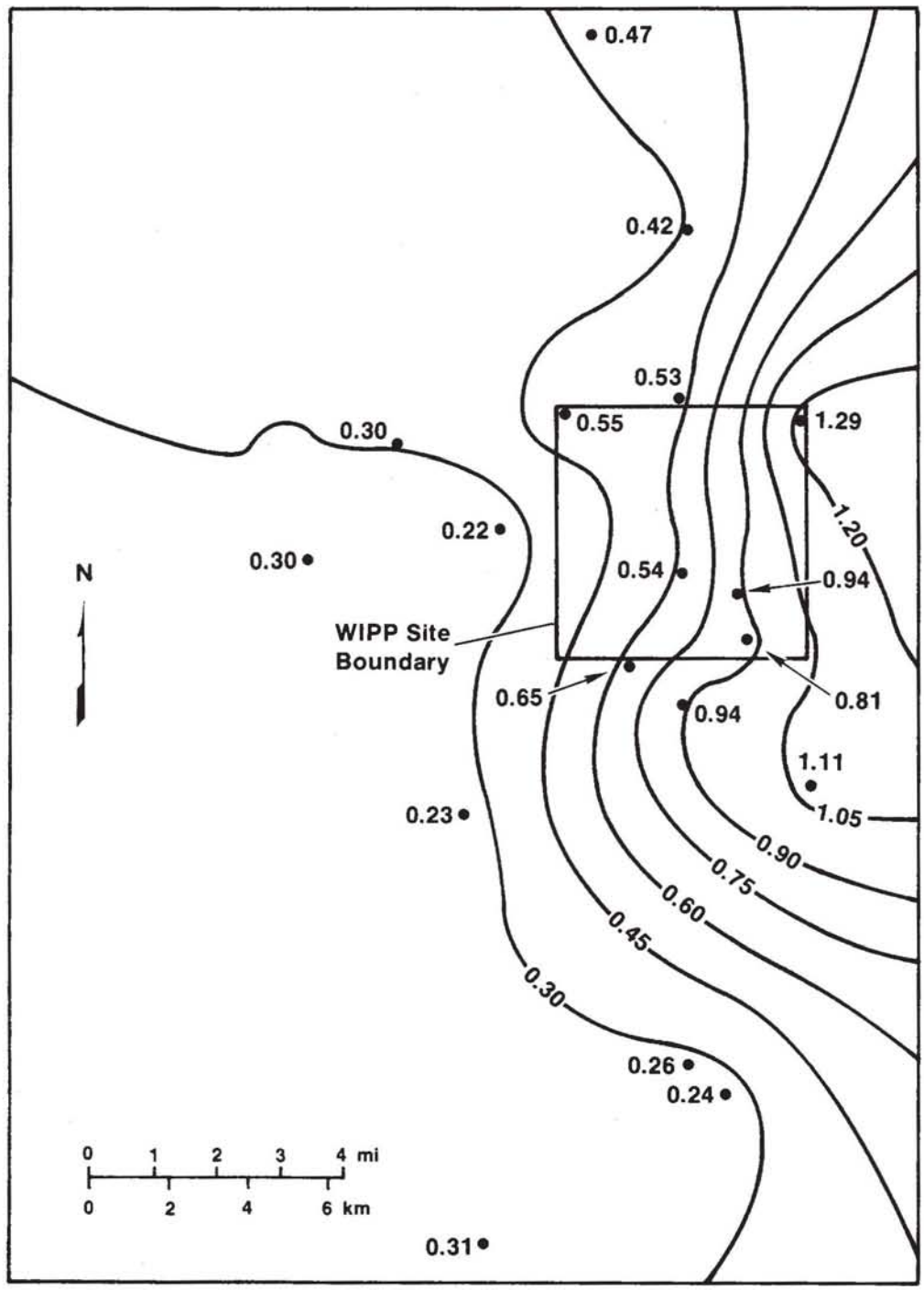

Figure 2-5. Contour plot of Mg/Ca weight ratios ([mg/L]/[mg/L]) in Culebra groundwaters.

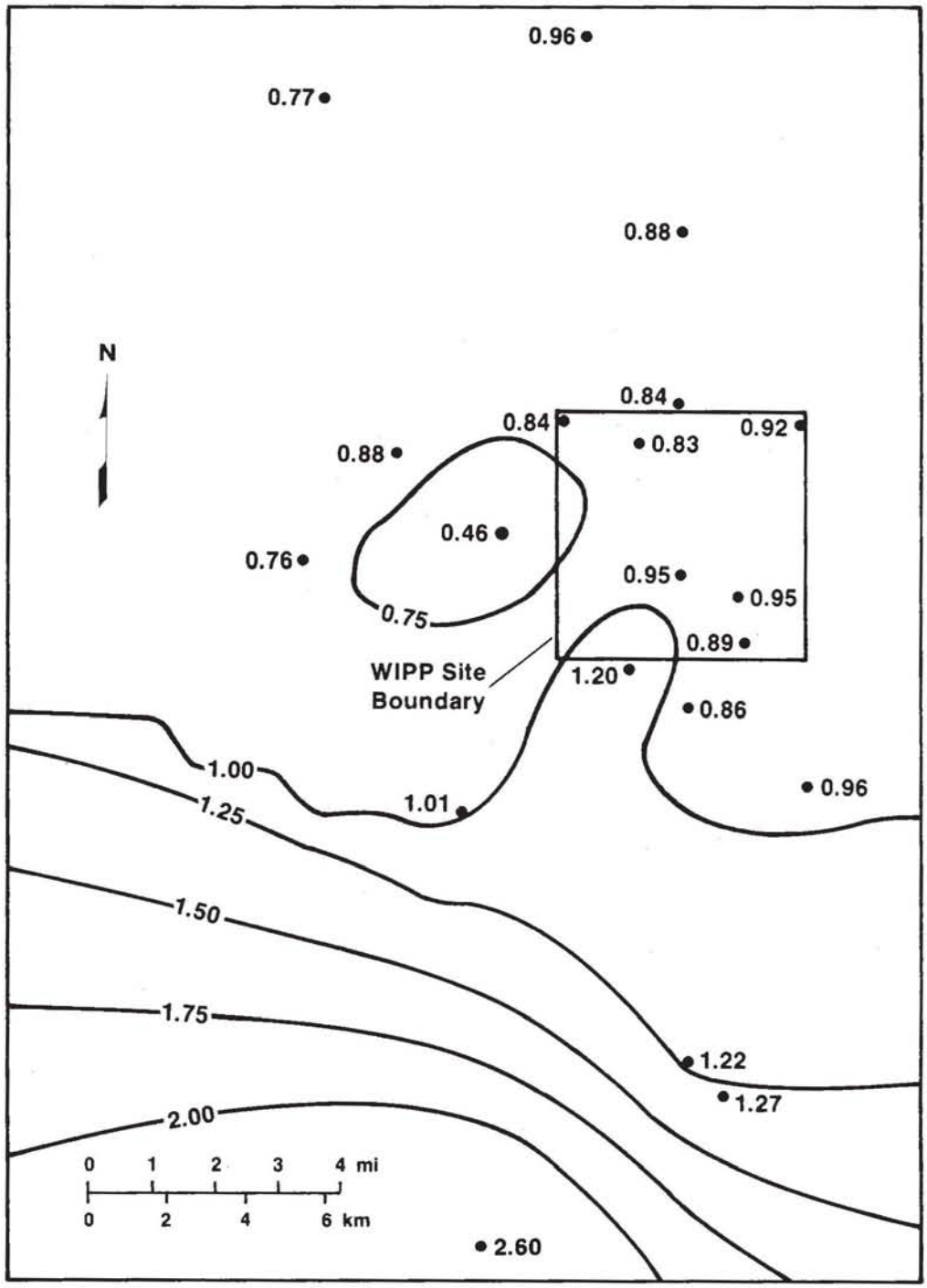

Figure 2-6. Contour plot of Na/Cl molar ratios ([mol/L]/[mol/L]) in Culebra groundwaters.

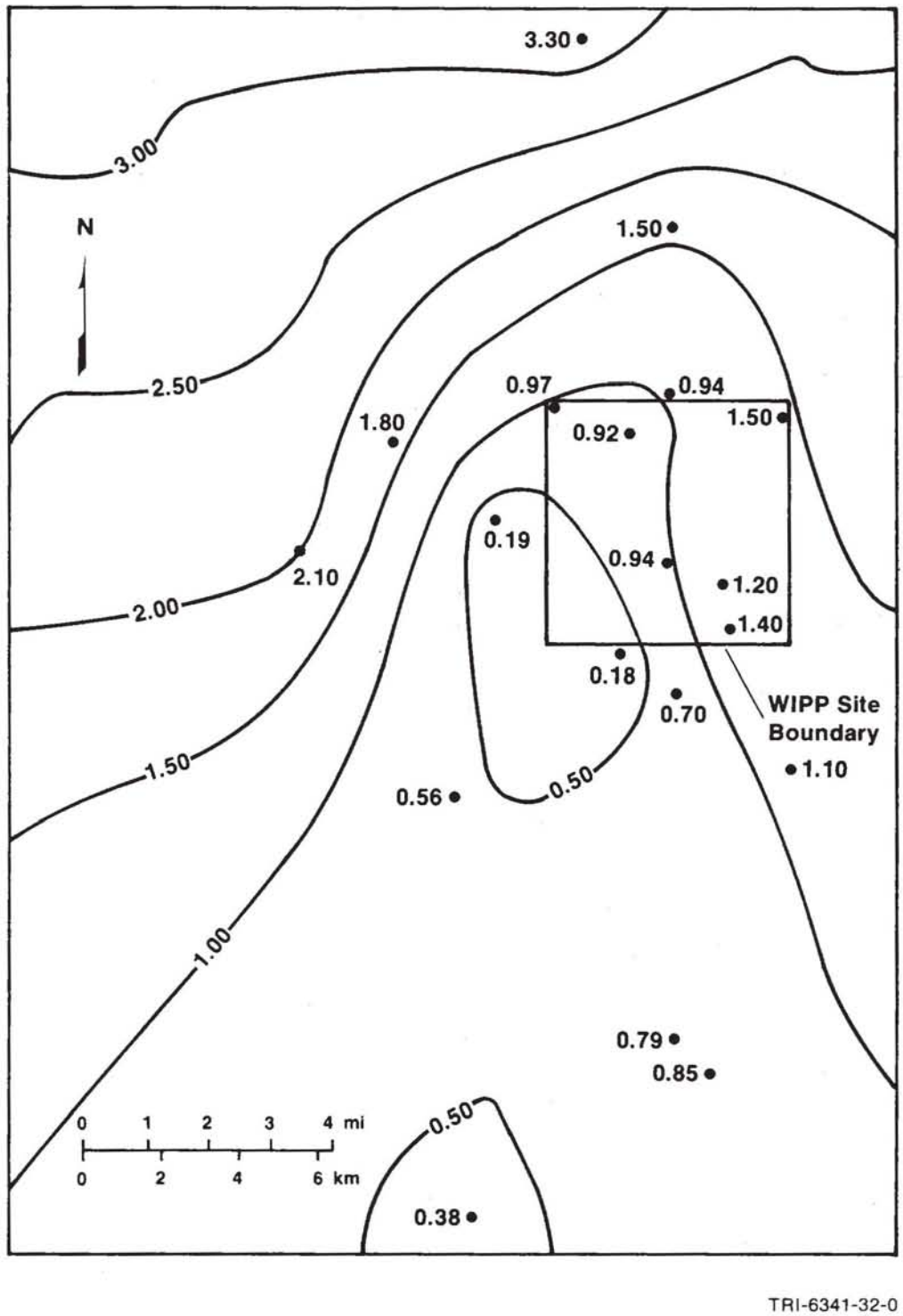

Figure 2-7. Contour plot of Cl/Br weight ratios ([g/L]/[mg/L]) in Culebra groundwaters.

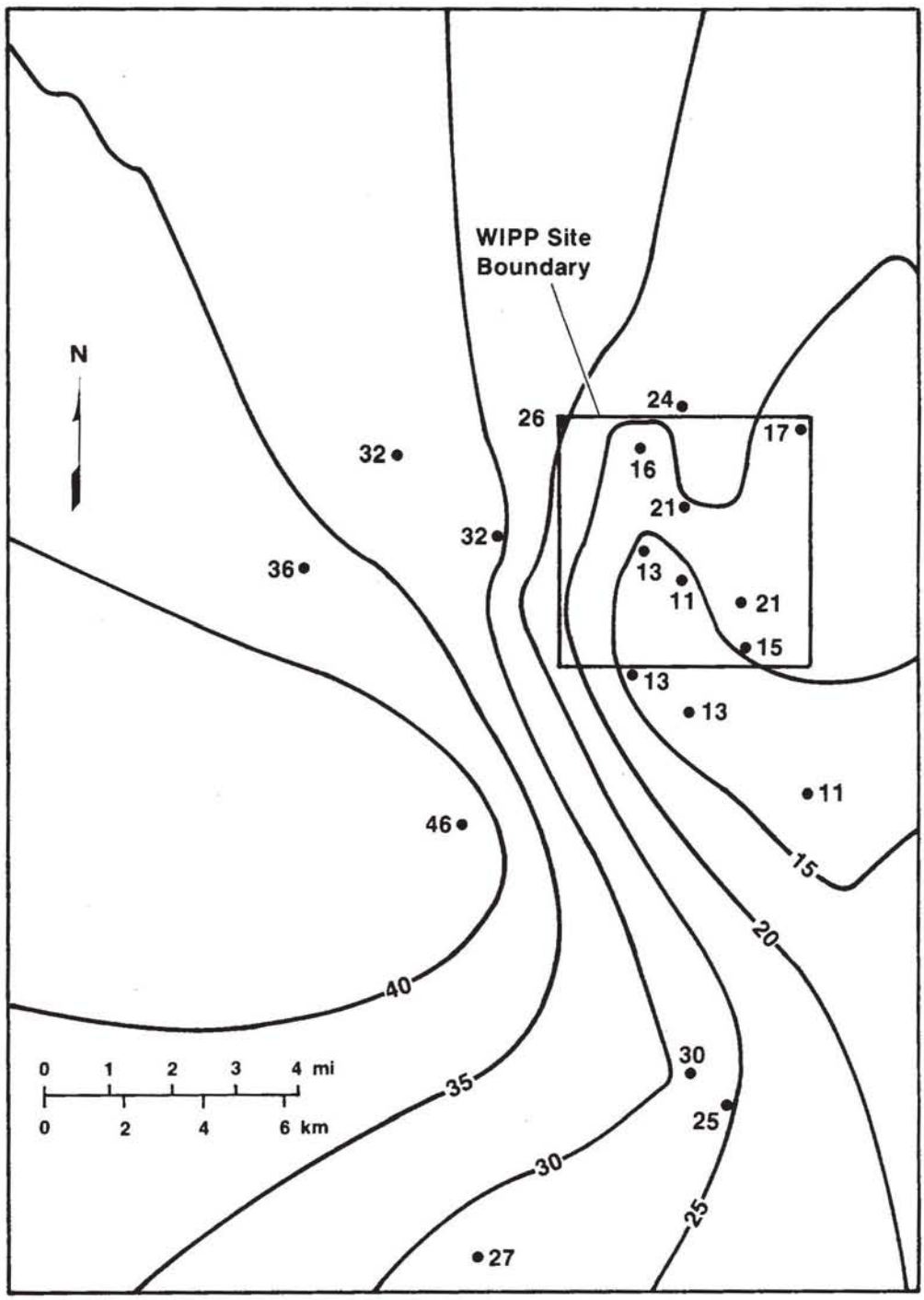

Figure 2-8. Contour plot of silica concentrations (mg/L as SiO_2) in Culebra groundwaters.

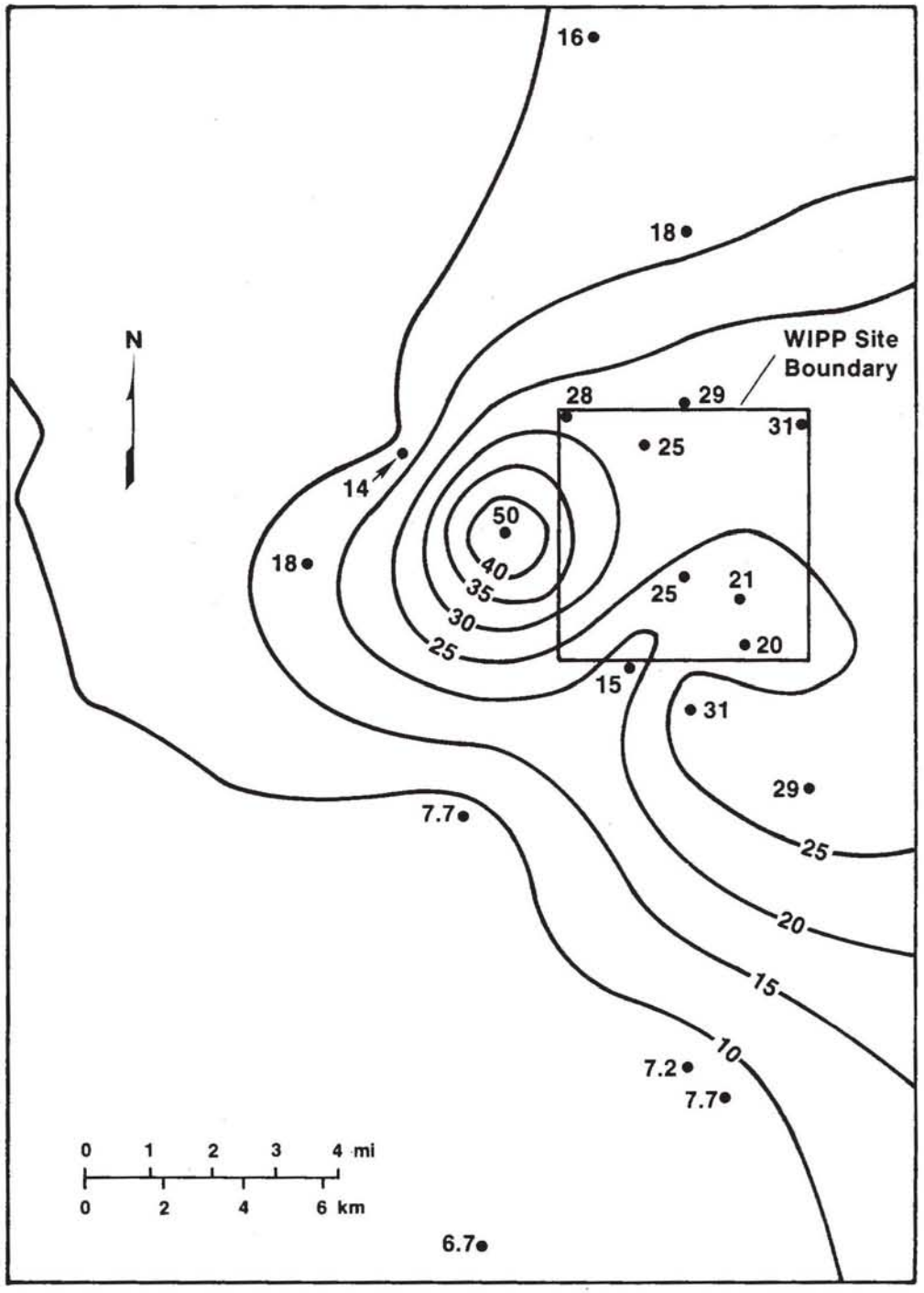

Figure 2-9. Contour plot of strontium concentrations (mg/L) in Culebra groundwaters.

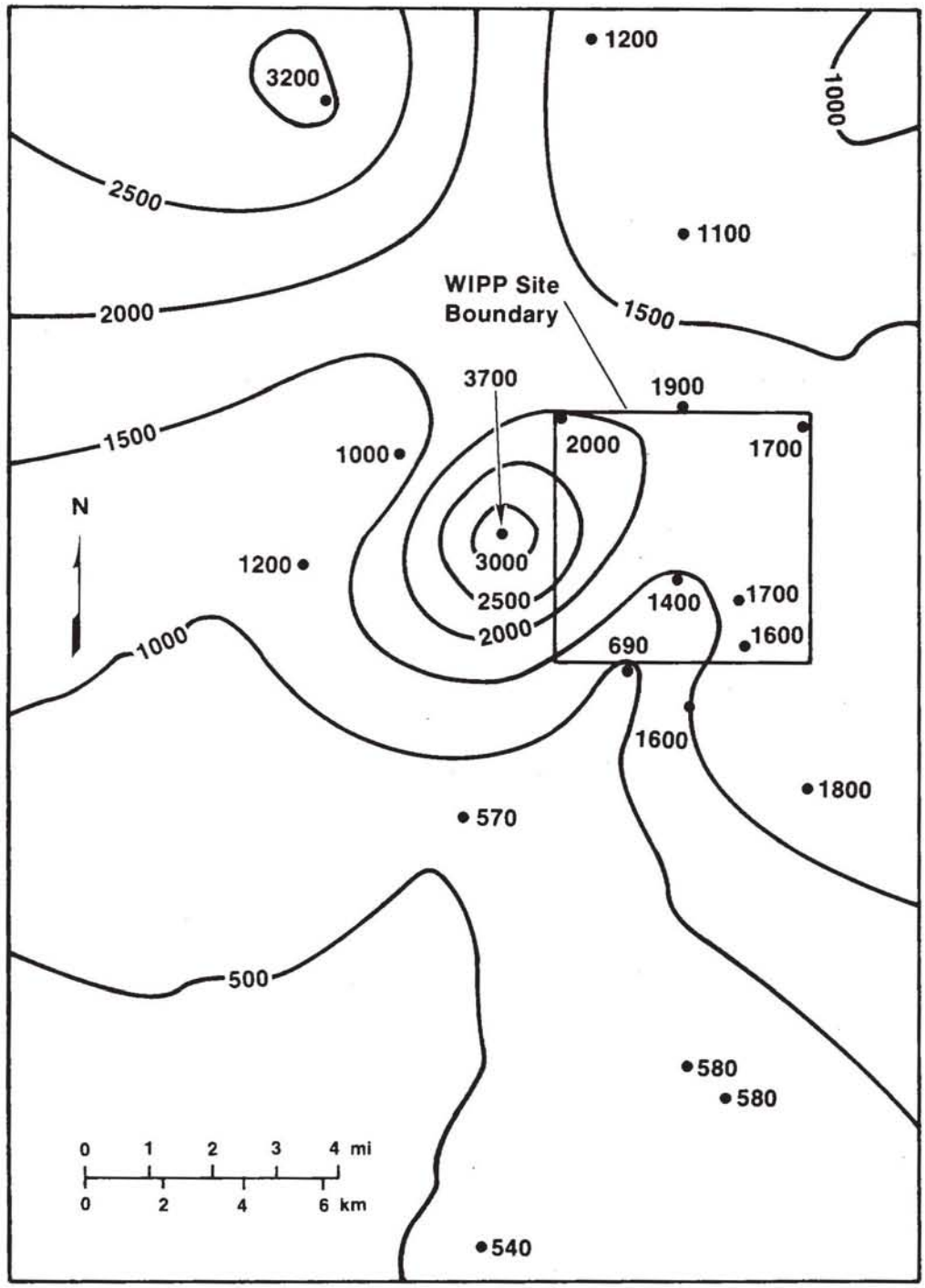

Figure 2-10. Contour plot of calcium concentrations (mg/L) in Culebra groundwaters.

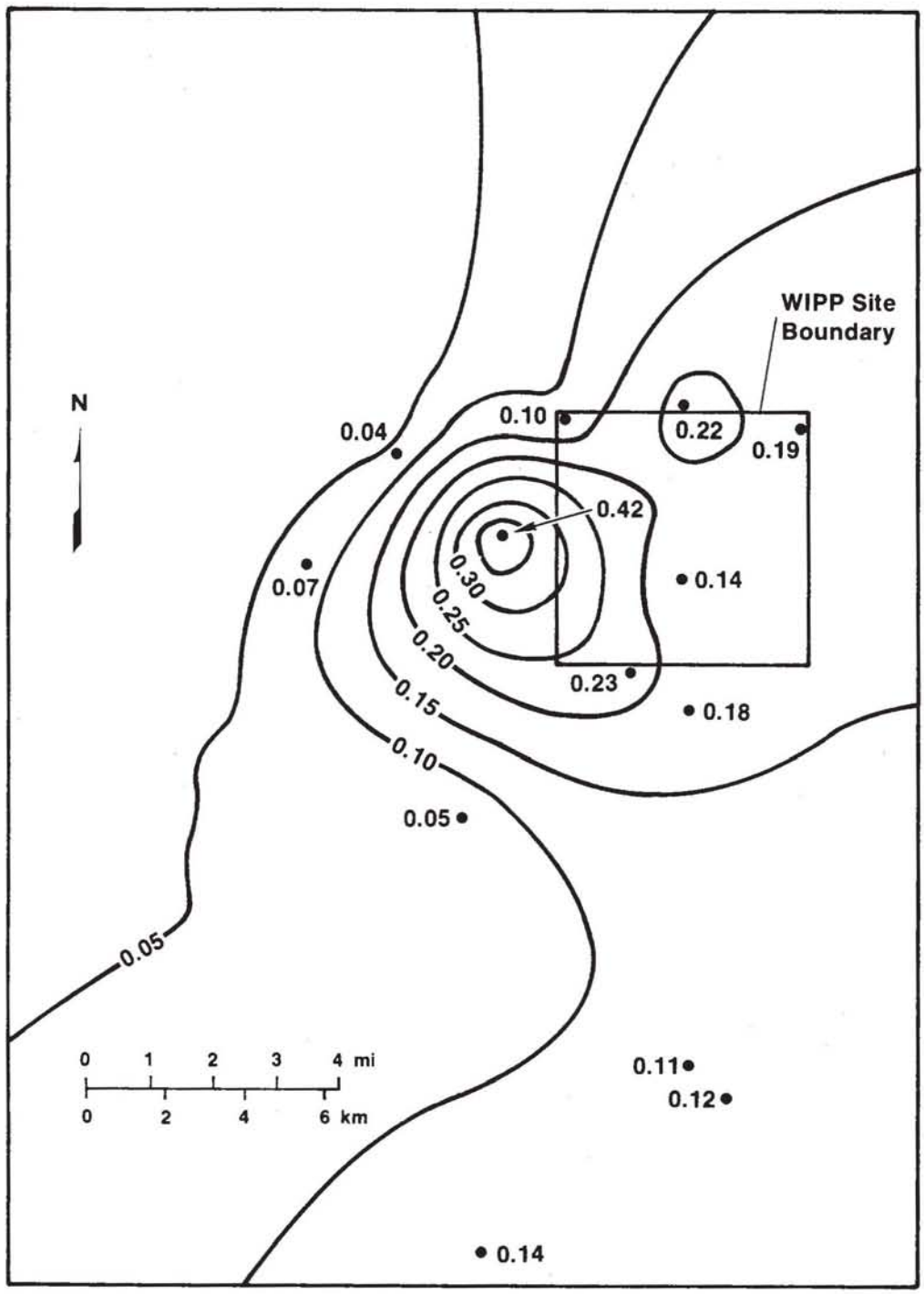

Figure 2-11. Contour plot of iodide concentrations (mg/L) in Culebra groundwaters.

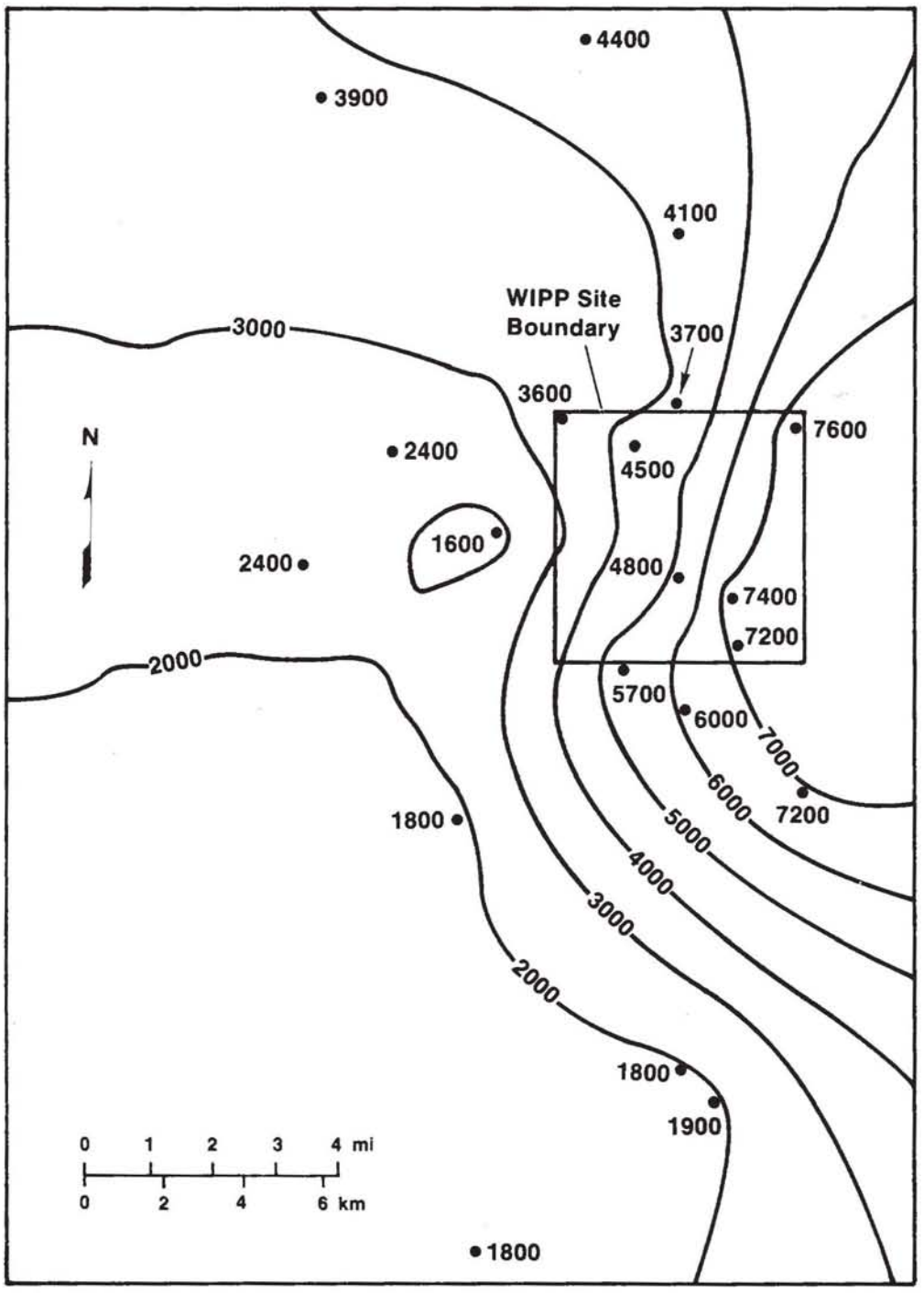

Figure 2-12. Contour plot of sulfate concentrations (mg/L) in Culebra groundwaters.

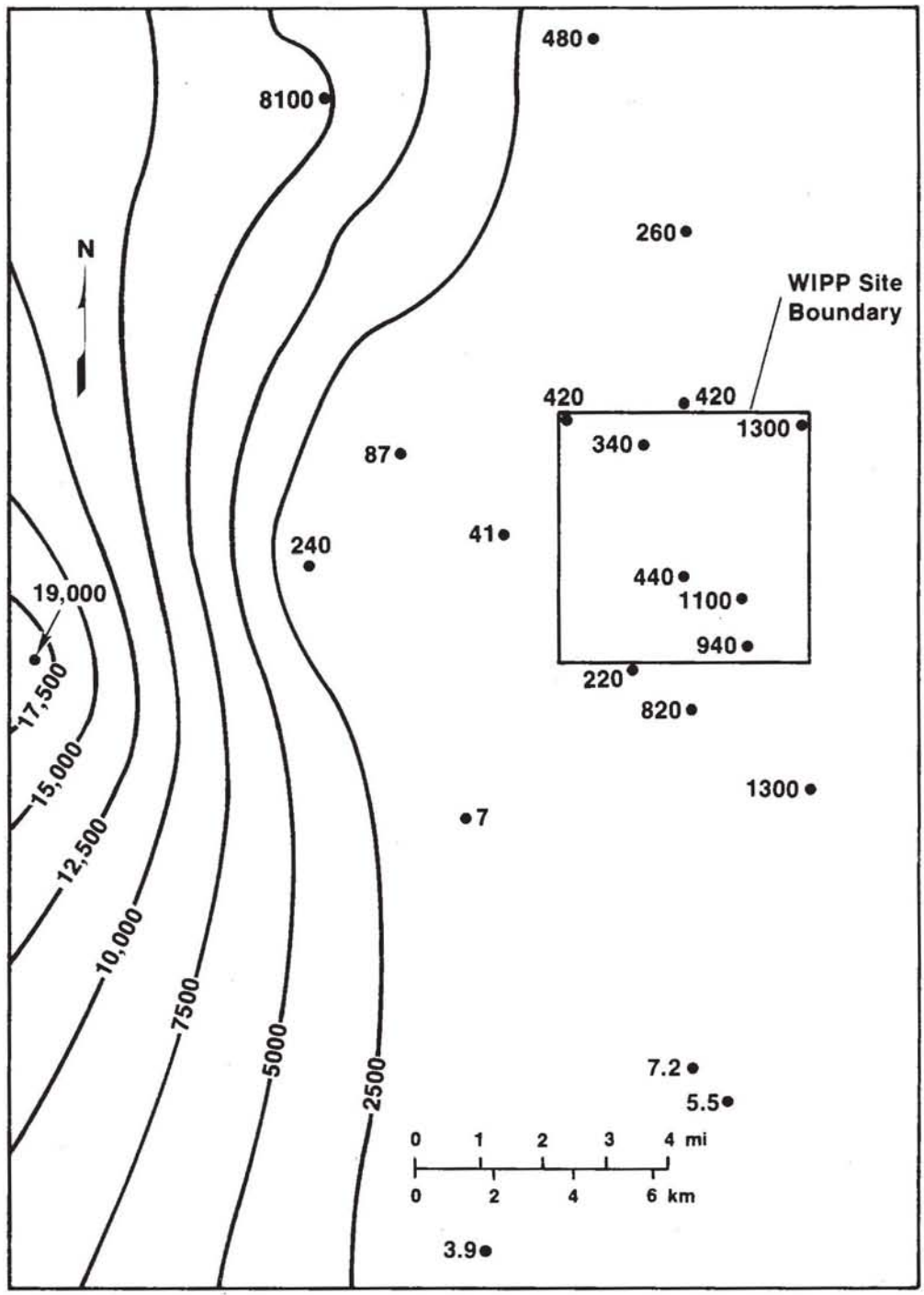

Figure 2-13. Contour plot of potassium concentrations (mg/L) in Culebra groundwaters including samples from WIPP-27 and WIPP-29.

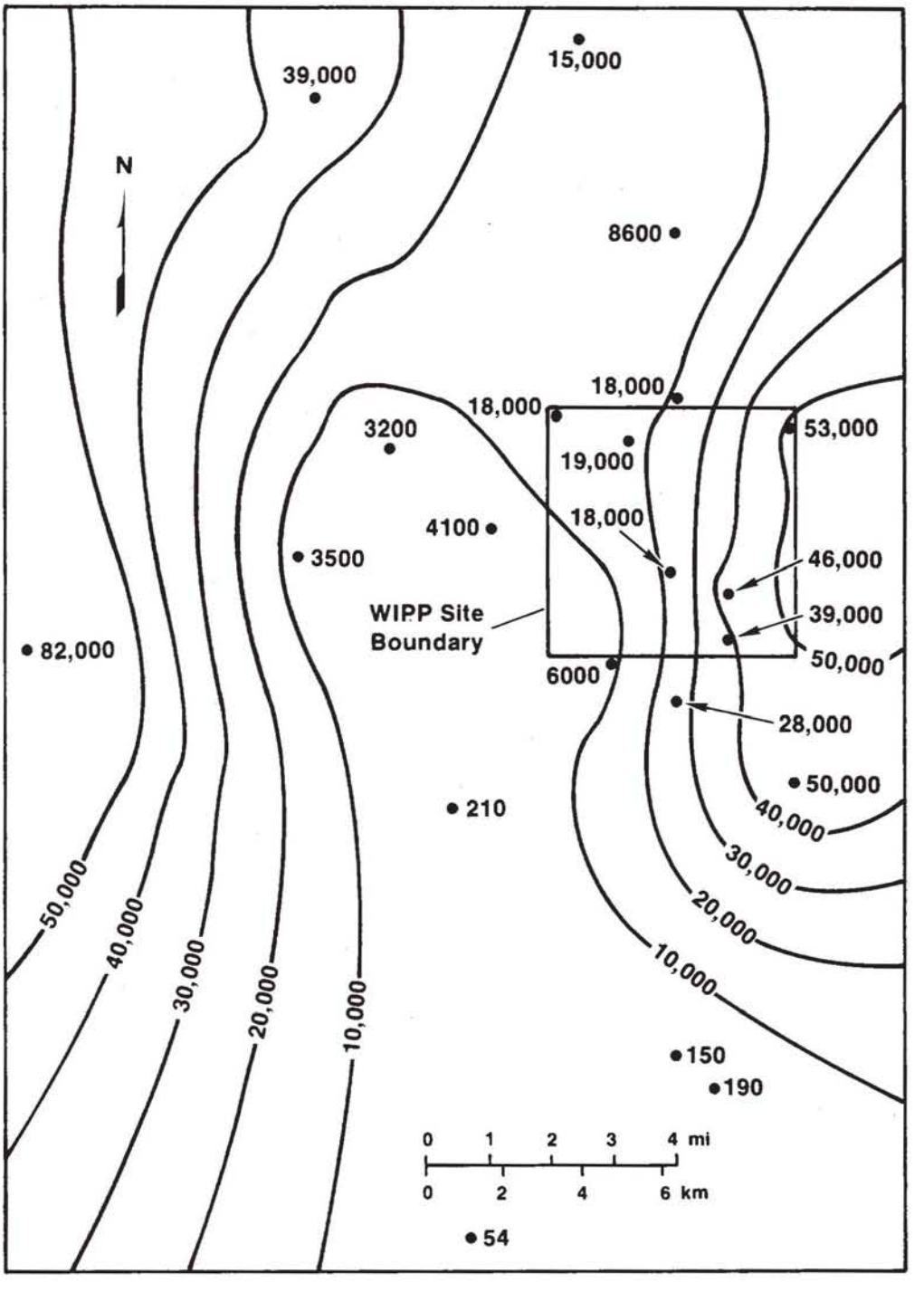

Figure 2-14. Contour plot of sodium concentrations (mg/L) in Culebra groundwaters including samples from WIPP-27 and WIPP-29.

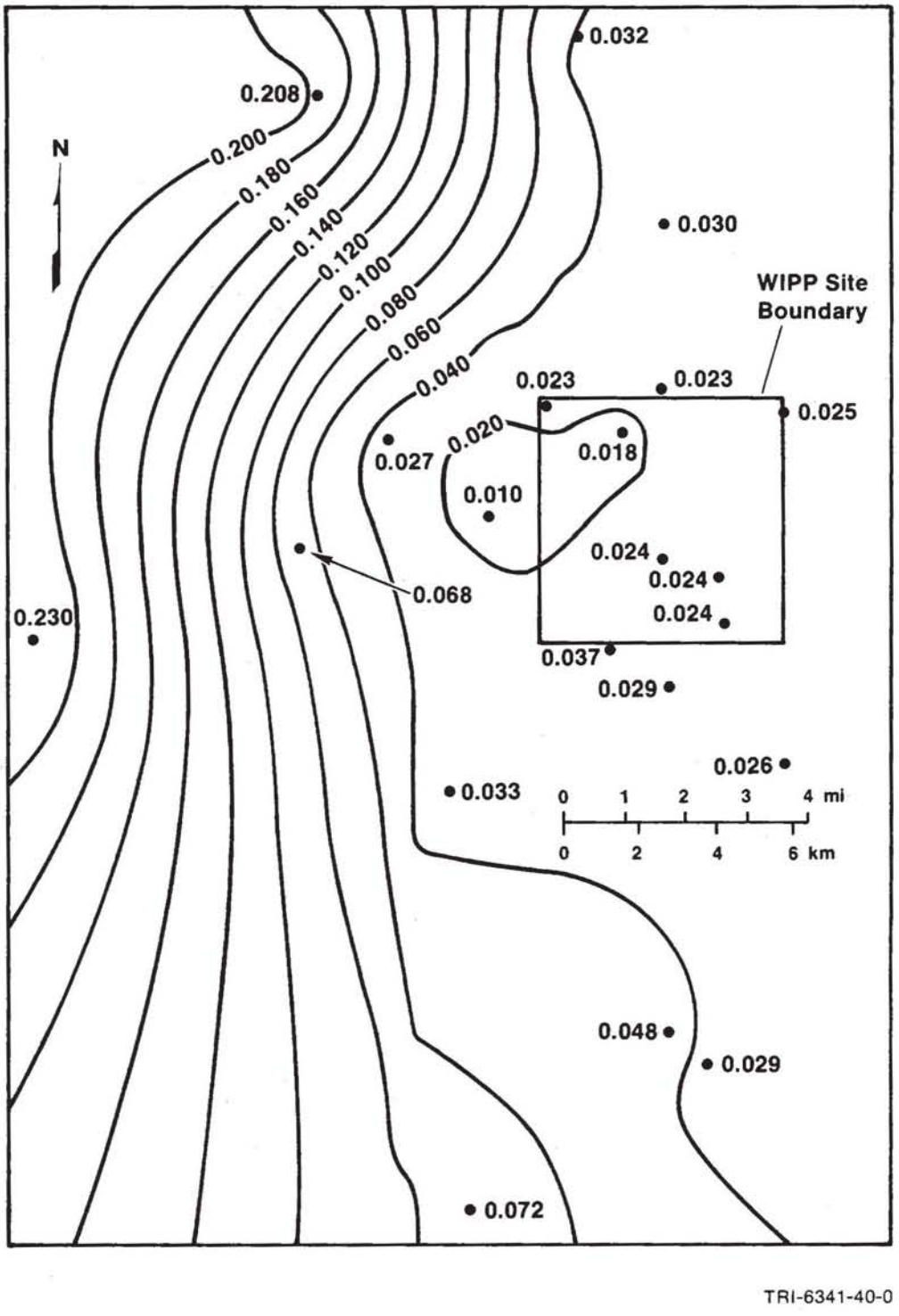

Figure 2-15. Contour plot of K/Na weight ratios ([mg/L]/[mg/L]) in Culebra groundwaters including samples from WIPP-27 and WIPP-29.

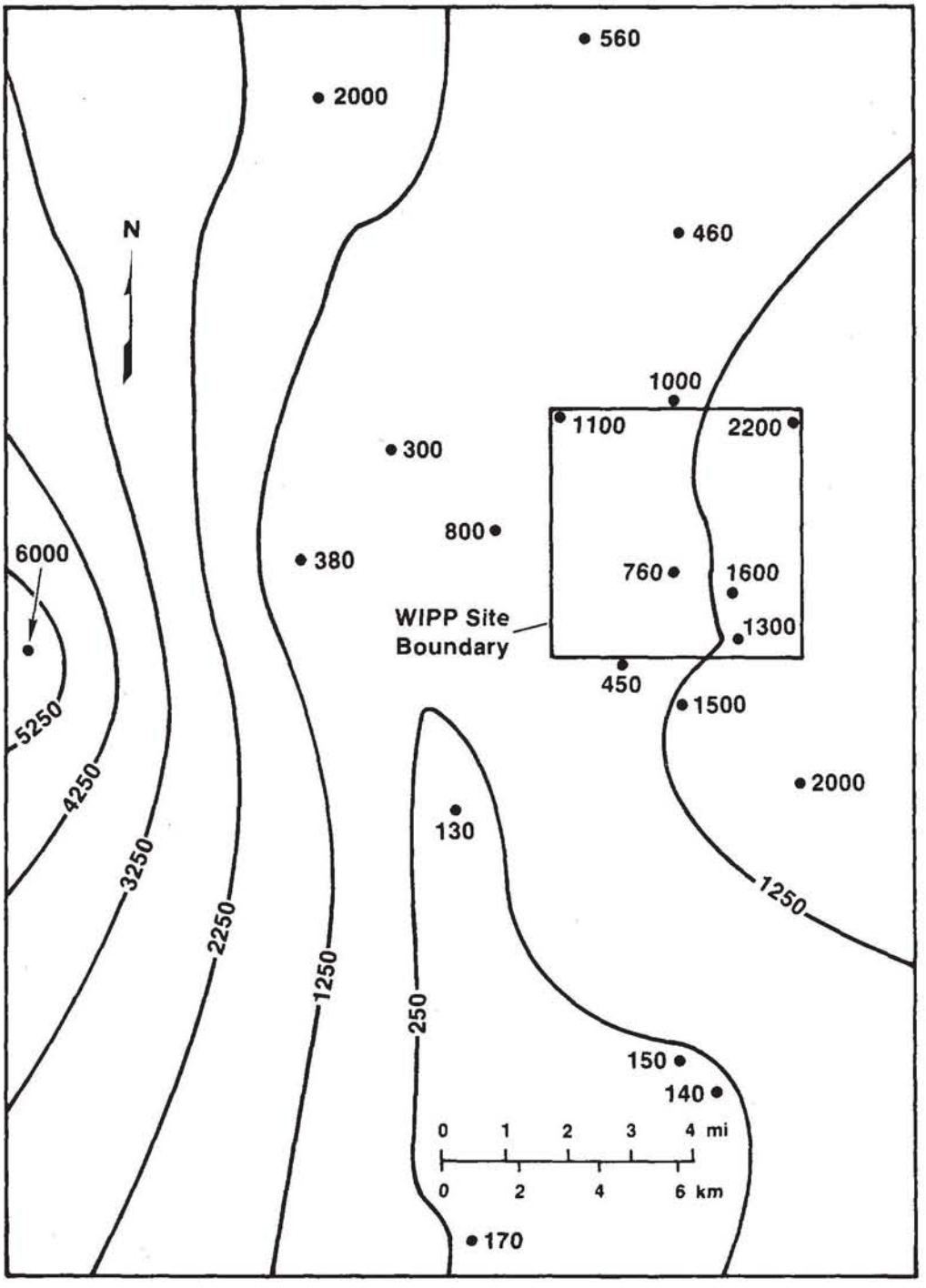

Figure 2-16. Contour plot of magnesium concentrations (mg/L) in Culebra groundwaters including samples from WIPP-27 and WIPP-29.

2.3.1.3 Na/Cl Ratio

The distribution of Na/Cl molar ratios is shown in Figure 2-6. The ratios are very close to unity in the northern and central areas (with the exception of P-14), increase in the south to values of 1.20 and 1.28 at H-9B and Engle, and reach a maximum of 2.56 at H-8B. If dissolution of halite is the main source of the Na and Cl, the Na/Cl molar ratio should be close to 1.0 in solution. The elevated ratios in the southern area indicate a contribution of Na from an additional source, such as the weathering of Na-bearing feldspars or clays. However, the absolute concentrations of Na and Cl are considerably lower in the southern area. Thus, there may also be small contributions of Na from nonhalite sources in the north and central areas that are effectively overwhelmed by the contributions from halite dissolution, creating a Na/Cl ratio close to unity.

2.3.1.4 Distribution of Cl/Br Ratios

The distribution of Cl/Br weight ratios ([g/L]/[mg/L]) is shown in Figure 2-7. The values range from 3.30 at WIPP-28 to 0.37 at H-8B, with the exception of P-14 and H-4B, which have values of 0.20 and 0.18, respectively. The Cl/Br weight ratio in seawater is about 0.30. As seawater evaporates, this ratio rises slightly (0.33 at the onset of halite precipitation; Sonnenfeld, 1984, p. 229) and then decreases in the remaining brine due to the limited incorporation of Br in the halite lattice (Braitsch, 1971). The ratio is further increased at the onset of the precipitation of late-stage minerals such as carnallite, kainite, bischofite, and sylvite, which incorporate more Br into their lattices than halite does. Castile brines from ERDA-6 have average Cl/Br weight ratios of 0.19 (Popielak et al., 1983), and analyses of brine samples collected from the floor of the WIPP Facility have Cl/Br ratios of 0.12 (Stein and Krumhansl, 1986). The fact that the Cl/Br ratios at P-14 and H-4B are lower than seawater may indicate that the wells were contaminated. Alternatively, if the Cl/Br ratios at these wells are reliable, this may suggest that the Br and Cl at these wells originated either from residual concentrated seawater (such as fluid inclusions) or from the dissolution of late-stage evaporite minerals that have lower Cl/Br ratios than halite.

2.3.1.5 Distribution of Silica

The distribution of silica is shown in Figure 2-8. Silica values reported by ITAS were used in this figure; these values differ from values reported by UNC (see Table 2-2). As discussed previously, the silica concentrations may be affected by precipitation of a Fe-Si floc after sample collection. The values range from 11 to 46 mg/L SiO_2 and are highest in the south and west and decrease toward the east. This silica distribution pattern is roughly the inverse of the general salinity distribution pattern (Figures 2-2, 2-3, and 2-4). Possible controls on the distribution of silica are discussed in Section 2.4.3.2.

2.3.1.6 Solute Concentrations and Ratios at P-14

As discussed in Section 2.2, the possibility that the samples from P-14 are contaminated cannot be ruled out; several isoconcentration plots indicate apparently anomalous concentrations and element ratios at P-14. Plots of the distributions of Sr, Ca, and I (Figures 2-9, 2-10, and 2-11) show an elevation of these elements at P-14, which in each case is nearly 2 times higher than the next highest observed value. However, the increased Sr and Ca concentrations in the vicinity of P-14 could be caused by variations in compositions of carbonate and sulfate minerals. The P-14 sample is also depleted in sulfate, as shown in Figure 2-12. The lowest concentrations of sulfate were measured at P-14 (1,600 mg/L), suggesting that Ca and Sr concentrations are currently controlled by equilibria with sulfate minerals.

The anomalously low Cl/Br ratio (0.200 [g/L]/[mg/L]) at P-14 (discussed above) is accompanied by an unusually low Na/Cl molar ratio of 0.46, which is approximately half the value at most of the other wells (Figure 2-6). This low value suggests a major contribution of Cl from some nonhalite source. One such source may be the leakage of high-Mg or high-Ca brine from underlying stratigraphic zones, such as the Rustler/Salado contact. The Ca and Mg concentrations will eventually be buffered by reactions with sulfates and carbonates, but the Cl will remain in solution, depressing the Na/Cl ratio.

2.3.1.7 Solute Concentrations and Ratios at WIPP-27 and WIPP-29

WIPP-27 and WIPP-29 represent anomalies with respect to K and to a lesser extent Na and Mg. Figures 2-13 through 2-16 show the distributions of K, Na, K/Na, and Mg including WIPP-27 and WIPP-29. The anomalies are probably caused by contamination from potash-mining wastes introduced into the Culebra near the eastern edge of Nash Draw. Although both K and Na are elevated at these two wells, the distribution of K/Na ratios (Figure 2-15) clearly indicates a relative enrichment of K by nearly an order of magnitude.

2.3.2 Definition of Hydrochemical Facies Based on Relative Proportions of Major Solutes

2.3.2.1 Definition of Hydrochemical Facies in the Culebra Dolomite

Based on the major solute compositions given in Table 2-2, four hydrochemical facies have been delineated and are shown in Figure 2-17. Compositions of waters from several other locations (indicated by open circles, open squares, or parentheses around the well name) were not included in the original data set used to define the facies, but their compositions are consistent with the facies boundaries. Compositions of waters in each zone are described in Figure 2-18.

Zone A (DOE-1, H-5, H-11, H-12, P-17) contains saline (~2 to 3 molal) NaCl brines with Mg/Ca molar ratios of about 1.2 to 2 (cf. Figure 2-19). This water is found in the eastern third of the study area; the zone coincides roughly with the region of low transmissivity, although at some of the wells (e.g., DOE-1 and H-11B3) the transmissivities are greater than 1 ft^2/day. On the western side of the zone, halite in the Rustler has been found only in the lower unnamed member; in the eastern portion of the zone, halite has been observed above and below the Culebra.

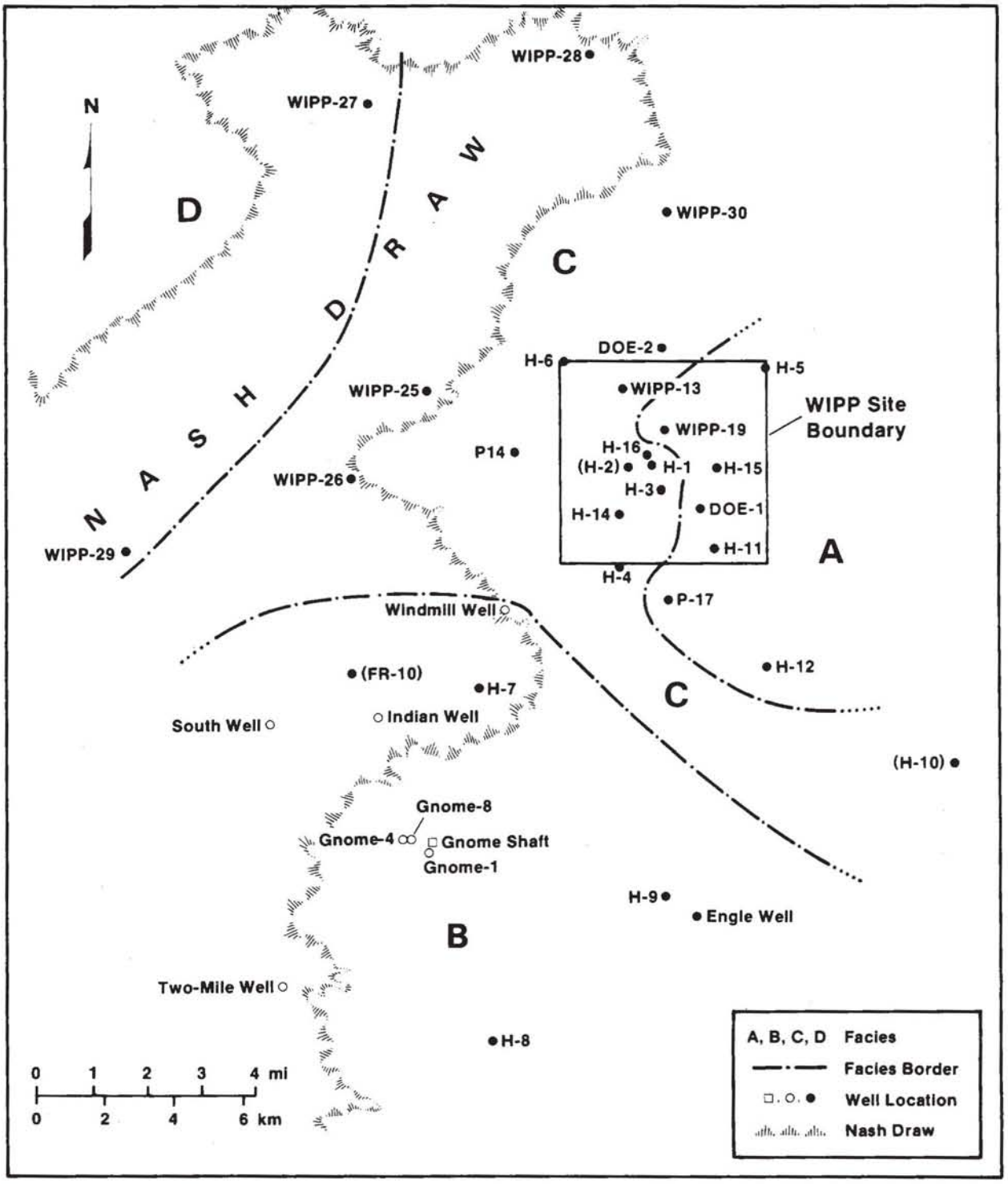

TRI-6331-78-1

Figure 2-17. Hydrochemical facies of the Culebra dolomite.

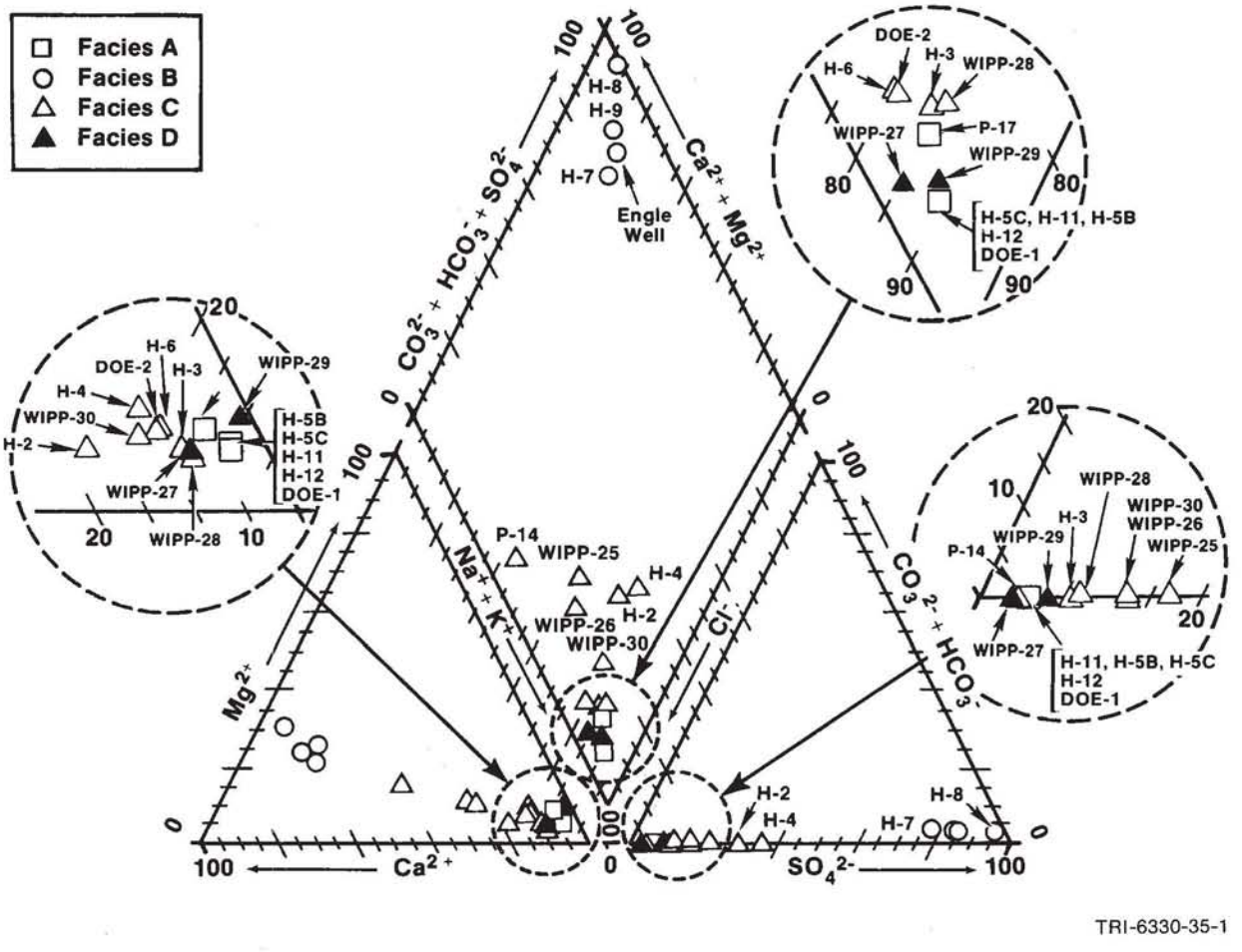

Figure 2-18. Trilinear diagram showing compositions of Culebra groundwaters.

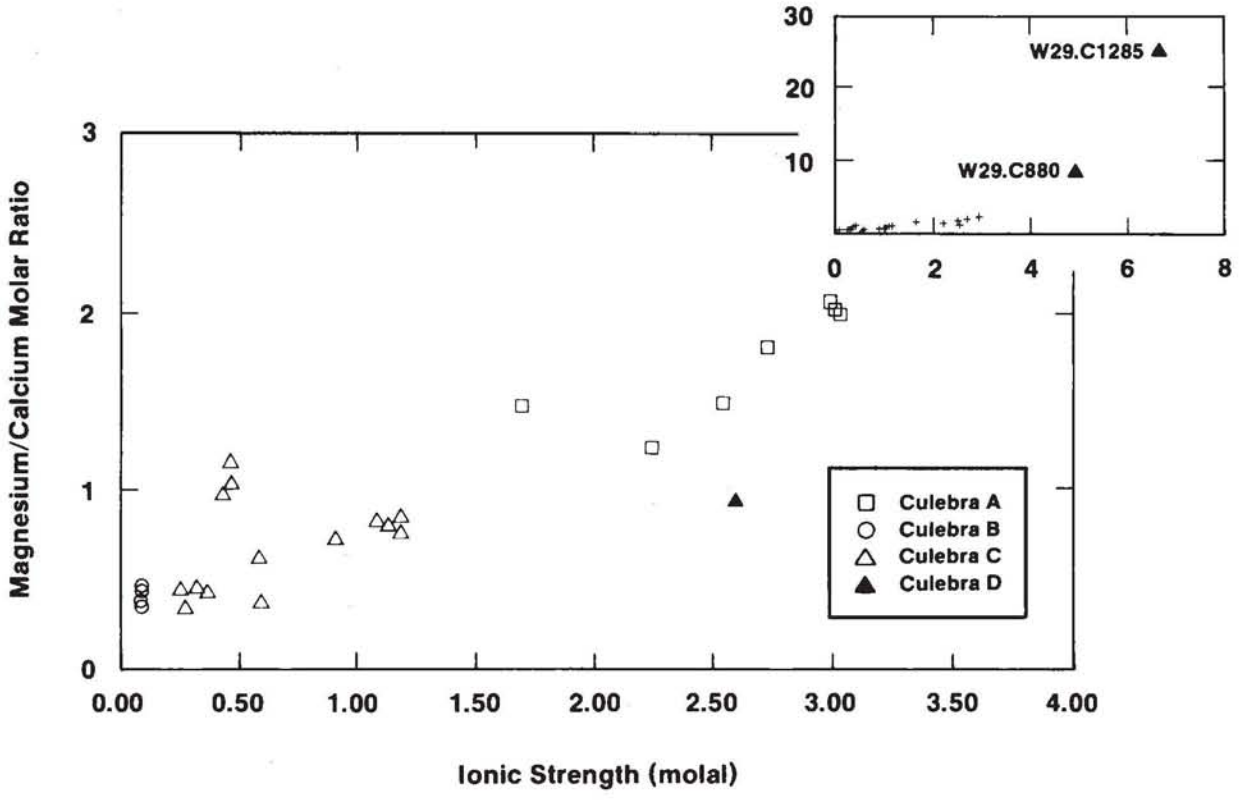

Figure 2-19. Relationship between Mg/Ca molar ratios and ionic strengths of Culebra groundwaters.

Zone B (H-7, H-8, H-9, Engle) contains relatively dilute $CaSO_4$-rich groundwater (ionic strength <0.1 m). This water is found in the southern part of the study area. This zone coincides with a region of high transmissivity; halite is not found in the Rustler in this zone. Chemical data from Bodine et al. (Chapter 4) suggest that several stock wells (Windmill, Indian, South, and Two-Mile) and the Gnome (USGS) wells are also part of this zone.

Zone C contains waters of variable composition with low to moderate ionic strength (0.3 to 1.6 m). These waters occur in the western part of the WIPP Site and the eastern side of Nash Draw. Mg/Ca molar ratios of the fresher waters in this zone (I <1.25 m) range from about 0.3 to about 1.2. This zone coincides with a region of generally high transmissivity (except wells WIPP-30, H-1, H-2, H-4, H-14, and H-16). In the eastern part of this zone, halite is present in the lower unnamed member of the Rustler; on the western side of the zone, halite is not observed in the formation. The most saline (Na-Cl rich) water is found in the eastern edge of the zone, close to borehole locations where halite is observed in the Tamarisk member.

Zone D (WIPP-27, WIPP-29) is defined based on inferred contamination related to potash-refining operations in the area. The Culebra groundwaters from these wells have anomalously high salinities (3-7 m) and K/Na weight ratios (0.2) compared to other wells in the study area (salinities <3 m; K/Na weight ratios 0.01 to 0.09). At WIPP-29, the composition of the Culebra water has changed over the course of a 7-year monitoring period.

Many of the chemical characteristics of the facies are illustrated by the Piper (trilinear) diagram shown in Figure 2-18. This plot summarizes relationships between the major solutes in the Na-K-Mg-Ca-Cl-SO_4-CO_3 system. The diagram shows the relative proportions of the ions on an equivalents/liter basis. Relative proportions of cations and anions are displayed separately in the triangular plots in the bottom half of the figure. In the

rhombus in the upper portion of the diagram, the ratio of divalent to monovalent cations and the ratio of chloride to the sum of sulfate + carbonate + bicarbonate are shown.

Groundwater samples from each well in Zone A have nearly identical ionic proportions and plot very near the Na-Cl corner of the trilinear diagram. They are distinguished from Zone-C groundwaters primarily on the basis of Mg/Ca ratio and ionic strength (see Figure 2-19). Waters from Zone C cover a wide area in the diagram, whereas the relatively fresh waters from Zone B plot near the Ca-SO_4 corner of the diagram. Waters in Zone D have similar ionic proportions to those of Zone A and are distinguished primarily on the basis of the K/Na ratio (see Figure 2-15).

2.3.2.2 Solute Proportions for Other Groundwater Samples

Appendix 2D discusses the major solute compositions of selected samples from the Rustler/Salado contact zone, the Magenta dolomite, the Dewey Lake Red Beds, and the Bell Canyon Formation. There are insufficient data for meaningful isoconcentration or element ratio contours. No hydrogeochemical facies have been defined for these stratigraphic horizons because of the small number of analyses. Additional descriptions of solute relationships in these waters are found in the discussion of factor analysis in Section 2.3.3 and in Appendix 2D.

2.3.3 Principal Component Analysis of Water Chemistry Data

In the previous section, hydrochemical facies for Culebra groundwaters were defined using the relative proportions of the concentrations of seven major solutes. These solute ratios can be represented by a trilinear plot as shown in Figure 2-18. To show relationships among the 17 independent chemical variables presented in Table 2-2, PCA was used. This method summarizes the relationships among the variables and shows how these relationships differ for each water composition. This information can be used to refine the definitions of the hydrochemical facies and to suggest the nature of chemical reactions that control groundwater composition. This section contains a brief introduction to the

principles of PCA and then describes the application of this technique to waters from the Culebra dolomite and related rock units.

2.3.3.1 Introduction to Principal Component Analysis

PCA is a method of multivariate statistics that can be used to examine the relationships in complex data sets. It can be used in two ways: (1) to express the relationships among a large number of variables in terms of correlations with a smaller number of underlying components or factors; or (2) to describe the characteristics of a sample suite by defining hypothetical end members of the population.

When the objective of the analysis is to find correlations among variables, R-mode analysis is employed; when the similarities among samples are examined, Q-mode analysis is used.

Appendix 2B explains the basic concepts and vocabulary of PCA. The origins of the factor-loading matrices and factor-score matrices, the significance of factor rotations, and the need for data transformations are explained. A detailed explanation of the mathematical principles that underly the technique is not required to understand this section and is beyond the scope of this work. Similarly, a review of previous applications of PCA in geochemical studies is not included here. References to works that contain excellent discussions of the theory and applications of PCA can be found in Appendix 2B.

In this report, the terms "factor" and "principal component" are used interchangeably. However, as discussed in Appendix 2B, the analysis presented below is, in the strictest sense, a PCA and not a classical factor analysis.

2.3.3.2 Sample Populations Examined by Principal Component Analysis

Table 2-4 describes the two sample populations that were examined using PCA. Population 1 contains 21 water samples from the Culebra dolomite of the Rustler Formation. Where multiple samples from the same well are available, the most recent sample was used. Where data from both UNC and other laboratories were available, data

Table 2-4. Populations Used in Principal Component Analysis

Pop.	Wells	Variables used in PCA
1	Culebra: DOE-1, DOE-2, H-2A, H-3B3, H-4B, H-5B, H-5C, H-6B, H-7B1, H-8B, H-9B, H-12, P-14, P-17, WIPP-25, WIPP-26, WIPP-27, WIPP-28, WIPP-29, WIPP-30, Engle	Ca, Mg, K, Na, Cl, SO_4, B, Li, SiO_2, Br, Sr, HCO_3, pH
2	Dewey Lake: Ranch, Twin-Pasture	Ca, Mg, K, Na, Cl, SO_4, B, Li, SiO_2, Br, Sr, HCO_3, pH,
	Magenta: H-3B1, H-4C, H-5C, H-6C	Fe, Mn, F, I
	Culebra: DOE-2, H-2A, H-3B3, H-5B, H-6B, H-7B1, H-8B, H-9B, P-14, P-17, WIPP-26, WIPP-29, Engle	
	Bell Canyon: DOE-2	

from the UNC laboratory were used. The reasons for these choices are discussed in Section 2.2. Factor analysis of population 1 is discussed in detail in the following sections and in Appendix 2C.

Population 2 contains 20 groundwater samples from the Dewey Lake Red Beds, Magenta dolomite, Culebra dolomite, and Bell Canyon Formation. The objective in selecting analyses for this data set was to include as many different solutes as possible. For this reason, several Culebra samples from population 1 that lack minor and trace-element data (Mn, Fe, I) were not included. The interelement correlations involving these additional solutes are described in Section 2.3.3.6. Additional information about factor analysis of population 2 is found in Appendix 2D.

2.3.3.3 Q-mode Analysis of Culebra Water Samples

A Q-mode PCA was carried out on population 1 to determine if the data set was homogeneous and therefore amenable to R-mode analysis. The factor analysis programs of SAS (Statistical Analysis System Institute, 1982) were used to extract the principal components. The data set consisted of the logarithms of the raw concentrations; all principal components (factors) that accounted for at least 1% of the total variance were extracted.

Both the unrotated and varimax solutions were examined; the former was more interpretable and was retained for further discussion. The results of the unrotated analysis are presented in Table 2-5 and Figures 2-20 and 2-21. Table 2-5 shows the factor loading matrix; it can be seen that two principal components account for nearly all of the variance. The communalities of all samples are at least 0.93, indicating that combinations of these factors accurately reconstruct the compositions of most of the water samples.

The "Factor A" and "Factor B" columns of Table 2-5 describe the similarity between each sample and principal components A and B, respectively. The rows across the table show the composition of each sample in terms of the components. Figure 2-20 provides a graphical representation of Table 2-5 and describes the water compositions in terms of the two principal components. Figure 2-21 is a graphical representation of the Q-mode factor-score matrix and describes the components in terms of the chemical variables.

The first principal component (factor A) accounts for 96% of the variance of the population (Table 2-5). Most of the samples are similar to this factor (that is, they have factor loadings close to unity), which represents a grand average of all the compositions. H-6 is closest in composition to this hypothetical entity. A few water samples deviate considerably from this grand average composition. The second principal component (factor B) describes this deviation; it accounts for 4% of the variance. WIPP-29 and H-8 are the extrema of this principal component.

Table 2-5. Unrotated Q-mode Factor Loadings of Culebra Groundwaters (Population 1)

Well	Coll. Date	Facies[1]	Factor A	Factor B	Communality (h_i^2)
DOE-1	4/85	A	0.98	-0.19	0.994
H-5C	10/81	A	0.98	-0.15	0.990
H-5B	8/85	A	0.98	-0.18	0.993
H-12	8/85	A	0.98	-0.19	0.992
P-17	3/86	A	0.98	-0.13	0.989
H-7B1	3/86	B	0.94	0.33	0.998
H-8B	1/86	B	0.90	0.43	0.990
H-9B	11/85	B	0.93	0.35	0.997
ENGLE	3/85	B	0.94	0.34	0.998
DOE-2	3/85	C	0.99	-0.09	0.996
H-2A	4/86	C	0.99	0.08	0.985
H-3B3	2/85	C	0.99	-0.08	0.992
H-4B	7/85	C	0.99	0.00	0.981
H-6B	9/85	C	0.99	-0.09	0.997
P-14	2/86	C	0.97	0.04	0.936
WIPP-25	2/86	C	0.99	0.10	0.994
WIPP-26	11/85	C	0.99	0.05	0.987
WIPP-28	9/80	C	0.98	-0.04	0.974
WIPP-30	9/80	C	0.99	0.03	0.985
WIPP-27	9/80	D	0.95	-0.20	0.956
WIPP-29	12/85	D	0.90	-0.34	0.939

Amount and Percent of Variance Explained by Each Factor

Factor A	Factor B
19.778	0.888
96%	4%

1. Hydrochemical facies in the Culebra, as defined in Section 2.3.2.1.

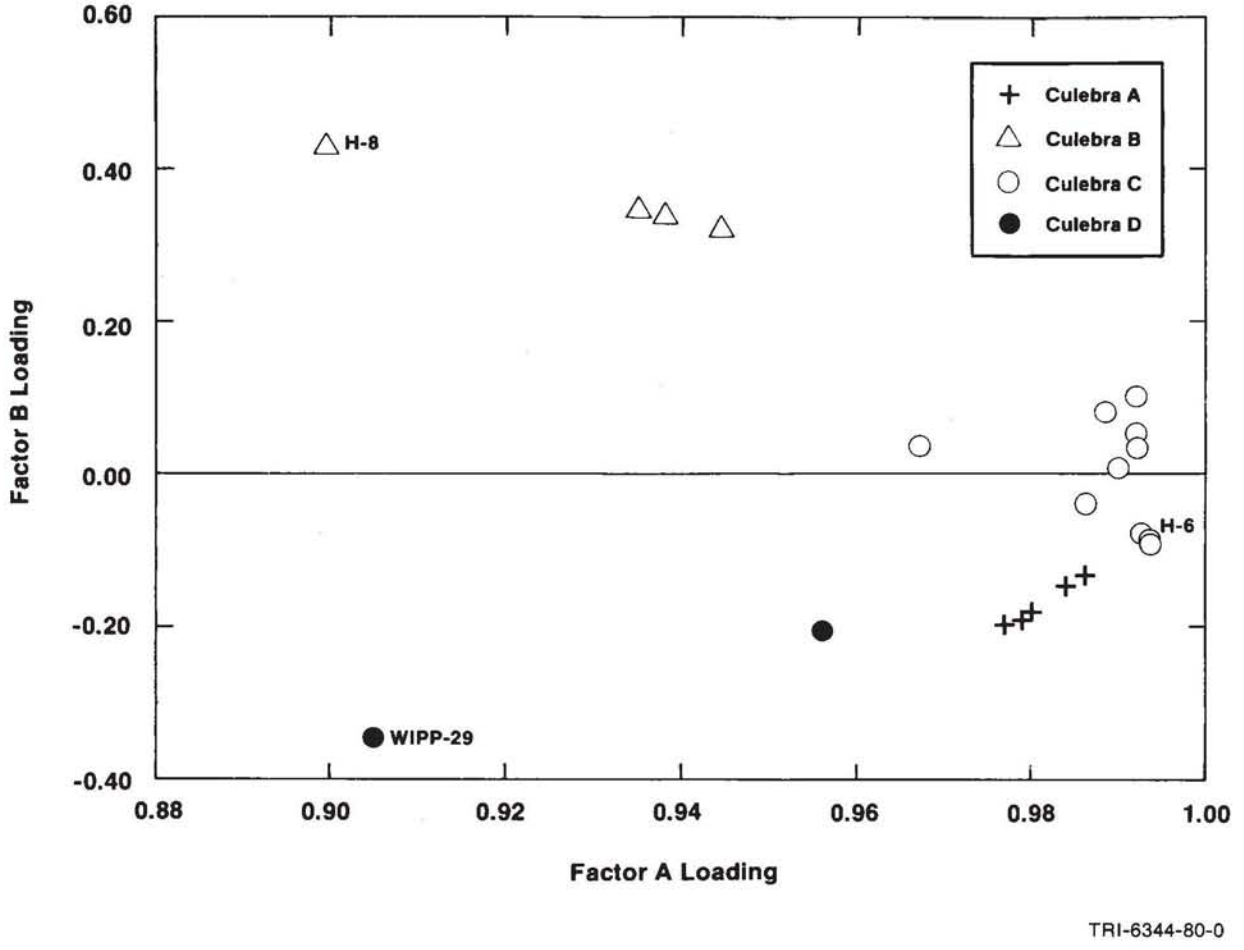

Figure 2-20. Relationship between unrotated Q-mode factor loadings for factors A and B of Culebra groundwaters (population 1).

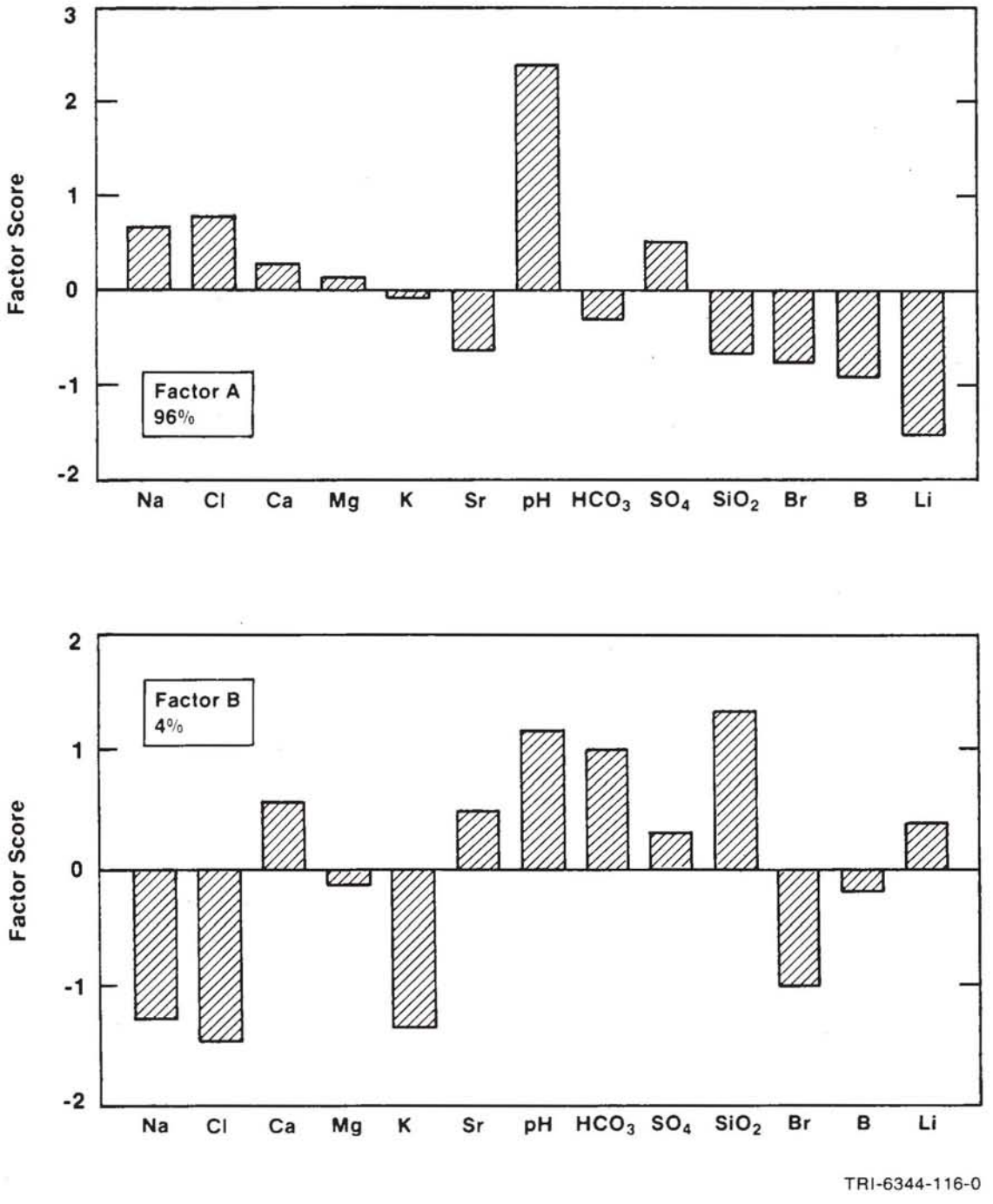

Figure 2-21. Unrotated Q-mode factor scores for factors A and B of Culebra groundwaters (population 1).

In general, as discussed in Appendix 2B, if two or three Q-mode principal components account for most of the sample variance, the population can be considered homogeneous enough for R-mode analysis (Hitchon et al., 1971; Klovan, 1975; Drever, 1982). The results, shown in Table 2-5, indicate that population 1 is homogeneous and therefore amenable to R-mode analysis.

2.3.3.4 R-mode Principal Component Analysis of Culebra Water Samples

2.3.3.4.1 FACTOR LOADINGS

R-mode PCA was carried out on population 1 using the factor-analysis programs in SAS. The common logarithms of the raw chemical data were calculated; the resulting distributions of the transformed variables were close to normal. The correlation matrix of the transformed data is shown in Table 2-6.

The factor-loading matrix of the principal components extracted from the correlation matrix is described in Table 2-7. Three factors account for approximately 96% of the total variance of the sample population; these three factors are shown in Figure 2-22.

Factor 1 accounts for approximately 67% of the total variance of the data set. It is characterized by high positive loadings for all of the variables except pH, bicarbonate alkalinity, and silica. The factor accounts for most of the variance of sodium and chloride. For this reason, the factor is referred to as the "salinity factor" in this report.

Factor 2 accounts for approximately 18% of the variance of the data set. It is characterized by large loadings for pH, bicarbonate alkalinity, and silica and boron concentrations. It is referred to as the "silicate/bicarbonate factor" in this report.

Table 2-6. Correlation Matrix for Solute Data[1] in Culebra Groundwaters (Population 1)

	Ca	Mg	K	Na	Cl	SO_4	B
Ca	1.000	0.492	0.414	0.568	0.606	0.042	0.361
Mg	0.492	1.000	0.905	0.906	0.893	0.835	0.638
K	0.414	0.905	1.000	0.945	0.930	0.847	0.663
Na	0.568	0.906	0.945	1.000	0.993	0.810	0.797
Cl	0.606	0.893	0.930	0.993	1.000	0.759	0.753
SO_4	0.042	0.835	0.847	0.810	0.759	1.000	0.755
B	0.361	0.638	0.663	0.797	0.753	0.755	1.000
Li	0.456	0.882	0.801	0.886	0.859	0.839	0.864
SiO_2	-0.259	-0.583	-0.544	-0.649	-0.601	-0.703	-0.842
Br	0.638	0.853	0.819	0.934	0.944	0.695	0.763
Sr	0.940	0.712	0.624	0.750	0.780	0.310	0.508
pH	-0.118	-0.412	-0.351	-0.223	-0.239	-0.187	0.187
HCO_3	-0.221	-0.155	-0.095	-0.229	-0.198	-0.226	-0.577

	Li	SiO_2	Br	Sr	pH	HCO_3
Ca	0.456	-0.259	0.638	0.940	-0.118	-0.221
Mg	0.882	-0.583	0.853	0.712	-0.412	-0.155
K	0.801	-0.544	0.819	0.624	-0.351	-0.095
Na	0.886	-0.649	0.934	0.750	-0.223	-0.229
Cl	0.859	-0.601	0.944	0.780	-0.239	-0.198
SO_4	0.839	-0.703	0.695	0.310	-0.187	-0.226
B	0.864	-0.842	0.763	0.508	0.187	-0.577
Li	1.000	-0.778	0.864	0.647	-0.123	-0.397
SiO_2	-0.778	1.000	-0.633	-0.396	-0.422	0.729
Br	0.864	-0.633	1.000	0.816	-0.153	-0.329
Sr	0.647	-0.396	0.816	1.000	-0.202	-0.266
pH	-0.123	-0.442	-0.153	-0.202	1.000	-0.572
HCO_3	-0.397	0.729	-0.329	-0.266	-0.572	1.000

1. The data are the natural logarithms of the solute concentrations in mg/L (except for pH).

Table 2-7. Unrotated R-mode Factor Loadings for Culebra Groundwaters (Population 1)

Element	Factor 1	Factor 2	Factor 3	Factor 4	Factor 5	Communality (h_i^2)
Ca	0.590	0.177	0.773	0.017	0.005	0.979
Mg	0.922	0.255	-0.128	-0.146	-0.160	0.980
K	0.901	0.251	-0.212	0.107	-0.144	0.953
Na	0.976	0.125	-0.039	0.135	0.010	0.990
Cl	0.962	0.168	0.019	0.159	0.001	0.981
SO_4	0.818	-0.031	-0.564	-0.030	-0.042	0.992
B	0.848	-0.385	-0.106	0.048	0.320	0.985
Li	0.944	-0.081	-0.123	-0.116	0.120	0.942
SiO_2	-0.748	0.616	0.115	-0.001	0.132	0.971
Br	0.947	0.059	0.126	0.055	0.052	0.924
Sr	0.778	0.198	0.582	-0.038	-0.044	0.988
pH	-0.145	-0.903	0.162	0.344	-0.100	0.993
HCO_3	-0.379	0.799	-0.208	0.360	0.049	0.960

Amount and Percent of Variance Explained by Each Factor

Factor 1	Factor 2	Factor 3	Factor 4	Factor 5
8.4033	2.2385	1.4456	0.3470	0.2006
67%	18%	11%	3%	2%

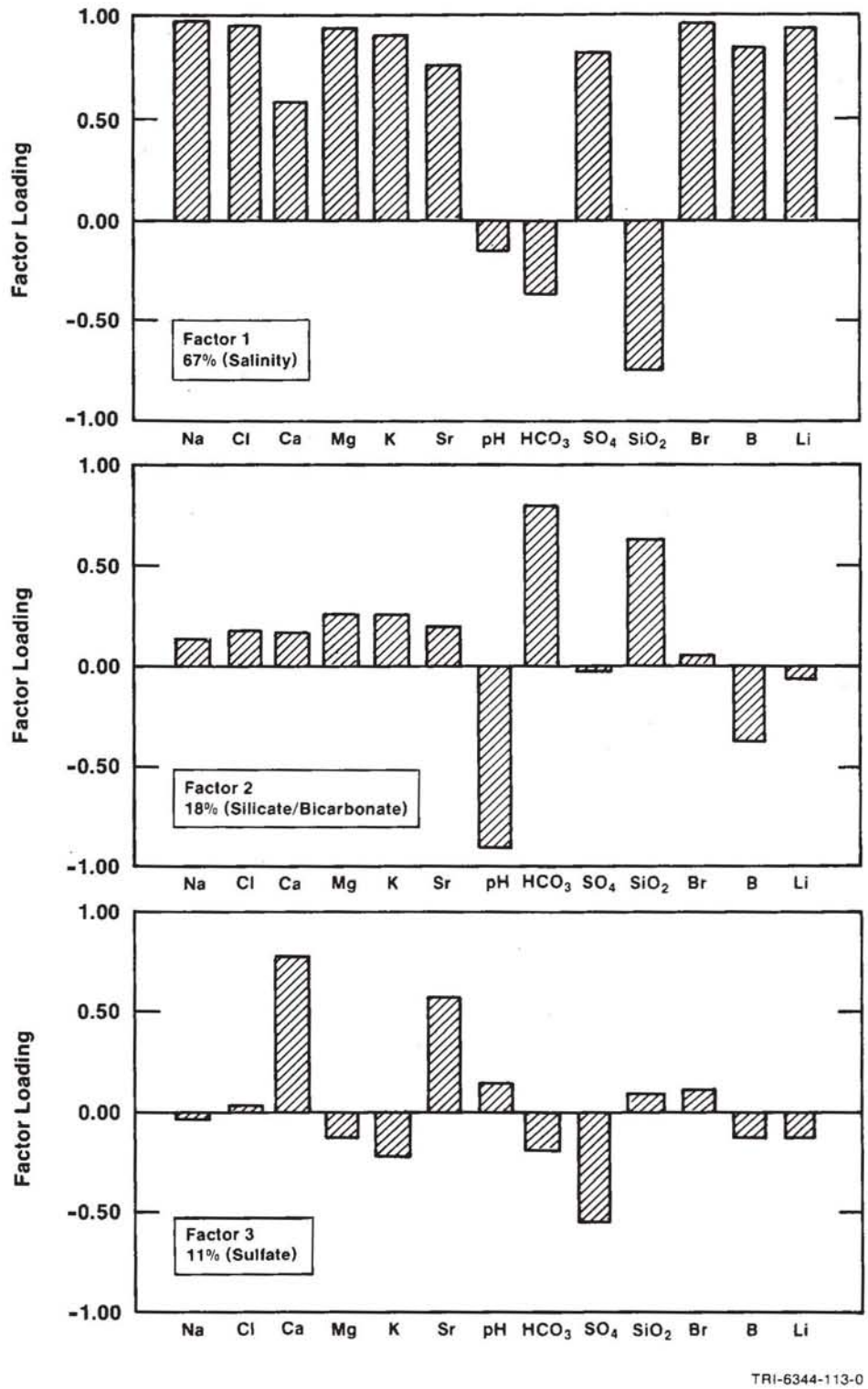

Figure 2-22. Unrotated R-mode factor loadings for factors 1, 2, and 3 of Culebra groundwaters (population 1).

Factor 3 accounts for approximately 11% of the total variance and exhibits high positive loadings for calcium and strontium. It also exhibits a high negative loading for sulfate and is referred to as the "sulfate factor " in this report.

As discussed in Appendix 2B, the factor loadings and scores of the unrotated principal components are strongly influenced by the requirement that the first principal component account for the highest possible amount of variance. As discussed in the appendix, this mathematical constraint may obscure the true relationships among the variables. Other orientations or rotations of the factor axes are possible and are equally mathematically correct in describing the variance of the data set. For this reason, the SAS factor-analysis factor-rotation subroutines were used to examine other factor structures. The mathematical basis for the different rotations is discussed clearly in Nie et al. (1975).

Factor loadings obtained from varimax, equamax, and quartimax rotational schemes were examined to determine if any element associations were common to alternative orientations of the factor axes. It was found that the factor-loading matrices from all rotational schemes contained the same key element associations described above for the unrotated components. The loading matrices differed primarily in the relative loadings of other elements and the variance explained by the salinity, silicate/bicarbonate, and sulfate factors. These differences and similarities are illustrated by examining the results of the varimax rotation discussed in the following section.

2.3.3.4.2 VARIMAX FACTOR LOADINGS

As discussed in Appendix 2B, the varimax rotation is most commonly used in analysis of hydrochemical and mineralogical data. This rotation is based on numerical criteria that seek to simplify the columns of the factor-loading matrix. This means that in the "ideal" varimax factor-loading matrix, every factor is important for as few elements as possible.

The first three varimax factors are described in Figure 2-23; they are similar to the three unrotated factors shown in Figure 2-22. By convention, the factor loadings are scaled in

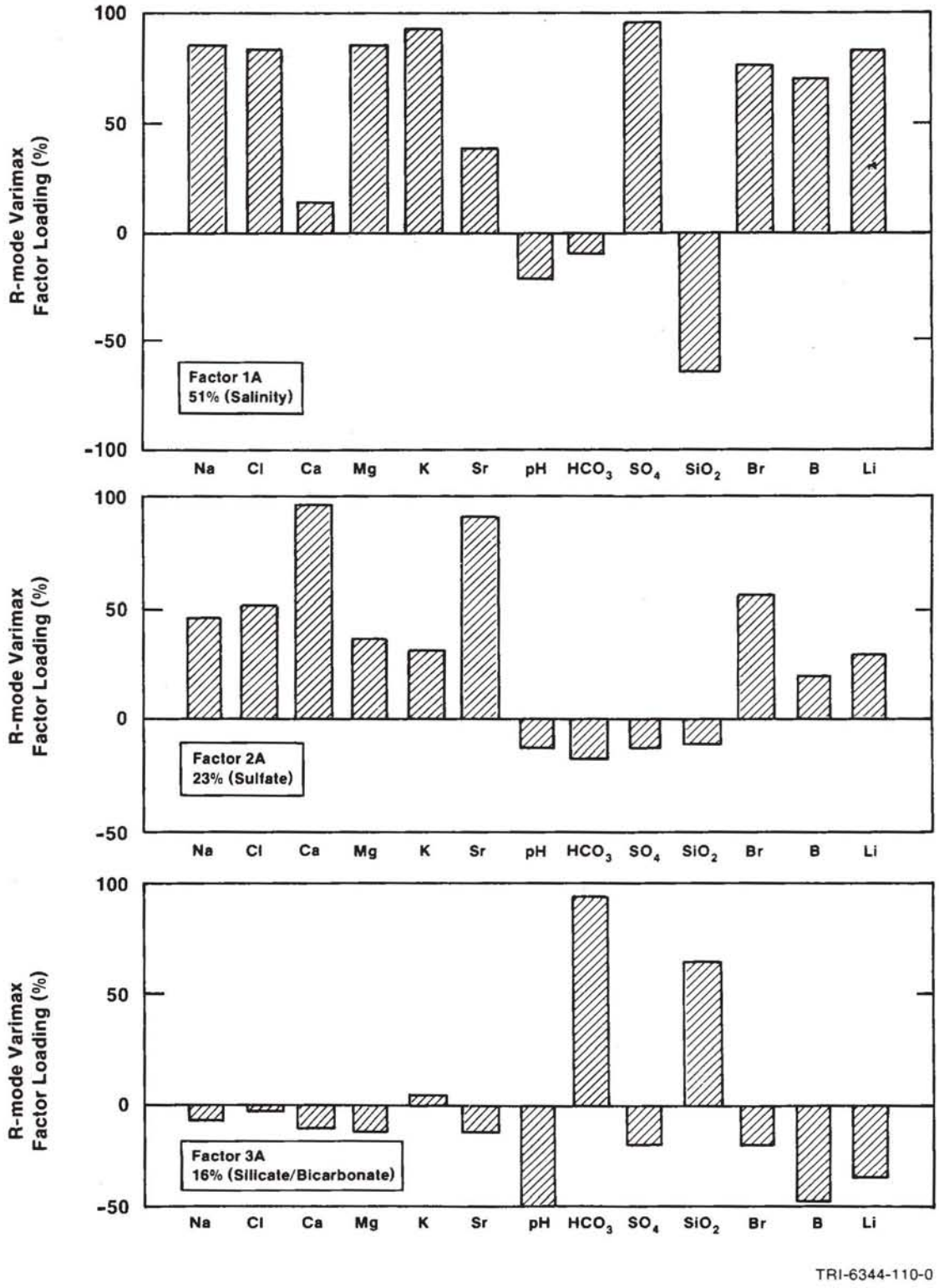

Figure 2-23. Varimax R-mode factor loading for factors 1A, 2A, and 3A of Culebra groundwaters (population 1).

units of percent after rotation, whereas the the unrotated factor loadings are scaled in fractional units. Factors are assigned numbers in order of decreasing variance, also by convention.

Factor 1A contains the same elemental associations as factor 1, the salinity factor, but accounts for slightly less variance. Factor 2A contains the same calcium-strontium correlation as factor 3, the sulfate factor, but is less influenced by sulfate concentration. The varimax factor is more strongly affected by the concentrations of elements such as sodium and bromine and accounts for more variance than its unrotated counterpart. Factor 3A is very similar to factor 2, the silicate/bicarbonate factor. It is more strongly influenced by elements such as sodium and chlorine and explains more variance than the unrotated factor.

More details of the varimax factor loadings and scores are given in Appendix 2C. Because of the similarity of the factors obtained from the different rotations, the discussion of the factor-score matrix that follows is relevant to all four rotations examined. In this discussion, the water sample compositions are compared in terms of the relative importances of the key elemental associations described above as the "salinity," "sulfate," and "silicate/bicarbonate" factors.

2.3.3.4.3 VARIMAX FACTOR SCORES

The compositions of the samples in terms of the factors are described by the factor scores. Relationships between varimax factor scores for the three most important factors are presented as bivariate plots in Figures 2-24 and 2-25. Scores for the salinity and sulfate factors are plotted in Figure 2-24. This figure shows that the first two principal components can be used to delineate the same groups of wells identified in Figures 2-17 through 2-19. Thus, the definition of hydrochemical facies, based on the proportions of major solutes, is supported by correlations among the major and minor elements examined in this study.

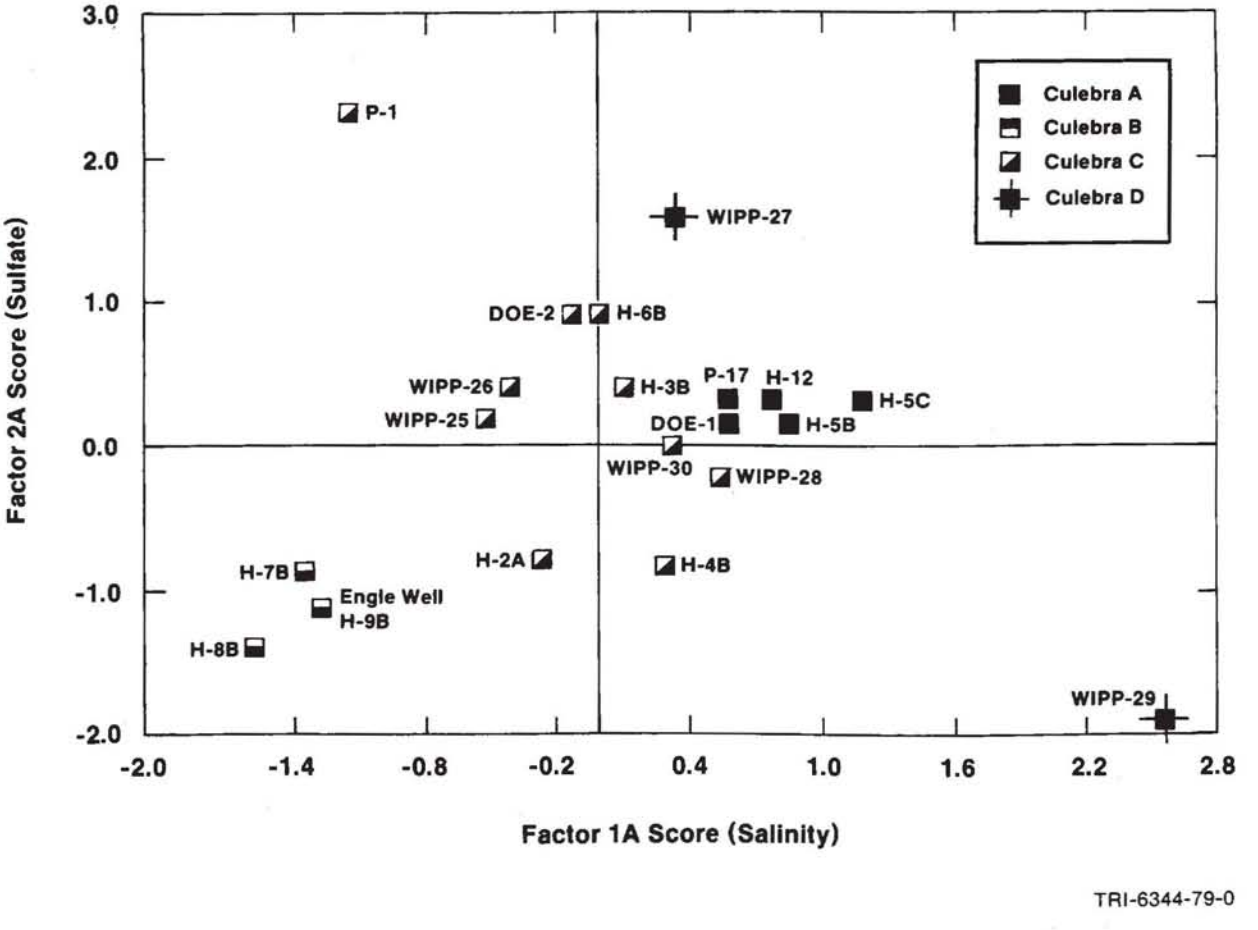

Figure 2-24. Relationship between varimax R-mode factor scores for factors 1A and 2A of Culebra groundwaters (population 1).

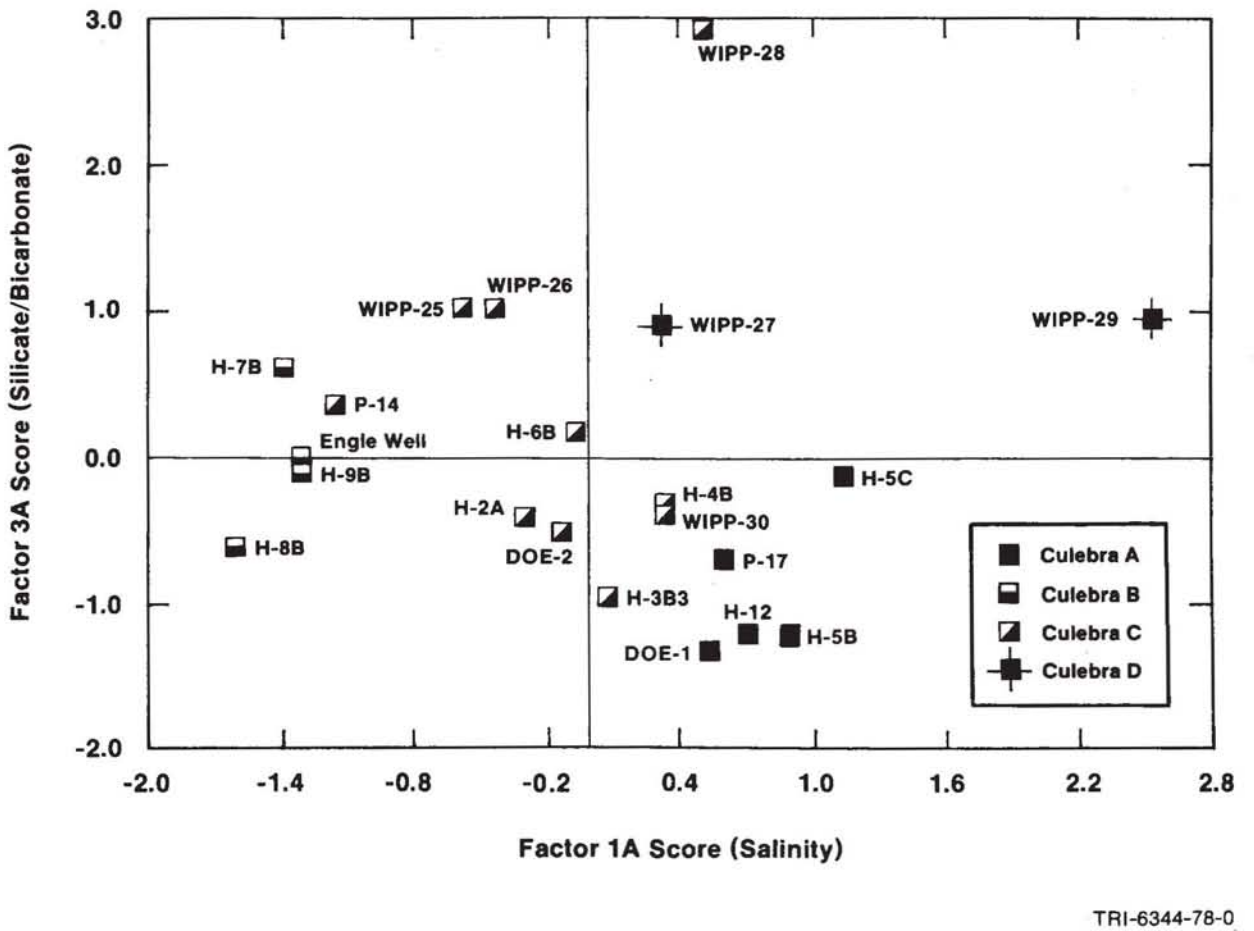

Figure 2-25. Relationship between varimax R-mode factor scores for factors 1A and 3A of Culebra groundwaters (population 1).

Scores for the salinity factor (1A) are lowest for wells in Zone B and are highest for WIPP-29 (Zone D) and for wells in Zone A. In Zone C, the scores for the salinity factor are intermediate; within the zone, the scores are lowest for P-14 and increase radially to the east, west, and north. The contours for the scores of salinity factor are similar to those for sodium concentration (Figure 2-14). This supports the suggestion that this factor is dominated by the effects of halite dissolution. The scores of the salinity factor (1A) are plotted and contoured in Figure 2C-3 in Appendix 2C.

P-14 has the highest score for the sulfate factor (2A). As discussed in Section 2.3.1, the concentrations of several elements in P-14 are anomalous, perhaps because of contamination. Ca, Sr, I, and Br exhibit local highs in their element contours; SO_4 and the Na/Cl ratio are anomalously low. The lowest (most negative) score for this factor is exhibited by WIPP-29; this well also has an anomalously high concentration of SO_4. The scores for the sulfate factor (2A) are plotted and contoured in Figure 2C-5 in Appendix 2C.

Figure 2-25 shows the scores of the salinity (1A) and silicate/bicarbonate (3A) factors for each well. The scores for the silicate/bicarbonate factor show little relationship to the hydrochemical facies, although there is a general increase in the value of the score from west to east. WIPP-28 has the highest score and is anomalous compared to wells surrounding it. The bicarbonate concentration at WIPP-28 is also anomalously high because of contamination (see Table 2-3, Section 2.2) and dominates the score for this well. Contours of the spatial distribution of scores for the silicate factor are not plotted; the pattern is similar to that of SiO_2 presented in Figure 2-8.

2.3.3.5 R-mode Factors Obtained After Partialling Out Total Dissolved Solids

2.3.3.5.1 OBJECTIVES AND PROCEDURE

The three major factors obtained from the R-mode analysis described above are strongly affected by halite dissolution. Solutes are added directly from the halite or indirectly because the solubilities of sulfate and carbonate phases increase as the ionic strength increases (see Section 2.4.2). A second R-mode PCA was carried out to examine interelement correlations independent of the effects of halite dissolution. The analysis was carried out as follows. First, regression equations for each of the chemical variables as a function of the TDS were obtained. Next, the partial correlation matrix with respect to TDS was obtained by calculating the correlations between the residuals from the regression equations. Finally, the eigenvectors of the partial correlation matrix were extracted to give the principal components. A detailed description of the procedure can be found in Appendix 2B.

This PCA was carried out on the variance in the population that is not correlated with variation in the TDS. The amount of this residual variance for each variable is shown in the last column of Table 2-8. After accounting for the correlation with TDS, very little of the variance of Na, Mg, K, and Cl remains. In contrast, a significant portion of the variation in the concentrations of Ca, Sr, B, and SiO_2, the pH, and the alkalinity cannot be correlated with the TDS. The results of this analysis are summarized in the following section; a more detailed discussion of the analysis is found in Appendix 2C.

2.3.3.5.2 DESCRIPTION OF FACTORS

Five factors account for 99% of the variance that remains after the TDS is partialled out. The varimax factor-loading matrix for the five factors is shown in Table 2-8. In Figure 2-26, the variables with the highest loadings for each factor are identified. Table 2-9 recasts the factor loadings in terms of the percentage of the total variance (including the variance correlated to TDS) of each variable that each factor explains. These percentages of the

Table 2-8. Varimax R-mode Factor Loadings (Percent) Obtained from Partial-Correlation Matrix with Respect to TDS of Culebra Groundwaters (Population 1)

Element	Factor 1B	Factor 2B	Factor 3B	Factor 4B	Factor 5B	Communality (h_i^2)	Residual Variance[1]
Na	12	-10	76	-58	4	98.7	4%
Cl	28	3	84	-36	- 4	96.1	7%
Ca	97	- 1	14	- 8	- 1	99.2	71%
Mg	- 3	23	-23	92	10	98.1	7%
K	-30	22	5	-13	-25	98.8	9%
Sr	94	- 1	25	9	1	97.1	39%
pH	- 1	-93	19	-26	7	98.7	91%
HCO_3	-11	79	- 4	3	-22	97.1	96%
SO_4	-94	-18	-14	5	17	98.2	27%
SiO_2	18	93	4	9	-24	99.0	58%
Br	27	-16	86	8	13	96.2	19%
B	-19	-52	14	-55	47	97.3	43%
Li	-12	-34	7	7	90	99.5	18%

Table 2-8. Varimax R-mode Factor Loadings (Percent) Obtained from Partial-Correlation Matrix with Respect to TDS of Culebra Groundwaters (Population 1) (Continued)

Amount and Percent of Variance[1] Explained by Each Factor				
Factor 1B	Factor 2B	Factor 3B	Factor 4B	Factor 5B
3.071	2.903	2.251	1.737	1.265
27%	26%	20%	16%	11%

1. Variance not correlated to TDS; that is, the amount of variance remaining after TDS was partialled out.

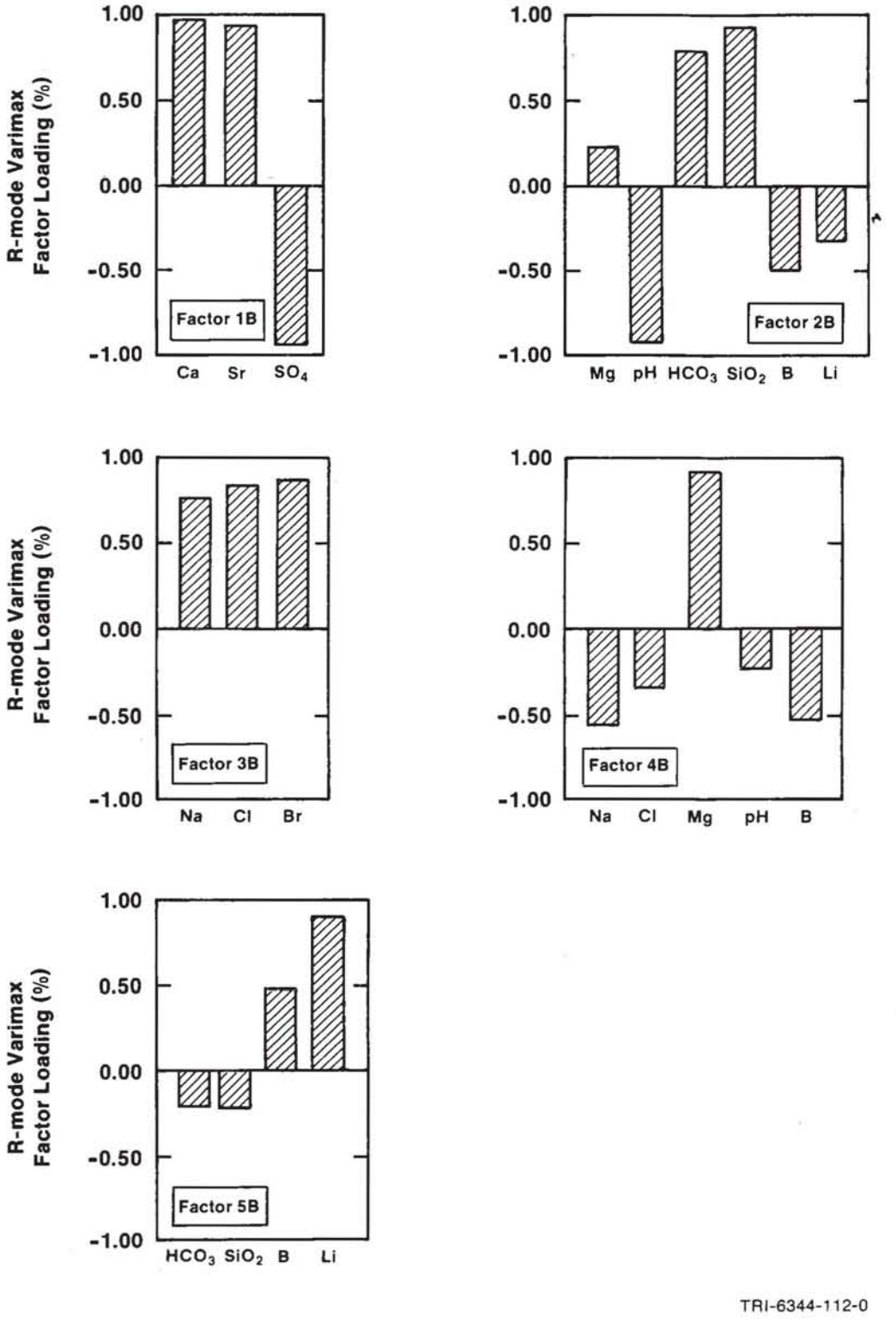

Figure 2-26. Varimax R-mode factor loadings of key (loading >0.23) elements for factors 1B, 2B, 3B, 4B, and 5B obtained from partial-correlation matrix with respect to TDS of Culebra groundwaters (population 1).

Table 2-9. Percent of Total Variance[1] Explained by Varimax R-mode Factors Obtained from Partial-Correlation Matrix with Respect to TDS of Culebra Groundwaters (Population 1)

Element	Factor 1B	Factor 2B	Factor 3B	Factor 4B	Factor 5B	Residual Variance[2]
Na	*	*	*	*	*	4%
Cl	*	*	5%	*	*	7%
Ca	67%	*	*	*	*	71%
Mg	*	*	*	6%	*	7%
K	*	*	*	*	*	9%
Sr	35%	*	*	*	*	39%
pH	*	-79%	*	-6%	*	91%
HCO_3	*	60%	*	*	-5%	96%
SO_4	-24%	*	*	*	*	27%
SiO_2	**	50%	**	**	-3%	58%
Br	*	*	14%	*	*	19%
B	*	-12%	*	-13%	10%	43%
Li	*	*	*	*	15%	18%

1. Percent of total variance. Signs indicate type of correlation shown in Table 2-8. An asterisk indicates that the percent variance is <5%; a double asterisk indicates that the percent variance is <3%.
2. Amount of variance that is not correlated with the TDS.

total variance are plotted in Figure 2-27. Figure 2-27 plots variances only for elements for which the factors explain approximately >5% of the total variance.

Factor 1B is dominated by the negative correlation of Ca and Sr with sulfate and is suggestive of dissolution/coprecipitation of Sr and Ca in a sulfate phase such as gypsum or anhydrite. It accounts for 67% of the total variance of Ca, 35% of the total variance of Sr, and 24% of the total variance of sulfate. This factor is similar to the sulfate factors (3 and 2A) described in Section 2.3.3.4. The factor scores are plotted in Figure 2-28. The spatial distribution of the scores is not related to hydrochemical facies; the scores are contoured in

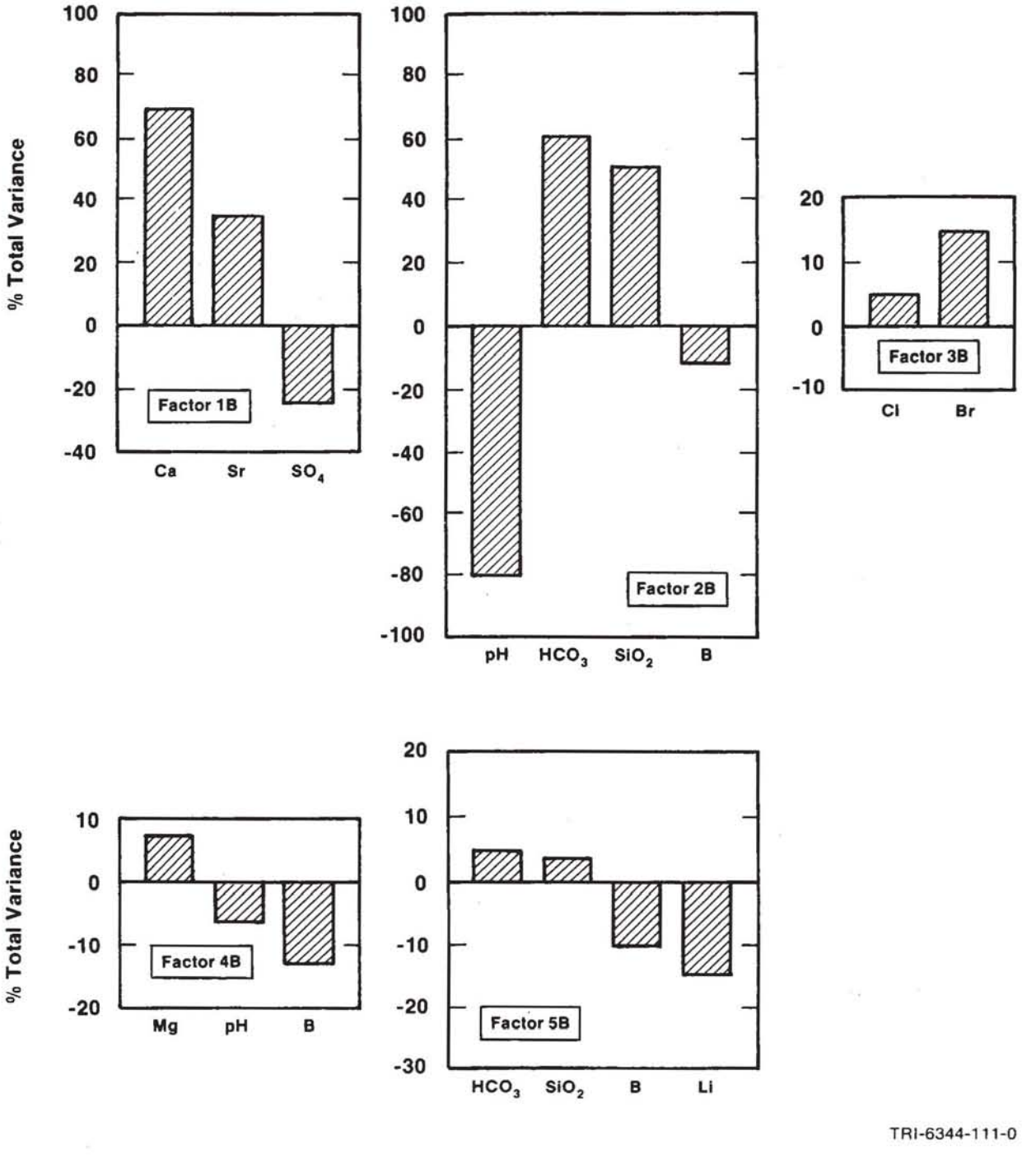

Figure 2-27. Amount of total variance of key elements explained by factors 1B to 5B obtained from the partial-correlation matrix with respect to TDS of Culebra groundwaters (population 1).

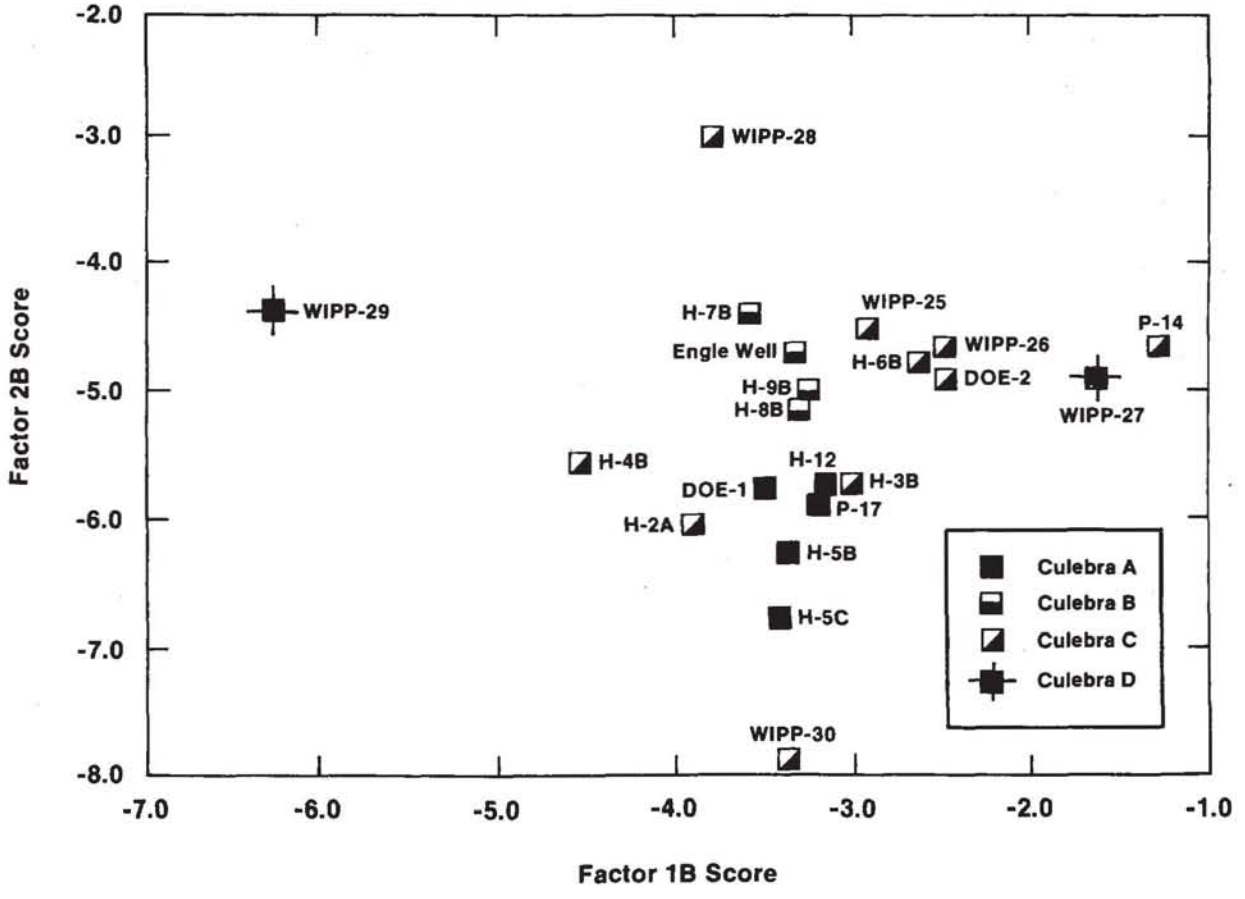

Figure 2-28. Relationship between varimax R-mode factor scores for factors 1B and 2B obtained from the partial-correlation matrix with respect to TDS of Culebra groundwaters (population 1).

Figure 2C-8 in Appendix 2C. Well P-14 has the highest score for this factor; WIPP-29 has the lowest score.

Factors 2B, 4B, and 5B are similar to the silicate factors (2 and 3A) described in Section 2.3.3.4. They contain all or portions of two negatively correlated groups of variables. One group involves the correlation of Mg, K, bicarbonate alkalinity, and silica; the other group contains Na, pH, B, and Li. This pattern of element associations may be due to a combination of processes including sorption, ion exchange, carbonate diagenesis, and silicate diagenesis. The pattern is discussed in more detail in Section 2.4.3.

Figure 2-28 shows that Factor 2B clearly distinguishes hydrochemical facies A from facies B. The extreme values of the factor score, however, are both in Zone C. Both of the extrema, WIPP-30 and WIPP-28, are anomalous with respect to neighboring wells. WIPP-30 exhibits the lowest silica concentration (4 mg/L). WIPP-28 exhibits the highest bicarbonate alkalinity in the population, but is known to be contaminated (Section 2.2). Figure 2-29 shows that on a regional scale, the value of the score increases from east to west. In Section 2.4.3, it is suggested that this trend could be related to a westward increase of the amount of silicates exposed to groundwaters. The increased amounts of silicates are consistent with the greater degree of evaporite dissolution and formation of a residual fraction in the parts of the aquifer in contact with the groundwater.

2.3.3.6 Principal Component Analysis of Culebra, Magenta, Dewey Lake, and Bell Canyon Groundwater Samples

PCA was carried out on a second data set containing water compositions from wells in the Culebra dolomite, Magenta dolomite, Dewey Lake Red Beds, and Bell Canyon Formation. The sample population is designated "population 2" and is described in Table 2-4. The primary purpose of this analysis was to examine the relationships between the major solutes and several minor elements not included in population 1 (which included Culebra data only). Concentrations of iron, manganese, fluoride, and iodide were included in this

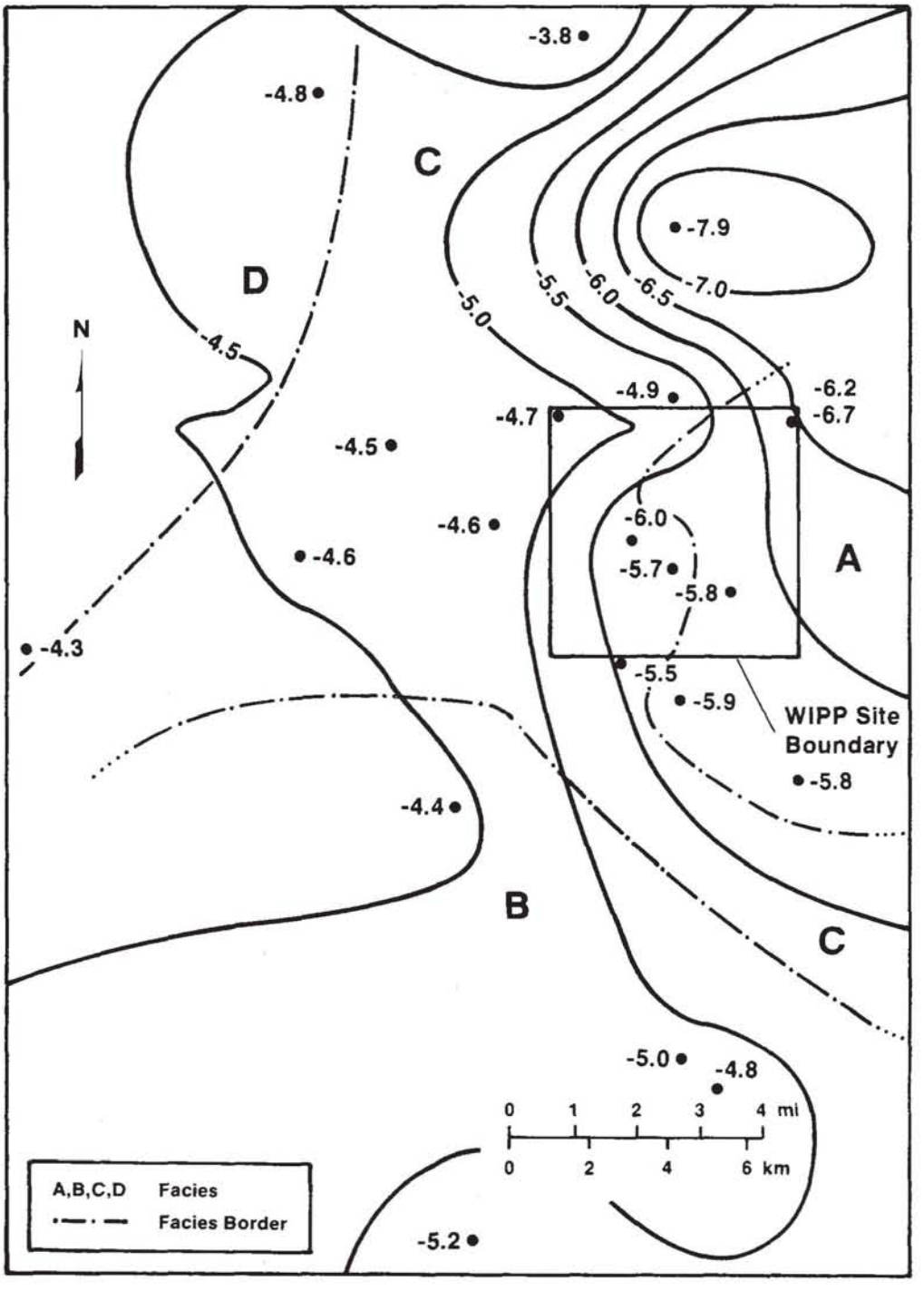

Figure 2-29. Contour plot of varimax R-mode factor scores for factor 2B obtained from the partial-correlation matrix with respect to TDS of Culebra groundwaters (population 1).

data set, in addition to the 13 variables included in the analysis of Culebra data. Only data from the chemical analyses carried out at UNC laboratory and listed in Table 2-2 were used. The results of the analysis pertinent to the primary objective are summarized in this section.

A secondary objective of the analysis of population 2 was to determine if the relationships among chemical variables observed in the Culebra were present in a larger data set drawn from the Rustler and related formations. In Appendix 2D, the solute relationships in population 2 are compared to those of population 1. In addition, the methods of data pretreatment, factor extraction, and rotations, and the factor-loading and score matrices are described in detail in the appendix.

2.3.3.6.1 R-MODE PRINCIPAL COMPONENT ANALYSIS

The Q-mode analysis, described in Appendix 2D, showed that the data set was homogeneous enough for R-mode analysis. R-mode PCA was carried out on this data set in the same manner that it was carried out with data from the Culebra in the previous section. Seven varimax factors that account for nearly all of the variance (99%) were extracted. The factor loadings are described in Table 2D-5 (Appendix 2D); the five most important factors are shown in Figure 2-30. At least 93% of the variance of each variable could be explained by these factors.

Relationships among major solutes in population 2 are similar to those in population 1. The first three principal components shown in Figure 2-30 account for 67% of the total variance of the sample population. For most elements, they are similar to the salinity, sulfate, and silicate/bicarbonate varimax factors (factors 1A, 2A, and 3A) extracted from the Culebra data set (population 1) and shown in Figure 2-2. The two important exceptions are sulfate and magnesium, discussed below.

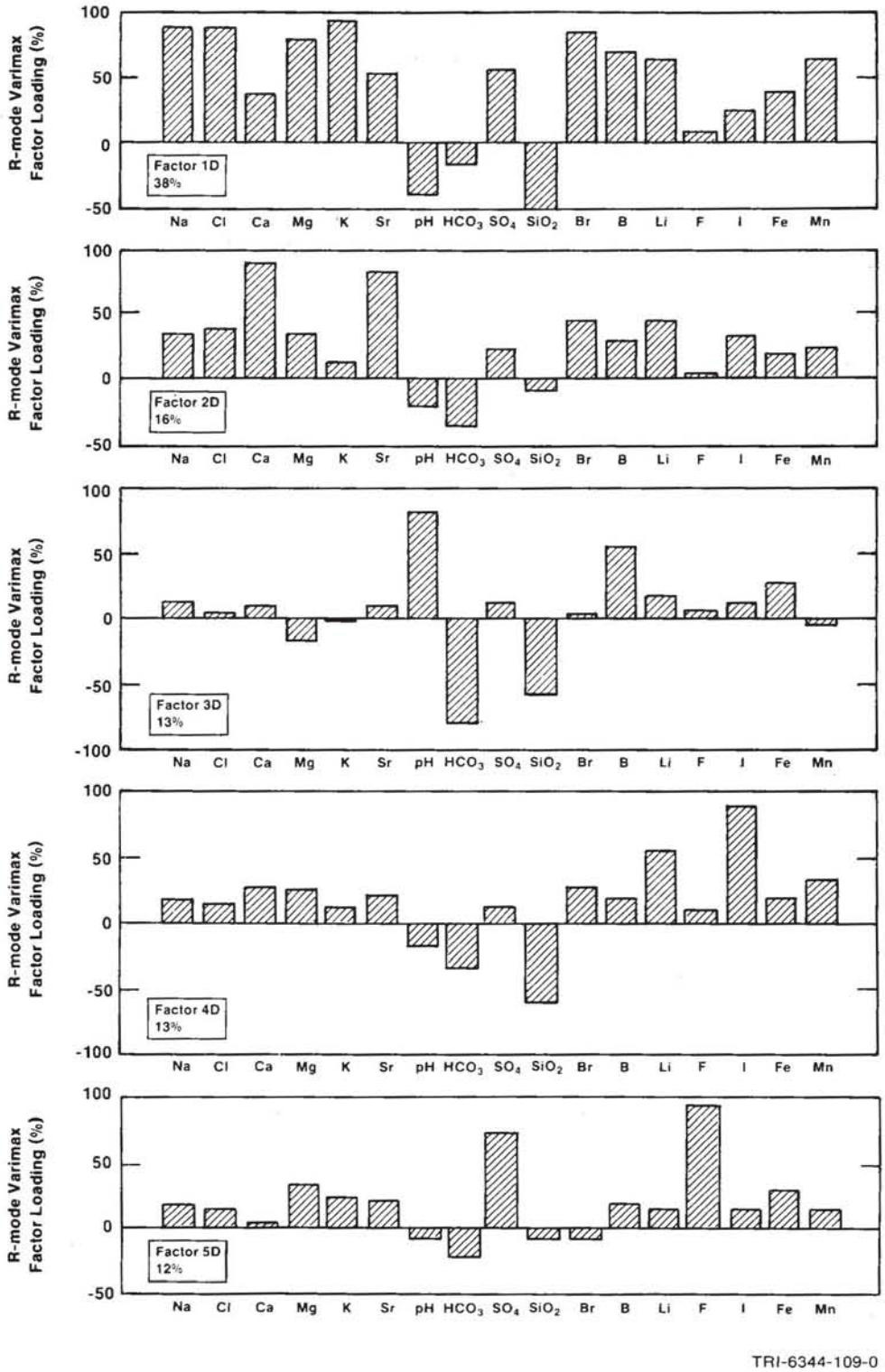

Figure 2-30. Varimax R-mode factor loadings for factors 1D, 2D, 3D, 4D, and 5D of Rustler, Dewey Lake, and Bell Canyon groundwaters (population 2).

The inclusion of data for fluoride concentrations in population 2 affected the factor loadings for sulfate and magnesium in the sulfate and silicate factors. Factor 5D is the most significant factor for both F and SO_4 (see Table 2D-5 in Appendix 2D). Fluorine occurs most commonly in fluorite (CaF_2) and sellaite (MgF_2). Sonnenfeld (1984) notes that typically MgF_2 occurs as an accessory mineral associated with anhydrite, whereas CaF_2 more commonly occurs with carbonates. The association of F, SO_4, and Mg in factor 5D may indicate that MgF_2 in anhydrite is the source of fluoride in these waters.

This PCA also allows an examination of the behavior of iodide, iron, and magnanese. Iodide is correlated with Na and Cl and inversely correlated with Si on all factors. Factor 4D of population 2 is dominated by the behaviors of I, Si, and Li and has no counterpart in the Culebra analysis. The geochemical significance of this factor is unclear. Nearly all of the waters in population 2 are enriched in iodide relative to the seawater evaporation curve (cf. Collins, 1975). Potential sources of the excess iodide include dissolution of iodide from evaporite minerals or organic material and desorption from clays. As discussed in Appendix 2D, examination of the factor scores and element ratios suggests that the relative importance of these sources probably varies vertically and horizontally throughout the study area.

Iron loads primarily onto its own principal component, factor 6D; Mn has an appreciable loading onto this factor also (see Table 2D-5). The lack of correlation between Fe and Mn with other major and minor solutes may be due to random errors in sampling or analyses as discussed in Section 2.2. Manganese also loads strongly onto factor 1D and factor 7D; the geochemical significance of these elemental associations is unclear, but might be related to borehole pipe corrosion.

2.3.3.6.2 R-MODE ANALYSIS WITH SALINITY PARTIALLED OUT

A second R-mode PCA was carried out in which the correlation of each element with the TDS concentration was partialled out. The resulting factor pattern shows the interelement

correlations independent of the effects that may be attributed to halite dissolution. The results are described in Appendix 2D.

2.3.4 Saturation Indices for Culebra Groundwaters

2.3.4.1 Introduction

Calculations of saturation indices of groundwaters are useful in suggesting the identity of the minerals that may control solute concentrations, in detecting evidence of metastable persistence of mineral phases, and in indicating possible errors in chemical analyses or sampling procedures. Saturation indices for common evaporite minerals for Culebra brine samples are presented in Table 2-10.

The calculations were carried out using the geochemical reaction and speciation code PHRQPITZ (Plummer et al., 1988). This code uses a specific interaction model to calculate activity coefficients in the system Na-Ca-Mg-K-H-OH-HCO_3-CO_3-CO_2-SO_4-Cl-H_2O. The theory, data, and implementation are based primarily on previous work by Pitzer and coworkers (Pitzer, 1973, 1975; Pitzer and Kim, 1974; Pitzer and Mayorga, 1973, 1974) and Harvie et al. (Harvie and Weare, 1980; Harvie et al., 1984). Estimates of the maximum ionic strength for which the model accurately predicts mineral solubilities range from 6 to 20 molal. For comparison, the Davies equation used in codes such as PHREEQE (Parkhurst et al., 1980) is accurate up to about 0.5 molal.

Given the dissolution of a solid:

$$M_aL_b \rightarrow aM^{m+} + bL^{n-} \qquad \text{(where } a \cdot m = b \cdot n\text{)} \qquad [1]$$

the equilibrium constant is given by:

$$\log K_{sp} = \frac{-\Delta G_R}{2.303\ RT} \qquad [2]$$

Table 2-10. Mineral Saturation Indices for Culebra Groundwaters

Well[3]	Date	Density (g/mL)	Temp[4] (°C)	Ionic Str.[1]	pH[5]	a_{H_2O}[1]	CBE[1,6]	Saturation Indices[1,2] Anh	Cal	Dol	Gyp	Hal	Mag	log pCO_2[1]
DOE-1	4/85	1.09	22	2.53	7.10	0.923	9.05E-03	-0.12	-0.34	-0.13	0.03	-1.26	-0.62	-2.60
DOE-2	3/85	1.04	22	1.19	7.00	0.968	-6.52E-02	-0.18	-0.21	-0.14	0.01	-2.03	-0.77	-2.33
ENGLE	3/85	1.00	22	0.09	7.40	0.999	1.00E-03	-0.22	0.22	0.38	0.00	-6.02	-0.68	-2.44
H-2A	4/86	1.01	22	0.27	8.00	0.994	-4.33E-03	-0.25	0.45	0.78	-0.04	-3.49	-0.52	-3.38
H-3B3	2/85	1.04	22	1.08	7.40	0.971	-2.53E-03	-0.20	-0.08	0.12	0.00	-2.11	-0.65	-2.86
H-3B3	6/84	1.03	26	1.08	7.40	0.972	-2.56E-02	-0.15	-0.02	0.23	0.04	-2.13	-0.59	-2.83
H-4B	5/81	1.01	22	0.455	8.00	0.991	-1.49E-02	-0.17	0.36	1.07	0.04	-3.13	-0.13	-3.35
H-4B	7/85	1.02	22	0.42	7.70	0.991	4.14E-03	-0.20	0.07	0.46	0.01	-3.17	-0.45	-3.04
H-4C	8/84	1.01	21	0.45	7.80	0.991	4.82E-03	-0.20	0.19	0.77	0.01	-3.12	-0.26	-3.11
H-5B	6/81	1.10	22	2.993	7.90	0.906	-1.18E-01	-0.10	0.71	2.12	0.04	-1.08	0.57	-3.21
H-5B	8/85	1.10	22	2.97	7.40	0.908	8.46E-02	-0.11	-0.02	0.68	0.03	-1.09	-0.15	-2.86
H-5C	10/81	1.10	24	3.002	7.90	0.906	-1.20E-01	-0.08	0.75	2.20	0.05	-1.08	0.61	-3.17
H-6B	5/81	1.04	22	1.178	7.00	0.969	2.24E-04	-0.15	-0.04	0.16	0.05	-2.05	-0.64	-2.16
H-6B	9/85	1.04	22.5	1.13	6.90	0.970	-1.28E-02	-0.20	-0.16	-0.07	-0.01	-2.08	-0.75	-2.07
H-7B1	3/86	1.00	22	0.089	7.20	0.999	-4.09E-04	-0.23	0.07	0.01	-0.01	-5.86	-0.90	-2.20
H-8B	1/86	1.00	22	0.083	7.60	0.999	-1.97E-04	-0.23	0.33	0.66	-0.01	-7.45	-0.52	-2.70
H-9B	11/85	1.00	22	0.087	7.40	0.999	3.70E-04	-0.22	0.24	0.37	0.00	-6.23	-0.71	-2.43
H-11B3	6/85	1.09	22.7	2.23	7.20	0.934	-3.60E-02	-0.13	-0.17	0.12	0.03	-1.39	-0.54	-2.63
H-12	8/85	1.10	24	2.72	7.20	0.916	4.42E-02	-0.12	-0.15	0.34	0.02	-1.18	-0.35	-2.61
P-14	2/86	1.02	21.5	0.582	6.80	0.988	-9.06E-03	-0.15	0.14	0.18	0.05	-3.01	-0.81	-1.81

Table 2-10. Mineral Saturation Indices for Culebra Groundwaters (Continued)

Well[3]	Date	Density (g/mL)	Temp[4] (°C)	Ionic Str.[1]	pH[5]	a_{H_2O}[1]	CBE[1,6]	Saturation Indices[1,2] Anh	Cal	Dol	Gyp	Hal	Mag	log pCO_2[1]
P-17	3/86	1.06	21.2	1.67	7.50	0.953	-3.61E-02	-0.18	0.10	0.73	0.00	-1.70	-0.22	-2.90
WIPP-25	8/80	1.01	23	0.26	6.90	0.995	3.21E-03	-0.24	0.03	0.04	-0.03	-3.56	-0.84	-1.69
WIPP-26	8/80	1.00	22	0.329	6.90	0.993	-5.12E-03	-0.18	-0.04	-0.10	0.03	-3.36	-0.91	-1.86
WIPP-26	8/80	1.01	22	0.330	6.90	0.993	-3.71E-02	-0.23	0.09	0.14	-0.02	-3.32	-0.79	-1.84
WIPP-26	11/85	1.01	22	0.371	7.10	0.992	-9.29E-03	-0.20	0.10	0.18	0.02	-3.22	-0.77	-2.14
WIPP-27	9/80	1.09	22	2.573	6.30	0.922	-7.62E-02	-0.12	-0.38	-0.40	0.03	-1.29	-0.87	-1.33
WIPP-28	9/80	1.03	22	0.903	6.50	0.976	-2.42E-02	-0.26	0.16	0.53	-0.07	-2.27	-0.48	-0.76
WIPP-29	8/80	1.16	20	4.908	6.10	0.840	-2.06E-01	0.02	-0.72	0.01	0.09	-0.61	-0.21	-0.87
WIPP-29	8/80	1.17	20	4.472	6.10	0.853	-2.74E-01	-0.15	-0.45	0.61	-0.07	-0.64	0.21	-1.10
WIPP-29	12/85	1.22	21.5	6.57	5.90	0.773	-2.07D-01	-0.01	-1.25	-0.56	-0.01	-0.20	-0.16	-0.75
WIPP-30	9/80	1.02	21	0.582	8.80	0.986	-2.50E-02	-0.18	1.12	2.37	0.02	-2.73	0.41	-4.41

1. Unless otherwise indicated, the solute data from UNC Geotech given in Table 2-2 were used in the PHRQPITZ (Plummer et al., 1988) calculations of the ionic strength (molal), the activity of water (a_{H_2O}), the charge-balance error, the log pCO_2 (atm.), and the saturation indices.
2. Anh = anhydrite; Cal = calcite; Dol = dolomite; Gyp = gypsum; Hal = halite; Mag = magnesite.
3. Samples from WIPP-26 and WIPP-29 were analyzed by the USGS Central Laboratory; the data are given in Mercer (1983).
4. Temperature measured at the wellhead during sampling test and assumed in saturation-index calculations.
5. The pH values used in the PHRQPITZ calculations; a few differ slightly from those given in Table 2.
6. The charge-balance error (CBE in equivalents per kilogram of water) was calculated as: CBE (eq/kg H_2O) = Σ cations (eq/kg H_2O) - Σ anions (eq/kg H_2O)

where ΔG_R is the free energy of reaction [1] in units of Kcal/mol, R is the gas constant, and T the absolute temperature.

Saturation indices (SI) are calculated as:

$$SI = \log IAP - \log K_{sp} \qquad [3]$$

where the IAP is the ion activity product in the solution ($[M^{m+}]^a \cdot [L^{n-}]^b$).

At saturation, the saturation index equals zero; positive and negative values indicate supersaturation and undersaturation, respectively. All of the saturation index calculations in this report used unscaled activity coefficients (Plummer et al., 1988).

2.3.4.2 Saturation Indices of Sulfates

Figure 2-31 illustrates the relationship between ionic strength and the saturation indices of gypsum ($CaSO_4 \cdot 2H_2O$) and anhydrite ($CaSO_4$). All water samples are saturated (SI = 0.00 ± 0.09) with respect to gypsum. This is expected given the common presence of gypsum in the Culebra (Sewards et al., Chapter 3) and the rapid dissolution rates of this mineral under natural conditions (Back et al., 1983).

With the exception of the Culebra samples from WIPP-29 (collected in 9/80 and 12/85 and analyzed by UNC), all samples are undersaturated with respect to anhydrite. Saturation with respect to anhydrite is related to the high ionic strengths of these waters. As discussed previously, the high salinities of these waters are caused by contamination from nearby potash refining operations.

Previous calculations for groundwaters from the Culebra showed nontrivial deviations from gypsum saturation. These may have been due in part to the failure of the ion-pairing

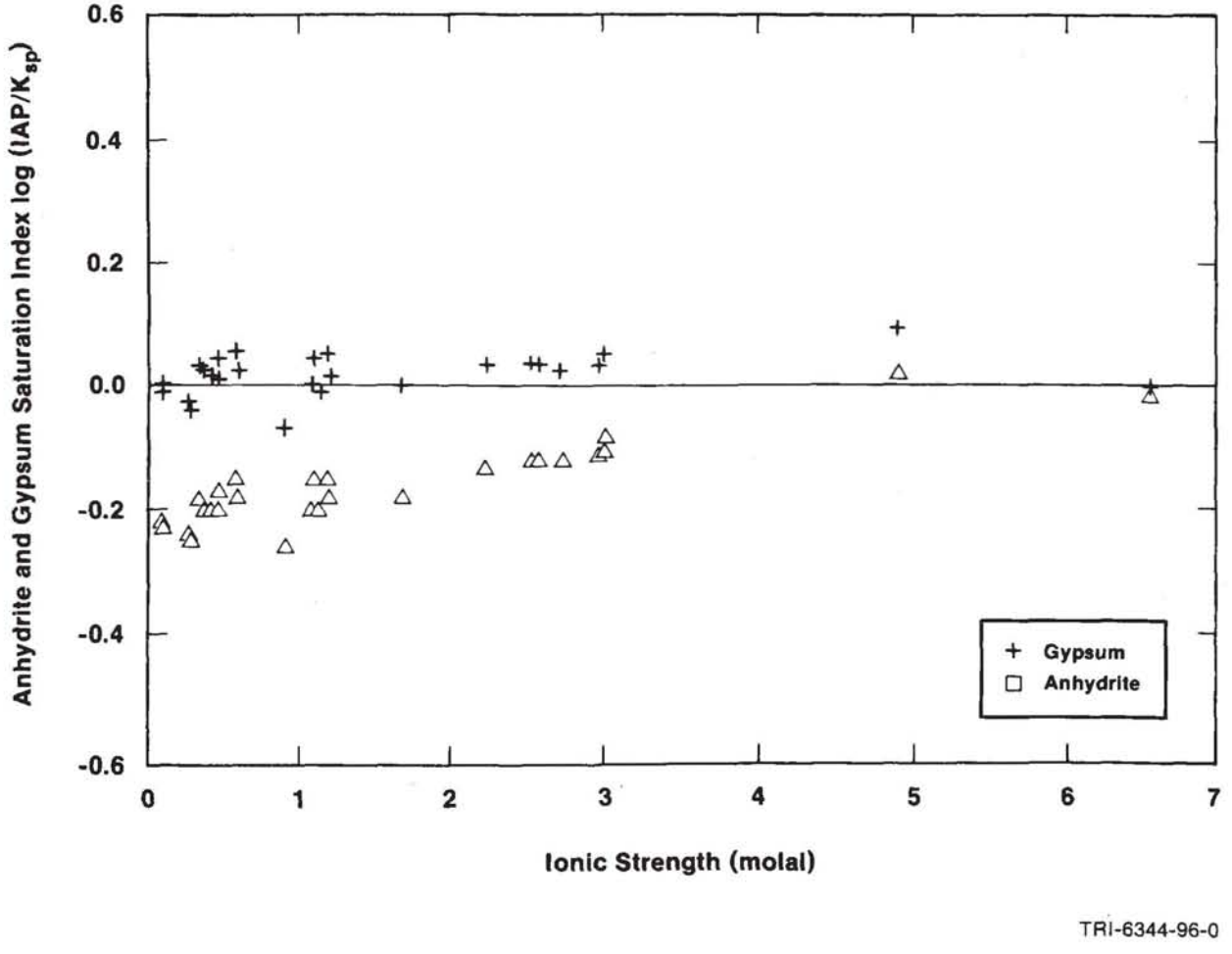

Figure 2-31. Relationship between anhydrite and gypsum saturation indices and ionic strengths of Culebra groundwaters.

chemical model used in WATEQFC and PHREEQE at high ionic strength (Ramey, 1985; Meijer et al., 1987). The calculations presented here show excellent agreement between field observations and predictions based on thermodynamic data.

2.3.4.3 Saturation Indices of Evaporite Salts

Figure 2-32 shows the relationship between ionic strength and the calculated saturation indices for halite. All of the waters analyzed from the Culebra are undersaturated with respect to this mineral. Saturation indices were also calculated for other common evaporite salts (listed in Table 2A-1); all waters were undersaturated with respect to these minerals.

2.3.4.4 Saturation Indices of Carbonates

Figures 2-33 and 2-34 show saturation indices for dolomite and calcite as functions of ionic strength. Many of the samples show appreciable supersaturation or undersaturation with respect to these carbonates. It has been suggested that waters in carbonate aquifers that are older than several hundreds of years should be saturated with these phases (Meijer et al., 1987). Available radiocarbon ages for Culebra waters suggest that they are at least 10,000 years old (Lambert, Chapter 5); thus, the apparent lack of carbonate equilibrium is problematic.

Previous saturation-index calculations for Culebra waters using the PHREEQE and WATEQFC codes also indicated that some samples were supersaturated with respect to the carbonate minerals (Ramey, 1985; Meijer et al., 1987). It was suggested that calculated deviations from saturation were due in part to failures of the aqueous model used in these codes. However, it is unlikely that the supersaturations calculated in Table 2-10 are due to errors in the aqueous model because the Pitzer formulation for the activity coefficients used in PHRQPITZ has been validated against experimental data (Plummer et al., 1988) in chemical systems similar to the Culebra waters. The version of PHRQPITZ used in these calculations does not include speciation of boron. This exclusion introduces a potential

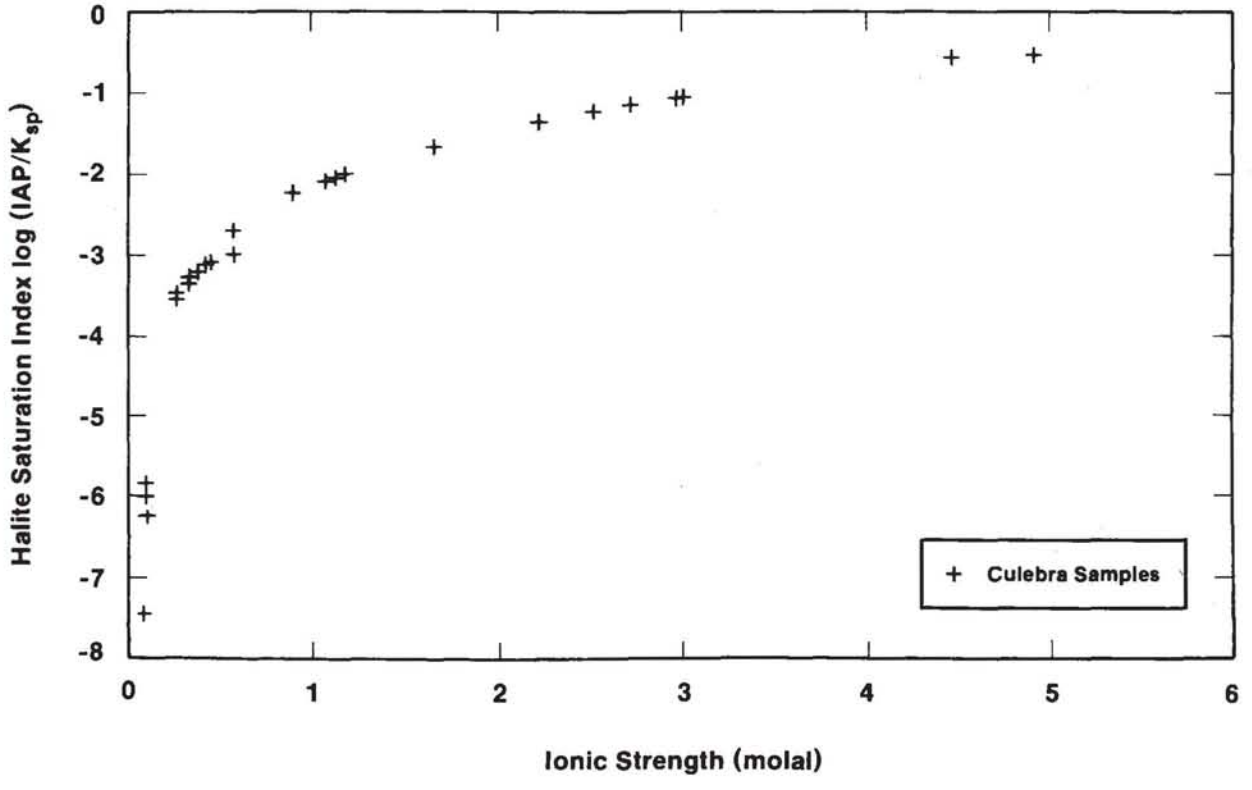

Figure 2-32. Relationship between halite saturation indices and ionic strengths of Culebra groundwaters.

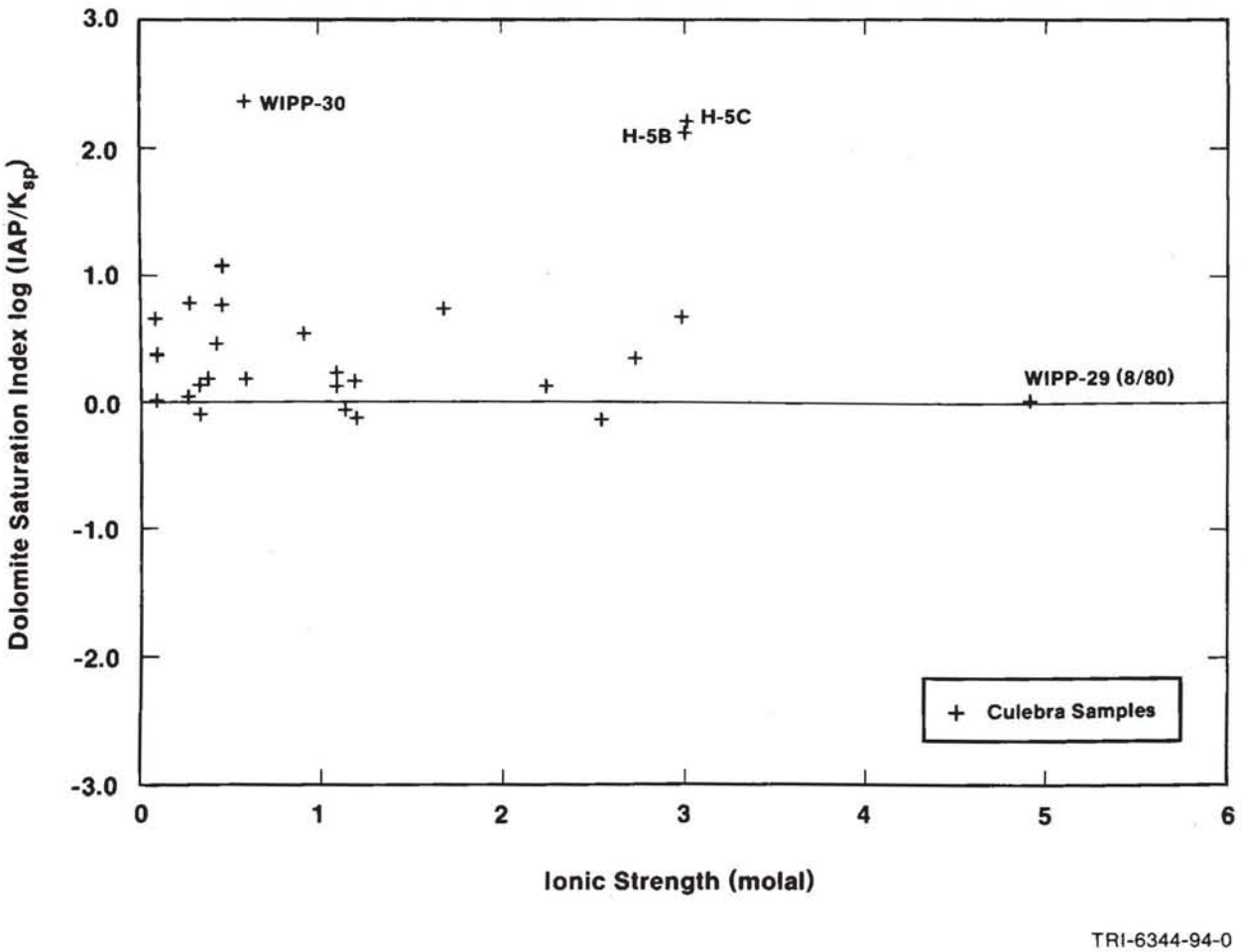

Figure 2-33. Relationship between dolomite saturation indices and ionic strengths of Culebra groundwaters.

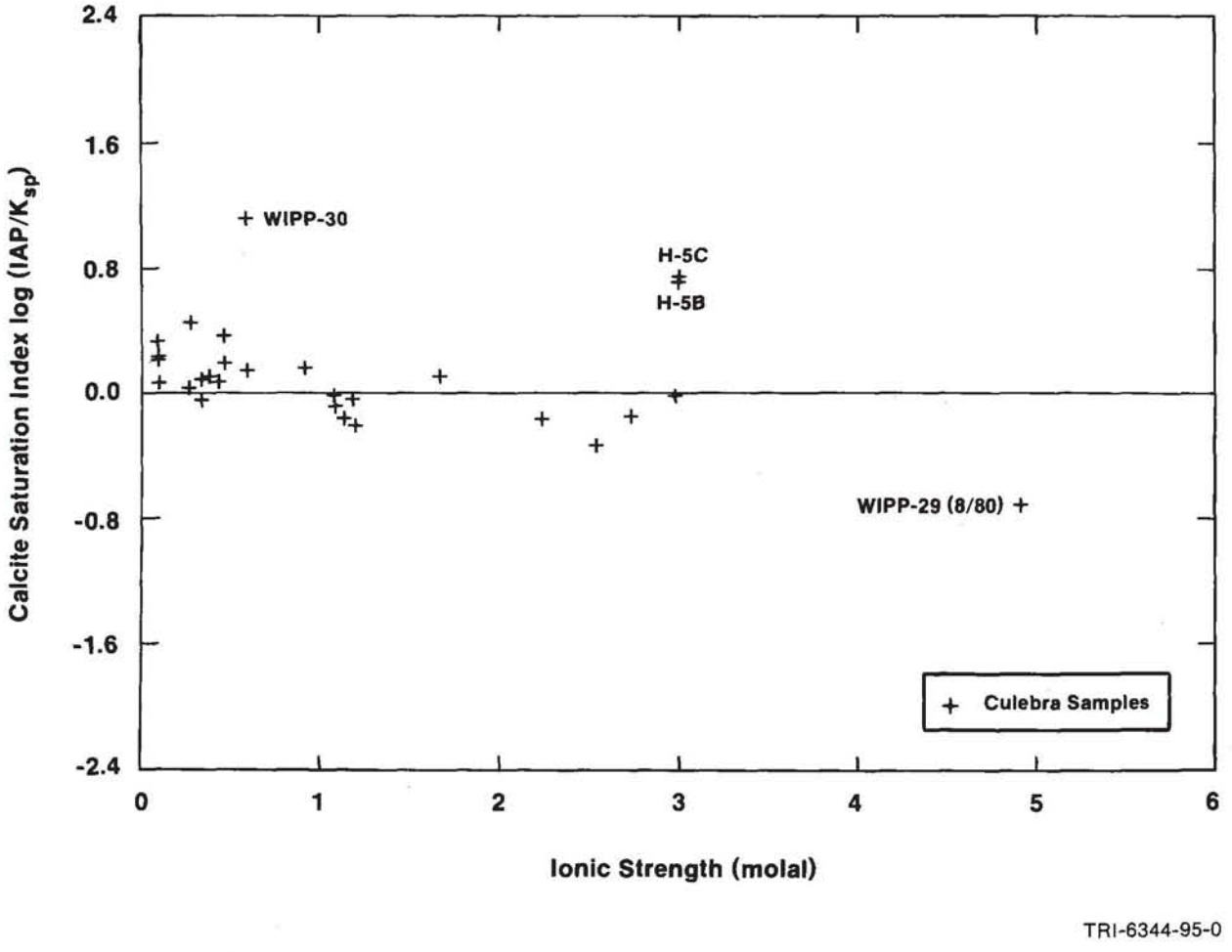

Figure 2-34. Relationship between calcite saturation indices and ionic strengths of Culebra groundwaters.

source of error in the calculated exclusion total inorganic carbon and carbon speciation. As discussed in Section 2.2.3.2, however, the low concentrations of boron in these waters suggest that this error is relatively small. This suggests that the calculated disequilibria may be real or due primarily to other factors such as errors in chemical analysis or sampling.

Errors in analysis of calcium could be responsible for errors in the saturation indices for the carbonates. However, the near-zero values of saturation indices for gypsum reported above and shown in Figure 2-35 suggest that this is not the cause of the calculated super-saturation.

In the following sections, several other possible sources of error are discussed. These include errors associated with pH measurements in brines, uncertainties in the free energies of carbonate solid phases, and CO_2 gas loss during sampling.

Finally, evidence that the Culebra waters are actually supersaturated with respect to dolomite and/or calcite is summarized.

2.3.4.4.1 UNCERTAINTY IN pH MEASUREMENTS IN BRINES

The inconsistency between the activity scales of the measured pH and the computed ion activities can lead to errors in calculated saturation indices. As discussed by Plummer et al. (1988), the activity scales are different because the buffers used to define the pH do not have the same composition as the brine of interest. In addition, due to the liquid-junction potentials, the measured pH is subject to deviations that are not accounted for in the theoretical speciation calculations.

Plummer et al., (1988) show that the magnitude of the error introduced by the use of different activity scales in a speciation calculation can be large, especially for the carbonate system. Plummer et al. (1988, sample problem 1) show that the saturation index for

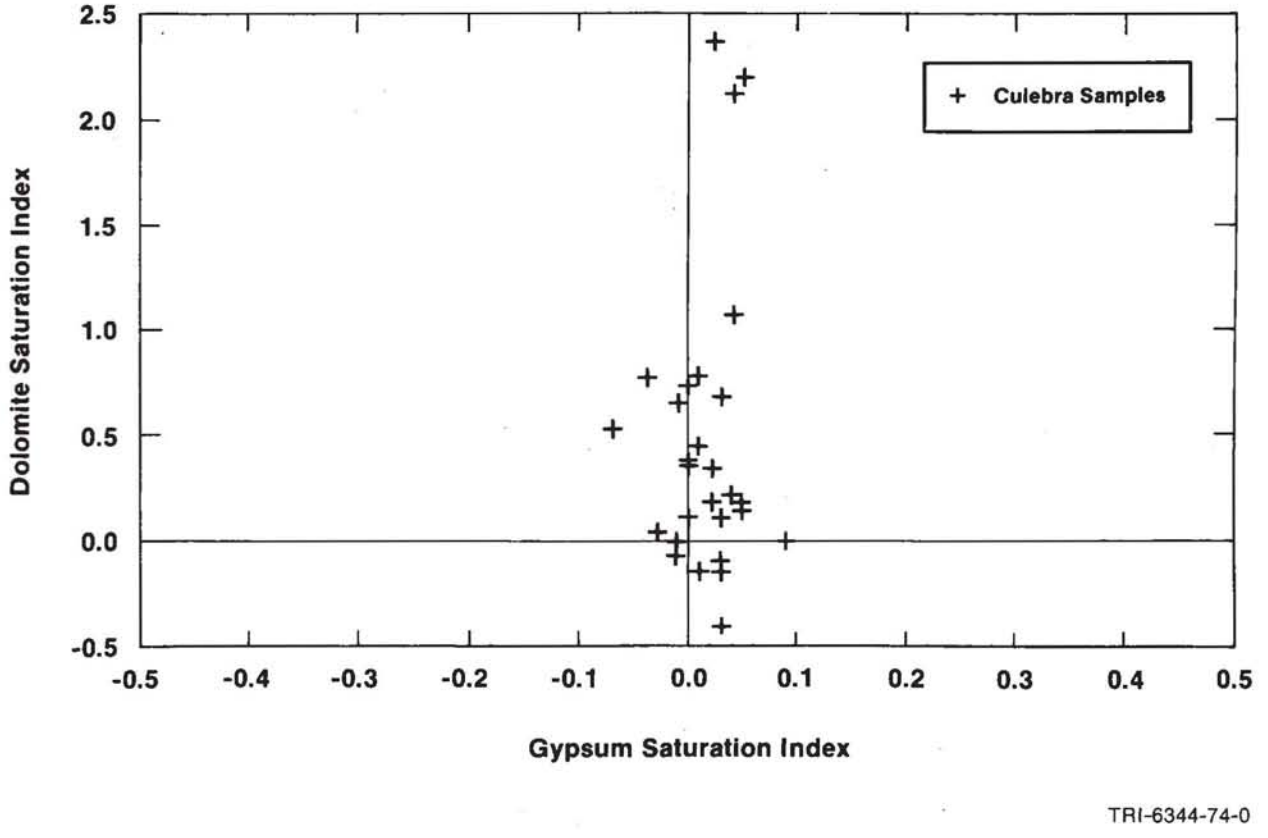

Figure 2-35. Relationship between gypsum and dolomite saturation indices in Culebra groundwaters.

dolomite calculated with two different commonly used scales varies from -1.08 (MacInnes scale) to -0.13 (not adjusted or unscaled) in a Canadian Shield brine sample (ionic strength of 8.5). They also show for the saline brine that the computed total concentration of inorganic carbon and pCO_2 varied by 300%, depending on the scale convention used. The error in less saline brines is also significant; individual ion activities in seawater (I = 0.7m) were shown to differ by as much as 10% when calculated with different scales.

In this study, all saturation indices are calculated with unscaled activities. The activity scale error may be responsible for part of the apparent supersaturation in the saturation indices shown in Figures 2-33 and 2-34. Only if the total alkalinity and either total inorganic carbon or pCO_2 are measured can the carbonate system be unambiguously defined. With such an approach, the pH is calculated rather than measured and problems associated with the different activity scales are avoided.

2.3.4.4.2 UNCERTAINTY IN THERMODYNAMIC DATA FOR MINERAL PHASES

Calculations of dolomite saturation indices for Culebra water samples are hindered by lack of reliable values for the free energy of the Culebra dolomite. Studies of carbonates from other areas (Reeder and Wenk, 1979; Reeder, 1981) suggest that nonstoichiometry and disorder may be sources of uncertainty in the Gibbs free energy of formation of the Culebra dolomites. Figure 2-36 compares saturation indices calculated using three different reference values for the free energy of dolomite. Note that these calculations were carried out with the EQ3NR computer code (Wolery, 1983) using the water composition data reported by Uhland and Randall (1986). The thermodynamic data base for EQ3NR contains free energies for disordered (EQ3NR-DIS) and ordered (EQ3NR-ORD) dolomites. Saturation indices calculated with EQ3NR with the free energy for dolomite found in the PHRQPITZ data base are also shown.

Figure 2-36 shows that the uncertainty in the saturation index of dolomite resulting from the choice of the value of free energy is about 1.5 units. This potential error is as large as

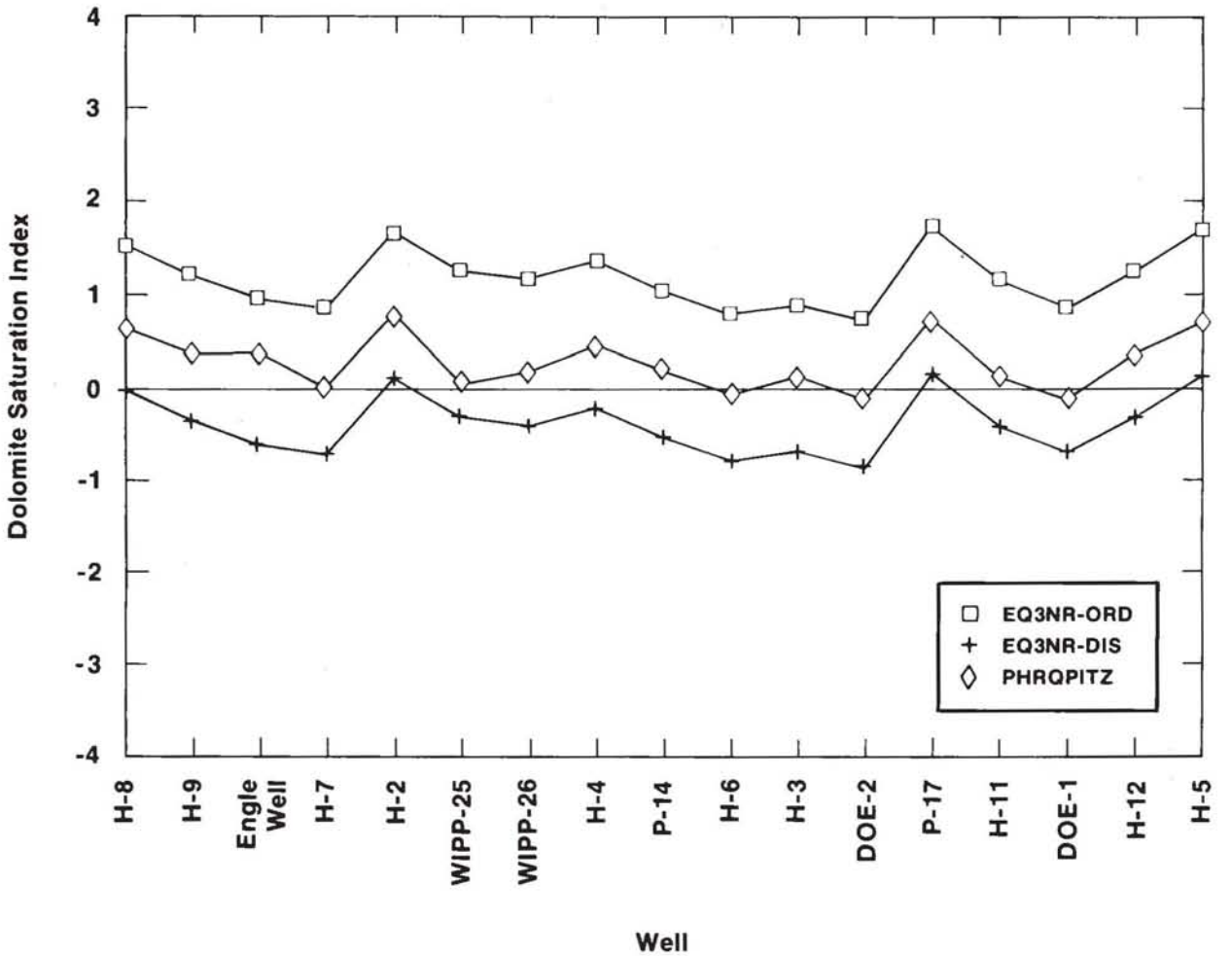

Figure 2-36. Dolomite saturation indices calculated for Culebra groundwaters using alternative values for the ΔG_f of dolomite. (SI = log [IAP/K_{sp}]. EQ3NR-ORD = value for "ordered" dolomite from the data base of EQ3NR [Wolery, 1983]; EQ3-DIS = value for "disordered" dolomite from EQ3NR data base; PHRQPITZ = data for dolomite from PHRQPITZ data base. Wells are arranged in order of increasing ionic strength).

or larger than the degree of supersaturation calculated for most of the samples in Figure 2-33.

2.3.4.4.3 *ERRORS RELATED TO LOSS OF CO_2 GAS DURING SAMPLING*

In the PHRQPITZ calculations described above, the pCO_2 and saturation indices were calculated from the field pH and alkalinity. The relationship in these samples between pH and saturation indices for dolomite and calcite are shown in Figures 2-37 and 2-38.

Changes in pH due to loss of CO_2 gas during water sampling result in apparent supersaturation of carbonate minerals; H^+ production from oxidation of Fe^{+2} results in apparent undersaturation (Bassett, 1982). For solutions at equilibrium with calcite in the pH range of waters in the Culebra (pH ~6 to 8), the error in the measured pH, ΔpH (where $\Delta pH = pH_{measured} - pH_{equilibrium}$), is equal to the saturation index (i.e., ΔpH = SI) (Pearson et al., 1978). For such waters, plots of saturation index versus pH have slopes of unity and two for calcite and dolomite, respectively.

Bassett (1982) calculated saturation indices for calcite and dolomite for 121 brines from the Permian Wolfcamp carbonates in the Palo Duro, Dalhart, and Anadarko Basins. Many of those water samples are apparently supersaturated with respect to these phases; others are apparently undersaturated. Bassett estimated the pCO_2 of the Wolfcamp samples before outgassing using the code AQ/SALT and found that the calculated values were similar to those measured in waters in natural gas reservoirs in the Texas Panhandle. He suggested that these results indicate that pCO_2 in both sets of waters were buffered by equilibrium with carbonates but that the Wolfcamp brines lost CO_2 during sampling.

Pearson et al. (1978) have estimated the significance of this effect for several dilute calcium-bicarbonate well waters. They calculated the pH from the total inorganic carbon and pCO_2 measured in the laboratory and compared it to field pH. They showed that in warm (T = 55°C), weakly-buffered waters (alkalinity = 90-140 mg/L HCO_3^-) an error of 1 pH

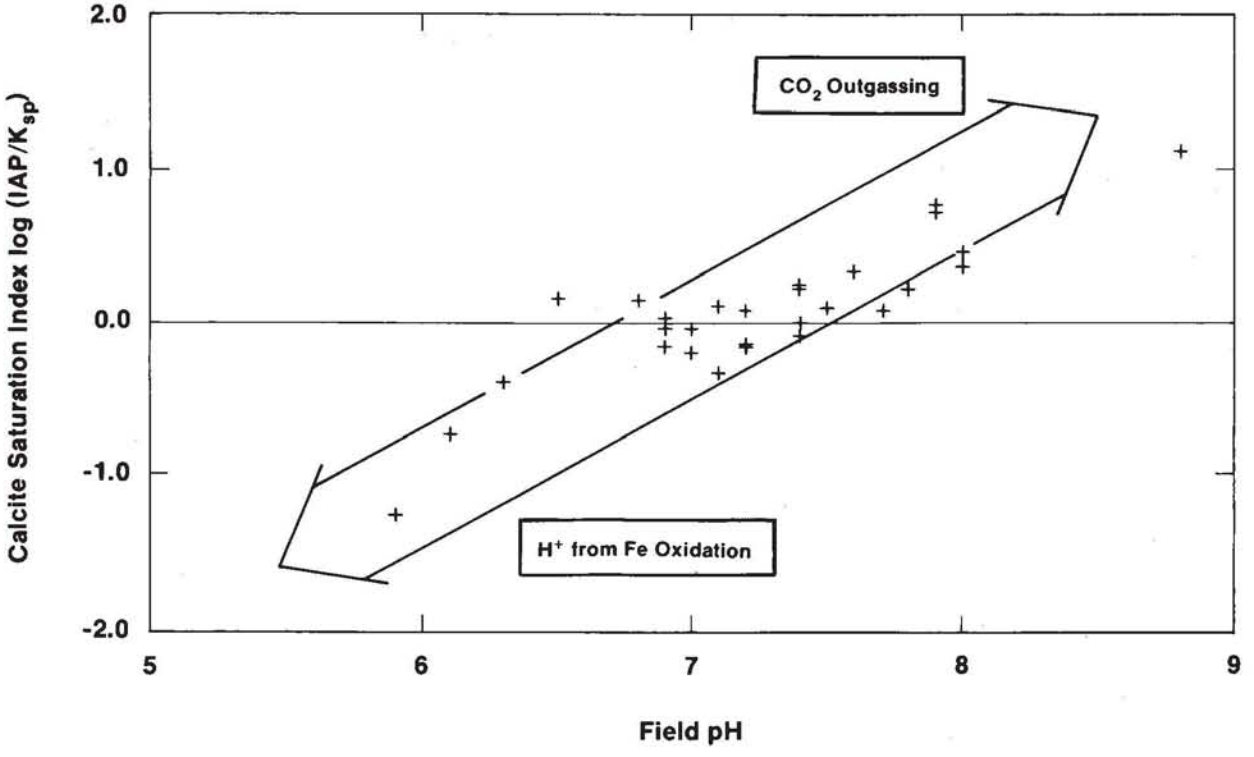

Figure 2-37. Relationship between calcite saturation indices and field pH values for Culebra groundwaters.

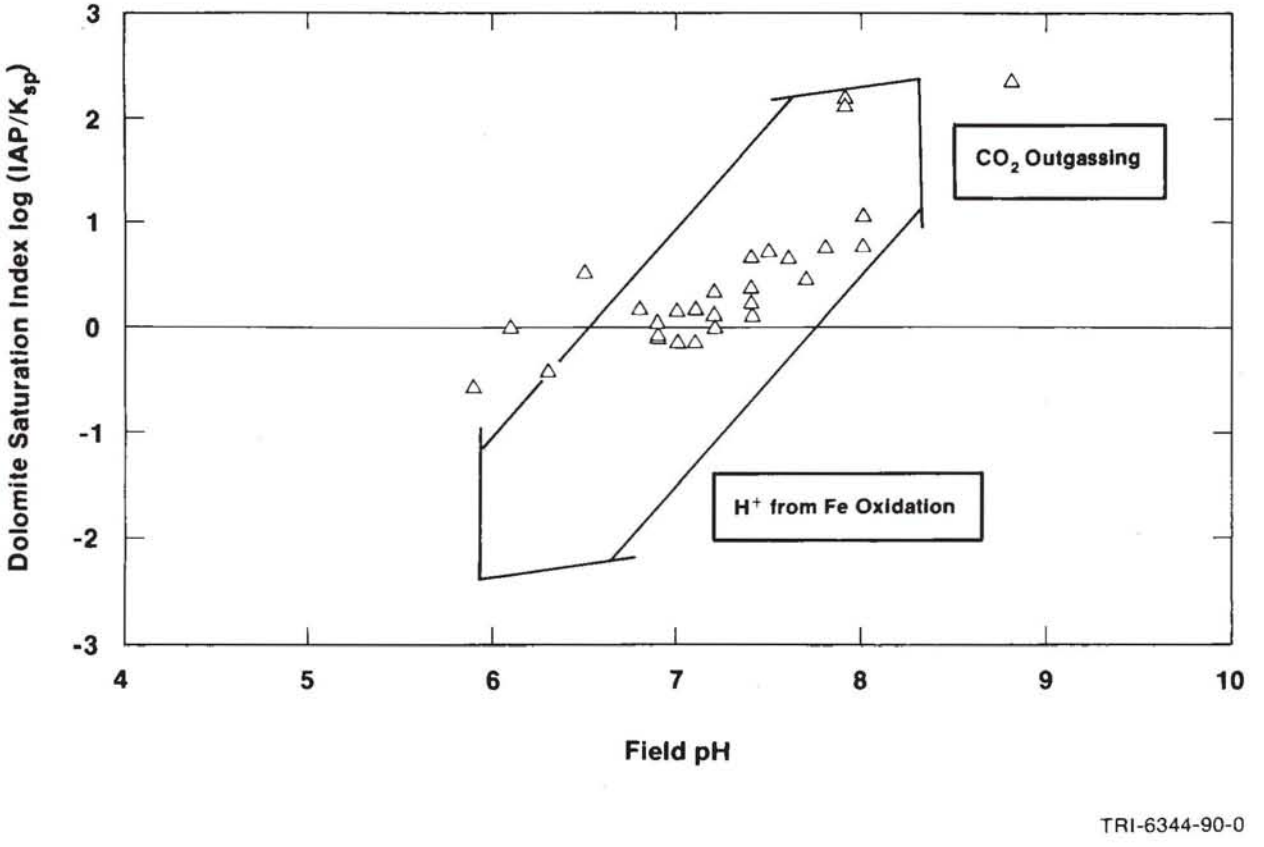

Figure 2-38. Relationship between dolomite saturation indices and field pH for Culebra groundwaters.

unit and 1 log unit in the computed calcite saturation index is possible. In cooler waters, the rates of CO_2 loss are lower and the probable error is smaller (about 0.3 pH units).

Many of the data in Figures 2-37 and 2-38 lie along trends that are consistent with the aforementioned mechanisms leading to errors in the field pH. Arrows with slopes of unity and two slopes are superimposed on the data in Figures 2-37 and 2-38, respectively. Most of the plotted points fall between the parallel sides of arrows. There are considerable deviations from these trends, however, and the width of the arrows would have to be very large to accommodate all of the data, suggesting that other processes may also be affecting the saturation indices.

2.3.4.4.4 EVIDENCE OF SUPERSATURATION OF CARBONATE MINERALS

Meijer et al. (1987) suggest that one can determine the degree of carbonate mineral saturation independent of the effects of CO_2 outgassing by examining the value of the saturation index expression:

$$2\,SI_{calcite} - SI_{dolomite} .$$

The value of this expression is independent of the uncertainty in the carbonate ion activity and equals zero when the solution is saturated with respect to both calcite and dolomite. Based on the near zero values of the saturation index expression, Meijer et al. concluded that the waters from the H-3B3 well were saturated with respect to both dolomite and calcite.

Figure 2-39 shows that the value of the saturation index expression for the Culebra waters decreases as a function of ionic strength. This indicates that when the effects of the CO_2 outgassing are corrected for, it can be seen that many of these waters are supersaturated with respect to dolomite and/or undersaturated with respect to calcite. The degree of

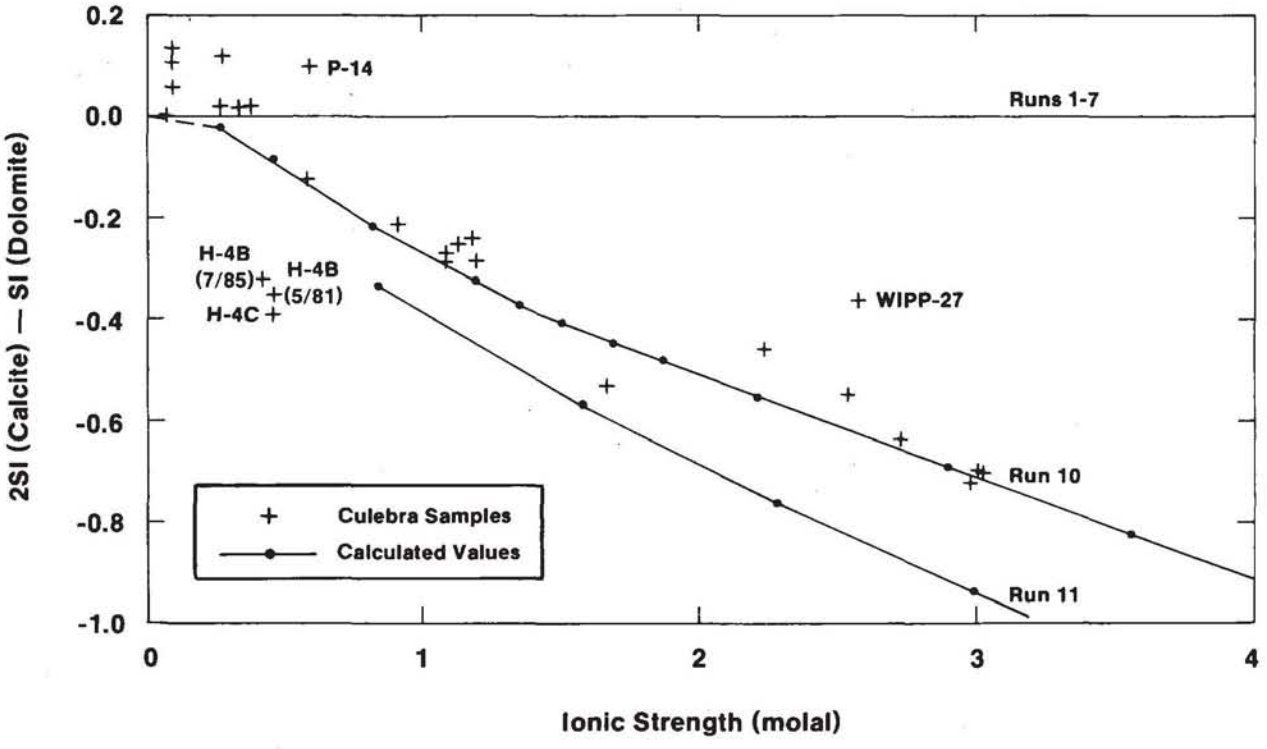

Figure 2-39. Relationship between saturation index expression ($2SI_{calcite} - SI_{dolomite}$) and ionic strengths for Culebra groundwaters.

disequilibrium increases with ionic strength; a chemical model that accounts for this trend is described in the next section.

2.4 DISCUSSION: PROCESSES AFFECTING WATER CHEMISTRY

2.4.1 Introduction: Summary of Important Solute Relationships

In the previous sections, the complementary techniques of plotting spatial distributions of solutes and element ratios, factor analysis, and thermodynamic models have been used to summarize solute relationships in the Culebra waters. Several of these relationships may provide indications of the chemical processes that affect the groundwater composition.

The following solute relationships were described in the preceding sections:

- Increase in concentrations of Na, Cl, Ca, Mg, K, SO_4, Br, B, and Li with ionic strength. This relationship can be seen by examination of the data in Table 2-1 and is illustrated by the "salinity factors" described in Section 1.4.3 and by simple scatterplots such as Figure 2-40, where the total analytical concentrations of calcium and sulfate and the saturation quotient of gypsum and anhydrite are shown as functions of chloride concentration.

- The increase in the Mg/Ca ratio as the ionic strength increases (cf. Figure 2-19).

- The near-perfect saturation of the solutions with respect to gypsum over the entire range of ionic strength. Figure 2-40 shows that while the saturation indices (expressed as IAP/K_{sp}) for gypsum and anhydrite are nearly constant over the entire range of chloride the concentration up to 180,000 mg/L, the sum of the concentrations of calcium and sulfate increase nearly continuously. Any local deviation in the trend of increasing calcium concentration is offset by a deviation in sulfate concentration due to the

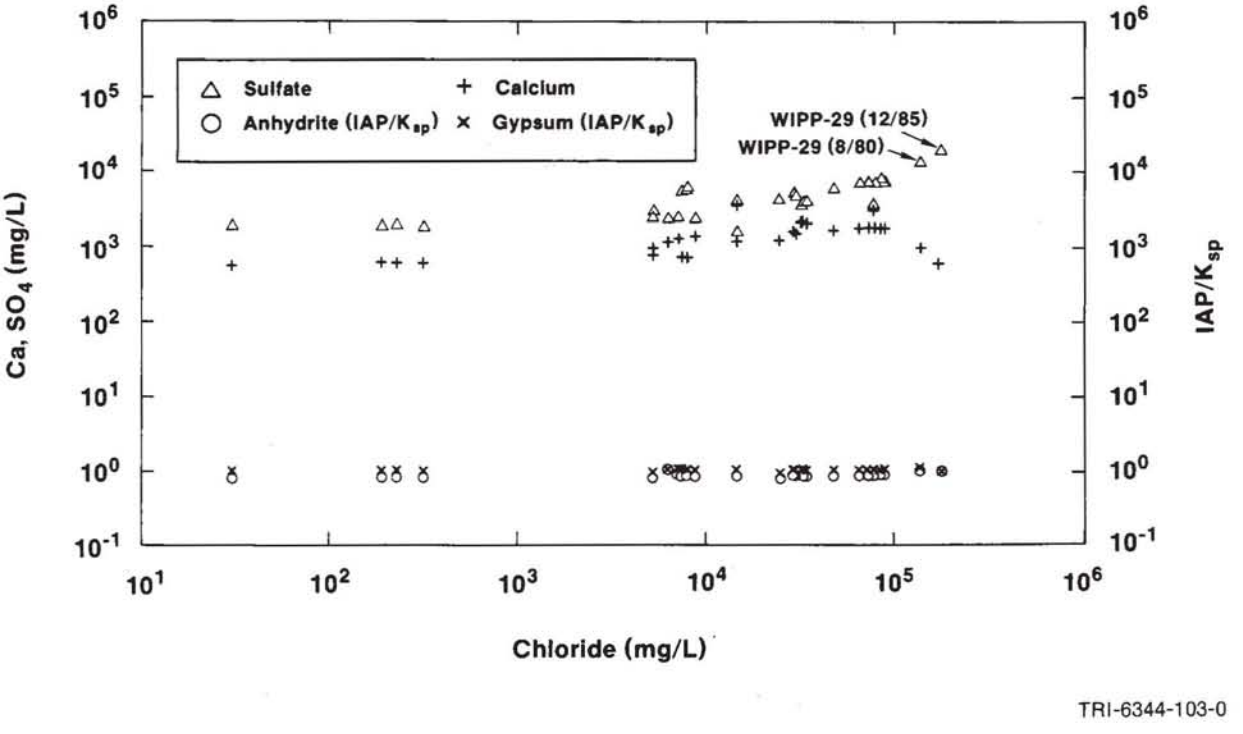

Figure 2-40. Calcium sulfates in Culebra groundwater samples.

saturation control exerted by equilibrium with gypsum. For example, in the two WIPP-29 samples, sulfate concentrations are anomalously high, and calcium concentrations are correspondingly low.

- The apparent supersaturation of dolomite. Outgassing of CO_2 during sample collection is a probable source of error in the pH and calculated saturation indices. However, a saturation index expression independent of this uncertainty indicates that the degree of supersaturation increases with ionic strength (cf. Figure 2-39).

- Negative correlation between pH and bicarbonate alkalinity shown in the "silicate/bicarbonate factor" (e.g., factor 2B described in Section 2.3.3.5). This relationship may be an artifact of the CO_2 outgassing or may reflect an underlying reaction whose effects are not completely obscured by the the pH shift associated with the CO_2 loss.

- An underlying correlation of Mg with SiO_2 and negative correlation of both these elements with Li and B observed after the effects of salt dissolution are factored out. This relationship is most clearly indicated by the "silicate/ bicarbonate factor."

In the Rustler Formation, two broad types of chemical processes are likely to affect the water chemistry and produce the above solute relationships: (1) precipitation and dissolution of carbonates, sulfates, halite, and other evaporite salts; and (2) ion exchange and silicate diagenesis involving clays that occur as fracture linings and matrix inclusions.

The purpose of this section is to describe these processes, discuss their probable importance and provide a conceptual framework within which future hydrochemical, mineralogical, and petrographic studies can be conducted. Section 2.4.2 describes the effect of ionic strength on the solubilities of carbonate and sulfate minerals present in the Culebra. The PHRQPITZ code is used to evaluate the effect of reactions involving these minerals and other evaporite salts on groundwater composition. Section 2.4.3 assesses the

effect of reactions involving silicate minerals on the concentrations of several solutes (Si, Li, B, and Mg). Other processes that may affect the groundwater composition are discussed in Section 2.4.4.

2.4.2 Precipitation and Dissolution

2.4.2.1 Salt Dissolution as an Irreversible Process in Partial Equilibrium Systems

In this study, saturation indices for groundwaters have been used to identify minerals that may control solute concentrations and to determine if the water is capable of dissolving additional rock. However, as Plummer (1984) notes, even if the saturation index of a mineral is zero, this does not indicate whether the mineral is at equilibrium in the system or is continually responding to an irreversible process. In the latter case, the system is said to be at partial equilibrium, and the mineral/water equilibria are shifting along a reaction path driven by the irreversible process. Examples of irreversible processes are temperature and pressure changes, changes in activity coefficients due to changes in salinity that might accompany dissolution of salt, or addition of a component by the exposure of certain minerals (e.g., nodules in a dissolving matrix).

Halite and other evaporite salts are strongly undersaturated in groundwaters in the Culebra dolomite. It is likely that dissolution of halite in strata adjacent to the Culebra acts as an irreversible driving force for changes in water composition. The dissolution of evaporite salts will add solutes directly and will also increase the solubilities of gypsum, calcite, and dolomite as discussed below.

Figure 2-41 shows the relationship between ionic strength and the unscaled activity coefficients for magnesium, calcium, sulfate, and carbonate in the Culebra samples. The unscaled activity coefficients were calculated for the specific composition of each water sample with the PHRQPITZ code (Plummer et al., 1988), according to the formalism described by Pitzer and coworkers (Pitzer, 1973, 1975; Pitzer and Kim, 1974; Pitzer and

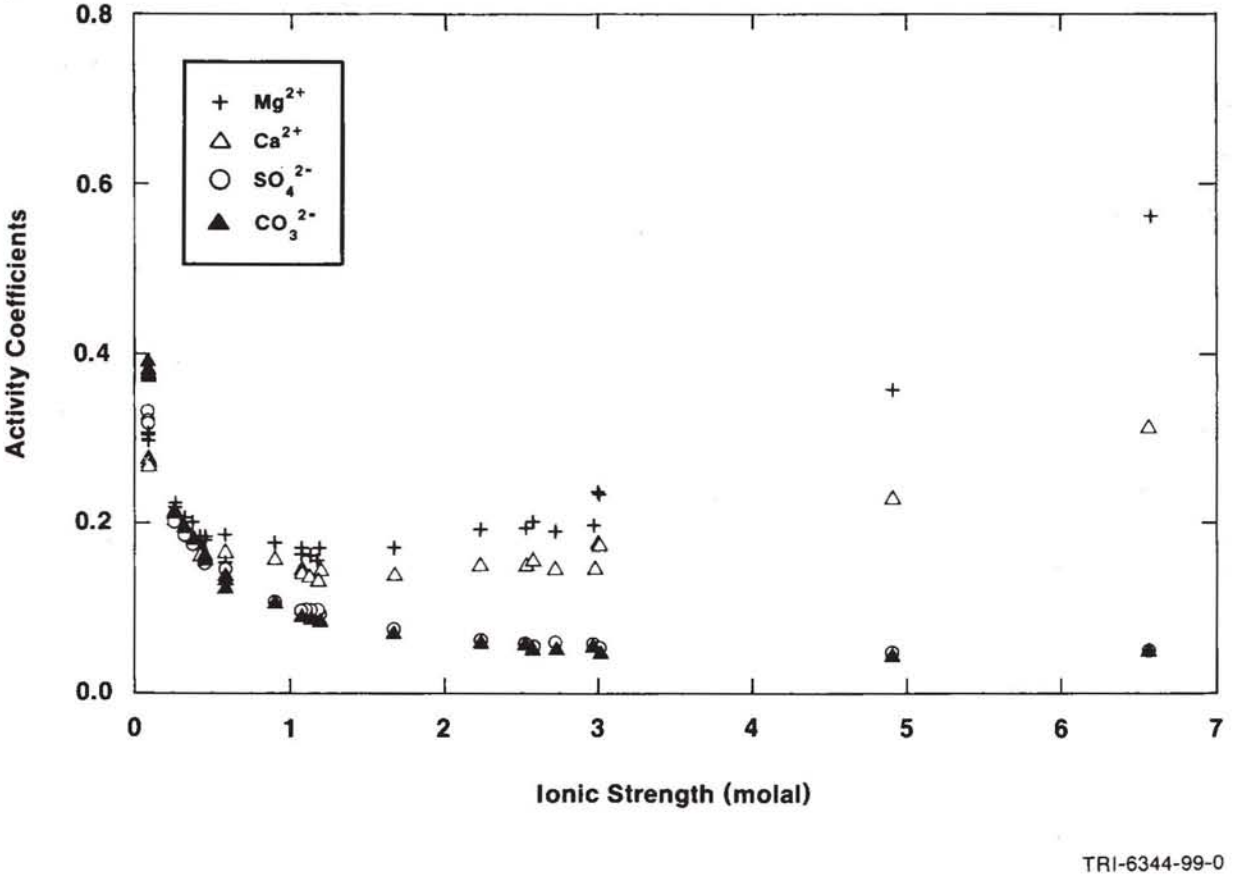

Figure 2-41. Relationships between activity coefficients for magnesium, calcium, sulfate, and carbonate, and ionic strengths of Culebra groundwaters.

Mayorga, 1973, 1974), and using the UNC Geotech data given in Table 2-2. The calculated activity coefficients are functions of the specific interactions in the solutions and the ionic strength.

The relationships between activity coefficient and ionic strength for the anions differ from that of the cations. For these particular water compositions, the activity coefficients of the anions decrease until the ionic strength reaches about 1.0 molal; thereafter, they remain level at about 0.05. The activity coefficients of the cations decrease to minima at an ionic strength of about 1.0 and then increase.

The effect of these changes in activity coefficients on the apparent solubility products of gypsum and dolomite are shown in Figures 2-42 and 2-43. The apparent solubility product for gypsum in each solution was calculated as:

$$\log Q_{gyp} = \log K_{sp(gyp)} - \log(\gamma_{Ca^{2+}} \cdot \gamma_{SO_4^{2-}} \cdot a^2_{H_2O}) \qquad [4]$$

where $\log K_{sp(gyp)}$ = the equilibrium solubility product for gypsum at the temperature of interest,

$\gamma_{Ca^{2+}}$ and $\gamma_{SO_4^{2}}$ = the activity coefficents for Ca^{2+} and SO_4^{2-}, respectively, in a specific sample, and

a_{H_2O} = activity of water.

Similarly, the apparent solubility product for dolomite in a water sample was calculated as:

$$\log Q_{dol} = \log K_{sp(dol)} - \log(\gamma_{Ca^{2+}} \cdot \gamma_{Mg^{2+}} \cdot \gamma^2_{CO_3^{2-}}) \qquad [5]$$

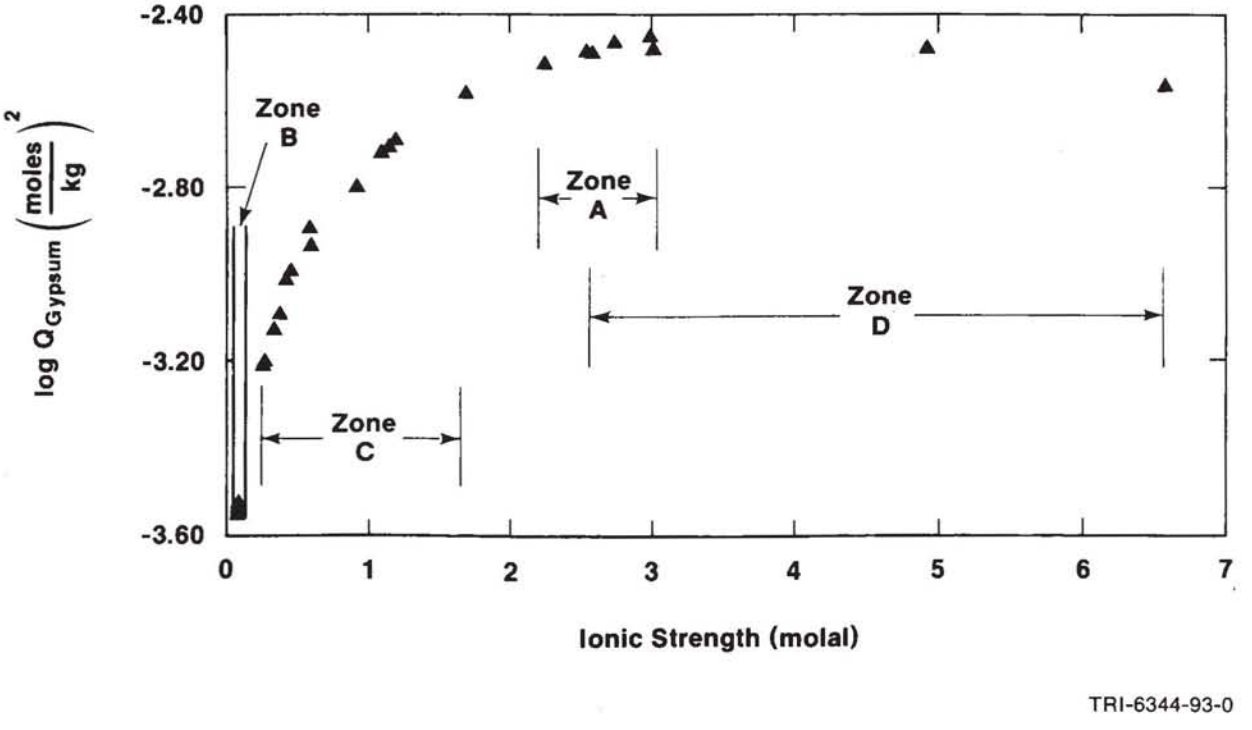

Figure 2-42. Relationship between apparent equilibrium constants for gypsum, log Q, and ionic strengths of Culebra groundwaters.

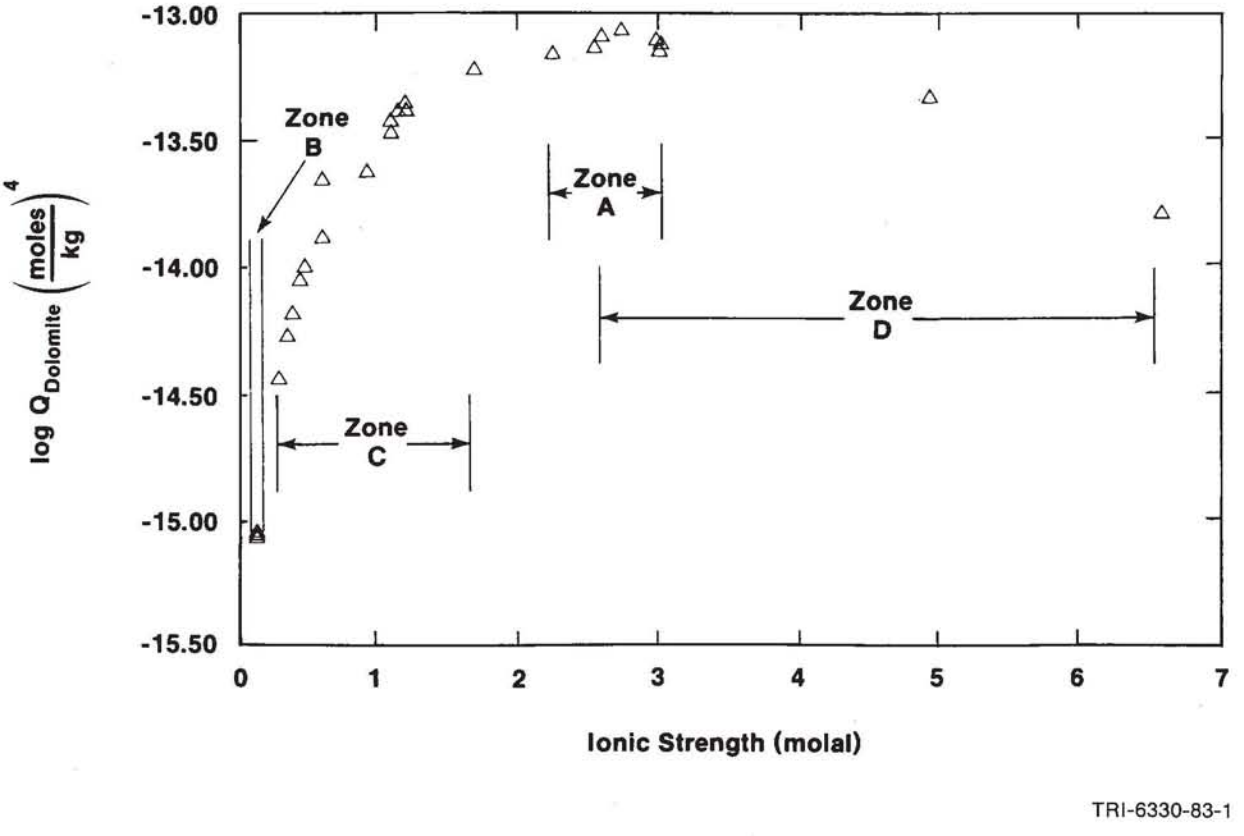

Figure 2-43. Relationship between apparent equilibrium constants for dolomite, log Q, and ionic strengths in Culebra groundwaters.

where $K_{sp(dol)}$ = the equilibrium solubility product for dolomite at the temperature of interest, and

$\gamma_{Mg^{2+}}$ and $\gamma_{CO_3^{2-}}$ = the activity coefficients of Mg^{2+} and CO_3^{2-} in the particular sample.

Dissolution of gypsum, dolomite, and calcite could account for the increase in the concentrations of Mg, Ca, and SO_4 as a function of ionic strength. The ability of this process alone to account for the observed solute relationships in the Culebra is examined by the reaction path modeling described in the next section.

2.4.2.2 Reaction Path Models of Culebra Waters

The PHRQPITZ code was used to calculate the compositions of waters that would be produced by several hypothetical reaction paths. A series of parametric simulations was carried out to determine the effect of certain assumptions about chemical reaction rates, sources of solutes, and initial conditions on the groundwater compositions. The simulations are described in Table 2-11. All of the simulations contained two parts.

In the first part, the composition of water (referred to as the "starting solution") in equilibrium with calcite, gypsum, and dolomite at a specified pCO_2 was calculated. The initial water assumed in this calculation was distilled water, and therefore the resulting solution (i.e., the "starting solution") consisted only of species containing Ca, Mg, CO_3, and H_2O.

In the second part of the simulations, the addition of solutes (Na, Cl, Mg, SO_4, and K) to the starting solution by dissolution of halite and other evaporite salts was simulated. The progress of the dissolution reaction was specified by adding the halite in successive increments of 0.3 or 0.6 moles until a total of 6 moles of NaCl had been added. In Runs 1 to 4, only halite was added to the starting solution. For Runs 5 to 11, a different dissolution reaction was described by specifying the ratio of NaCl to a particular accessory mineral.

Table 2-11. Summary of Parameters for Reaction Path Calculations

Run	CO_2 System[1]	log pCO_2 (atmos)	Minerals at fixed saturation index (SI)[2,3]	Molar ratio of accessory mineral[4]/halite
1	closed	-2	c(0),g(0),d(0)	none
2	closed	-3.5	c(0),g(0),d(0)	none
3	open	-2	c(0),g(0),d(0)	none
4	open	-3.5	c(0),g(0),d(0)	none
5	closed	-2	c(0),g(0),d(0)	poly (0.007)
6	closed	-2	c(0),g(0),d(0)	mag (0.02) carn (0.014)
7	closed	-2	c(0),g(0),d(0)	leon (0.007)
8	closed	-2	c(0),g(0),d(0.5)	carn (0.007)
9	closed	-2	c(0),g(0),d(1.0)	poly (0.007)
10	closed	-2	c(0),g(0)	leon (0.007) $MgCl_2$ (0.025)
11	closed	-2	c(0),g(0)	leon (0.007) mag (0.025)

1. Closed or open to exchange of CO_2 with atmosphere.
2. Minerals: c = calcite; g = gypsum; d = dolomite.
3. Saturation index for mineral: log (IAP) - log (K_{sp})(see Section 3.4).
4. Poly = polyhalite; mag = magnesite; carn = carnallite; leon = leonite.

Solutes (Mg, Ca, CO_2, and SO_4) were added or removed from the solution in amounts needed to maintain saturation levels specified for CO_2 gas, calcite, gypsum, and dolomite.

The effect of the following conditions or processes were considered in the various simulations:

- Closed versus open system with respect to CO_2 gas
- Identity of accessory evaporite salts used as sources of Mg, K, and SO_4
- Degree of saturation of the waters with respect to dolomite.

Table 2-11 summarizes the conditions assumed for the simulations; the results of the calculations are presented in Figures 2-44 to 2-53. In each figure, the concentration of a solute at each reaction step is plotted as a function of the amount of added chloride and compared to the composition of Culebra waters. The types of mass transfers (i.e., precipitation or dissolution) in each simulation are summarized in Table 2-12. The most important results are summarized below.

2.4.2.2.1 EFFECT OF CO_2 PARTIAL PRESSURE ON WATER COMPOSITIONS

Runs 1 to 4 assume the simplest partial equilibrium model in which pure NaCl is added to the solution while the groundwaters are maintained at equilibrium with respect to calcite, dolomite, and gypsum. The concentrations of Ca, Mg, SO_4, and CO_3 change due to the changes in the solubilities of calcite, dolomite, and gypsum described in Section 2.4.2.1.

The four runs differ only in the assumptions made about the CO_2 gas. In Runs 1 and 2, the system is closed with respect to CO_2 gas exchange. This means that the sources of the carbonate species in the solutions are the original CO_2, dissolved in the recharge and soil water, and carbonate dissolved from the Culebra or adjacent strata.

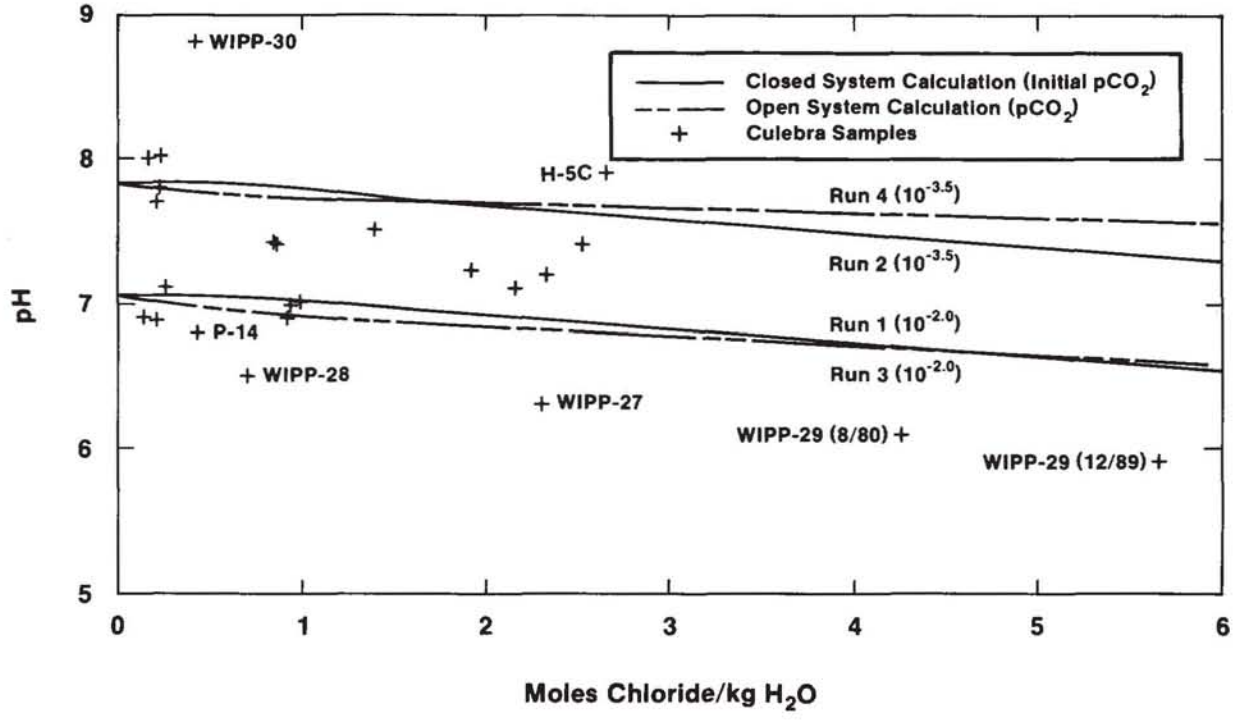

Figure 2-44. Change in pH as a function of reaction progress for simulated evolution of Culebra groundwater compositions.

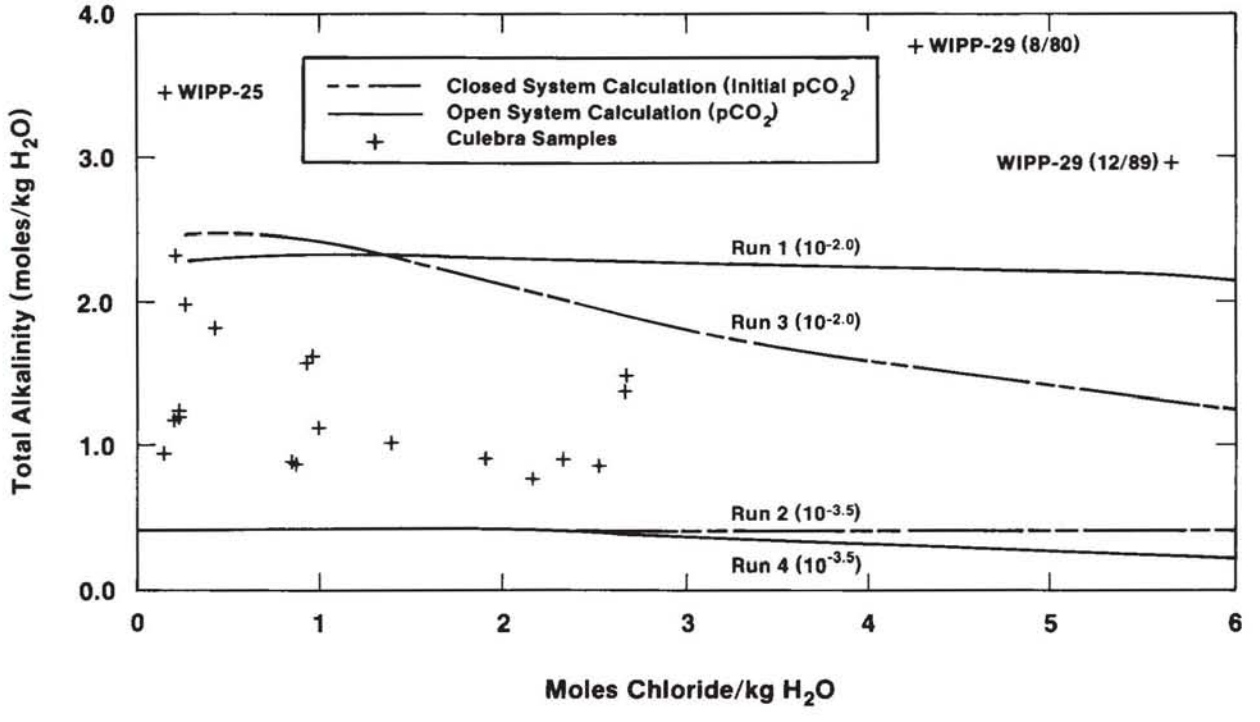

Figure 2-45. Change in total alkalinity as a function of reaction progress for simulated evolution of Culebra groundwater compositions.

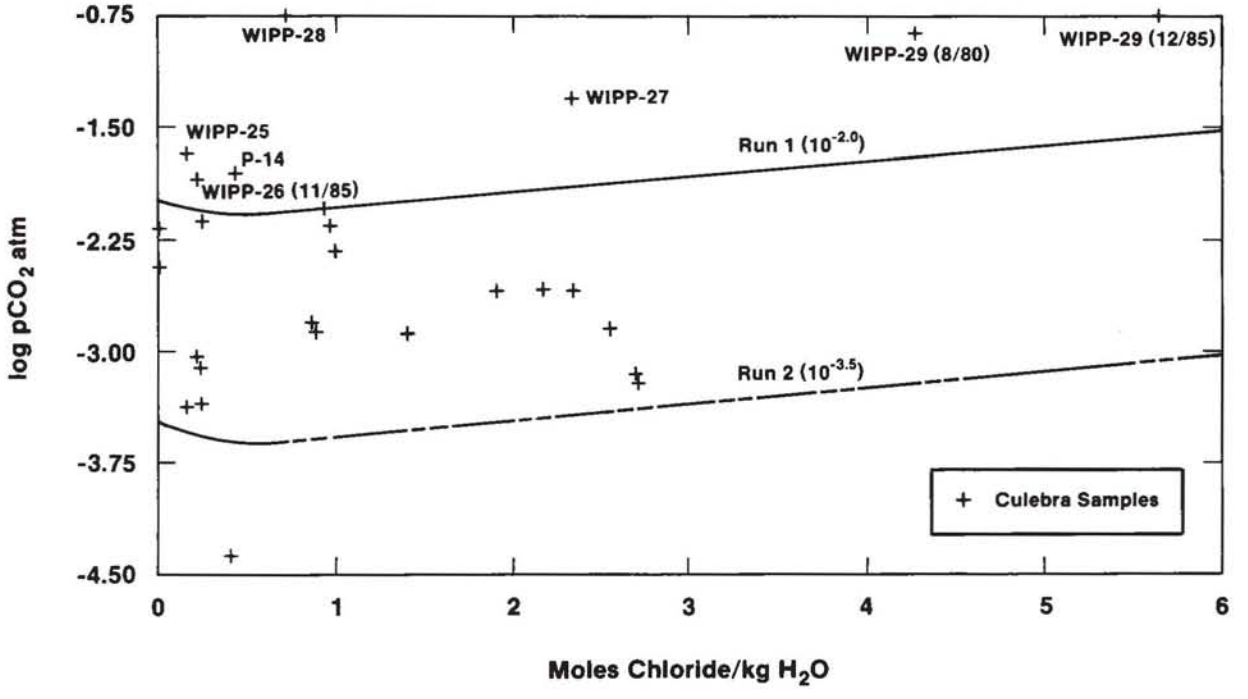

Figure 2-46. Change in pCO_2 for systems closed to atmospheric conditions as a function of reaction progress for simulated evolution of Culebra groundwater compositions.

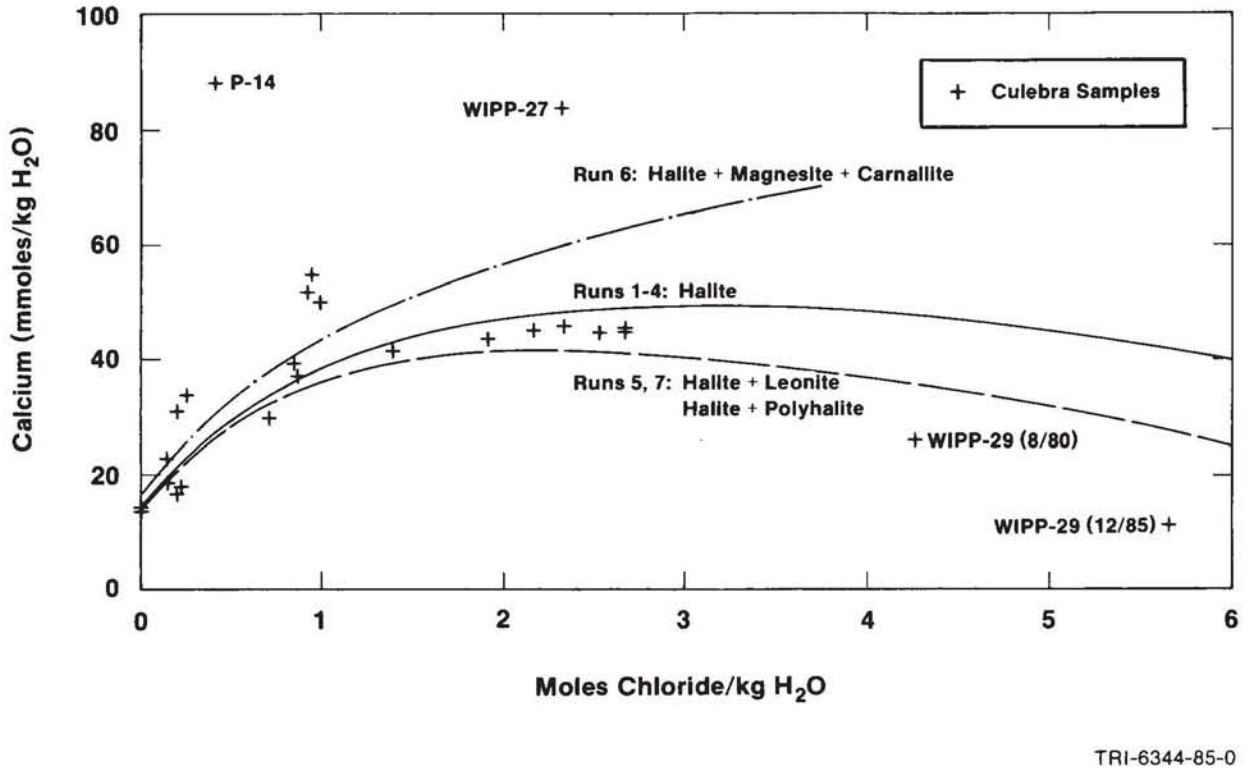

Figure 2-47. Change in calcium concentration as a function of reaction progress and types of added salts for simulated evolution of Culebra groundwater compositions.

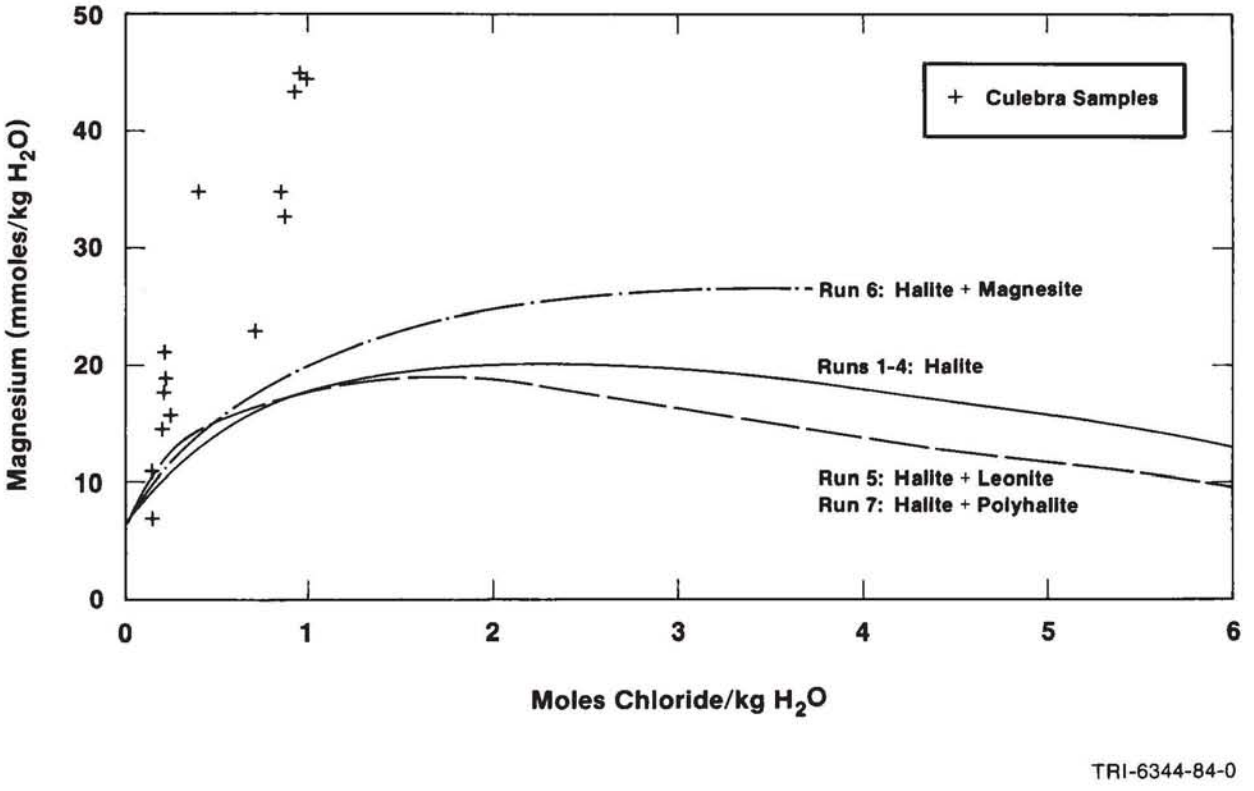

Figure 2-48. Change in magnesium concentration as a function of reaction progress and types of added salts for simulated evolution of Culebra groundwater compositions.

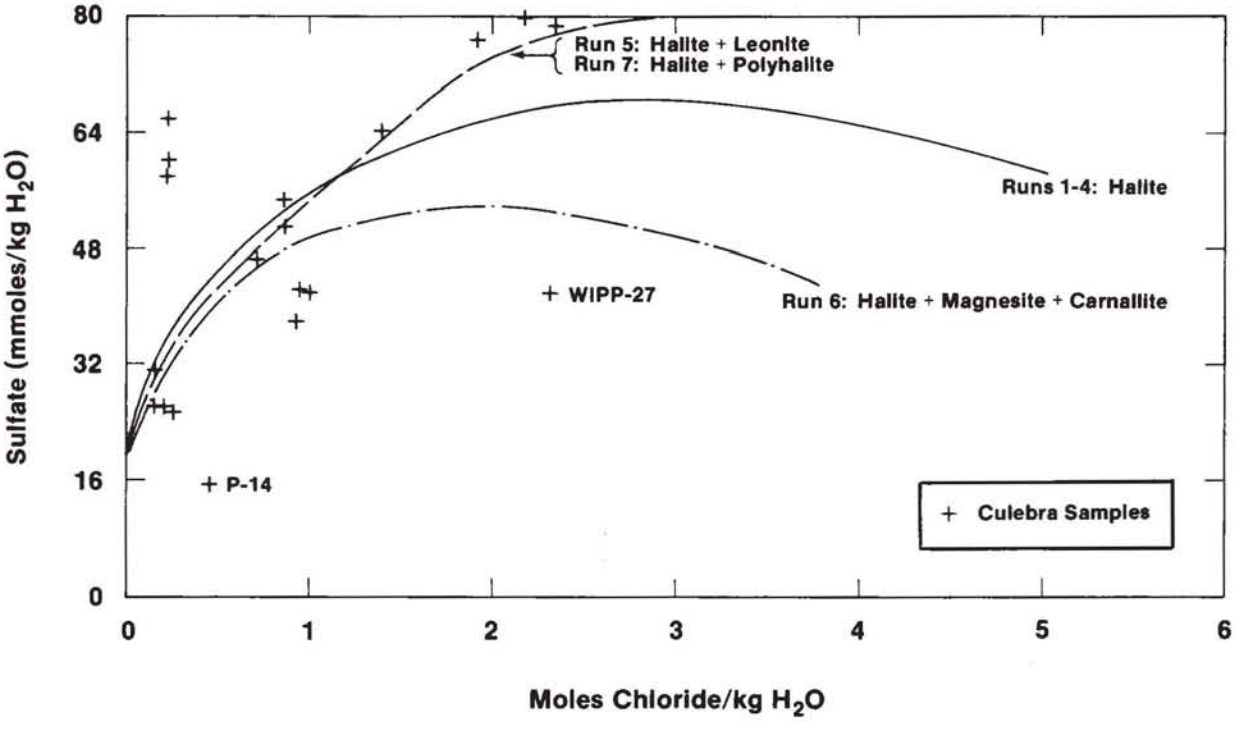

Figure 2-49. Change in sulfate concentration as a function of reaction progress and types of added salts for simulated evolution of Culebra groundwater compositions.

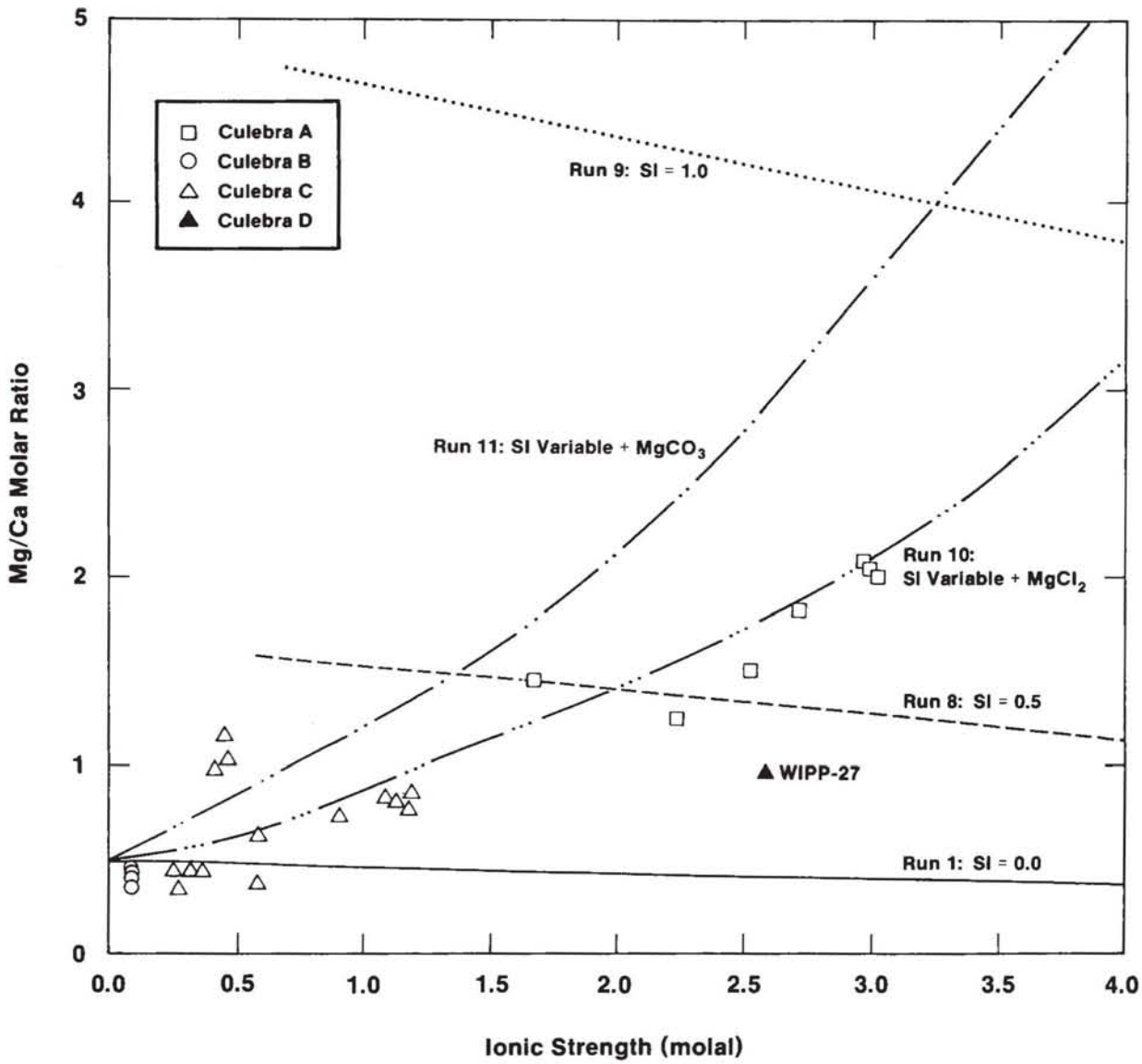

Figure 2-50. Change in Mg/Ca molar ratio as a function of reaction progress, types of added salts, and dolomite saturation index for simulated evolution of Culebra groundwaters.

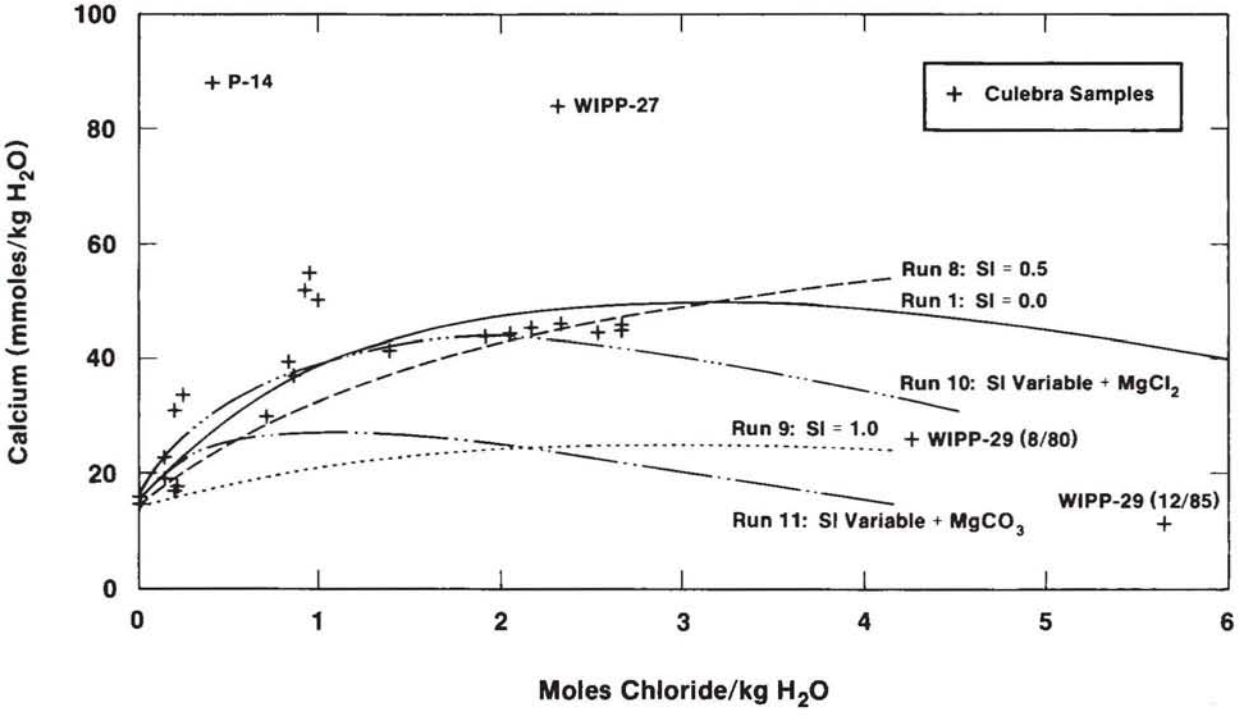

Figure 2-51. Change in calcium concentration as a function of reaction progress, types of added salts, and dolomite saturation index for simulated evolution of Culebra groundwater compositions.

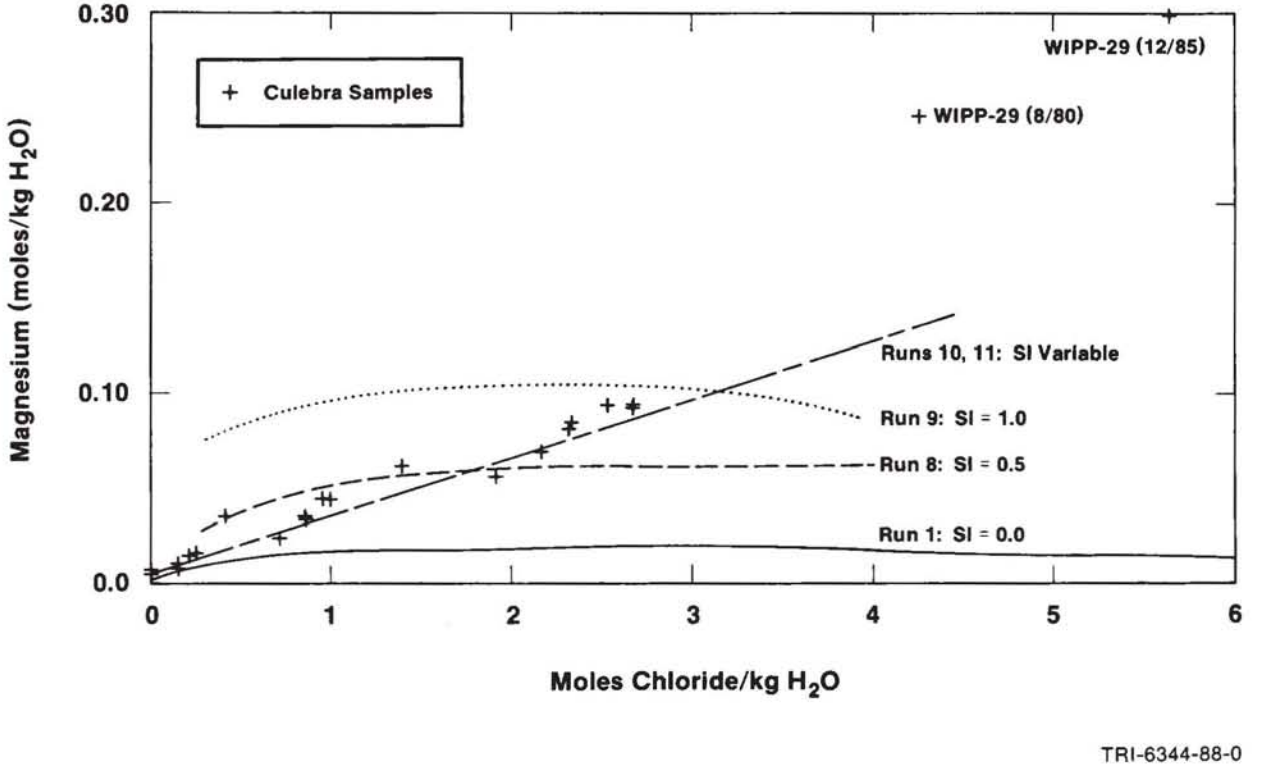

Figure 2-52. Change in magnesium concentration as a function of reaction progress, types of added salts, and dolomite saturation index for simulated evolution of Culebra groundwater compositions.

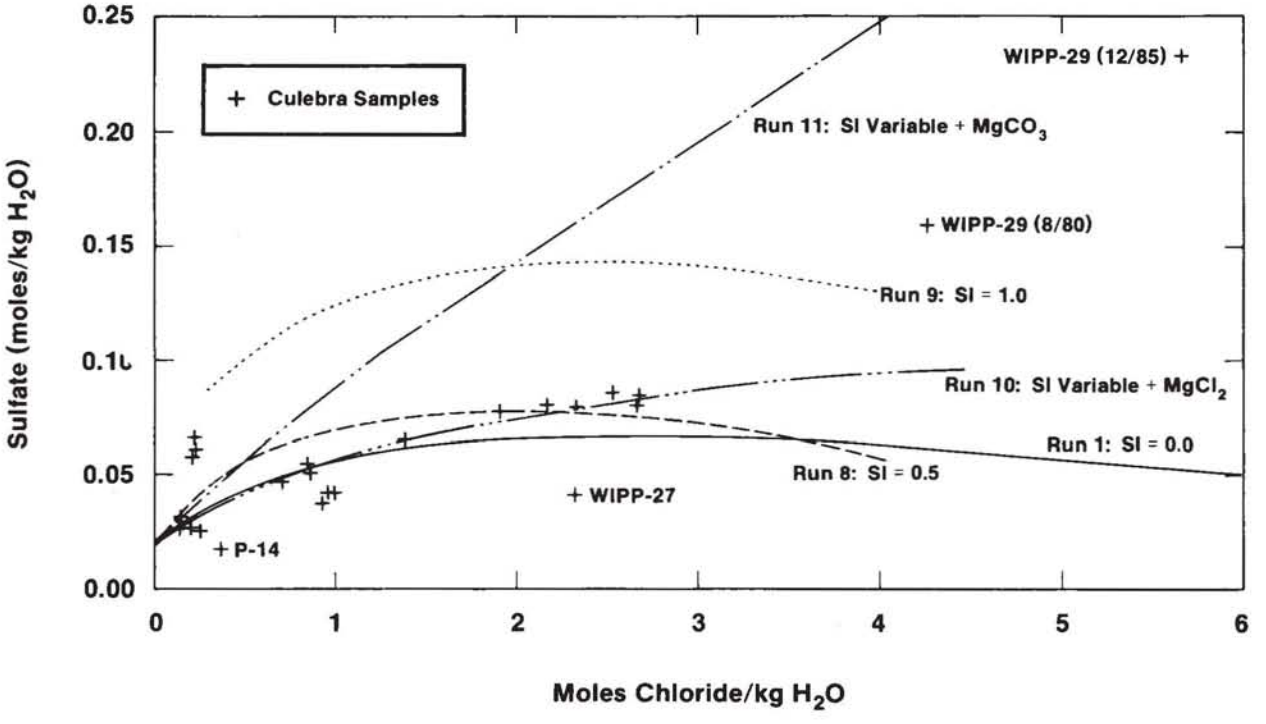

Figure 2-53. Change in sulfate concentration as a function of reaction progress, types of added salts, and dolomite saturation index for simulated evolution of Culebra groundwater compositions.

Table 2-12. Mass Transfers During Reaction Path Calculations[1]

	Minerals and Gases at Saturation				
Run	Calcite	Gypsum	Dolomite	CO_2	Cl Range (Molal)
1	ppt[2]	dis[3]	dis	na[4]	0.3 - 6
2	ppt	dis	dis	na	0.3 - 6
3	ppt	dis	dis	dis	0.3 - 6
4	ppt	dis	dis	dis[5]	0.3 - 1.5
	ppt	dis	dis	exs[5]	1.8 - 6
5	ppt	dis	dis	na	0.3 - 1.5
	dis	dis	ppt	na	1.8
	dis	ppt	ppt	na	2.1 - 6
6	dis	dis	ppt	na	0.3 - 6
7	ppt	dis	dis	na	0.3 - 1.5
	dis	dis	ppt	na	1.8 - 4.2
	dis	ppt	ppt	na	4.5 - 6
8	ppt	dis	dis	na	0.3 - 3.9
	dis	dis	ppt	na	4.2 - 6
9	ppt	dis	dis	na	0.3 - 3.9
	ppt	ppt	dis	na	4.2 - 6
10	dis	dis	na	na	0.3 - 6
11	ppt	dis	na	na	0.3 - 6

1. The starting solutions for all runs were saturated with respect to calcite, gypsum, dolomite, and CO_2 by dissolving gypsum, dolomite, and CO_2 and precipitating excess calcite.
2. ppt = mineral precipitates.
3. dis = mineral or gas dissolves.
4. na = reaction not allowed (closed system).
5. exs = gas exsolves.

This closed system assumption is consistent with the models used to interpret the carbon isotope systematics discussed by Lambert (Chapter 5). In Run 1 the initial partial pressure of CO_2 is 10^{-2} atmospheres; this is a reasonable value for near-surface groundwater in carbonate aquifers that have received CO_2 from both the atmosphere and soil organic matter (Drever, 1982). In Run 2, the initial pCO_2 is atmospheric ($10^{-3.5}$ atm) corresponding to the case in which there is no CO_2 contribution from soil organic matter.

The changes in pH, alkalinity, and pCO_2 as a function of added chloride are shown in Figures 2-44 and 2-45. The compositions of the simulated solutions are compared to compositions of Culebra waters in each figure. There is no apparent relationship between the concentrations measured in the Culebra and the theoretical trends predicted by the simple partial equilibrium model. This is consistent with the potential effects of CO_2 outgassing, H^+ production, and contamination discussed in Section 2.3.4.4.

Figure 2-44 shows that for all simulations the pH decreases as the dissolution reaction proceeds and that the pH is lower for $pCO_2 = 10^{-2.0}$ atmosphere than for $pCO_2 = 10^{-3.5}$ atmosphere. At a given pCO_2, the pH of the closed system drops below that of the open system as the reaction progresses. Many of the Culebra samples have pH values that fall outside of the range bound by these simple simulations. This is consistent with the possibility that the pH of many of the Culebra samples rose during sampling due to the loss of CO_2 gas or fell due to H^+ production during oxidation of ferrous iron from the well casing.

Figure 2-45 shows that the calculated total alkalinity at $pCO_2 = 10^{-3.5}$ atmosphere is a lower limit for measured alkalinities in the Culebra waters. Alkalinities computed for a pCO_2 of 10^{-2} atmosphere are higher than those measured at all Culebra wells except for WIPP-25, WIPP-28, and WIPP-29. As discussed previously, the value measured for WIPP-28 is not considered representative because the field alkalinity had not reached steady-state when the final samples were collected. Lambert (Chapter 5) reports the presence of significant amounts of modern carbon in WIPP-25 and WIPP-29. Contamination of the wells by organic compounds during drilling and the subsequent production of bicarbonate by

heterotrophic bacteria may be responsible for the anomalously high values of alkalinity. Such contamination may also be responsible for the high pCO_2 (Figure 2-46) and low pH in these and other wells.

The changes in concentrations of Ca, Mg, and SO_4 as a function of reaction progress for Run 1 are plotted in Figures 2-47 to 2-49. The plots for Runs 2 to 4 are virtually identical to those of Run 1. The figures show that the simple partial equilibrium model provides a good fit to many of the observed calcium concentrations. However, concentrations of Mg and SO_4 are considerably below the predicted values.

2.4.2.2.2 EFFECT OF ADDITION OF SOLUTES FROM EVAPORITE SALTS

Potential sources of additional Mg and SO_4 for the Culebra groundwaters are polyhalite ($K_2Ca_2Mg(SO_4)_4 \cdot 2H_2O$), carnallite ($KMgCl_3 \cdot 6H_2O$), and magnesite ($MgCO_3$). All of these minerals have been observed in at least trace amounts in the Rustler. Simulations (Runs 5 and 6) were carried out in which one or more of these salts were added to the solution at constant ratios to halite. The ratios of carnallite and polyhalite to halite were set by the observed K:Cl ratio of Culebra waters. A molar ratio of K/Cl = 0.007 was estimated by examination of scatter plots of K to Cl. The proportion of $MgCO_3$ (magnesite/halite = 0.025) added was determined by the amounts of the other salts and the difference between the observed Mg and the amount calculated in Run 1.

In nature, polyhalite dissolves incongruently to form gypsum plus a solution containing K^+, Mg^{+2} and SO_4^{2-}. In Run 7, this process was simulated by adding these solutes as leonite ($K_2Mg(SO_4)_2 \cdot 4H_2O$). Because the solutions are saturated with respect to gypsum, congruent (Run 5) and incongruent (Run 7) dissolution of polyhalite produced virtually identical results. Only the amount of gypsum precipitated depended on the method of dissolution in the simple model considered here.

Figures 2-47 to 2-49 show the concentrations of Ca, Mg, and SO_4 as a function of reaction progress (indicated by the chloride concentration) for these simulations. In all of these

calculations, saturation was maintained with respect to calcite, gypsum, and dolomite. The system was closed with respect to CO_2 gas; the initial pCO_2 was 10^{-2} atmosphere. None of the theoretical reaction paths reproduce the observed Culebra groundwater compositions. Although the sulfate concentrations are improved at intermediate chloride concentrations by addition of polyhalite/leonite, the magnesium concentrations are not improved.

2.4.2.2.3 EFFECT OF DEGREE OF DOLOMITE SATURATION

The Mg/Ca ratio of a solution can be specified by specifying the ratio of the saturation indices of dolomite and calcite. A set of reaction path simulations (Runs 8 and 9) was carried out in which halite was added to the starting solution while maintaining saturation with respect to calcite and gypsum and various levels of supersaturation with respect to dolomite (Run 8: SI = 0.5; Run 9: SI = 1.0). Mg, K, SO_4, and CO_3 were added to the reaction solution by specifying various proportions of polyhalite, carnallite, and magnesite to halite. The results are presented in Figures 2-50 to 2-53.

Figure 2-50 shows that a constant dolomite saturation index leads to a Mg/Ca ratio that decreases slightly as the halite dissolution reaction progresses. Figures 2-51 and 2-52 show that this effect is due to an increase in the calcium concentration and a decrease in the Mg concentration over most of the range of chloride concentration (cf. Runs 1, 8, and 9). This differs from the increase in the Mg/Ca ratio as a function of ionic strength that is observed in the Culebra waters. In addition, the sulfate concentrations calculated with Runs 8 and 9 do not match the concentrations observed in the Culebra either (cf. Figure 2-53).

A final set of simulations (Runs 10 and 11) were run in which saturation with dolomite was not maintained. The starting solution was produced by equilibrating distilled water with calcite, dolomite, and gypsum at an initial pCO_2 of 10^{-2} atmosphere. The system was then closed to pCO_2 gas, and halite plus accessory minerals were added. The saturation index of dolomite was calculated as the reaction progressed, but dolomite was not allowed to dissolve or precipitate.

Run 10 simulated addition of K, Mg, and SO_4 by incongruent dissolution of polyhalite and carnallite. Carnallite dissolves incongruently to form KCl and a solution containing Mg^{2+} and Cl^-. In Run 10, this was simulated by adding $MgCl_2$ to the reaction solution. Incongruent dissolution of polyhalite was simulated by addition of leonite to the solution. The K:Cl ratio of the Culebra waters was used to estimate a reasonable leonite:halite ratio. The $MgCl_2$:halite ratio was then adjusted to fit the observed Mg:Cl ratio of the Culebra waters. In Run 11, magnesite ($MgCO_3$) was added instead of $MgCl_2$ to adjust the Mg:Cl ratio.

Figures 2-50 through 2-53 show that Run 10 reproduces the trends of the Ca, Mg, and SO_4 concentrations in this suite of Culebra groundwaters. The calculated dolomite saturation indices for Run 10 were used to calculate values of the saturation index expression ($2SI_{calcite}$ - $SI_{dolomite}$) described previously and are plotted in Figure 2-39. The good correspondence between the theoretical and observed solute concentrations in these figures show that addition of solutes (Mg, SO_4, and K) to the Culebra from evaporite minerals such as polyhalite is consistent with the observed groundwater compositions if dolomite does not precipitate from supersaturated solutions.

2.4.2.2.4 MASS TRANSFER

Table 2-12 summarizes the nature of mass transfers (dissolution, precipitation, and gas exsolution) that occur during the reaction simulations. For the simplest partial-equilibrium model (Runs 1 through 4) dedolomitization (dissolution of dolomite and precipitation of calcite) and dissolution of gypsum occur over the entire salinity range. In Run 4, which has a constant pCO_2 ($10^{-3.5}$ atmosphere), gas begins to exsolve at a chloride concentration of about 1.8 molal. Addition of Mg by dissolution of polyhalite and/or carnallite (Runs 5, 7, and 8) leads to dolomitization (dissolution of calcite and precipitation of dolomite) at intermediate ionic strengths. Dedolomitization occurs over the entire salinity range in a solution maintained at dolomite supersaturation (SI = 1.0, Run 9). If magnesite is added to the solution (Run 6), dolomitization can occur over the entire salinity range. If dolomite precipitation and dissolution are suppressed, addition of K, Mg, and SO_4 by incongruent

dissolution of polyhalite and carnallite (as leonite and $MgCl_2$, Run 10) leads to dissolution of calcite and gypsum over the entire reaction path. If magnesite is added instead of $MgCl_2$ (Run 11), calcite precipitates and gypsum dissolves.

The nature of these mass transfers is dependent on the proportions and stoichiometry of the minerals added to the reaction solution, and many plausible combinations exist. Solution compositions during Run 10 are closest to those observed in the Culebra. This simulation predicts dissolution of both calcite and gypsum. However, gypsum and minor calcite have been observed in Culebra fractures (Sewards et al., Chapter 5), and it cannot be stated that these minerals are currently dissolving in the Culebra. In Run 10, if sufficient anhydrite were added to the reaction solution, gypsum would precipitate rather than dissolve.

2.4.2.2.5 COMPARISON OF RESULTS FROM REACTION PATH MODELS AND PRINCIPAL COMPONENT ANALYSIS

The assumptions of Run 10 are also consistent with the results of the principal component analysis (PCA) described in Section PCA . The slight change in gypsum solubility with ionic strength leads to a moderate positive correlation between Na, Cl, and Ca seen in the salinity factor. This factor accounts for about 35% of the variance of calcium. The equilibrium with gypsum, however, produces a strong negative correlation between Ca and SO_4 that is expressed in the sulfate factor and accounts for more than 50% of the variance in calcium. Run 10 assumes that Mg and K are added to the solution along with the halite and are not appreciably controlled by solubility equilibria. This is consistent with the salinity factor, which accounts for more than 80% of both of these elements.

The behavior of sulfate is affected both by addition from salt dissolution and by solubility equilibrium in Run 10. This is consistent with the PCA: the salinity and sulfate factors account for about 60% and 25% of the variance, respectively.

The negative correlation between pH and bicarbonate alkalinity shown in the silicate/bicarbonate factor (e.g., factor 2B) is also consistent with the reactions included in Run 10. For example, a negative correlation could result from dissolution of calcite:

$$CaCO_3 + H^+ \rightarrow Ca^{2+} + HCO_3^- \quad [6]$$

The mass action expression for these reactions can be written as:

$$pH = -\log a_{HCO_3^-} - \log a_{Ca^{2+}} - \log K_6 , \quad [7]$$

where K_6 is the equilibrium constant for the reaction described by Equation 6.

Although dolomite was not allowed to dissolve in Run 10 (except in the preparation of the starting solution), the negative correlation between pH and bicarbonate could also reflect dissolution of dolomite in the Culebra:

$$CaMg(CO_3)_2 + 2H^+ \rightarrow Mg^{2+} + Ca^{2+} + 2HCO_3^- \quad [8]$$

with the corresponding mass action expression:

$$2pH = -2\log a_{HCO_3^-} - \log a_{Ca^{2+}} - \log a_{Mg^{2+}} - \log K_8 , \quad [9]$$

where K_8 is the equilibrium constant for Equation 8. In a closed chemical system, the inverse relation between pH and alkalinity expressed by either of these equations could show up in a factor such as factor 2B.

The reaction path models described above correspond to a simple hydrologic model in which recharge water enters the Culebra and dissolves dolomite, gypsum, and calcite. As the water migrates within the aquifer, it obtains solutes from fluids that have dissolved

halite and other evaporite salts from adjacent strata. This model is no doubt much simpler than the real system. There is no reason to assume that the ratio of halite to accessory minerals is constant over the entire flow path. It is possible that other combinations of reactants could be added to the "starting solution" to produce the observed trends in the Culebra. Although Run 10 provides the best average fit to the observed Culebra compositions over the entire range of ionic strengths, some of the Culebra waters more closely match the compositions of other runs. Thus, it is likely that each of the water samples in the Culebra has a unique history that does not conform to the simple model described above.

2.4.3 Ion Exchange, Sorption, and Silica Diagenesis

2.4.3.1 Introduction: Potential Significance of the Silicate/Bicarbonate Factor

The reaction path model described in the previous section includes dissolution and precipitation of chloride, sulfate, and carbonate minerals and accounts for most of the variance of Na, Cl, Ca, SO_4, Mg, and K. The model is consistent with the solute relationships expressed by the salinity and sulfate factors from the PCA. In addition, the model is consistent with the negative correlation between pH and bicarbonate that is part of the silicate/bicarbonate factor. This factor also accounts for large portions of the variances of Li, B, and SiO_2; however, the variances in the concentrations of these solutes may be related to other processes in addition to salt dissolution or carbonate and sulfate mineral equilibria. For example, factor 2B, obtained from the partial R-mode PCA of Culebra samples (Figure 2-26), shows a moderate Li-B association negatively correlated to a Mg-Si association. The following amounts of the total variance of these elements are explained by the above correlation: SiO_2 - 53%; B - 35%; Li - 15%; Mg - 6%.

The relationships among these elements may be partially controlled by reactions involving silicate minerals. Potential processes include release of Si and Mg by dissolution of silica and silicates, and sorption of Li and B by clays.

This hypothesis is supported by the studies of the mineralogy of samples from intact core. Sewards et al. (Chapter 3) report that clays comprise about 3 to 5% by weight of the bulk mineralogy of intact Culebra core samples that have been studied. They occur as discrete seams, as fracture surface coatings, or are finely dispersed throughout the matrix; they are commonly associated with silt-sized quartz. The dominant clay minerals are corrensite (a mixed-layer chlorite/smectite), illite, and serpentine.

Because silica will be released by dissolution of both quartz and clays, the distribution of silica may be controlled by the accessibility of the clays to groundwaters. The extent to which clays react with groundwater is of interest because of their ability to sorb radionuclides. In areas where clays are abundant, both dissolution and ion exchange may affect water chemistry. In Section 2.4.3, relevant laboratory and field data are summarized to assess whether these processes are likely for Culebra groundwaters.

2.4.3.2 Dissolution of Clay Minerals and SiO_2

2.4.3.2.1 SOLUBILITY OF SILICA IN WIPP GROUNDWATERS

The distribution of aqueous silica at the WIPP Site may be controlled by saturation with respect to a silica or silicate phase or by the rate of dissolution from a silica-rich rock. The degree of control that saturation with respect to SiO_2 polymorphs plays in controlling silica activity may be assessed from Figure 2-54. This figure shows the relationships between the activity of water, the total measured silica concentration for Culebra samples, and the saturation concentrations of $Si(OH)_4^o$ for several silica polymorphs ($SiO_2(s)$). The equilibrium silica concentrations were calculated for the reaction:

$$SiO_2(s) + 2H_2O \rightarrow Si(OH)_4^o \qquad [10]$$

from the relation:

$$[Si(OH)_4^o] = [H_2O]^2 \; K_{10} \qquad [11]$$

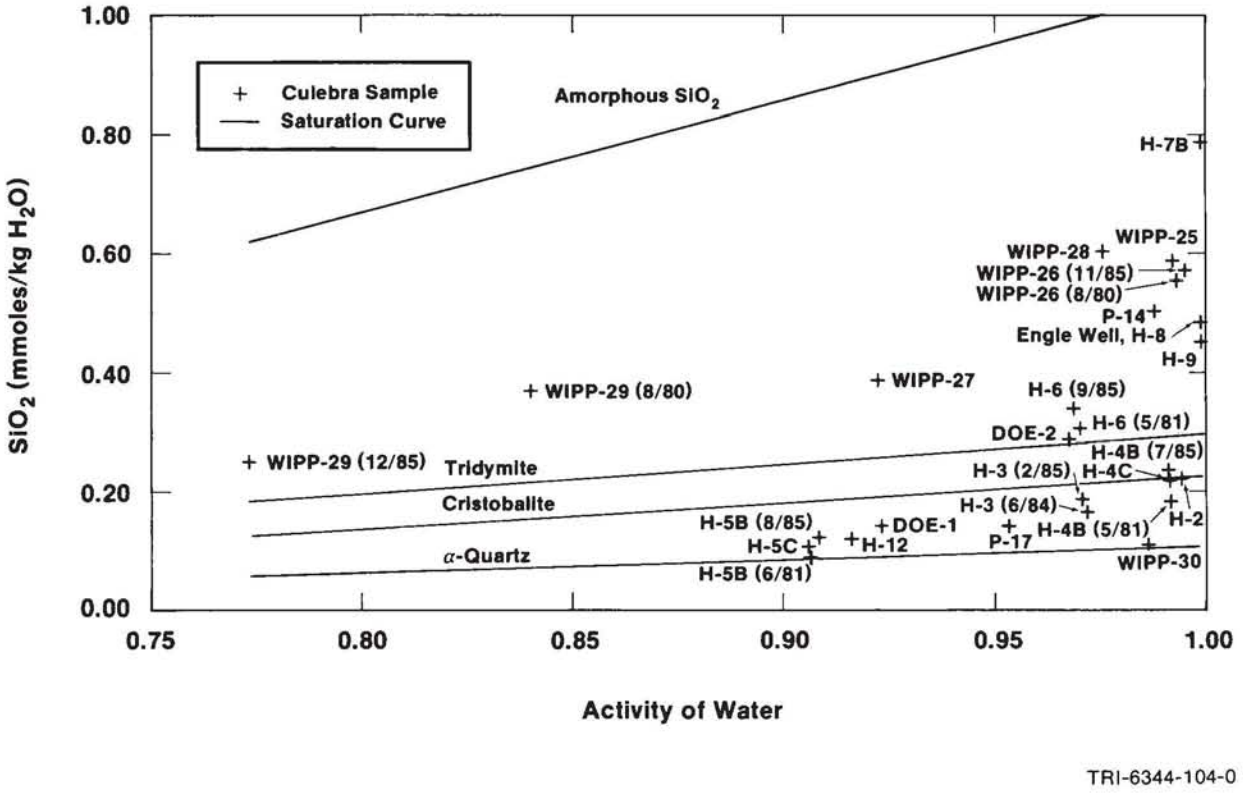

Figure 2-54. Relationship between measured concentrations of aqueous silica (mmoles/L), calculated saturation curves for silica polymorphs, and the activities of water in Culebra groundwaters.

where K_{10} is calculated from the relationship:

$$\Delta G_r = \Delta G_{Si(OH)_4^o} - 2\Delta G_{H_2O} - \Delta G_{SiO_2(s)} = RTlnK_{10} \quad [12]$$

The current version of PHRQPITZ does not have data for any silica species; therefore, two approximations were made in this calculation. First, the contribution of other silica species to the measured silica total has been ignored. This is reasonable because in the pH range of interest (pH 6 to 8) in 0 to 3 M NaCl solutions, $Si(OH)_4^o$ is by far the dominant silica species in solution (cf. Stumm and Morgan, 1981, Figure 9.5). For example, the $Si(OH)_3^-/Si(OH)_4^o$ ratio is <0.05 at pH = 8 in 3 M NaCl solution (using thermodynamic data from Phillips et al., 1985). The second assumption was that the activity coefficent of $Si(OH)_4^o$ was equal to unity because it is an uncharged species.

Figure 2-54 shows that the solutions are all undersaturated with respect to amorphous silica. Saline waters in hydrochemical facies Zone A lie close to quartz saturation, and fresh waters from Zone B have silica contents between tridymite and amorphous silica saturation. No pattern is apparent for water samples from Zone C. In general, the silica concentrations do not seem to be related to saturation constraints for the silica polymorphs.

The relationship between the silica concentration and the activity of water might be due to a kinetic effect. Precipitation of SiO_2 from solution involves dehydration of $Si(OH)_4^o$. If the rate of this reaction increases with salinity, then equilibrium with alpha quartz might be more rapidly approached by the more saline waters in Zone A and lead to lower concentrations than those of the fresher waters in Zone B. The role of kinetic factors, however, cannot be resolved within the scope of this report.

2.4.3.2.2 SILICA DISSOLUTION AND LEACHING

The spatial pattern of silica concentration contours is different from patterns for elements that are assumed to be dissolved from halite and associated evaporite salts (cf. Figures 2-2 and 2-8). Figure 2-8 shows the concentrations of total silica in Culebra samples analyzed by the ITAS laboratories. The contours illustrate that in general, silica concentrations are highest in the west and decrease to the east. Uncertainties in the silica values were discussed in Section 2.2. The actual range of silica concentrations measured at each site can be found in Table 2-2. In general, UNC Geotech analyses in the eastern section of the site show lower concentrations than the corresponding ITAS values. Use of the UNC Geotech values in Figure 2-8 would reinforce the observed trend of decreasing silica concentrations from west to east.

The lack of solubility control on silica concentration discussed above and the spatial trend shown in Figure 2-8 suggest that the distribution of silica is strongly controlled by the rate of supply of silica to the groundwater (leach-limited). Source rocks in the western part of the site may contain more silica that is accessible to leaching than rocks in the east. This may be due to the greater amount of evaporite dissolution and concomitant concentration of residual detrital silicates in the western and southern parts of the site compared to the eastern section.

2.4.3.2.3 DISSOLUTION OF AUTHIGENIC MIXED-LAYER CLAYS AND THE Mg-SiO_2 ASSOCIATION

The correlation of Mg and Si in factor 2B could result from dissolution of a Mg-Si rich phase, possibly a trioctahedral Mg-rich layer in corrensite. The following equation qualitatively illustrates this process:

$$MgSiX_{(am)} + 2H_2O + 2H^+ \rightarrow Mg^{2+} + Si(OH)_4^o \qquad [13]$$

Evidence that an amorphous Mg-rich layer ($MgSiX_{(am)}$) in authigenic mixed-layer clays is more soluble than the Al-Fe-rich smectite layer is found in studies of Salt Lake sediments by Spencer et al. (1985). It is not known if the rate of reaction expressed by equation 13 is rapid enough to affect groundwater chemistry on the time scale of interest to this study (≈10,000 years). The reverse precipitation reaction is probably fast enough to affect the solution composition on this time scale. Jones and Weir (1983) found that sediments in alkaline Lake Albert are ≈2500 years old yet have developed a Mg-rich trioctahedral component in mixed-layer smectite clays.

2.4.3.3 Sorption of Lithium and Boron in Saline Water/Clay Systems

2.4.3.3.1 LITHIUM

Approximately 15% of the variance of lithium is not correlated with ionic strength. Figure 2-55 shows that over most of the ionic strength range, increase in Li concentration is associated with a decrease in the Li/Cl ratio. The depletion of Li relative to Cl in these waters could be due to increasingly lower Li contents of the salt that supplies the Cl, or removal by clays of Li supplied by the salt dissolution.

The importance of the first mechanism is difficult to assess with the available data. A systematic study of the lithium contents in salts adjacent to the Culebra dolomite has not been carried out. In general, in evaporite basins, Li is not taken up appreciably by precipitating salts. Accessory evaporite minerals have different Li contents (e.g., halite, 0.2 ppm; polyhalite, 10 ppm; carnallite, 8 to 9 ppm; sylvite, 16 ppm) (Holser, 1979; Sonnenfeld, 1984). It is possible that the Li/Cl ratio reflects the ratio of accessory salts to halite in dissolving evaporite layers.

The decrease of Li/Cl with increasing Li and Cl concentrations is also consistent with release of Li from clays in relatively fresh Li-poor waters and uptake of Li by clays in saline Li-rich waters. Clays have the highest Li contents of all rock types (up to 120 ppm in shales; Holser, 1979) and can act both as sources and sinks for Li. Evaporitic clays can be sources of Li in oil-field brines (Collins, 1975).

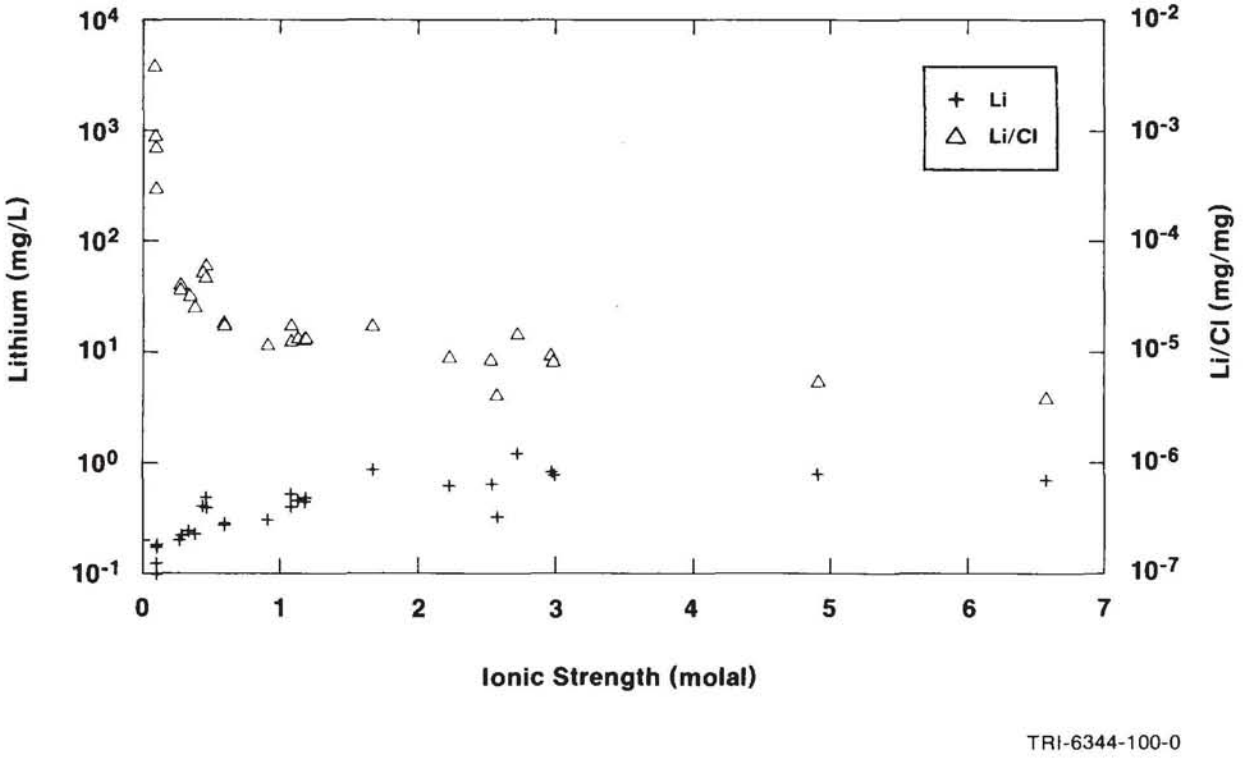

Figure 2-55. Relationship between Li concentrations (mg/L), Li/Cl weight ratios ([mg/L]/[mg/L]), and ionic strengths of Culebra groundwater samples.

The uptake of Li into clays is well documented. Based on a comparison of rates of supply of dissolved Li to the amounts of Li salt in evaporite beds, G. Smith (1976) suggests that 95% of the Li originally supplied to Searles Lake, California was removed by uptake by lake sediments prior to deposition of salt beds. C. Smith (1976) notes that the Li/Cl ratios of Li-rich brines from across the western United States decrease as the Cl content increases, indicating removal or fixation of Li from waters in the vadose zone and surface waters (near surface) during evaporation.

Seyfried et al. (1984) cite ample evidence suggesting that pelagic clays are efficient scavengers of Li from seawater and could remove up to 75% of the total riverine-Li input to the oceans. The uptake of Li by clays may involve substitution (Collins, 1975) or irreversible uptake up by vacant octahedral sites in Al-rich smectites (Schultz, 1969).

The extent of release or uptake of Li by clays could depend on a large number of solution/substrate parameters including surface area, salinity, temperature, and past diagenetic history. It is not possible at this time to formulate a quantitative model for the exchange of Li between clays and Culebra waters. The information provided above, however, suggests that this mechanism is plausible in Culebra waters and may exert some control on the distribution of Li in this aquifer.

2.4.3.3.2 Boron

About 43% of the variance of B is not correlated with the TDS concentration (Table 2-8). Like Li, B can be either released or sorbed by clays in saline waters. Equation 14 qualitatively illustrates the sorption of borate ion onto a clay surface:

$$SOH + B(OH)_4^- + H^+ \rightarrow SOH_2^+ B(OH)_4^- \quad , \qquad [14]$$

where SOH represents a surface site.

There is abundant field and laboratory evidence that illite and montmorillonite effectively scavenge B from saline solutions such as seawater (Seyfried et al., 1984, and cited references; Harriss, 1969; Goldberg and Glaubig, 1986). In evaporite systems, B is primarily associated with clay minerals and initially substitutes for Al in Si tetrahedra or occupies empty sites in the crystal lattice (Sonnenfeld, 1984; Harder, 1961). During alteration in hypersaline brines when Mg-rich, mixed-layer clays are formed, the original crystal lattice is destroyed and the B is released. The liberated B can form independent minerals or become associated with sulfates such as anhydrite.

A quantitative model for the exchange of B between clays and water in the Culebra cannot be formulated at this time. However, both the negative correlation of B with silica (that is independent of the effects of salt dissolution) and the laboratory and field data discussed above are consistent with the hypothesis that clays in the Culebra could scavenge B from Culebra waters.

2.4.3.4 Determining the Potential Significance of Ion Exchange, Sorption, and Silicate Diagenesis in Culebra Waters: Limitations of Available Information

The role that clay minerals have in affecting the concentration of trace solutes through ion-exchange, sorption, and silicate diagenesis is of particular interest to the WIPP Site characterization studies. Studies of the distribution of minor solutes in waters from the Culebra dolomite may provide some insight into the ability of small amounts of clays in fractures to affect the transport of solutes in general.

The attempt to use the data for B, Si, Mg, and Li to study in-situ ion exchange and sorption onto clays has several limitations. First, it is likely that multiple sources exist for these elements. This problem was addressed by using PCA to distinguish the individual contributions of potential sources that are identified by diagnostic element correlations. The correlations are consistent with the hypothesis that clays remove B and Li from solution and release Mg and silica.

A second limitation in this analysis is the small size of the sample set. The computation of the correlation matrix used in the PCA requires a population with a normal distribution. The small population available hindered the identification of outliers that may exert a disproportionate influence on the orientation of the principal components. This effect may be especially important for minor elements such as B and Li. Because PCAs account for all of the variance in the data set, random variations due to analytical errors may have strongly influenced or dominated the minor factors.

This limitation could be addressed in future studies by carrying out a classical factor analysis of a larger data set. As discussed in Appendix 2B, in classical factor analysis, a proportion of the variance of each variable is assigned to random error and does not influence the orientation of the extracted factors. If the experimental error for each chemical variable could be equated with the unique variance, the disproportionate influence of the analytical imprecision of the trace solute analyses could be reduced.

A final problem is related to the method of PCA itself. This method provides no insights into the identity of the factors, nor does it provide the means to identify meaningless or spurious correlations; additional sources of information are always required. A survey of the literature provides ample evidence that sorption of B and Li and release of Mg and silica from clays in saline waters is possible. However, geochemical and mineralogical evidence supporting or contradicting this model for the WIPP are ambiguous. There are insufficient trace element analyses of clay minerals in the Culebra to allow an independent assessment of the magnitude of the effect of ion exchange on groundwaters at the WIPP. While Sewards et al. (Chapter 3) suggest that the probable high solution-volume/clay ratios in the Culebra indicate that the clays do not significantly affect major solute chemistry, no reliable estimate of the solution/clay ratio is available at this time. Additional analyses of mineral compositions from rock samples and better estimates of the amount of clay that have been in contact with the Culebra fluids are required to test the hypotheses suggested by the PCA.

2.4.4 Other Processes

There are several other potential sources of solutes for waters in aquifers in evaporite environments that are discussed briefly here and described in more detail in other chapters of this report. These include:

- Mixing with primitive waters. Waters from fluid inclusions and intergranular fluids are potential sources of solutes which are discussed by Bodine et al. (Chapter 4).

- Mixing with waters from other water-bearing zones or mixing with introduced (contaminant) waters such as process brines, proprietary additives, lubricants, or special treatments in hydrologic testing. These may not always be detectable without knowing the long-term sampling history (over many years) of any single well.

2.4.5 Formulation of a Combined Hydrological-Hydrochemical Model for the Chemical Evolution of Waters in the Rustler Formation

One accepted framework for the formulation of a model for the geochemical evolution of a groundwater is a series of mass-balance and reaction path calculations along the hydrologic flow path (Plummer, 1984; Back et al., 1983); such calculations involve using codes like PHRQPITZ and BALANCE (Parkhurst et al., 1982) to simulate the chemical and isotopic reactions that produce a given groundwater composition at the end of a flow path from the composition found at the beginning of the path. Plummer (1984) shows that the data required for these calculations are substantial. The compositions (solutes and isotopes) of waters from wells along a well defined flow path, the textural and compositional data of minerals at the wells, and the equilibrium and rate constants for important reactions are required to produce a well constrained model. Even if these data are available, however, a unique reaction path model is generally not obtainable. Systems with significant fracture flow, systems with hydrochemically undefined vertical mixing, and systems not at hydrological and chemical steady state are not amenable to this kind of modeling.

The available mineralogical, thermodynamic, kinetic, and hydrologic data are not adequate to support a meaningful reaction path calculation along groundwater flow paths at the WIPP Site. Even if additional data are collected, the information summarized in this chapter and in other chapters in this report suggest that the WIPP Site has many attributes that are unfavorable for successful simulation of the chemical evolution of the waters along hydrologic flow paths. As discussed in other sections of this report (cf. Lambert, Chapter 5), there is abundant evidence that the hydrologic flow system is not at steady state. Isotopic, stratigraphic, and geochemical data are consistent with the hypothesis that the direction of groundwater flow changed from a direction with a strong west to east component to one with a dominant north to south component since the late Pleistocene.

2.5 SUMMARY AND CONCLUSIONS

The purpose of this chapter is to summarize solute concentration data and to delineate hydrochemical facies in the Culebra Member of the Rustler Formation. These data are used as a basis for hypotheses concerning the chemical evolution of the groundwaters and to show the relationship between patterns of solute distribution and groundwater flow. The composition of waters in the Culebra dolomite is emphasized in this chapter. Preliminary results from work dealing with the Magenta dolomite, the Rustler/Salado contact zone, the Dewey Lake Red Beds, and the Bell Canyon Formation are found in Appendix 2D.

Several kinds of relationships among groundwater chemical variables were examined. These included spatial distributions of element concentrations and ratios (hydrochemical facies and geochemical signatures), interelement correlations expressed by PCA, and mass action (solubility constant) constraints. The methods used, results, and limitations of the analysis are summarized below.

2.5.1 Delineation of Hydrochemical Facies in the Culebra

Based on the major solute compositions, four hydrochemical facies have been delineated. Zone A, containing saline (about 3.0 m) NaCl brine with a Mg/Ca molar ratio between 1.2

and 2.0, is found in the eastern third of the study area, roughly coincident with the region of low transmissivity and the occurrence of halite in several units of the Rustler Formation. Zone B, containing a dilute Ca-SO_4-rich water (I <0.1 m), is found in the southern part of the study area and coincides with a zone of high transmissivity where halite is absent from the Rustler. Zone C contains waters of variable composition and ionic strengths (0.3 to 1.6 m); Mg/Ca molar ratios range from 0.5 to 1.2. The zone extends from the western part of the four-mile zone where halite is present in the unnamed lower member of the Rustler to the eastern side of Nash Draw where no Rustler halite has been found. Zone D contains WIPP-27 and WIPP-29 and is defined on the basis of anomalously high salinities (3 to 6 m) and K/Na weight ratios (0.2). The composition of the Culebra groundwater at WIPP-29 has changed over the course of a 7-year monitoring period, probably due to contamination from potash-refining operations in the area.

2.5.2 Geochemical Signatures as Indicators of Hydrologic Flow Direction

In simple hydrologic systems, spatial trends in element concentrations and ratios (geochemical signatures) can be used to delineate sites of recharge or interaquifer leakage, to provide independent evidence of groundwater flow, and to determine the presence of hydrologic divides. The use of geochemical signatures to delineate groundwater flow direction assumes the following:

- The hydrologic system has been at steady state for at least as long as the residence time of the solutes in the system

- The signature involves elements that are not appreciably removed from solution by chemical processes or do not have multiple sources that supply the solutes at different rates.

In general, those conditions are not present at the WIPP Site. As discussed in Section 2.3.2.1 and by Ramey (1985), the geochemical signatures are inconsistent with the assumption of steady-state hydrologic flow. The regional variation in salinity at the WIPP Site, as shown by the sodium concentration contours in Figure 2-2 and the hydrochemical facies map in Figure 2-1, suggest a southwest-to-northeast groundwater flow direction across the site. The present day flow direction indicated by available hydrologic data (cf. Lappin, 1988) is approximately north to south. Independent isotopic evidence suggests that the flow system has been transient over at least the last 12,000 years and the direction of flow has changed since the late Pleistocene (Lambert, Chapter 5). Paleo-flow directions indicated by $^{234}U/^{238}U$ relationships have a west to east component consistent with the regional variation of most of the solutes.

There is agreement between geochemical signatures and present day flow directions only in limited sections of the WIPP area. Local contours for K, K/Na, Mg, and Na near WIPP-27 and WIPP-29 are consistent with the introduction of wastes from nearby potash refining operations. In the vicinity of the WIPP Site (four-mile zone), the series of wells (H2 → H3 → P-17) may lie along a modern flow path. The salinity of waters sampled from the wells increases along this path. The concordance of flow direction and solute concentration is ambiguous, however, because of uncertainties in the flow direction and in the chemistry of the Culebra water at the H-2 well.

2.5.3 Use of Principal Component Analysis to Identify Geochemical Processes Affecting Water Chemistry

Three factors were extracted by R-mode PCA from the major and minor solute data. The first factor (salinity factor) is dominated by Na, K, Mg, Br, and Cl. The second most important factor (sulfate factor) also has a strong Na-Cl influence, but is dominated by Ca, sulfate, bicarbonate alkalinity, and Sr. Geologic data from the site suggest that these two factors represent addition of solutes by the dissolution of halite, gypsum/anhydrite, and carbonates. A third factor (silicate/bicarbonate factor) showed the interelement correlations independent of effects attributable to halite dissolution. This factor contains two

inversely correlated groups of elements: Mg, bicarbonate alkalinity, and SiO_2 form one group; and pH, B, and Li form another group. This pattern of element associations might reflect sorption of B and Li by clays, release of Mg and SiO_2 by dissolution of authigenic clays, and carbonate diagenesis.

The reification of the principal components in terms of geochemical processes must be done cautiously. The results of the PCA should only be used to suggest possible reactions; independent confirmation must be obtained before the proposed mechanisms are accepted. Other limitations of the PCA presented here are the small size of the data set and the large relative uncertainties in the concentrations of some of the minor and trace solutes.

2.5.4 Thermodynamic (Mass Action) Calculations with Solute Concentration Data

2.5.4.1 Use of Saturation Index Calculations to Evaluate Chemical Equilibria

Saturation indices of groundwaters can be used to suggest the identity of minerals that control solute concentrations, to detect evidence of the metastable persistence of mineral phases, and to indicate possible errors in chemical analyses, sampling procedures, and chemical speciation models. Waters from the Culebra are saturated with respect to gypsum and undersaturated with respect to halite. Calculated saturation indices for calcite and dolomite indicate saturation for some wells, but many of the waters show apparent supersaturation. The Mg/Ca ratios of the waters are consistent with increasing degrees of dolomite supersaturation with ionic strength.

Uncertainties in the saturation indices must be evaluated on a mineral by mineral basis. Analytical error, errors in calculated activity coefficients, and uncertainties in the equilibrium constants will contribute to the uncertainty in the saturation index. For chemical analyses of Culebra waters, uncertainties in pH will be important for carbonates, and uncertainties in equilibrium constants will be important for phases such as dolomite that exhibit order/disorder.

The uncertainty in the carbonate analyses is especially important for the waters in the dolomite aquifers and can be resolved by modification of sampling techniques in the field. Only if the total alkalinity and either total inorganic carbon or pCO_2 are measured can the carbonate system be unambiguously defined. With this approach the pH is calculated rather than measured, and problems associated with loss of CO_2 gas and the different activity scales are minimized.

Even if the actual saturation indices of dolomite, calcite, and gypsum are zero, it is likely that these minerals are dissolving in areas where halite dissolution is increasing the ionic strength of the groundwaters over the range of 0 to 3 molal. The Culebra may be a partial-equilibrium system in which the mineral/water equilibria are shifting along a reaction path driven by the irreversible process of halite dissolution. Theoretical calculations show that the increase in salinity caused by the dissolution of halite changes the solubilities of carbonates and sulfates; solubilities increase up to 3 molal ionic strength and then decrease. Additional evidence for the mass transfer could come from petrographic investigations of textural relations in the rock, isotopic data for minerals and aqueous species, and mass balance calculations based on concentration changes along the flow path.

2.5.4.2 Reaction Path Modeling

The PHRQPITZ code was used to calculate the compositions of waters that would be produced by several hypothetical reaction paths. A series of parametric simulations was carried out to determine the effects of certain assumptions about chemical reaction rates, sources of solutes, and initial conditions on the groundwater compositions. The results of the reaction path simulations are non-unique; it is possible that fluid compositions can be obtained by several different paths. However, simulations described in Section 2.4.2.2 suggest that equilibrium with dolomite plays a minor role in controlling the chemistry of the more saline Culebra waters in Zones A and C. The relationships between K, Mg, Ca, and SO_4 with chloride are consistent with a partial-equilibrium model in which saturation is maintained with respect to calcite and gypsum while these solutes are added to the Culebra by dissolution of halite containing minor amounts of polyhalite and carnallite. Recharge

waters entering the Culebra may initially reach equilibrium with dolomite, but as the ionic strength increases, due to dissolution of halite and the accessory minerals, the solutions become increasingly supersaturated with respect to dolomite.

2.5.5 Summary of Chemical Processes Affecting Groundwater Chemistry

Table 2-13 summarizes chemical processes that may affect the chemistry of water samples described in this report. The mixing of connate formation waters with recharge waters is discussed by Bodine et al. (Chapter 4) and cannot be ruled out with the available solute composition data.

Table 2-13. Chemical Processes That May Affect the Solute Compositions of Culebra Groundwaters

Chemical Process	Potential Effect(s) on Concentrations of Solutes in Culebra Groundwaters
Halite dissolution	increase Na, Cl, Br, Li; increase Cl/Br; increase solubility of carbonates and sulfates up to 3 molal ionic strength and then decrease solubility causing changes in Ca, Mg, SO_4, CO_3
Precipitation/dissolution of gypsum	decrease/increase Ca, SO_4
Precipitation/dissolution of calcite and dolomite	decrease/increase Ca, Mg, CO_3
Dolomitization[1]: calcite + Mg → dolomite + Ca	decrease Mg/Ca ratio
Dedolomitization[2]: dissolution of gypsum and dolomite with concurrent precipitation of calcite.	decrease pH, alkalinity, SO_4; must maintain Mg/Ca molar ratio < 1
Sorption/desorption by clays	loss/gain of Li and B by solution
Mixing of connate hypersaline formation water with recharge water that has dissolved gypsum[3]	increase Mg, Ca, K, Na, Cl; decrease SO_4, Cl/Br ratio
Incongruent dissolution of polyhalite	increase Mg, K, SO_4; decrease Ca, Cl/Br ratio
Dissolution of silicates	increase Si, Mg, Na
Dissolution of anhydrite with sellaite inclusions	increase Ca, SO_4, Mg, F

1. Process may be important locally.
2. Process may be important locally, for example, at WIPP-33.
3. Process discussed by Bodine et al. (Chapter 4).

2.6 REFERENCES

Back, W., B. B. Hanshaw, L. N. Plummer, P. H. Rahn, C. T. Rightmire, and M. Rubin. 1983. "Process and Rate of Dedolomitization: Mass Transfer and ^{14}C Dating in a Regional Carbonate Aquifer." *Geological Society of America Bulletin*, Vol. 94:1415-1429.

Barr, G. E., W. B. Miller, and D. D. Gonzalez. 1983. *Interim Report on the Modeling of the Regional Hydraulics of the Rustler Formation*. SAND83-0391. Albuquerque, NM: Sandia National Laboratories.

Bassett, R. L. 1982. "Geochemistry and Mass Transfer in Brines from Permian Wolfcamp Carbonates in the Palo Duro, Dalhart, and Anadarko Basins." *Geology and Geohydrology of the Palo Duro Basin, Texas Panhandle: A Report on the Progress of Nuclear Waste Isolation Feasibility Studies (1981)*. Bureau of Economic Geology.

Bates, R. G. 1975. "pH Scales for Sea Water." *The Nature of Seawater*, E. D. Goldberg, ed. Dahlem Workshop Report, Berlin, Abakon: Verlagsgesellschaft.

Bates, R. G., and C. H. Culberson. 1977. "Hydrogen Ions and the Thermodynamic State of Marine Systems." *The Fate of Fossil Fuel CO_2 in the Oceans*, N.R. Anderson and A. Malahoff, ed. New York: Plenum Publishing Company.

Bidoglio, G., G. Tanet, and A. Chatt. 1985. "Studies on Neptunium (V) Carbonate Complexes Under Geologic Repository Conditions." *Radiochimica Acta*, Vol. 38:21.

Bidoglio, G., G. Tanet, A. de Plano, and G. P. Lazzari. 1987. "Radionuclide Chemical Species Determination in Waste Management Studies." *Journal of Radioanalytical and Nuclear Chemistry* Articles, Vol. 110, No. 1:91-100.

Bopp, F. III, and R. B. Biggs. 1981. "Metals in Estuarine Sediments: Factor Analysis and its Environmental Significance." *Science*, Vol. 214:441-443.

Braitsch, O. 1971. *Salt Deposits: Their Origin and Composition*. New York: Springer-Verlag.

Collins, A. G. 1975. *Geochemistry of Oil Field Waters*. New York: Elsevier Scientific Publishing Company.

Colton, I. D. and J. G. Morse. 1985. *Water Quality Sampling Plan*. WIPP-DOE-215. Carlsbad, NM: Waste Isolation Pilot Plant Project Office.

Davis, J. C. 1973. *Statistics and Data Analysis in Geology*. New York: John Wiley and Sons, Inc.

Drever, J. I. 1982. *The Geochemistry of Natural Waters*. Englewood Cliffs, NJ: Prentice-Hall, Inc.

Goldberg, S., and R. A. Glaubig. 1986. "Boron Adsorption and Silicon Release by the Clay Minerals Kaolinite, Montmorillonite, and Illite." *Soil Science Society of America Journal*, Vol. 50:1442-1448.

Golden Software, Inc. 1987. *Surfer Version 3.00, Reference Manual*. Golden, CO: Golden Software, Inc.

Gonzalez, D. D. 1983. *Groundwater Flow in the Rustler Formation, Waste Isolation Pilot Plant (WIPP), Southeast New Mexico (SENM)*. SAND82-1012. Albuquerque, NM: Sandia National Laboratories.

Gould, S. J. 1981. *The Mismeasure of Man*. New York: W.W. Norton & Company.

Harder, H. 1961. "Einbau von Bor in detritische Tonminerale. Experimente zur Erklarung des Borgehaltes toniger Sediments." *Geochimica et Cosmochimica Acta*, Vol. 21:284-294.

Harriss, R. C. 1969. "Boron Regulation in the Oceans." *Nature*, Vol. 223:290-291.

Harvie, C. E., N. Mϕller, and J. H. Weare. 1984. "The Prediction of Mineral Solubilities in Natural Waters: The Na-K-Mg-Ca-H-Cl-SO_4-OH-HCO_3-CO_3-CO_2-H_2O System to High Ionic Strengths at 25°C." *Geochimica et Cosmochimica Acta*, Vol. 48:723-751.

Harvie, C. E., and J. H., Weare. 1980. "The Prediction of Mineral Solubilities in Natural Waters: The Na-K-Mg-Ca-Cl-SO_4-H_2O System from Zero to High Concentration at 25°C." *Geochimica et Cosmochimica Acta*, Vol. 44:981-997.

Hem, J. D. 1985. *Study and Interpretation of the Chemical Characteristics of Natural Water.* Water-Supply Paper 2254, Third Edition. Denver, CO: US Geological Survey.

Hitchon, B., G. K. Billings, and J. E. Klovan. 1971. "Geochemistry and Origin of Formation Waters in the Western Canada Sedimentary Basin: III. Factors Controlling Chemical Composition." *Geochimica et Cosmochimica Acta*, Vol. 35:567-598.

Holser, W. T. 1979. "Marine Minerals Chapter 9: Trace Elements and Isotopes in Evaporites" *Mineralogical Society of America Short Course Notes*. R. G. Burns, ed. Vol. 6:295-346. Washington, DC: Mineralogical Society of America.

Jones, B. F., and A. H. Weir. 1983. "Clay Minerals of Lake Albert, An Alkaline, Saline Lake." *Clays and Clay Minerals*, Vol. 31, No. 3:161-172.

Klovan, J. E. 1975. "R- and Q-Mode Factor Analysis." *Concepts in Geostatistics*. McCammon, R., ed. New York: Springer-Verlag.

Lambert, S. J., and K. L., Robinson. 1984. *Field Geochemical Studies of Groundwaters in Nash Draw, Southeastern New Mexico*. SAND83-1122. Albuquerque, NM: Sandia National Laboratories.

Lambert, S. J. 1987. *Feasibility Study: Applicability of Geochronologic Methods Involving Radiocarbon and Other Nuclides to the Groundwater Hydrology of the Rustler Formation, Southeastern New Mexico*. SAND86-1054. Albuquerque, NM: Sandia National Laboratories.

Lappin, A. R. 1988. *Summary of Site-Characterization Studies Conducted From 1983 Through 1987 at the Waste Isolation Pilot Plant (WIPP) Site, Southeastern New Mexico*. SAND88-0157. Albuquerque, NM: Sandia National Laboratories.

Lyon, M. L. 1989. *Annual Water Quality Data Report for the Waste Isolation Pilot Plant*. DOE/WIPP 89-001.

Meijer, A. J., J. L. Lolcama, and F. J. Pearson. 1987. "Appendix E: Consistency of Densities and Chemical Compositions of Water Samples from the Culebra Dolomite." *Modeling of Ground-Water Flow in the Culebra Dolomite at the Waste Isolation Pilot Plant (WIPP) Site: Interim Report*, A. Haug, V. A. Kelly, A. M. LaVenue, and J. F. Pickens, ed. SAND86-7167. Albuquerque, NM: Sandia National Laboratories.

Mercer, J. W. 1983. *Geohydrology of the Proposed Waste Isolation Pilot Plant Site, Los Medaños Area, Southeastern New Mexico*. Water Resources Investigation Report 83-4016. Albuquerque, NM: US Geological Survey.

Mercer, J. W., and B. R. Orr. 1979. *Interim Data Report on the Geohydrology of the Proposed Waste Isolation Pilot Plant Site, Southeast New Mexico*. Water Resources Investigation Report 79-98. Albuquerque, NM: US Geological Survey.

Møller, N., J. H. Weare, and J. Greenberg. 1985. "Prediction of Mineral Solubilities and Diagenesis in Rock/Water Association at High Temperature." *Proceedings of the Conference on the Application of Geochemical Models to High-Level Nuclear Waste Repository Assessment*, G. K. Jacobs and S. K. Whatley, ed. NUREG/CP-0062, ORNL/TM-9585. Oak Ridge, TN: Oak Ridge National Laboratory.

Nie, N. H., C. H. Hull, J. G. Jenkins, K. Steinbrenner, and D. H. Bent. 1975. *SPSS: Statistical Package for the Social Sciences*. 2nd ed. New York: McGraw-Hill, Inc.

Parkhurst, D. L., D. C. Thorstenson, and L. N. Plummer. 1980. *PHREEQE - A Computer Program for Geochemical Calculations*. Water Resources Investigation Report 80-96. Reston, VA: US Geological Survey.

Parkhurst, D. L., L. N. Plummer, and D. C. Thorstenson. 1982. *BALANCE - A Computer Program for Calculation of Chemical Mass Balance*. Water Resources Investigation Report 82-14, NTIS Technical Report PB-82-255902. Reston, VA: US Geological Survey.

Pearson, F. J. Jr., D. W. Fisher, and L. N. Plummer. 1978. "Correction of Ground-Water Chemistry and Carbon Isotope Composition for Effects of CO_2 Outgassing." *Geochimica et Cosmochimica Acta*, Vol. 42:1799-1807.

Phillips, S. L., C. A. Phillips, and J. Skeen. 1985. *Hydrolysis, Formation and Ionization Constants at 25°C, and at High Temperature-High Ionic Strength*. LBL-14996. Berkeley, CA: Lawrence Berkeley Laboratory Report.

Phillips, S. L., F. V. Hale, L. F. Silvester, and M. D. Siegel. 1988. *Thermodynamic Tables for Nuclear Waste Isolation, Aqueous Solutions Database*. US Nuclear Regulatory Commision Report. NUREG/CR-4864 Vol. 1 (also LBL-22860 and SAND87-0323).

Pitzer, K. S. 1973. "Thermodynamics of Electrolytes. 1. Theoretical Basis and General Equations." *Journal Physical Chemistry*, Vol. 77:268-277.

Pitzer, K. S. 1975. "Thermodynamics of Electrolytes. 5. Effects of Higher-Order Electrostatic Terms." *Journal Solution Chemistry*, Vol. 4:249-265.

Pitzer, K. S., and J. J. Kim. 1974. "Thermodynamics of Electrolytes. 4. Activity and Osmotic Coefficients for Mixed Electrolytes." *Journal American Chemical Society*, Vol. 96:5701-5707.

Pitzer, K. S., and G. Mayorga. 1973. "Thermodynamics of Electrolytes. 2. Activity and Osmotic Coefficients for Strong Electrolytes with One or Both Ions Univalent." *Journal Physical Chemistry*, Vol. 77:2300-2308.

Pitzer, K. S., and G. Mayorga. 1974. "Thermodynamics of Electrolytes. 3. Activity and Osmotic Coefficients of 2-2 Electrolytes." *Journal Solution Chemistry*, Vol. 3:539-546.

Plummer, L. N., and E. T. Sundquist. 1982. "Total Individual Ion Activity Coefficients of Calcium and Carbonate in Seawater at 25°C and 35% Salinity, and Implications to the Agreement between Apparent and Thermodynamic Constants of Calcite and Aragonite." *Geochimica et Cosmochimica Acta*, Vol. 46:247-258.

Plummer, L. N. 1984. "Geochemical Modeling: A Comparison of Forward and Inverse Methods." *Proceedings First Canadian/American Conference on Hydrogeology*. B. Hitchon and E. I. Wallick, ed. Worthington, OH: National Water Well Association.

Plummer, L. N., and D. L. Parkhurst. 1985. "PHREEQE: Status and Applications" *Proceedings of the Conference on the Application of Geochemical Models to High-Level Nuclear Waste Repository Assessment*, G. K. Jacobs and S. K. Whatley, ed. Oak Ridge National Laboratory, NUREG/CP-0062, ORNL/TM-9585.

Plummer, L. N., D. L. Parkhurst, G. W. Fleming, and S. A. Dunkle. 1988. *PHRQPITZ - A Computer Program for Geochemical Calculations in Brines*. Water Resources Investigation Report 88-4153. Reston, VA: US Geological Survey.

Popielak, R. S., R. L. Beauheim, S. R. Black, W. E. Coons, C. T. Ellingson, and R. L. Olsen. 1983. *Brine Reservoirs in the Castile Formation, Waste Isolation Pilot Plant (WIPP) Project, Southeastern New Mexico*. Waste Isolation Pilot Plant Report TME 3153. Albuquerque, NM: US Department of Energy.

Ramey, D. S. 1985. *Chemistry of Rustler Fluids*. EEG-31. New Mexico Environmental Evaluation Group.

Randall, W. S., M. E. Crawley, and M. L. Lyon. 1988. *Annual Water Quality Data Report for the Waste Isolation Pilot Plant*. DOE-WIPP 88-006. Carlsbad, NM: Waste Isolation Pilot Plant Project Office.

Reeder, R. J. 1981. "Electron Optical Investigation of Sedimentary Dolomites." *Contributions to Mineralogy or Petrology*, Vol. 76:148-157.

Reeder, R. J., and H. R. Wenk. 1979. "Microstructures in Low Temperature Dolomites." *Geophysical Research Letters*, Vol. 6:77-80.

Robinson, K. L. 1988. *Analysis of Solutes in Groundwaters from the Rustler Formation at and near the WIPP Site*. SAND86-0917. Albuquerque, NM: Sandia National Laboratories.

Saulnier, G. J. Jr., G. A. Freeze, and W. A. Stensrud. 1987. *WIPP Hydrology Program, Waste Isolation Pilot Plant, Southeastern New Mexico, Hydrologic Data Report #4*. SAND86-7166. Albuquerque, NM: Sandia National Laboratories.

Schultz, L. G. 1969. "Lithium and Potassium Absorption, Dehydroxylation Temperature, and Structural Water Content of Aluminous Smectites." *Clays and Clay Minerals*, Vol. 17:115-149.

Seyfried, W. E., Jr., D. R. Janecky, and M. L. Mottl. 1984. "Alteration of the Oceanic Crust: Implications for Geochemical Cycles of Lithium and Boron." *Geochimica et Cosmochimica Acta*, Vol. 48:557-569.

Seyhan, E., A. A. van de Griend, and G. B. Engelen. 1985. "Multivariate Analysis and Interpretation of the Hydrogeochemistry of a Dolomite Reef Aquifer, Northern Italy." *Water Resources Research*, Vol. 21, No. 7:1010-1024.

Smith, C. L. 1976. "Use of Lithium and Chloride Concentrations in Ground Water for Lithium Exploration." *Lithium Resources and Requirements by the Year 2000*, J.D. Vine, ed. Professional Paper 1005. Washington, DC: US Geological Survey.

Smith, G. I. 1976. "Origin of Lithium and Other Components in the Searles Lake Evaporites, California." *Lithium Resources and Requirements by the Year 2000*, J. D. Vine, ed. Professional Paper 1005. Washington, DC: US Geological Survey.

Sonnenfeld, P. 1984. *Brines and Evaporites*. New York: Academic Press, Inc.

Spencer, R. J., H. P. Eugster, and B. F. Jones. 1985. "Geochemistry of Great Salt Lake, Utah II: Pleistocene-Holocene Evolution." *Geochimica et Cosmochimica Acta*, Vol. 49:739-747.

Statistical Analysis System Institute. 1982. *SAS User's Guide: Statistics*.

Stein, C. L., and J. L. Krumhansl. 1986. *Chemistry of Brines in Salt from the Waste Isolation Pilot Plant (WIPP), Southeastern New Mexico: A Preliminary Investigation*. SAND85-0897. Albuquerque, NM: Sandia National Laboratories.

Stumm, W., and J. J. Morgan. 1981. *Aquatic Chemistry: An Introduction Emphasizing Chemical Equilibria in Natural Waters*. 2nd ed. New York: John Wiley and Sons.

Tien, P. L., M. D. Siegel, C. D. Updegraff, K. K. Wahi, and R. V. Guzowski. 1985. *Repository Site Data Report for Unsaturated Tuff, Yucca Mountain, Nevada*. SAND84-2668 (also NUREG/CR-4110). Albuquerque, NM: Sandia National Laboratories.

Truesdell, A. H., and B. F. Jones. 1974. "WATEQ: A Computer Program for Calculating Chemical Equilibria of Natural Waters." *US Geological Survey Journal of Research*, Vol. 2:233-248.

Uhland, D. W., and W. S. Randall. 1986. *Annual Water Quality Data Report*. DOE-WIPP-86-006. Carlsbad, NM: Waste Isolation Pilot Plant Project Office.

Uhland, D. W., W. S. Randall, and R. C. Carrasco. 1987. *Annual Water Quality Data Report, March, 1987*. DOE-WIPP-87-006. Carlsbad, NM: Waste Isolation Pilot Plant Project Office.

Wolery, T. J. 1983. *EQ3NR, A Computer Program for Geochemical Aqueous Speciation-Solubility Calculations: User's Guide and Documentation*. UCRL-53414. Livermore, CA: Lawrence Livermore National Laboratory.

Wolery, T. J., D. J. Isherwood, K. J. Jackson, J. M. Delany, and I. Puigdomenech. 1985. "EQ3/6: Status and Applications." *Proceedings of the Conference on the Application of Geochemical Models to High-Level Nuclear Waste Repository Assessment*, G. K. Jacobs and S. K. Whatley, ed. NUREG/CP-0062, ORNL/TM-9585. Oak Ridge, TN: Oak Ridge National Laboratory.

APPENDIX 2A. MINERALS INCLUDED IN SATURATION INDEX CALCULATIONS WITH PHRQPITZ

As discussed in Section 2.3.4, the code PHRQPITZ (Plummer et al., 1988) was used to calculate saturation indices for many minerals found in evaporite environments. The minerals and their formulas are listed in Table 2A.1.

Table 2A.1. Chemical Formulas of Minerals Included in Saturation-Index Calculations with PHRQPITZ

Mineral (synonym)	Formula
Anhydrite	$CaSO_4$
Aragonite	$CaCO_3$
Arcanite	K_2SO_4
Bischofite	$MgCl_2 \cdot 6H_2O$
Bloedite	$Na_2Mg(SO_4)_2 \cdot 4H_2O$
Brucite	$Mg(OH)_2$
Burkeite	$Na_6CO_3(SO_4)_2$
Calcite	$CaCO_3$
Carnallite	$KMgCl_3 \cdot 6H_2O$
Dolomite	$CaMg(CO_3)_2$
Epsomite	$MgSO_4 \cdot 7H_2O$
Gaylussite	$Na_2Ca(CO_3)_2 \cdot 5H_2O$
Glaserite (Aphthitalite)	$K_3Na(SO_4)_2$
Glauberite	$Na_2Ca(SO_4)_2$
Gypsum	$CaSO_4 \cdot 2H_2O$
Halite	$NaCl$
Hexahydrite	$MgSO_4 \cdot 6H_2O$
Kainite	$KMgClSO_4 \cdot 3H_2O$
Kalicinite	$KHCO_3$
Kieserite	$MgSO_4 \cdot H_2O$
Leonhardtite (Starkeyite)	$MgSO_4 \cdot 4H_2O$
Leonite	$K_2Mg(SO_4)_2 \cdot 4H_2O$
Magnesite	$MgCO_3$
Mirabilite	$Na_2SO_4 \cdot 10H_2O$
Misenite	$K_2SO_4 \cdot 6KHSO_4$
Nahcolite	$NaHCO_3$
Natron	$Na_2CO_3 \cdot 10H_2O$
Nesquehonite	$Mg(HCO_3)(OH) \cdot 2H_2O$
Pentahydrite	$MgSO_4 \cdot 5H_2O$
Pirssonite	$Na_2Ca(CO_3)_2 \cdot 2H_2O$

Table 2A.1. Chemical Formulas of Minerals Included in Saturation-Index Calculations with PHRQPITZ (Continued)

Mineral (synonym)	Formula
Polyhalite	$K_2Ca_2Mg(SO_4)_4 \cdot 2H_2O$
Portlandite	$Ca(OH)_2$
Schoenite (Picromerite)	$K_2Mg(SO_4)_2 \cdot 6H_2O$
Sylvite	KCl
Syngenite	$K_2Ca(SO_4)_2 \cdot H_2O$
Trona	$Na_3H(CO_3)_2 \cdot 2H_2O$

APPENDIX 2B. USE OF PRINCIPAL COMPONENT ANALYSIS IN ANALYSIS OF HYDROCHEMICAL DATA: GENERAL PRINCIPLES

2B.1 Introduction

2B.1.1 Purpose and Background

This appendix will acquaint the reader with the basic concepts and vocabulary of principal component analysis (PCA). A detailed explanation of the mathematical principles that underly the technique is beyond the scope of this work. Similarly, a review of previous applications of PCA in geochemical studies is not included here. Excellent discussions of the theory and applications of PCA can be found in Davis (1973) and Klovan (1975). Applications of PCA in a study similar to the present one can be found in Hitchon et al. (1971). A number of other studies are reviewed by Drever (1982). An enlightening and entertaining explanation of the principles and history of PCA can be found in Gould (1981). The following discussion of the relationship between PCA and correlation coefficients is taken in part from that reference.

2B.1.2 Distinction Between Factor Analysis and Principal Component Analysis

The terms "factor" and "principal component" are often used interchangeably in the literature. There are important distinctions between classical PCA and classical factor analysis, however. In the present study, PCA was used exclusively.

In classical PCA, no assumption is made concerning the underlying structure of the data. The technique is primarily a mathematical method of transforming the original variables into another smaller set of variables. Classical factor analysis, on the other hand, requires

an *a priori* model for the underlying structure of the data set. Specifically, it is assumed that part of the variance of each variable is unique and not attributable to the influence of the factors (perhaps due to random error).

In most texts and publications, the strict definitions of factor analysis and PCA are not distinguished. The analysis presented below is a PCA; however, it is equivalent to analyses commonly referred to as "factor analysis" in the literature. In this report, the term "factor" is used interchangeably with the term "principal component" to improve readability and to save space in the data tables.

2B.2 Interelement Correlations

PCA is a mathematical method to find the basic structure underlying a large number of bivariate correlations. Understanding the significance of correlations among the concentrations of groundwater solutes is a prerequisite to understanding applications of PCA to water chemistry data. In addition, many of the limitations and potential misuses of PCA can be more easily illustrated by examples from bivariate correlation analysis.

2B.2.1 Bivariate Correlations

If the concentrations of two elements in a suite of chemical analyses vary sympathetically, then the concentrations are said to be "correlated." If the concentrations of both elements increase or decrease in concert, then the elements are "positively correlated;" if the increase in the concentration of one element is accompanied by a decrease in another element, then the elements are "negatively correlated." If the values of the two sets of concentrations have been normalized by dividing by the variance of their respective sample distributions, then the strength of the correlation is expressed by "r," the Pearson's product coefficient (often called the correlation coefficient). The value of r ranges from +1 for perfect positive correlation to -1 for a perfect negative correlation; a value of 0 denotes no correlation. The equations used to calculate the covariance and the correlation coefficient

and the assumptions underlying their use can be found in many standard statistics texts (such as Davis, 1973) and will not be presented here.

The fact that two variables are strongly correlated cannot be used to prove that a causal relationship exists between them. Gould (1981) provides a good discussion of the potential pitfalls of overinterpreting the significance of strong correlations. He notes that although some moderate correlations do have an underlying cause (e.g., the correlation between arm length and leg length in children), other strong correlations have no causal connection (e.g., the author's age and the price of gasoline during the 1970's). Similarly, the existence of a correlation between the concentrations of two elements alone does not prove the existence of a particular chemical process relating the elements. The techniques of correlation and PCA must be used in conjunction with other methods, such as thermodynamic or hydrologic modeling. This combination of techniques can be used to suggest alternative models for the chemical processes that have produced an observed groundwater composition.

2B.2.2 Examples of Bivariate Correlations Between Concentrations

Meaningful interpretation of observed interelement correlations requires an understanding of the types of chemical processes that are likely to occur in the groundwater system. Examples of correlations that may be produced by different kinds of chemical processes are given below.

1. A positive correlation could reflect a common source for two solutes.

$$CaSO_4 \rightarrow Ca^{2+} + SO_4^{2-} \qquad \text{(B1)}$$

Equation B1 describes the dissolution of anhydrite. The concentrations of calcium and sulfate would be positively correlated in a groundwater that is dissolving anhydrite, if there are no other significant sources of these two elements and if the

water is undersaturated with respect to other minerals containing Ca^{2+} and SO_4^{2-} (e.g., gypsum).

A related example involves substitution of a trace metal (such as strontium) for calcium in the anhydrite. The concentration of the trace metal would be positively correlated with those of calcium and sulfate in waters in which the anhydrite was dissolving.

2. A negative correlation could be due to mineral saturation and a common ion effect.

$$Ca^{2+} + SO_4^{2-} + 2H_2O \leftrightarrow CaSO_4 \cdot 2H_2O \qquad \text{(B2)}$$

$$K_{sp}^{gyp} = a_{Ca^{2+}} \cdot a_{SO_4^{2-}} \cdot a_{H_2O}^2 \qquad \text{(B3)}$$

Equation B2 describes the dissolution/precipitation of gypsum. If a groundwater is in equilibrium with gypsum, then the concentrations of calcium and sulfate will be related via the solubility product of gypsum, defined in Equation B3. If the concentration of one ion increases due to contributions from another source, then the concentration of the other ion will decrease (common ion effect), resulting in a negative correlation between the calcium and the sulfate.

3. Correlations can result from coupled chemical reactions.

$$CaMg(CO_3)_2 + 2H_2O + 2CO_2 \rightarrow Ca^{2+} + Mg^{2+} + 4HCO_3^- \qquad \text{(B4)}$$

$$CaSO_4 \cdot 2H_2O \rightarrow Ca^{2+} + SO_4^{2-} + 2H_2O \qquad \text{(B5)}$$

$$Ca^{2+} + HCO_3^- \rightarrow CaCO_3 + H^+ \qquad \text{(B6)}$$

Equations B4 through B6 represent a set of chemical reactions that occur during dedolomitization of carbonate aquifers (Back et al., 1983). In the rock, the net result of these reactions is the dissolution of dolomite and gypsum and the precipitation of calcite. In the groundwater, the net result is the decrease of pH and the increase in the concentrations of magnesium and sulfate as the reactions proceed. Thus, in a system in which dedolomitization is occurring along the hydrologic flow path, a negative correlation between pH and sulfate and magnesium could be observed.

2B.3 Principal Component Analysis

2B.3.1 Correlations Among Many Variables and the Goal of Principal Component Analysis

When relationships among many variables are important, a matrix of correlations between all possible pairs of variables can be constructed. Table 2B-1 is a correlation matrix for six major solutes in groundwaters at the WIPP Site. The matrix lists correlation coefficients describing the correlation between the elements identified in the corresponding row and column. PCA can be used to describe the information given by the bivariate correlations in the correlation matrix in terms of a smaller number of variables called principal components or factors.

The techniques and meaning of PCA can be understood more easily by using a geometric representation of correlation matrices as presented by Gould (1981). The set of variables in the correlation matrix is represented by a set of unit vectors radiating from a common origin. In six-dimensional space, the correlation coefficient between a pair of variables is equal to the cosine of the angle between their respective vectors. Thus, the vectors of two variables that are perfectly correlated coincide, and the cosine of the angle between them equals 1.00. The vectors of two variables that are completely uncorrelated are orthogonal, and the cosine of the angle between them equals zero. In Figure 2B-1, each variable in Table 2B-1 is represented by a unit vector. In this two-dimensional figure, the

Table 2B-1. Correlation Matrix for Major-Solute Data[1] in Culebra Groundwaters

Variable	Ca	Mg	K	Na	Cl	SO_4
Ca	1.000	0.492	0.414	0.568	0.606	0.043
Mg	0.492	1.000	0.906	0.907	0.893	0.836
K	0.414	0.906	1.000	0.946	0.930	0.847
Na	0.568	0.907	0.946	1.000	0.994	0.810
Cl	0.606	0.893	0.930	0.994	1.000	0.760
SO_4	0.043	0.836	0.847	0.810	0.760	1.000

1. The data are the common logarithms of the solute concentrations in mg/L.

angles are distorted from their true values. The figure shows principal components (factors) for a hypothetical unrotated R-mode analysis. The first principal component (or factor, labelled I) lies as close as possible to the largest number of vectors; the second principal component (or factor, labelled II) is orthogonal to the first.

In Figure 2B-1, five of the six variables are highly correlated and their vectors lie within a tight cluster. The extraction of the first principal component from the correlation matrix involves finding an axis that can be used as a grand average of all six vectors. This is equivalent to accounting for as much of the variance of the data set as possible with a single axis. The amount of variance of each variable that a principal component describes (or resolves) is represented by the length of the projection of the variable's vector onto the principal component axis (see Figure 2B-2). This resolving power is called the "loading" of the variable onto the factor and is listed in the factor-loading matrix. The amount of variance of variable A resolved or "explained" by the principal component (or factor, labelled I) is equal to the ratio of the length of OA', the projection of OA onto the axis I, to the length of vector OA. In Figure 2B-2, vector OA lies close to the principal component and has a high loading onto the axis. In contrast, vector OB lies far from the principal component axis I. The principal component I explains little of the variance of variable B, and the loading of this variable onto the principal component is low.

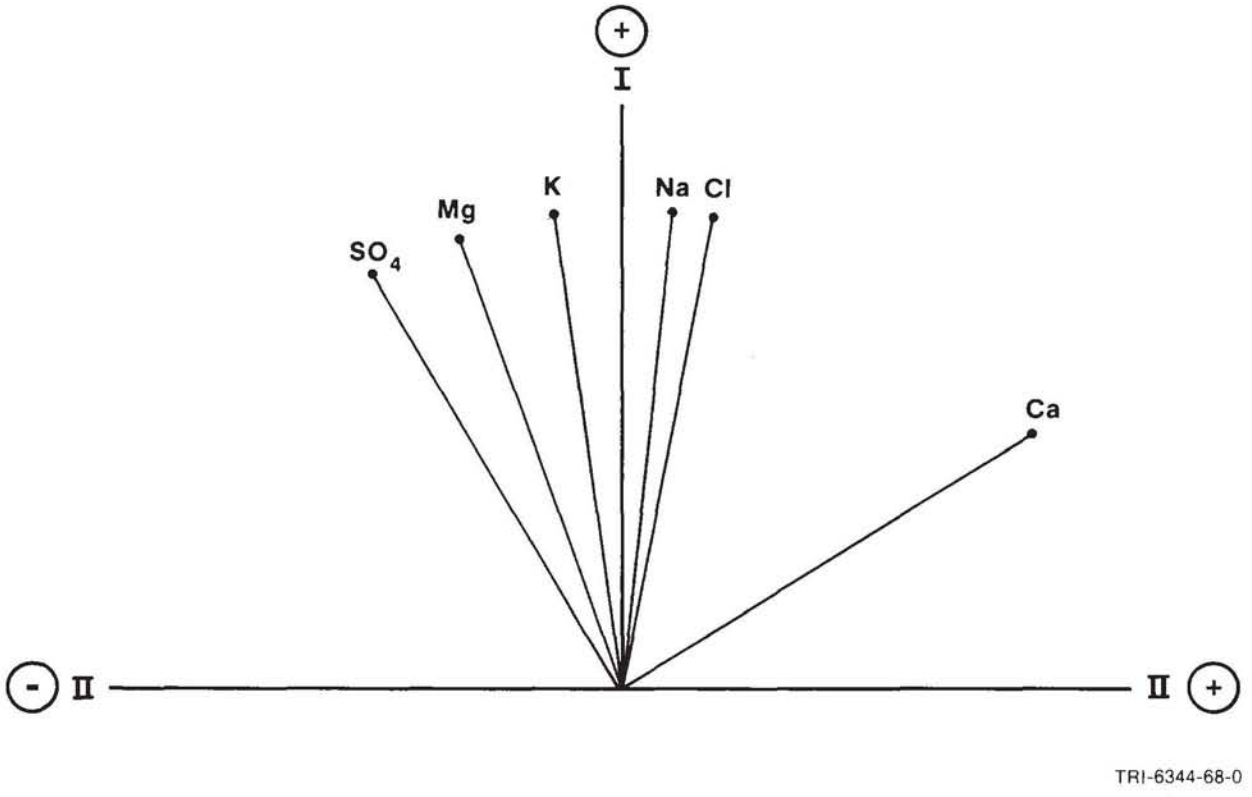

Figure 2B-1. Qualitative geometric representation of correlations among major solute concentrations for Culebra waters samples.

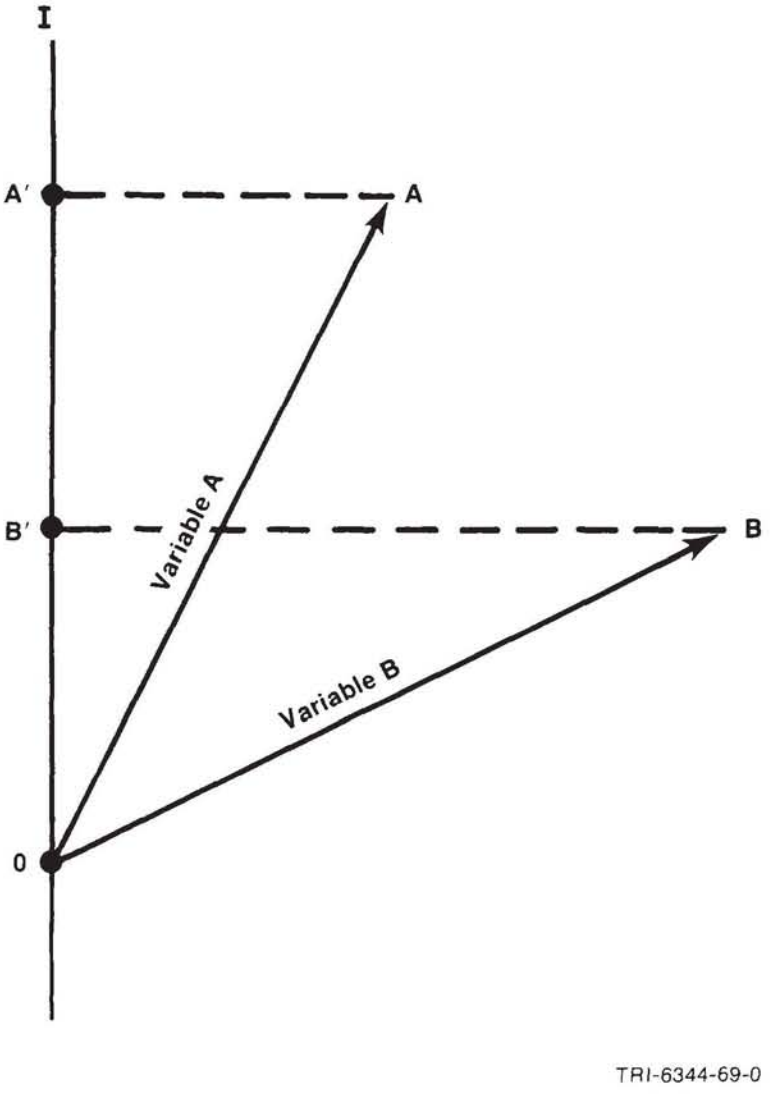

Figure 2B-2. Geometric representation of principal component (factor) loadings.

Mathematically, the principal components are obtained by extracting the eigenvectors of the correlation matrix. The necessary techniques can be found in many texts on linear algebra and will not be described here. In this example, the first principal component for the matrix in Table 2B-1 is shown in Figure 2B-1 and accounts for most of the variance of all the variables. A second principal component is located to account for as much of the remaining variance as possible. In most applications of PCA, all principal components are orthogonal to each other. Each succeeding principal component accounts for smaller and smaller amounts of the variance until either all of the variance in the data set has been accounted for or a predetermined amount of variance is resolved.

The communality, h_i^2, for the i^{th} variable (or i^{th} sample) is defined as the amount of variance of the i^{th} variable (or sample) that is accounted for by a set of principal components. It is calculated as:

$$h_i^2 = \sum_j F_{ij}^2$$

where F_{ij} is the loading of the i^{th} normalized variable (or sample) onto the j^{th} principal component.

The fraction of the variance of the i^{th} normalized variable (or sample) explained by the j^{th} principal component is F_{ij}^2 (the loading squared).

2B.3.2 Distinction Between R- and Q-Mode Principal Component Analysis

PCA can be used to express the relationships among a large number of variables in terms of correlations with a smaller number of underlying components, or to describe the characteristics of a sample suite by defining hypothetical end members of the population.

When the objective of the analysis is to find correlations among variables, R-mode analysis is employed. When the similarities among samples are examined, Q-mode analysis is used.

Figure 2B-1 was used to describe R-mode analysis; the unit vectors refer to individual variables (e.g., solute concentrations) and the cosines of the angles between the vectors equal the correlation coefficients. Figure 2B-3 provides the corresponding graphical representation for Q-mode analysis. Each vector in the figure corresponds to a different well water sample and the cosines of the angles between vectors are the similarity coefficients.

Q-mode analysis of the compositions of some Culebra water samples is described in Section 2.3.3.3. In the analysis, two principal components (factors) were sufficient to explain more than 99% of the total variance. The Q-mode factor-loading matrix is shown in Table 2-5 in Section 2.3.3.3. The two components can be thought of as "hypothetical entities that are completely dissimilar in terms of the proportions of their constituents" (Klovan, 1975, p. 51). Combinations of these components can be used to reconstruct the original water sample compositions. The "Factor A" and "Factor B" columns of Table 2-5 describe the similarity between a component and each sample. The rows of the table show the composition of each sample in terms of the components.

Q-mode analysis is used primarily to evaluate the statistical homogeneity of the sample population. If the data set is homogeneous, then it is amenable to R-mode analysis. A statistical criterion for recognizing homogeneity of a group of samples has not been developed for geological applications of PCA. In previous studies, if two or three Q-mode principal components accounted for most of the variance, then the population was considered homogeneous enough for R-mode analysis (see Hitchon et al., 1971; Klovan, 1975; Drever, 1982).

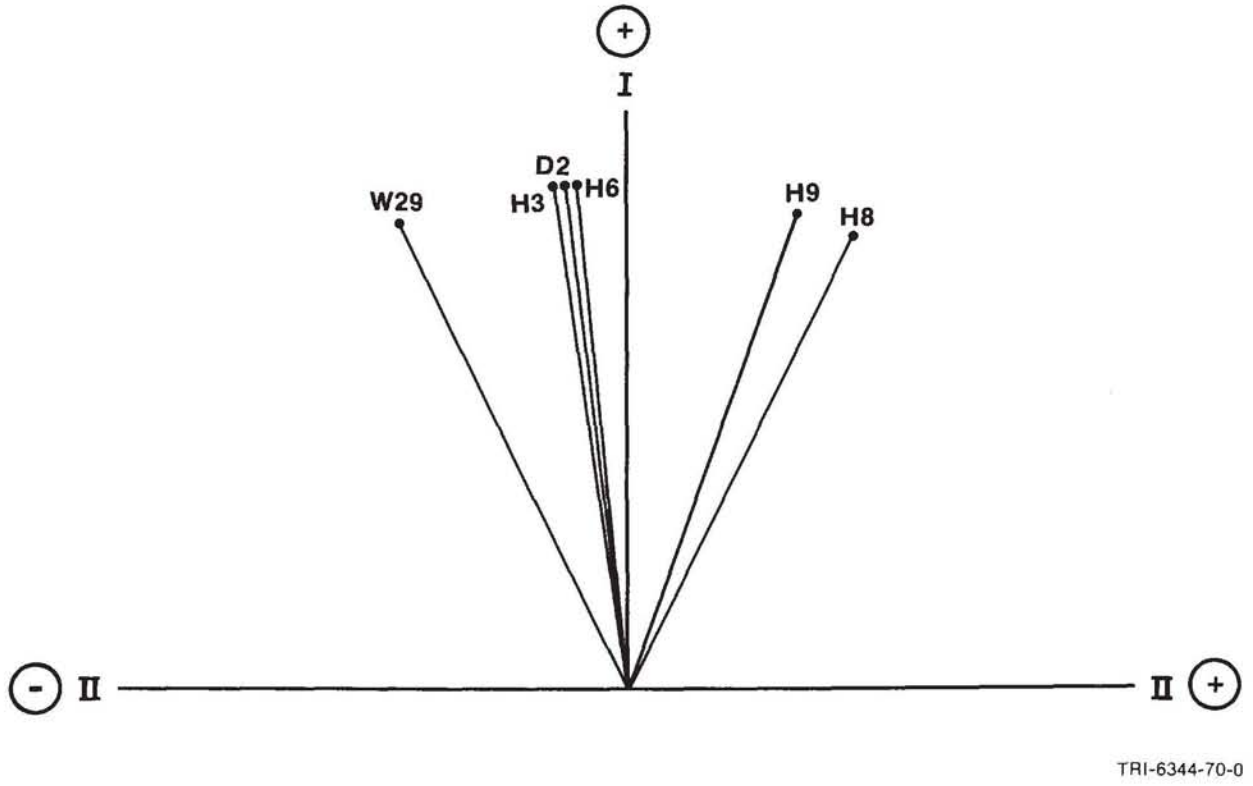

Figure 2B-3. Qualitative geometric representation of a similarity matrix for water sample compositions.

2B.3.3 Factor-Loading and Factor-Score Matrices

In R-mode analysis, the eigenvalues and eigenvectors of the correlation matrix are extracted; in Q-mode analysis, the similarity matrix (Klovan, 1975) is examined. The extraction of the eigenvectors in both R-mode and Q-mode analysis "decomposes" the original matrix into a "factor-loading matrix" and a "factor-score matrix:"

- The factor-loading matrix of a Q-mode analysis describes compositions of samples in terms of the Q-mode factors.

- The factor-loading matrix of an R-mode analysis describes the relations among the variables in terms of the R-mode factors.

Figure 2B-4 provides a graphical representation of the first two principal components (factors) of the correlation matrix shown in Table 2B-1 and the vectors shown in Figure 2B-1; it depicts the factor loadings. Factor loadings have values between +1 and -1 if they are expressed as fractions or between 100% and -100% if they are expressed as percents. In R-mode analysis, if the loadings of two variables have the same sign, the variables are positively correlated; if they have opposite signs, they are negatively correlated. If a sample has a high loading in a Q-mode factor-loading matrix, it is similar in composition to the factor. The absolute sign of any particular variable or sample in the factor-loading matrix is unimportant; only the relationships among the variables and samples provide useful information:

- The factor-score matrix from a Q-mode analysis describes the relations among the variables in terms of the Q-mode factors.

- The factor-score matrix from an R-mode analysis describes compositions of samples in terms of the R-mode factors.

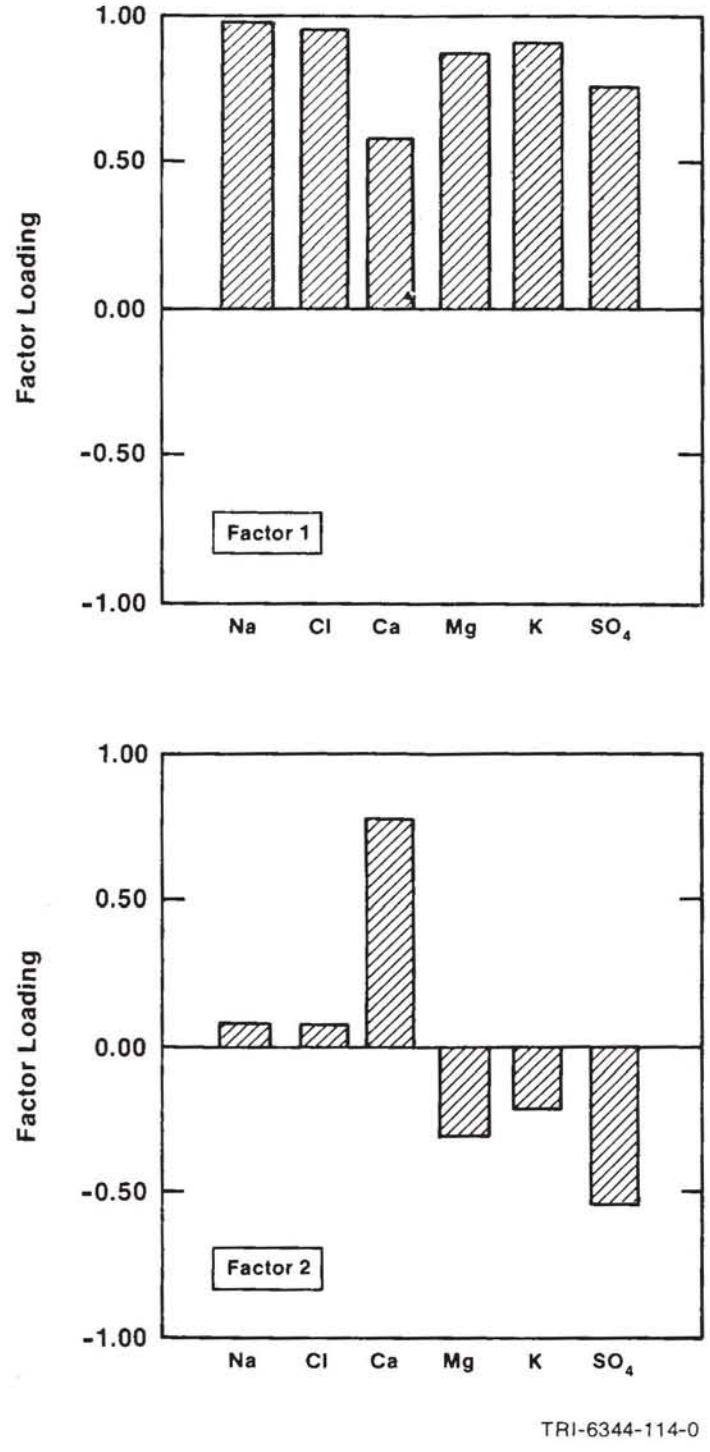

Figure 2B-4. Graphical representation of R-mode principal-component (factor) loadings.

The scales and absolute values of the factor-score matrix are not easily interpreted; the matrix should be examined in terms of the relative relationships between the samples or variables.

2B.4 Mathematical Options in PCA

2B.4.1 Data Pretreatment

Before the correlation or similarity matrix of the data set is calculated, the raw data may be transformed by arithmetic operations. Commonly used transformations include standardization (Davis, 1973), percent sample and percent range transformations, percent maximum value (Bopp and Biggs, 1981), and logarithmic transformations of raw or percent range/sample/maximum data (Seyhan et al., 1985).

The choice of the type of transformation often involves subjective judgment on the part of the analyst. For example, the solute concentrations could be represented as percents of the range of values or percents of the maximum value in order to prevent the variance of major elements from swamping the patterns of minor element variations.

A basic assumption of PCA is that the principal components are linearly related. A natural log or $\log_{10}$ transformation of water quality analyses may be appropriate since the total dissolved solid (TDS) concentrations of water samples often approximate log-normal distributions (Hitchon et al., 1971). Most of the uses of PCA in hydrochemical facies have factored the raw (untransformed) data; thus, transformation is not always necessary to obtain an interpretable set of principal components. In the present study, the $\log_{10}$ of the concentrations was used to calculate the correlation matrix.

2B.4.2 Partialling Out a Variable: PCA of Partial-Correlation Matrices

In some cases, many solutes may be strongly correlated with one or two major solutes, and the relationships among the other variables may be obscured by this effect. In this report, for example, nearly all variables were strongly correlated with the TDS and the sodium and chloride concentrations. To examine the relationships among the other solutes independent of this correlation, the principal components of the partial-correlation matrix with respect to TDS were extracted.

In this work, the effects of TDS were partialled out in the following way.

First, the linear regression equations were solved for each variable as a function of the TDS.

$$\log(Na) = a_1 + b_1 \log(TDS) + e_{Na} \quad \text{(B7a)}$$

$$\log(Ca) = a_2 + b_2 \log(TDS) + e_{Ca} \quad \text{(B7b)}$$

etc.

where a_1 and b_1 are the linear regression terms (intercept and slope), e_x is an error term, and (x) is the concentration of solute x.

Next, the residuals from each of these equations were calculated:

$$res(Na)_i = \log (Na)_i - \log (\hat{Na})_i \quad \text{(B8a)}$$

$$res(Ca)_i = \log (Ca)_i - \log (\hat{Ca})_i \quad \text{(B8b)}$$

etc.

where i refers to the i^{th} water sample and $(\hat{Na}_i)$, $(\hat{Ca}_i)$, etc., are the predicted values from the regression equations.

Then, the partial correlations with respect to TDS were calculated for all pairs of variables. The partial correlation between any two variables adjusted for the TDS is defined as the simple correlation of their residuals. For example, the partial correlation of Na and Ca adjusted for TDS is:

$$r_{Na,Ca.TDS} = \frac{\Sigma[\,res(Na_i) - \overline{res}(Na)][res(Ca_i) - \overline{res}(Ca)]}{\sqrt{\Sigma[res(Na_i) - \overline{res}(Na)]^2}\ \sqrt{\Sigma[res(Ca_i) - \overline{res}(Ca)]^2}} \qquad \text{(B9)}$$

where $\overline{res}(x)$ is the mean of the residuals for variable x.

The partial correlations with respect to TDS for all pairs of variables were calculated in this way.

Finally, these correlations were gathered into the partial-correlation matrix, and the eigenvectors for this matrix were extracted to obtain the principal components with the TDS partialled out.

The amount of variance of each variable that is explained by these factors can be calculated from R^2, the coefficient of determination for the regression equations (B7) above. R^2 is defined as the fraction of the variance of a variable explained by the regression expression. For example, the fraction of the variance of Na explained by the regression with TDS is the R^2 for Equation B7a. The percent of variance of Na that is not explained by correlation with TDS and that remains after the TDS is partialled out is equal to $1-R^2$ for Equation B7a. Thus, for each variable, $1-R^2$ is the total amount of variance that can be explained or resolved by the principal components extracted from the partial-correlation

matrix. The amount of variance that each of the principal components explains is calculated from the factor loadings as described above.

2B.4.3 Rotations

Extraction of the eigenvectors from the correlation or similarity matrix produces components that are constrained in two ways:

- The first principal component must account for the most variance, the second for the most of the remaining variance, and so on.

- The principal components must be orthogonal to one another.

Since the first component will represent a grand mean of all the correlations among variables, its orientation will be strongly influenced by the particular sample population. Therefore, the results of the PCA may not accurately reflect the true nature of the underlying independent components.

For example, in Figure 2B-1, the first principal component (factor) is drawn through the larger data cluster on the left. The loadings of all variables on the first factor are positive, whereas the loadings of some variables on the second factor are negative (Figure 2B-4). Both factors are important for Ca, Mg, K, and SO_4. Rotating the factors to coincide with clusters of samples, as shown in Figure 2B-5, "simplifies" the structure for these elements since only one factor is important for each variable. A graphical representation of the rotated factors is shown in Figure 2B-6. The effect of the rotation can be seen by comparing this figure with Figure 2B-4.

Several different rotational schemes exist; all attempt to "simplify" the structure or composition of the terminal (rotated) principal-component (factor) matrix. The rotation can be designed to simplify the complexity of the variables (quartimax rotation), the components (varimax rotation), or both (equimax rotation). In addition, rotations in which the principal

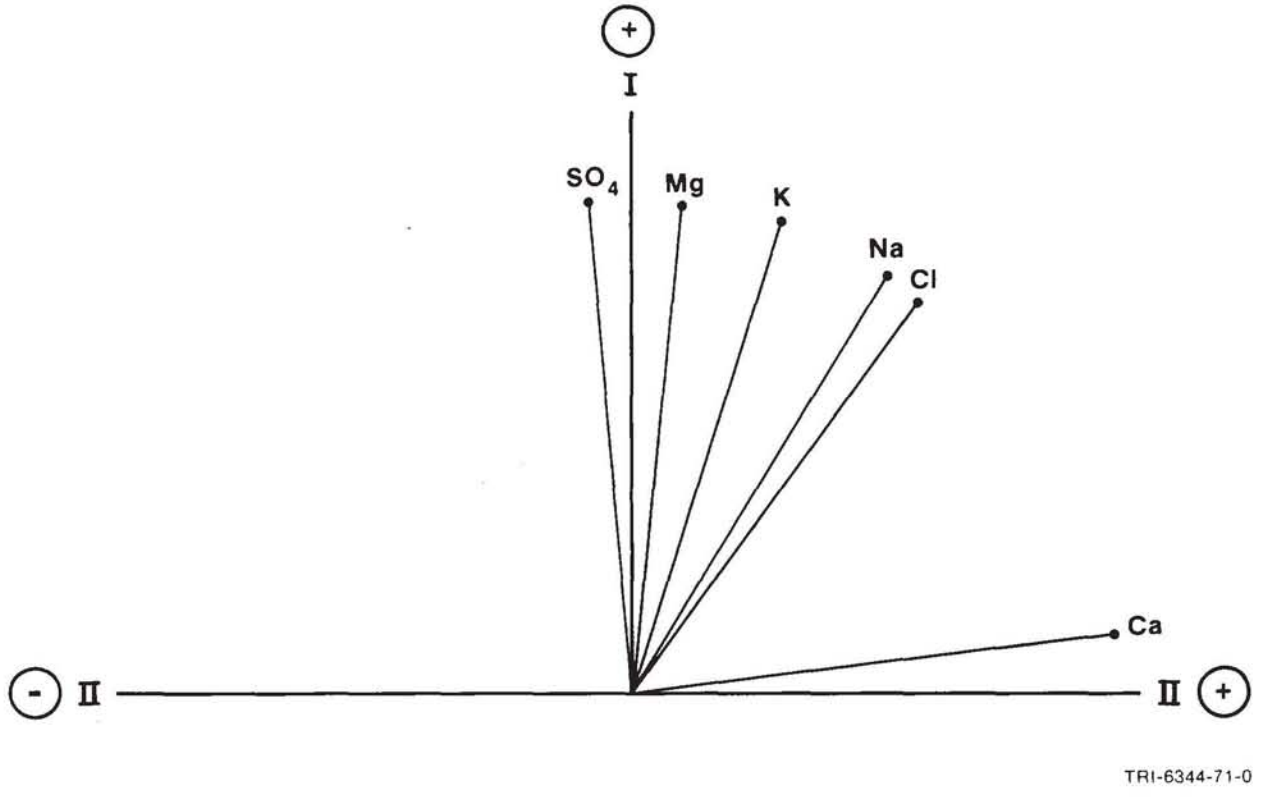

Figure 2B-5. Qualitative geometric representation of rotated principal components (factors).

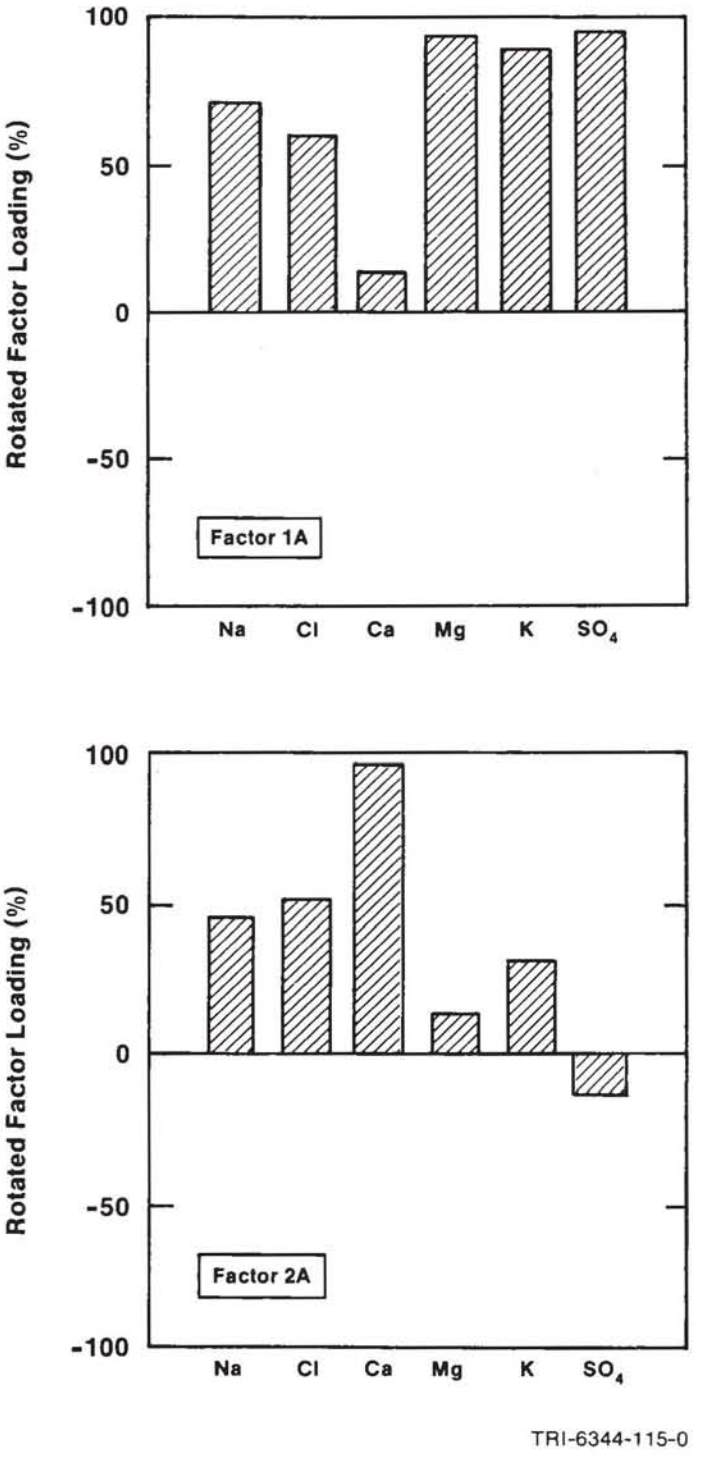

Figure 2B-6. Graphical representation of rotated R-mode principal-component (factor) loadings.

components (factors) are not constrained to be orthogonal (oblique transformations) are also used. Excellent descriptions of the mathematical criteria underlying the rotations used in this study can be found in Nie et al. (1975).

It cannot be said that any particular method of rotation is innately superior to another. All rotations are obtained from the same correlation matrix and therefore explain the same amount of variance. The insights provided by the different rotations are often complementary. In most cases, the choice of the "best" rotation will involve a great deal of subjectivity. PCA can only summarize the relationships among variables; the choice of rotational scheme must be based on the interpretability of the components and requires insight from other sources of information. In geochemical studies these other sources include thermodynamic constraints, geological data, and kinetic models.

APPENDIX 2C. VARIMAX R-MODE PRINCIPAL COMPONENT ANALYSIS OF CULEBRA WATERS: SUPPLEMENTAL RESULTS

2C.1 Introduction

Section 2.3.3 of this chapter summarizes the principal component analysis (PCA) of a data set comprising the chemical compositions of water samples from the Culebra dolomite. An introduction to the methods and objectives of PCA is given in Appendix 2B. Several rotations of the R-mode principal components were examined to assess the robustness of the factor-loading matrix. As discussed in Section 2.3.3, all the matrices contained the same key solute correlations observed in the unrotated principal components. Because the varimax rotation is the rotation most commonly used in the earth sciences, a more detailed PCA was carried out for this rotation. The results of this analysis are described in this appendix.

The data set examined in this analysis is designated as "population 1;" samples are listed in Table 2-4 in Section 2.3.3.2, and the solute data are given in Table 2-2 in Section 2.2.2. Q-mode and R-mode analyses of the data prior to varimax rotation are described in Sections 2.3.3.3 and 2.3.3.4. The interpretation of the factors in terms of geochemical processes is found in Section 2.2.4.

In this appendix, Section 2CVM discusses the varimax R-mode analysis of population 1. Section 2.CV- discusses the varimax R-mode analysis after total dissolved solids (TDS) were partialled out.

2C.2 Varimax R-Mode Analysis

2C.2.1 Factor Loadings

Five factors accounted for more than 99% of the variance. The factor-loading matrix is shown in Table 2C-1 and the first three factors (1A, 2A, and 3A) are shown in Figure 2C-1. At least 92% of the variance of each chemical variable is explained by the first five factors (that is, the communality, h_i^2, was > 0.92 for each variable). The first three factors account for 90% of the total variance of the data set. Because the other factors (4A and 5A) account for less than 10% of the variance, they are not considered further.

Factor 1A

Factor 1A accounts for 51% of the total variance of population 1 and is dominated by the covariance of nearly all the major and minor elements. The association Na-Cl-Br-B-Li may be due to the dissolution of halite and other evaporite salts. The association of K with this assemblage may reflect dissolution of polyhalite associated with halite. The B and Li could also be desorbed from iron oxyhydroxide inclusions in the polyhalite. Factor 1A accounts for 85% of the variance in K, for approximately 70 to 75% of the variance in Na, Cl, and Li, and for approximately 50 to 55% of the variance in B and Br.

The only element that has a significant negative loading on factor 1A is silicon; this factor accounts for 42% of the variance of this element.

Factor 1A also explains 74% of the variance of Mg and 94% of the variance of sulfate. The strong correlation of magnesium and sulfate with the solutes attributed to dissolution of halite and other evaporite salts may reflect dissolution of polyhalite or the increase of gypsum and dolomite solubility with increasing ionic strength as discussed in Section 2.4.

Table 2C-1. Varimax R-Mode Factor Loadings (Percent) for Culebra Groundwaters (Population 1)

Element	Factor 1A	Factor 2A	Factor 3A	Factor 4A	Factor 5A	Communality (h_i^2)
Na	88	45	- 6	- 1	10	99.0
Cl	85	50	- 2	0	9	98.1
Ca	14	97	- 9	- 2	4	97.9
Mg	86	36	-11	-29	-11	98.0
K	92	30	5	-10	- 7	95.3
Sr	39	90	-13	-10	0	98.8
pH	-22	-11	-49	83	3	99.3
HCO_3	-10	-15	94	-19	- 4	95.9
SO_4	97	-12	-18	-10	4	99.1
SiO_2	-65	-10	65	-33	- 1	97.1
Br	75	56	-17	- 2	14	92.3
B	72	20	-45	17	45	98.5
Li	82	30	-34	-11	21	94.2

Amount and Percent of Variance Explained by Each Factor

Factor 1A	Factor 2A	Factor 3A	Factor 4A	Factor 5A
6.418	2.936	1.981	0.996	0.304
51%	23%	16%	8%	2%

Factor 2A

Factor 2A accounts for 23% of the variance of population 1. It is qualitatively similar to factor 1A and includes a Na-Cl-Br association that may be indicative of halite dissolution. This factor accounts for only about 20 to 30% of the variance of these variables, however, and whereas factor 1A was dominated by Na and Cl, factor 2A is more strongly influenced by Br.

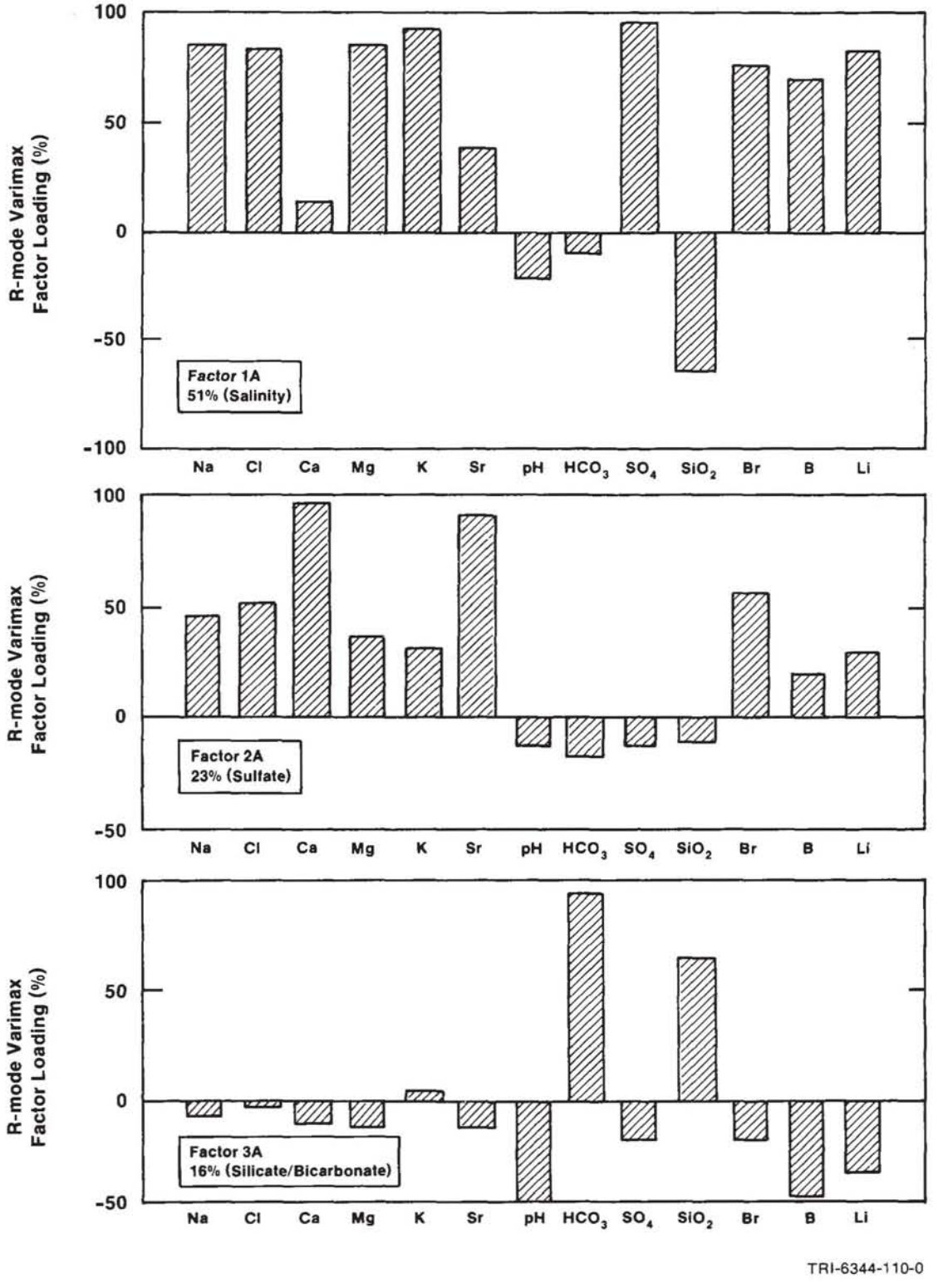

Figure 2C-1. Varimax R-mode factor loadings for factors 1A, 2A, and 3A of Culebra groundwaters (population 1).

Factor 2A is strongly influenced by the variance of Ca and Sr, accounting for 94% and 81% respectively of their variances. The negative correlations of these variables with both bicarbonate and sulfate are consistent with saturation with respect to both calcite and gypsum/anhydrite.

Factor 3A

Factor 3A accounts for approximately 16% of the total variance of population 1. It is dominated by the behavior of bicarbonate alkalinity, SiO_2, pH, B, and Li, and it accounts for 88%, 42%, 24%, 20%, and 12%, respectively, of their variances. It accounts for less than 5% of the variance of any of the other variables. The negative correlation between pH and alkalinity probably reflects carbonate equilibria. The relationship between Si, B, and Li may be related to ion exchange and silica diagenesis or desorption from clays as discussed in Section 2.4.

2C.2.2 Factor Scores

The compositions of the samples in terms of the three most important factors are described by the factor-score matrix, given in Table 2C-2. The scores are plotted in Figures 2C-2 through 2C-5 and are discussed in this section. Relationships between factor scores for the three most important factors are presented as bivariate plots in Figures 2C-2 and 2C-4. Spatial variation of the scores of factors 1A and 2A are plotted and contoured in Figures 2C-3 and 2C-5.

Factor 1A

Scores for factor 1A are lowest for samples from hydrochemical facies zone B and are highest for the sample from WIPP-29 (zone D) and for samples from zone A (Figure 2C-2). Factor 1A scores for samples from zone C are intermediate in value; within the zone, the scores are lowest for the P-14 sample and increase radially to the east, west, and north (Figure 2C-3).

Table 2C-2. Varimax R-Mode Factor Scores[1] for Culebra Groundwaters (Population 1)

Well	Coll. Date	Facies[2]	Factor 1A	Factor 2A	Factor 3A
DOE-1	4/85	A	0.59	0.22	-1.33
H-5C	10/81	A	1.16	0.34	-0.06
H-5B	8/85	A	0.84	0.23	-1.20
H-12	8/85	A	0.76	0.30	-1.25
P-17	3/86	A	0.61	0.32	-0.73
H-7B1	3/86	B	-1.36	-0.86	0.56
H-8B	1/86	B	-1.62	-1.39	-0.68
H-9B	11/85	B	-1.27	-1.13	-0.09
ENGLE	3/85	B	-1.27	-1.07	-0.05
DOE-2	3/85	C	-0.12	0.91	-0.48
H-2A	4/86	C	-0.30	-0.75	-0.42
H-3B3	2/85	C	0.09	0.39	-0.88
H-4B	7/85	C	0.29	-0.77	-0.32
H-6B	9/85	C	-0.03	0.86	0.16
P-14	2/86	C	-1.16	2.26	0.37
WIPP-25	2/86	C	-0.52	0.16	1.03
WIPP-26	11/85	C	-0.43	0.41	0.99
WIPP-28	9/80	C	0.53	-0.16	2.93
WIPP-30	9/80	C	0.32	-0.03	-0.38
WIPP-27	9/80	D	0.33	1.65	0.91
WIPP-29	12/85	D	2.54	-1.89	0.93

1. Factors 4A and 5A, which account for less than 10% of the total variance, are not given here or discussed in the text.
2. Hydrochemical facies in the Culebra, as defined in Section 2.3.2.1.

Factor 2A

The P-14 sample has the highest score for factor 2A; the WIPP-29 sample has the lowest score for this factor (Figure 2C-4). The hydrochemical facies zones are not clearly differentiated on the basis of this factor. Samples from zone A have factor scores of approximately 0.3 ± 0.1, whereas samples from zone B have values less than -0.8. Values for samples from zones C and D are quite variable, and no spatial pattern is evident (Figure 2C-5).

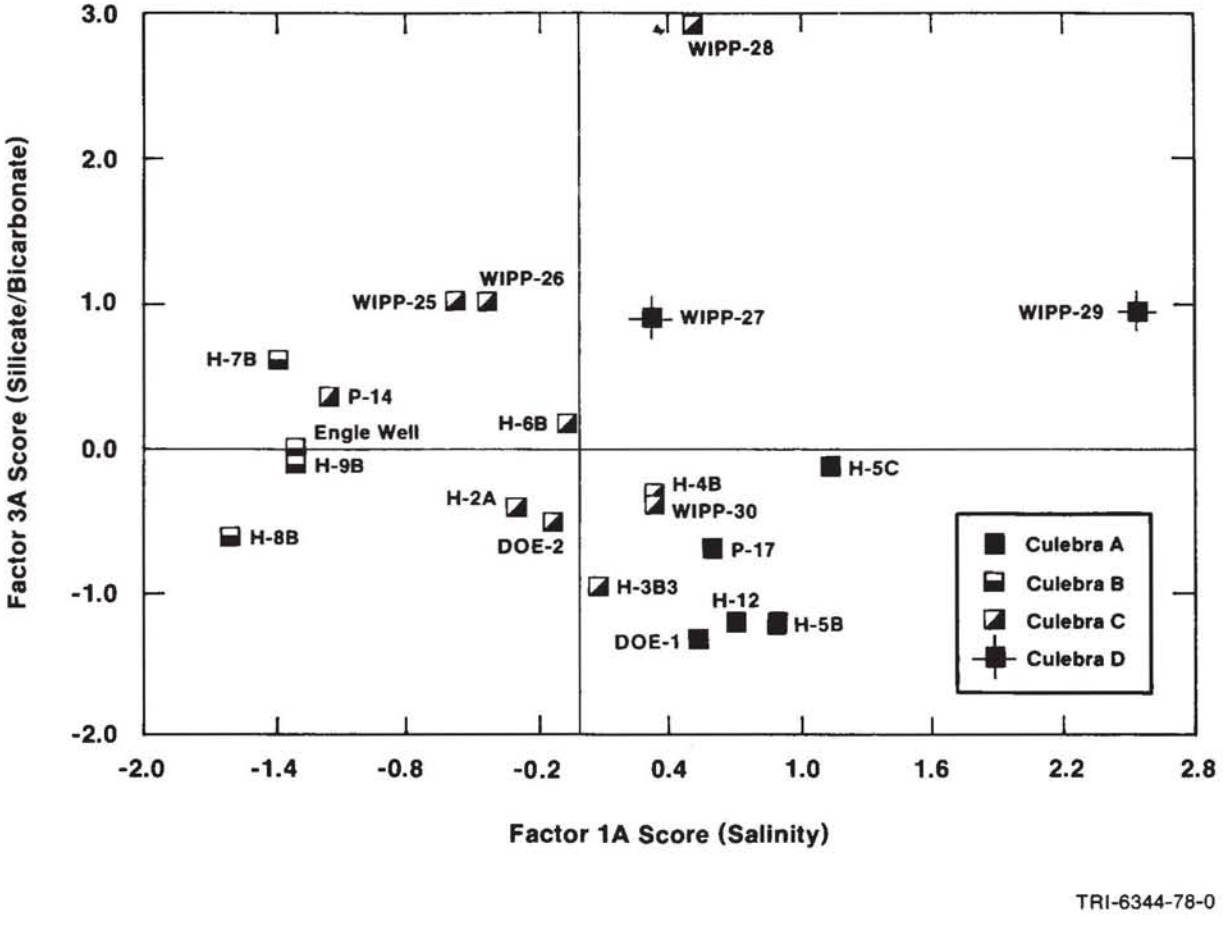

Figure 2C-2. Relationship between varimax R-mode factor scores for factors 1A and 3A of Culebra groundwaters (population 1).

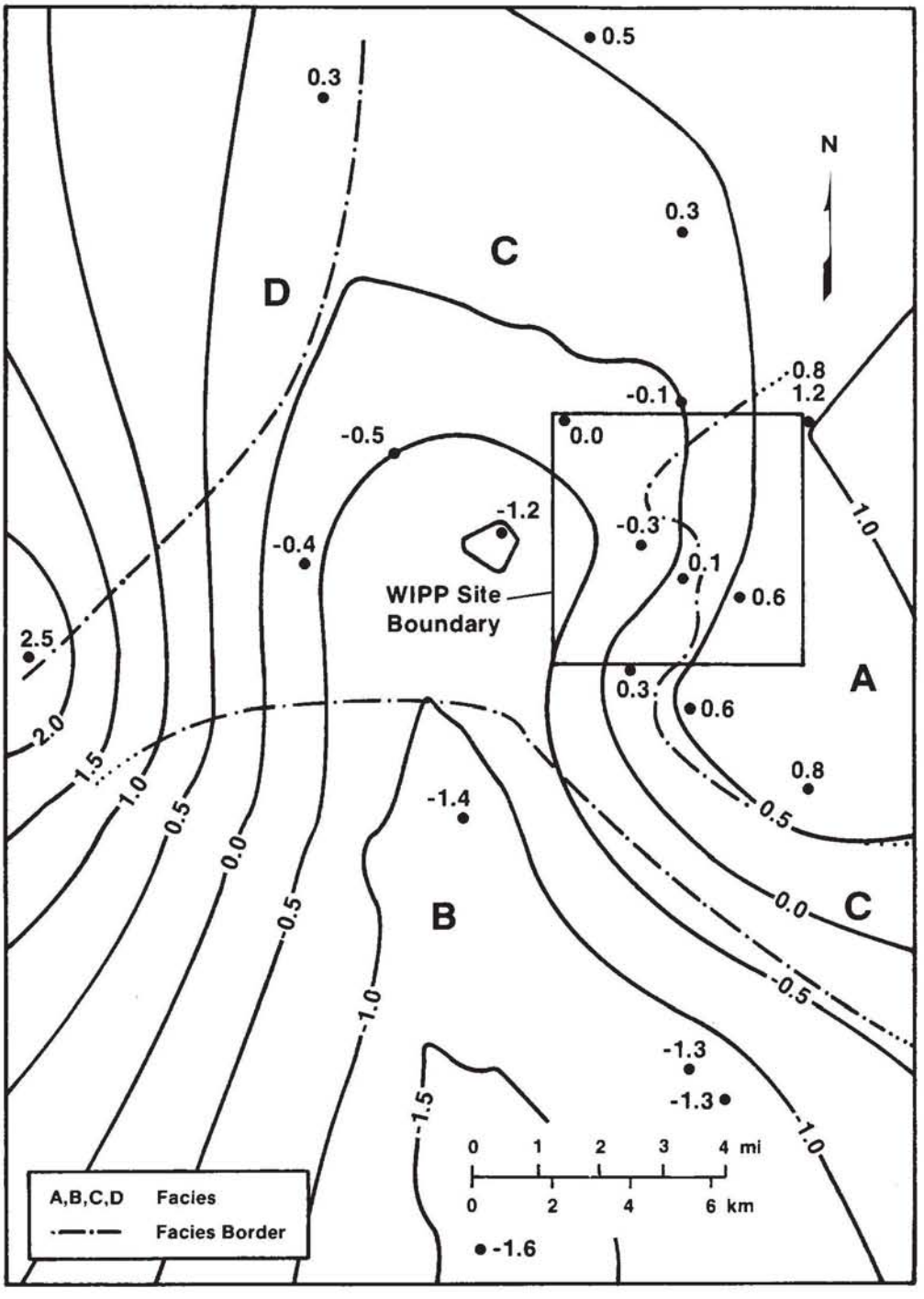

Figure 2C-3. Contours of varimax R-mode factor scores for factor 1A of Culebra groundwaters (population 1).

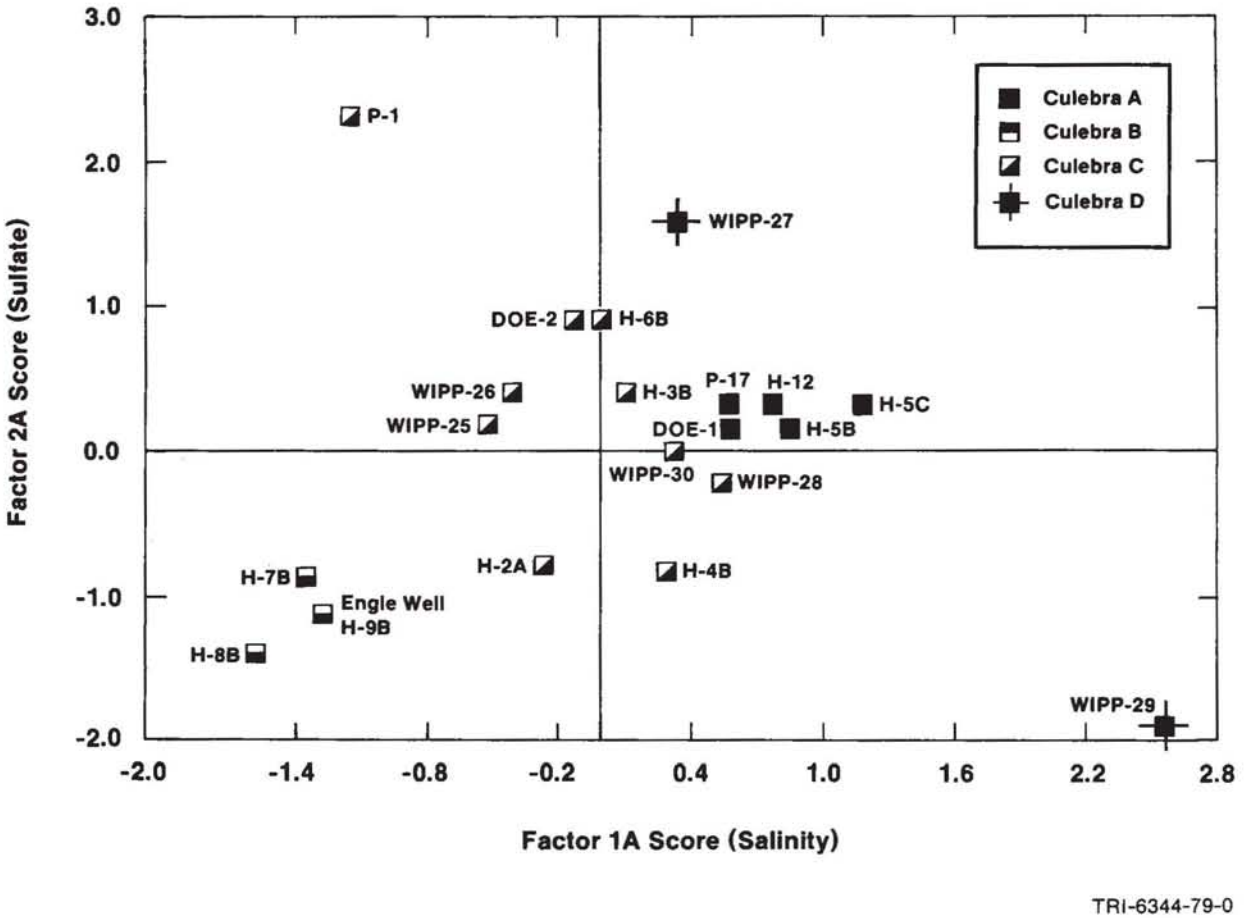

Figure 2C-4. Relationship between varimax R-mode factor scores for factors 1A and 2A of Culebra groundwaters (population 1).

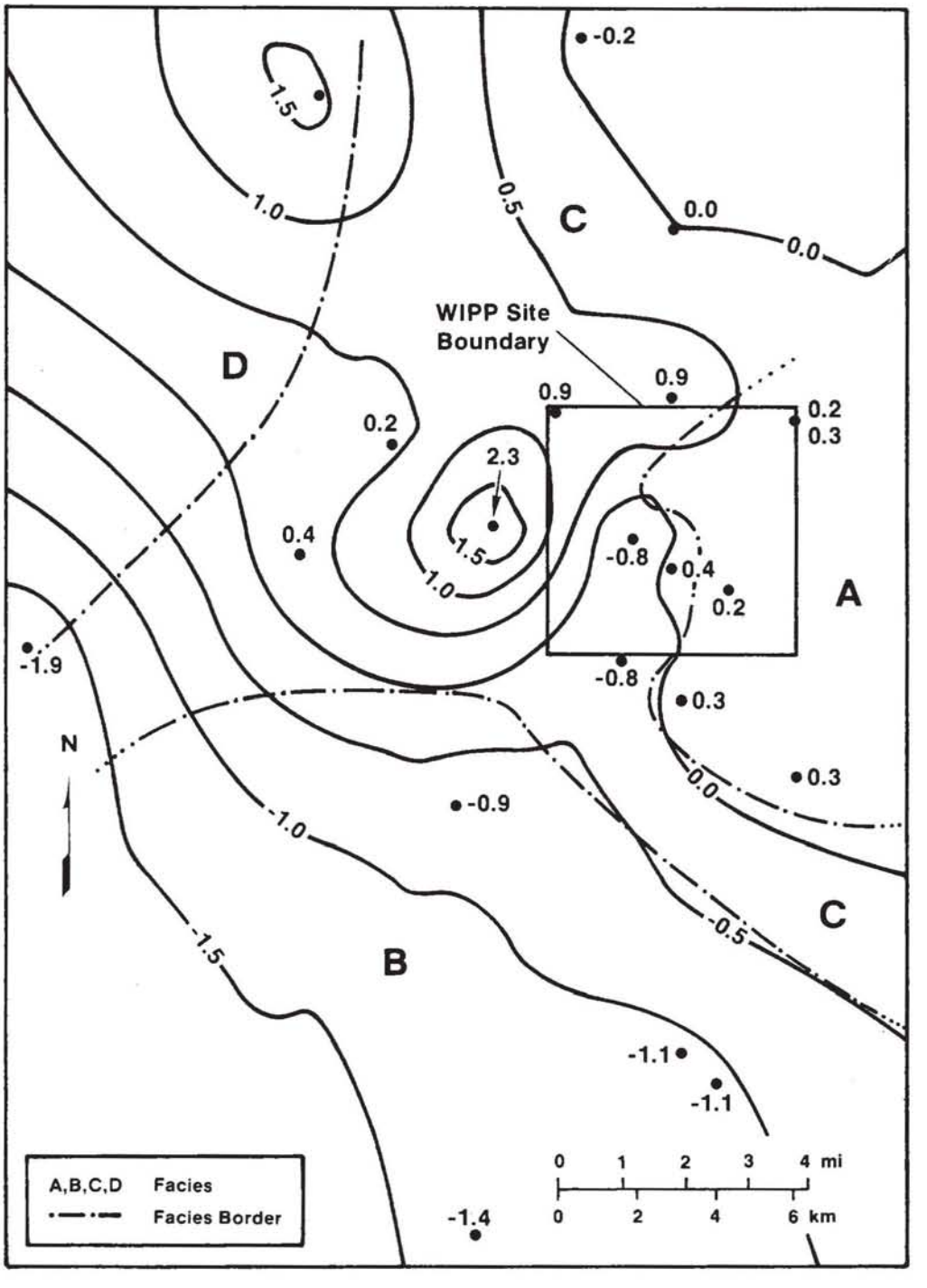

Figure 2C-5. Contours of varimax R-mode factor scores for factor 2A of Culebra groundwaters (population 1).

Factor 3A

The scores for factor 3A show little relationship to the hydrochemical facies (Figure 2C-2), although there is a general increase in the value of the score from west to east. The sample from WIPP-28 has the highest score and is anomalous compared to wells surrounding it; the bicarbonate content of the WIPP-28 sample, however, is known to be high because of contamination (see Section 2.2.2). Contours of the spatial distribution of scores for factor 3A are not plotted; however, the pattern is similar to that of SiO_2 presented in Figure 2-8 in Section 2.3.1.5.

2C.3 Varimax R-Mode Analysis With Total Dissolved Solids Partialled Out

2C.3.1 Objectives and Procedure

The three major factors obtained from the varimax R-mode analysis described above are all dominated by the effects of halite dissolution. Solutes are added directly from the halite or indirectly because the solubilities of sulfate and carbonate phases increase as the ionic strength increases (see Section 2.4.2).

A second varimax R-mode PCA was carried out to examine interelement correlations independent of the effects of halite dissolution. The analysis was carried out as follows. First, regression equations for each of the chemical variables as a function of the TDS were obtained. Next, the partial-correlation matrix with respect to TDS was obtained by calculating the correlations between the residuals from the regression equations. Then, the eigenvectors of the partial correlation matrix were extracted to give the factors. Finally, the varimax criterion was used to rotate the factors. A more detailed description of the procedure is in Appendix 2B.

This PCA is carried out on the variance in the population that is not correlated with variation in the TDS. The amount of this residual variance for each variable is shown in the last column of Table 2C-3. After accounting for the correlation with TDS, very little of the variance of Na, Mg, K, and Cl remains. In contrast, a significant portion of the variation in the concentrations of Ca, Sr, B, and SiO_2, the pH, and the alkalinity cannot be correlated with the TDS.

2C.3.2 Factor Loadings

Five factors accounted for 99% of the variance that remained after the TDS was partialled out. The factor-loading matrix for the five factors is shown in Table 2C-3. The factor loadings for the two most important factors are shown in Figure 2C-6 and are discussed below. For all five factors, the factor loadings for key elements (elements that have important geochemical significance or strongly influence the orientation of the factors, that is, with loadings >0.23) are discussed in Section 2.3.3.5.

Factor 1B

Factor 1B is dominated by the negative correlation of Ca and Sr with sulfate. It accounts for 67% of the total variance of Ca, 35% of the total variance of Sr, and 24% of the total variance of sulfate. This association is found in the factor 2A described previously and is suggestive of dissolution/coprecipitation of Sr and Ca in a sulfate phase such as gypsum or anhydrite.

Factor 2B

Factor 2B is similar to factor 3A. It shows two negatively correlated groups of variables. One group involves the correlation of Mg, K, bicarbonate alkalinity, and silica; the other group contains Na, pH, B, and Li. This pattern of element associations may be due to sorption onto a mineral surface, ion exchange, or silicate diagenesis. Several possible

Table 2C-3. Varimax R-Mode Factor Loadings (Percent) Obtained from Partial-Correlation Matrix with Respect to Total Dissolved Solids for Culebra Groundwaters (Population 1)

Element	Factor 1B	Factor 2B	Factor 3B	Factor 4B	Factor 5B	Communality (h_i^2)	Residual Variance[1]
Na	12	-10	76	-58	4	98.7	4%
Cl	28	3	84	-36	- 4	96.1	7%
Ca	97	- 1	14	- 8	- 1	99.2	71%
Mg	- 3	23	-23	92	10	98.1	7%
K	-30	22	5	-13	-25	98.8	9%
Sr	94	- 1	25	9	1	97.1	39%
pH	- 1	-93	19	-26	7	98.7	91%
HCO_3	-11	79	- 4	3	-22	97.1	96%
SO_4	-94	-18	-14	5	17	98.2	27%
SiO_2	18	93	4	9	-24	99.0	58%
Br	27	-16	86	8	13	96.2	19%
B	-19	-52	14	-55	47	97.3	43%
Li	-12	-34	7	7	90	99.5	18%

Amount and Percent of Variance[1] Explained by Each Factor

Factor 1B	Factor 2B	Factor 3B	Factor 4B	Factor 5B
3.071	2.903	2.251	1.737	1.265
27%	26%	20%	16%	11%

1. Variance not correlated to TDS; that is, the amount of variance remaining after TDS was partialled out.

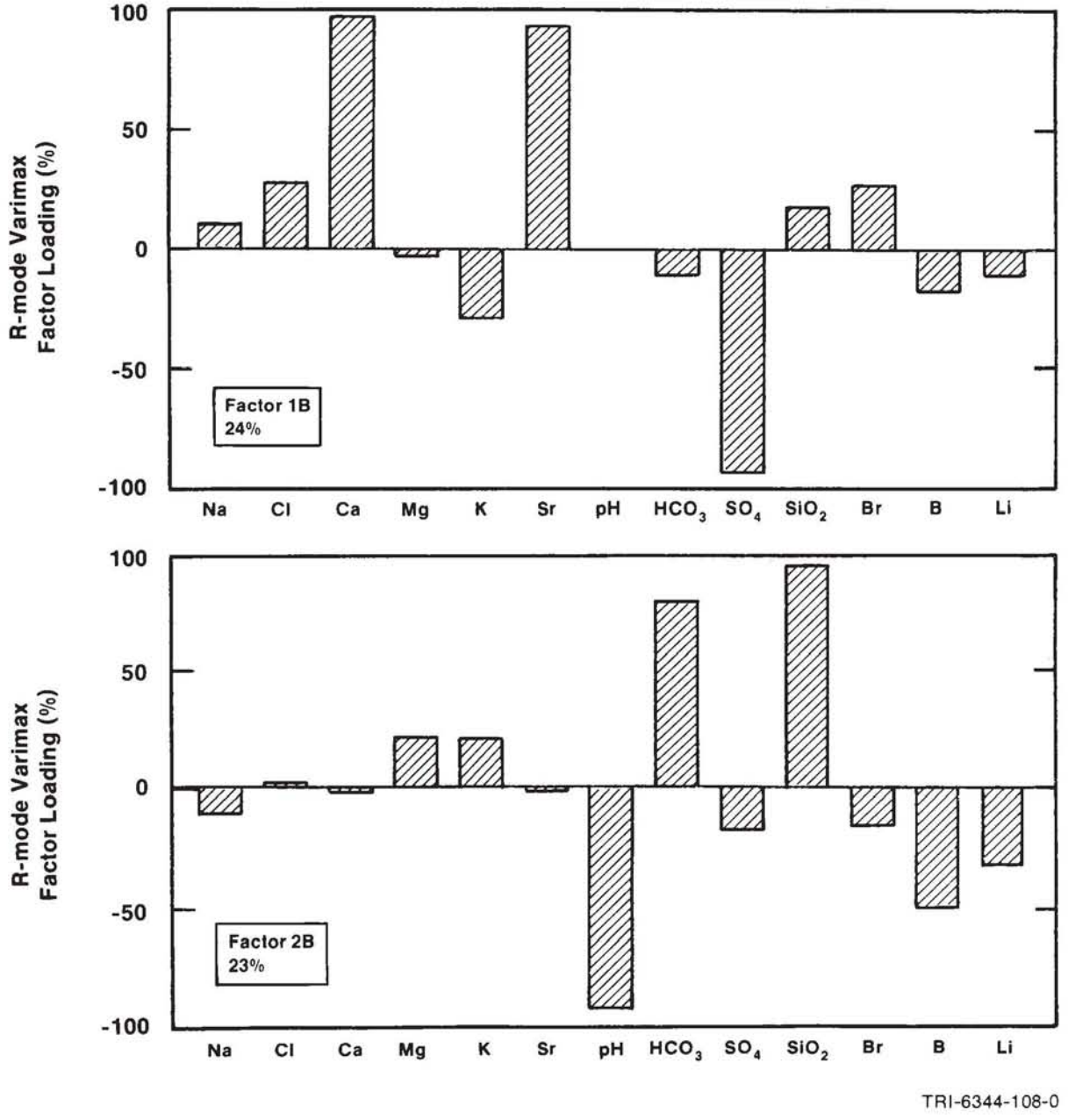

Figure 2C-6. Varimax R-mode factor loadings for factors 1B and 2B obtained from the partial-correlation matrix with respect to TDS of Culebra groundwaters (population 1).

chemical reactions that may cause these interelement correlations are discussed in Section 2.4.

2C.3.3 Factor Scores

The compositions of the samples in terms of the two most important factors are described by the factor scores plotted in Figure 2C-7. The spatial distributions of scores for factors 1B and 2B are plotted in Figures 2C-8 and 2C-9, respectively.

Factor 1B

Figure 2C-7 shows that the scores for factor 1B are not related to hydrochemical facies. Scores of this factor in samples from zone A and zone B are very similar; samples from zone C and zone D have the extreme score values.

The sample from P-14 has the highest score for this factor; locally, the values of the score decrease radially from this well (Figure 2C-7). As discussed in Section 2.2.3.1, the concentrations of several elements in the P-14 sample are anomalous, perhaps because of contamination. Ca, Sr, I, and Br exhibit local highs in their element contours; SO_4 and the Na/Cl ratio are anomalously low. The lowest (most negative) score for this factor is exhibited by the WIPP-29 sample; this sample has an anomalously high concentration of SO_4.

Factor 2B

Figure 2C-7 shows that factor 2B clearly distinguishes hydrochemical facies zone A from zone B. The extreme values of the factor score, however, are both in zone C. Both of the extrema, samples from WIPP-30 and WIPP-28, are anomalous with respect to neighboring wells. The sample from WIPP-30 exhibits the lowest silica concentration (4 mg/L). The sample from WIPP-28 exhibits the highest bicarbonate alkalinity in the population, but is known to be contaminated (Section 2.2.2). Figure 2C-9 shows that on a regional scale, the

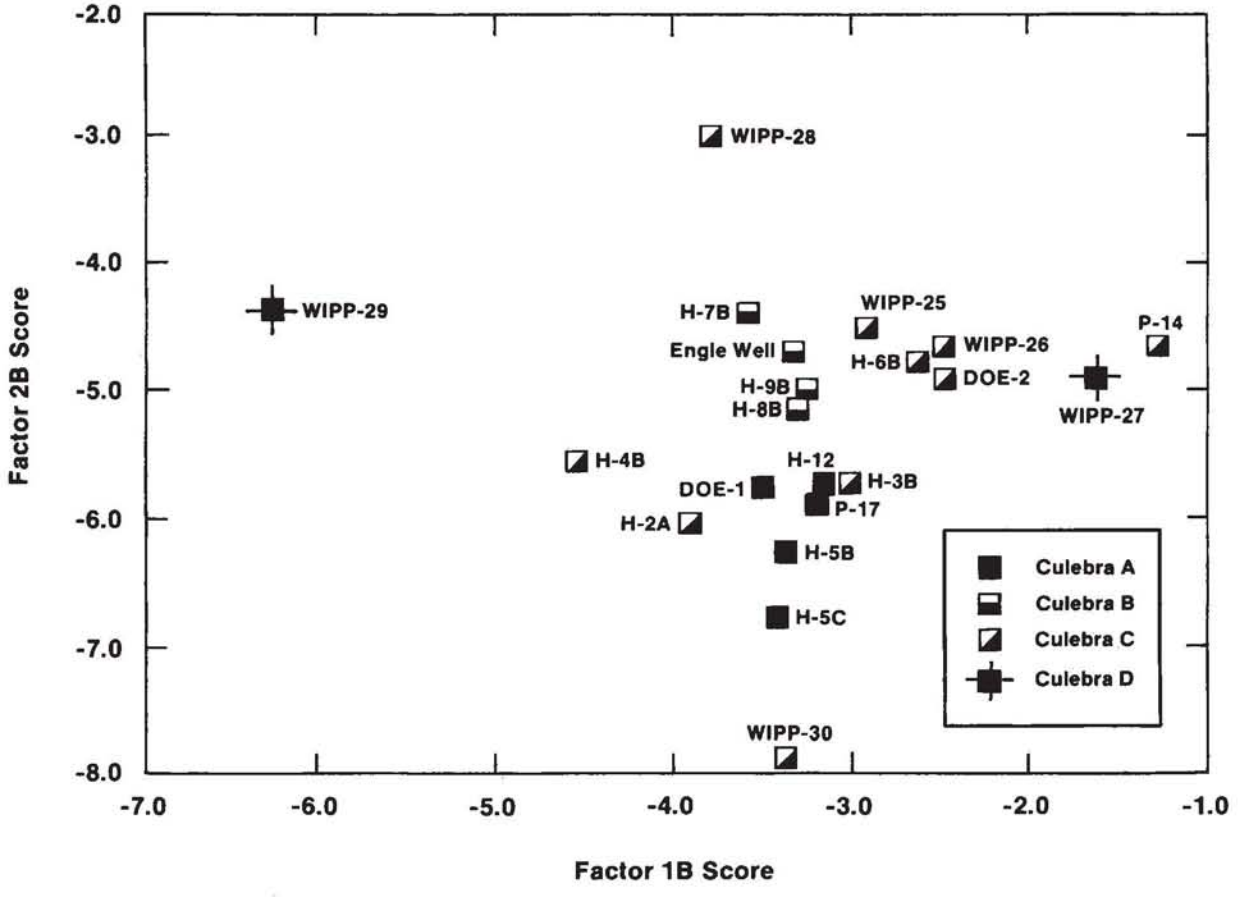

Figure 2C-7. Relationship between varimax R-mode factor scores for factor 1B and factor 2B obtained from the partial-correlation matrix with respect to TDS of Culebra groundwaters (population 1).

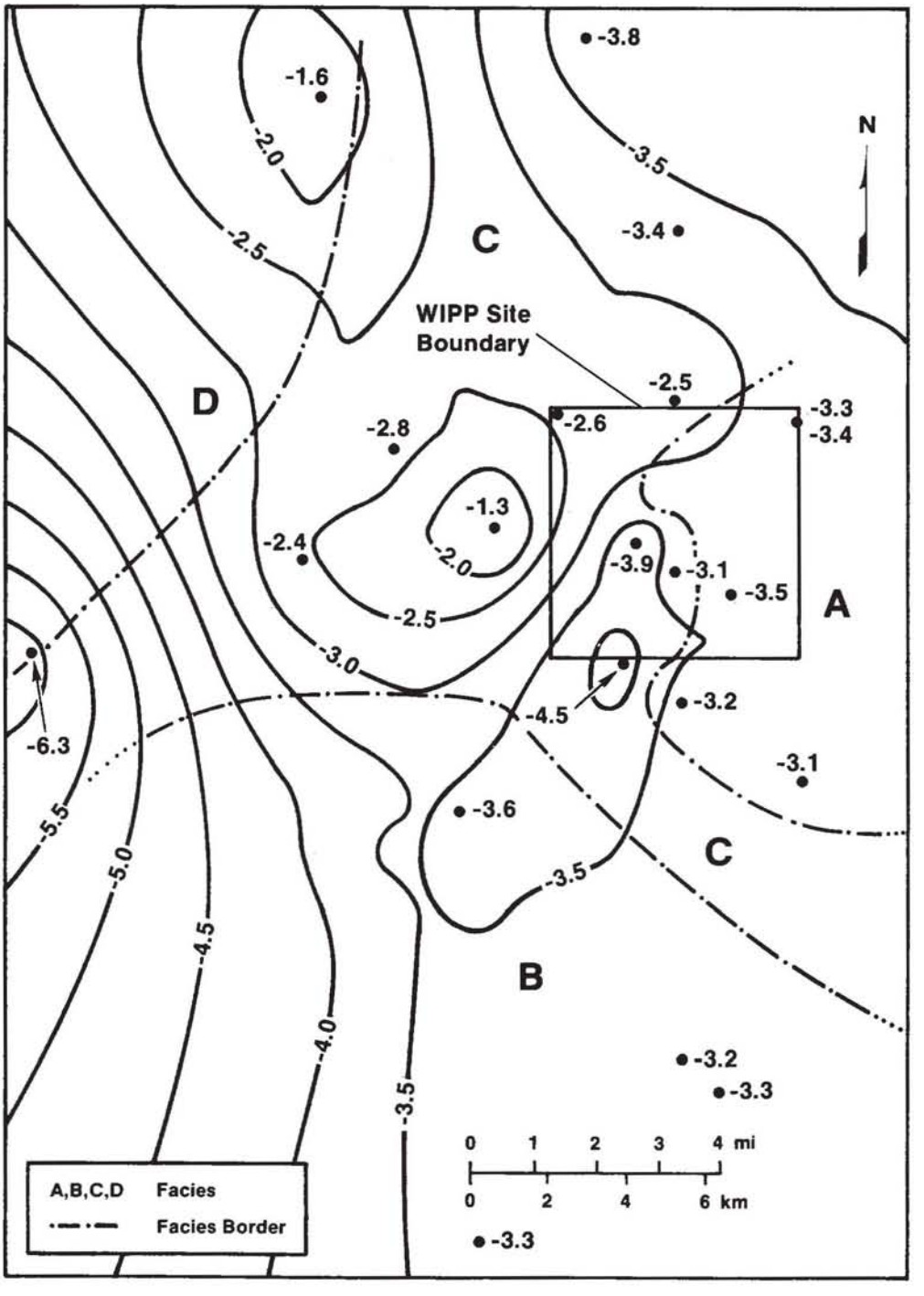

TRI-6341-46-0

Figure 2C-8. Contours of varimax R-mode factor scores for factor 1B obtained from the partial-correlation matrix with respect to TDS of Culebra groundwaters (population 1).

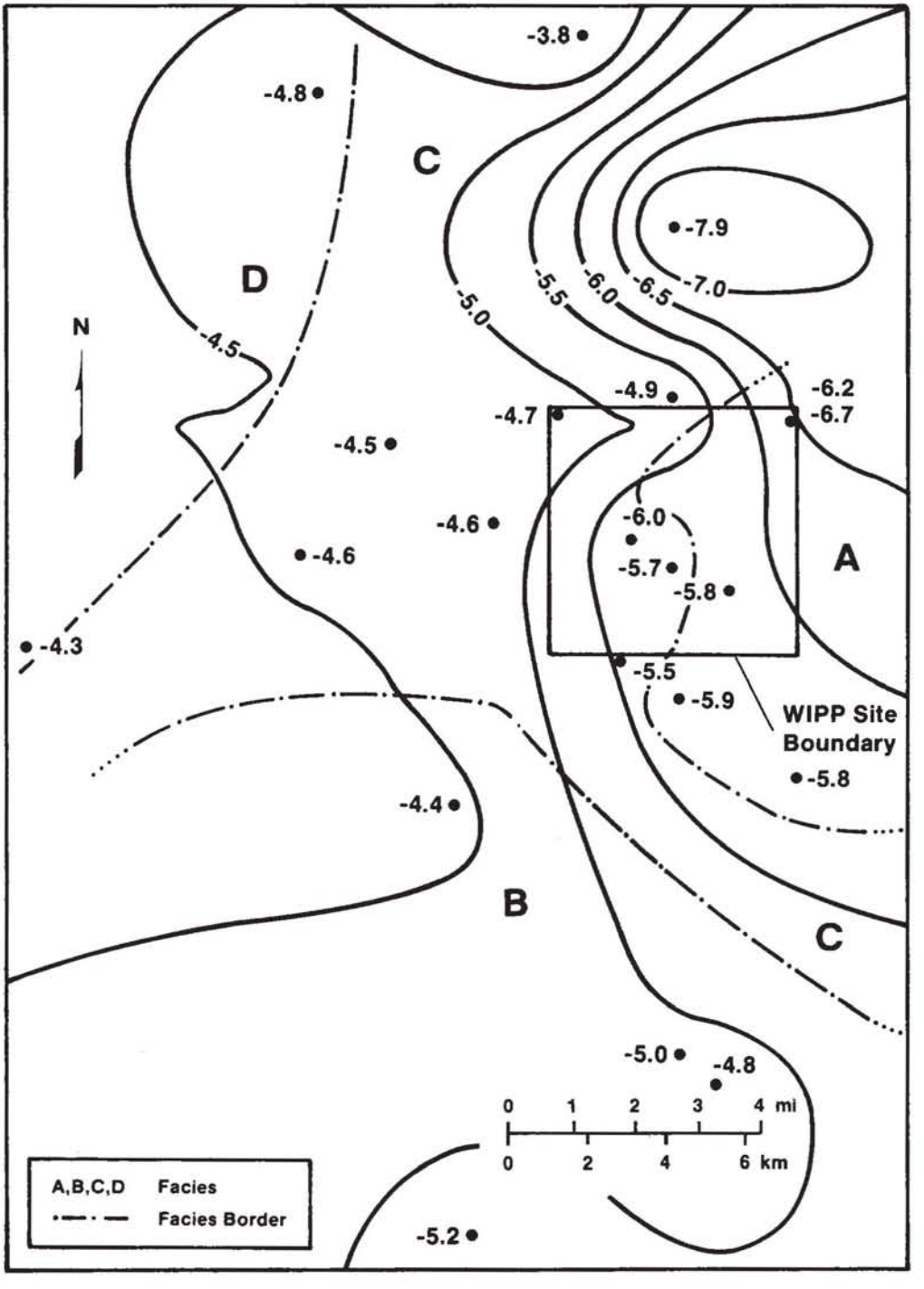

TRI-6341-43-0

Figure 2C-9. Contours of varimax R-mode factor scores for factor 2B obtained from the partial-correlation matrix with respect to TDS of Culebra groundwaters (population 1).

value of the score increases in a east to west direction. In Section 2.4.3, it is suggested that the east to west trend of increasing silica is consistent with an increase in the amount of detrital silicates exposed to groundwaters. The increased amounts of silicates are consistent with the greater degree of evaporite dissolution and formation of a residual fraction in the parts of the aquifer in contact with the groundwater.

APPENDIX 2D. SUPPLEMENTAL ANALYSIS OF SOLUTE RELATIONSHIPS IN SELECTED WATERS FROM THE CULEBRA AND MAGENTA DOLOMITES, RUSTLER/SALADO CONTACT ZONE, DEWEY LAKE RED BEDS, AND BELL CANYON FORMATION

2D.1 Introduction

Although for purposes of computer modeling, the Culebra is considered a confined aquifer (Lappin, 1988), leakage of groundwater into the Culebra from underlying and overlying units cannot be ruled out with the solute data available at this time (Siegel and Lambert, Chapter 1; Bodine et al., Chapter 4). In addition, even if the groundwaters in different units are completely isolated from each other, they may have evolved along similar geochemical reaction paths. Wherever possible, a comparison of water compositions from other units with Culebra waters is useful in obtaining a basic understanding of the water/rock interactions important in this hydrochemical system.

Mercer (1983) and Ramey (1985) have previously summarized water-chemistry data from the Magenta, Rustler/Salado contact zone, and other units.

This appendix documents preliminary analyses of solute relationships in a data set describing samples taken from the Magenta dolomite, the Culebra dolomite, the Rustler/Salado contact zone, the Dewey Lake Red Beds, and the Bell Canyon Formation. Descriptions of the locations, compositions, and histories of the samples are found in Sections 2.1 and 2.2 (see Figure 2-1 and Tables 2-1, 2-2, and 2-3). In this appendix, the solute relationships are examined using methods described in Section 2.3 and in Appendix 2B.

Section 2.D.2 summarizes the relationships among the major solutes using trilinear diagrams. Section 2.D.3 describes a principal component analysis (PCA) of major and minor solute data from the Culebra dolomite, the Magenta dolomite, the Dewey Lake Red Beds, and the Bell Canyon Formation.

2D.2 Solute Proportions in Samples from the Rustler Formation, Dewey Lake Red Beds, and Bell Canyon Formation

2D.2.1 Trilinear Plot of Solute Data

Figure 2D-1 uses a trilinear (Piper) diagram to compare the compositions of selected samples from the Rustler/Salado contact zone, the Magenta dolomite, and the Dewey Lake Red Beds. This plot summarizes relationships between the major solutes in the Na-K-Mg-Ca-Cl-SO_4-HCO_3 system. The diagram shows the relative proportions of the ions on an equivalents/liter basis. Relative proportions of cations and anions are displayed separately in the triangular plots in the bottom half of the figure. In the rhombus in the upper portion of the diagram, the ratio of divalent to monovalent cations and the ratio of chloride to the sum of sulfate + bicarbonate + carbonate are shown. Construction of trilinear diagrams is reviewed in Hem (1985).

Figure 2D-1 shows saline waters from the Rustler/Salado contact zone plot near the Na-Cl corner of the trilinear diagram in portions of the areas occupied by hydrochemical facies zone A, zone C, and zone D of the Culebra dolomite (cf. Figure 2-18). Samples from the Magenta dolomite have compositions intermediate between Culebra zones C and B. The Magenta samples from WIPP-25 and H-4C have solute proportions that overlap those found in Culebra zone C. The two samples from the Dewey Lake Red Beds are similar in composition to those from Culebra zone B. No hydrochemical facies have been defined for stratigraphic horizons other than the Culebra because of the small number of analyses.

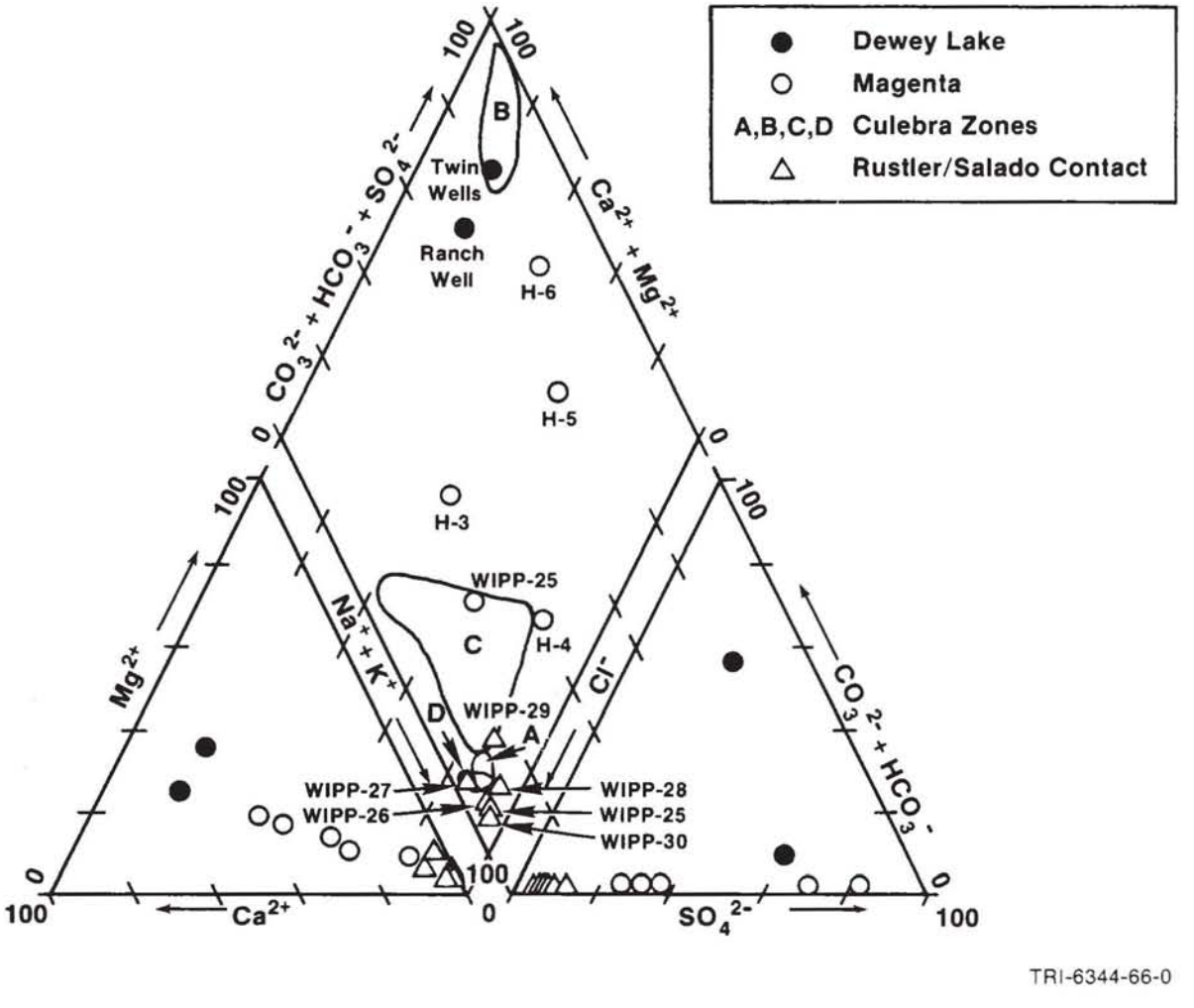

Figure 2D-1. Trilinear diagram showing compositions of groundwaters from the Rustler/Salado contact zone, the Magenta dolomite, and the Dewey Lake Red Beds.

2D.2.2 Comparison of Samples from Different Stratigraphic Horizons in the Same Well

Figure 2D-2 is a portion of a trilinear diagram showing the compositions of groundwater samples from locations where two or three stratigraphic horizons in the Rustler were sampled. Table 2D-1 compares the total dissolved solids (TDS) content of the same samples. For the majority of wells, groundwaters in the Magenta are relatively fresher and have higher proportions of Ca and SO_4, while groundwaters in the Culebra and at the Rustler/Salado contact are more saline and richer in Na and Cl. In addition, waters from the Rustler/Salado contact zone generally have higher concentrations of TDS than the waters from the Culebra. Notable exceptions to this are samples from the H-4, WIPP-25, WIPP-27, and WIPP-29 hydropads, discussed below.

Samples from the Magenta and Culebra at H-4 have similar TDS concentrations and proportions of major solutes. However, they differ dramatically in bromide and potassium concentrations (cf. Table 2-2).

Samples from the Magenta and Culebra at WIPP-25 are similar in TDS concentrations and proportions of all solutes. This similarity may indicate vertical connection between these two units at WIPP-25.

Samples from the Magenta and Culebra at WIPP-27 have nearly identical TDS and solute proportions. The similarity in composition in the Magenta and Culebra samples may indicate vertical connection between these two units at WIPP-27. The salinity of the Magenta samples at WIPP-27 is anomalously high compared to other Magenta samples. The high TDS and potassium concentrations of the Culebra and Magenta samples from WIPP-27 may be due to contamination from potash-refining operations in the area.

The hydrologic and isotopic evidence suggesting vertical connections between the Magenta and Culebra at WIPP-25 and WIPP-27 are summarized in Siegel and Lambert (Chapter 1).

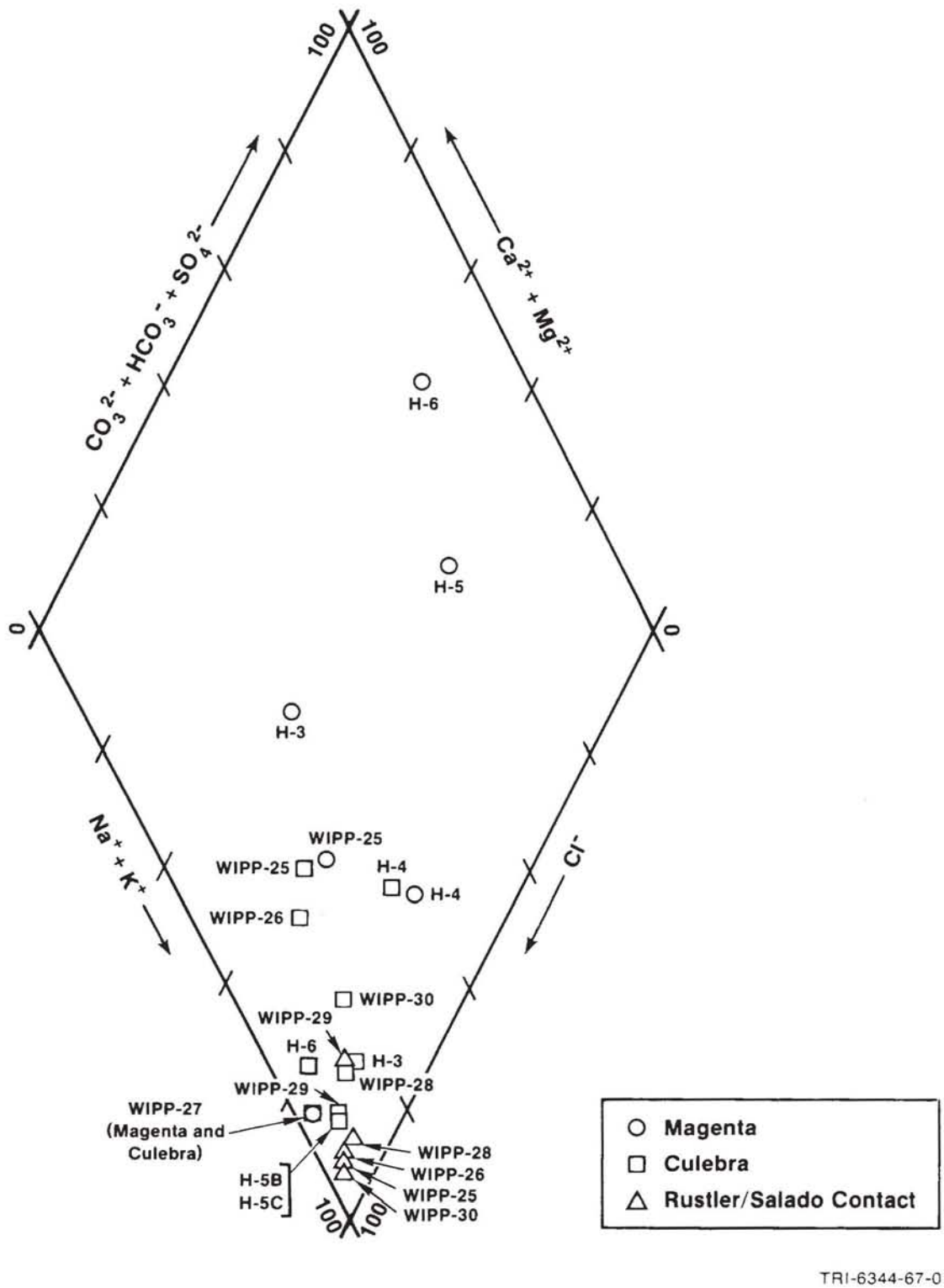

Figure 2D-2. Portion of a trilinear diagram showing compositions of Rustler groundwaters from wells where two or three stratigraphic horizons were sampled.

Table 2D-1. Concentrations of TDS in Groundwaters from the Rustler Formation, Dewey Lake Red Beds, and Bell Canyon Formation

Well	Strat. Hor.[1] (Facies)	Coll. Date	TDS (mg/L)
H-3B1	Mag	7/85	8560
H-3B3	Cul(C)	2/85	55800
H-4C	Mag	11/86	23900
H-4B	Cul(C)	7/85	20200
H-4C	Cul(C)	8/84	21200
H-5C	Mag	10/86	6980
H-5B	Cul(A)	8/85	152600
H-5C	Cul(A)	10/81	154500
H-6C	Mag	10/86	4540
H-6B	Cul(C)	9/85	57400
DOE-2	Cul(C)	3/85	60400
DOE-2	BC	7/85	149500
WIPP-25	Mag	9/80	11900
WIPP-25	Cul(C)	2/86	13600
WIPP-25	R/S	7/80	334400
WIPP-26	Cul(C)	11/85	17600
WIPP-26	R/S	7/80	188400
WIPP-27	Mag	9/80	145700
WIPP-27	Cul(D)	9/80	134700
WIPP-28	Cul(C)	9/80	46600
WIPP-28	R/S	7/80	277100
WIPP-29	Cul(D)	12/85	324100
WIPP-29	R/S	7/80	111000
WIPP-30	Cul(C)	9/80	29100
WIPP-30	R/S	7/80	325900
RANCH	DL	6/86	2520
TWIN-P	DL	1/86	401

1. Stratigraphic horizons: Cul = Culebra dolomite; Mag = Magenta dolomite; BC = Bell Canyon Fm.; DL = Dewey Lake Red Beds.
Facies (in parentheses) are the hydrochemical facies in the Culebra, as defined in Section 2.3.2.1.

At WIPP-29, the Culebra water samples are more saline and have different solute proportions than the samples from the Rustler/Salado contact. This difference indicates a lack of vertical connection between the two strata at this location.

2D.3 Principal Component Analysis of Groundwater Samples from the Rustler Formation, Dewey Lake Red Beds, and Bell Canyon Formation

PCA was carried out on a data set composed of samples from wells in the Dewey Lake Red Beds, Magenta and Culebra dolomites, and Bell Canyon Formation. An explanation of the methods and objectives of PCA is found in Appendix 2B. Only data from the UNC Geotech laboratory were used; the common logs ($\log_{10}$) of the raw concentration data were used in the analysis.

The objective in selecting analyses for this PCA was to include as many different elements as possible. For this reason, several Culebra samples that lack reliable minor and trace element data (Mn, Fe, I) were not included. A secondary objective in this PCA was to compare the solute relationships in this more extensive data set to those observed in the data set drawn from the Culebra alone. This PCA is in no way to be considered a comprehensive analysis of water from all water-bearing strata at the WIPP Site. Data from other stratigraphic horizons (the Rustler/Salado contact zone, the Castile Formation, and the Salado Formation) and additional data from the Magenta dolomite, Dewey Lake Red Beds, and Bell Canyon Formation would be required to produce a data set that is truly representative of the full range of solute compositions of water from rocks in the Ochoan. Table 2D-2 compares the data set (population 2) used in this analysis with the data set (population 1) used in the PCA of Culebra samples (described in Section 2.2.3.3).

2D.3.1 Q-Mode Principal Component Analysis

Q-mode analysis was carried out to determine if the samples were drawn from a statistically homogeneous population suitable for R-mode PCA. Both unrotated and varimax

Table 2D-2. Populations Used in Principal Component Analyses

Population	Wells	Variables used in PCA
1	Culebra: DOE-1, DOE-2, H-2A, H-3B3, H-4B, H-5B, H-5C, H-6B, H-7B1, H-8B, H-9B, H-12, P-14, P-17, WIPP-25, WIPP-26, WIPP-27, WIPP-28, WIPP-29, WIPP-30, Engle	Ca, Mg, K, Na, Cl, SO_4, B, Li, SiO_2, Br, Sr, HCO_3, pH
2	Dewey Lake: Ranch, Twin-Pasture Magenta: H-3B1, H-4C, H-5C, H-6C Culebra: DOE-2, H-2A, H-3B3, H-5B, H-6B, H-7B1, H-8B, H-9B, P-14, P-17, WIPP-26, WIPP-29, Engle Bell Canyon: DOE-2	Ca, Mg, K, Na, Cl, SO_4, B, Li, SiO_2, Br, Sr, HCO_3, pH, Fe, Mn, F, I

solutions were examined. The unrotated factors were the more interpretable and were retained for further discussion.

The factor loadings and scores are shown in Table 2D-3 and Figures 2D-3 and 2D-4. Table 2D-3 shows that two factors account for nearly all of the variance; at least 94% of the composition of all water samples can be mathematically expressed as a linear combination of these two hypothetical end-members. Figure 2D-4 shows the composition of the two factors.

Figure 2D-3 shows the composition of the samples in terms of the factors. Most of the samples are similar to factor 1C (97% of the variance); it represents a grand mean of the compositions. The Culebra sample from WIPP-25 is closest in composition to this factor. Along the factor-1C axis, Na, Cl, Ca, Mg, pH, SO_4, and TDS increase, and the

Table 2D-3. Unrotated Q-Mode Factor Loadings for Rustler, Dewey Lake, and Bell Canyon Groundwaters (Population 2)

Well	Strat.Hor.[1] (Facies)	Coll. Date	Factor 1C	Factor 2C	Communality (h_i^2)
H-5B	Cul(A)	8/85	0.97	0.22	0.993
P-17	Cul(A)	3/86	0.97	0.20	0.987
H-7B1	Cul(B)	3/86	0.98	-0.18	0.994
H-8B	Cul(B)	1/86	0.95	-0.29	0.987
H-9B	Cul(B)	11/85	0.97	-0.22	0.994
Engle	Cul(B)	3/85	0.97	-0.22	0.989
DOE-2	Cul(C)	3/85	0.98	0.16	0.983
H-2A	Cul(C)	4/86	0.99	0.01	0.984
H-3B3	Cul(C)	2/85	0.99	0.14	0.995
H-6B	Cul(C)	9/85	0.98	0.15	0.990
P-14	Cul(C)	2/86	0.98	0.06	0.956
WIPP-25	Cul(C)	2/86	0.99	<0.01	0.989
WIPP-26	Cul(C)	11/85	0.99	0.02	0.973
WIPP-29	Cul(D)	12/85	0.91	0.33	0.947
H-3B1	Mag	7/85	0.99	-0.05	0.982
H-4C	Mag	11/86	0.99	0.01	0.982
H-5C	Mag	10/86	0.98	-0.09	0.971
H-6C	Mag	10/86	0.99	-0.11	0.991
RANCH	DL	6/86	0.97	-0.18	0.973
TWIN-P	DL	1/86	0.95	-0.27	0.974
DOE-2	BC	7/85	0.93	0.31	0.963

Amount and Percent of Variance Explained by Each Factor

	Factor 1C	Factor 2C
	19.886	0.713
	96%	4%

1. Stratigraphic horizons: Cul = Culebra dolomite; Mag = Magenta dolomite; BC = Bell Canyon Fm.; DL = Dewey Lake Red Beds.
Facies (in parentheses) are the hydrochemical facies in the Culebra, as defined in Section 2.3.2.1.

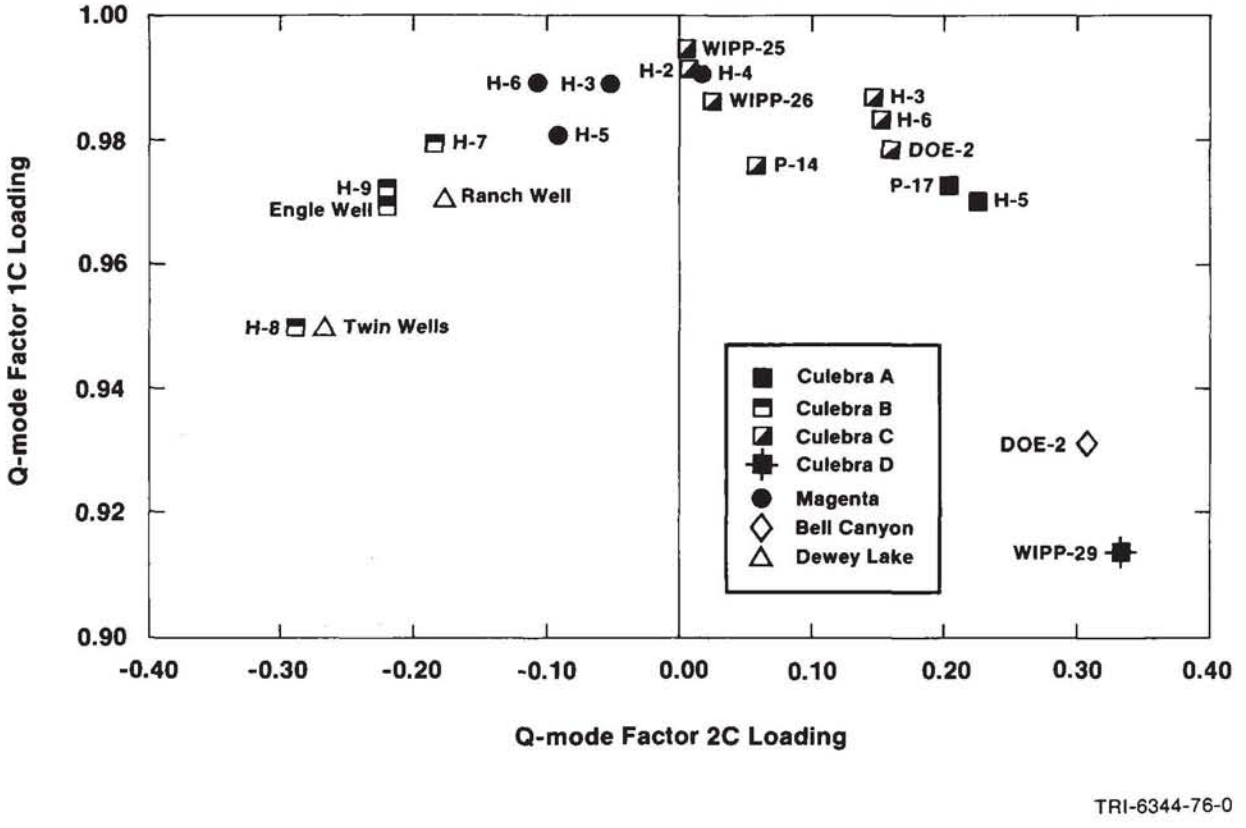

Figure 2D-3. Relationship between unrotated Q-mode factor loadings for factors 1C and 2C of Rustler, Dewey Lake, and Bell Canyon groundwaters (population 2).

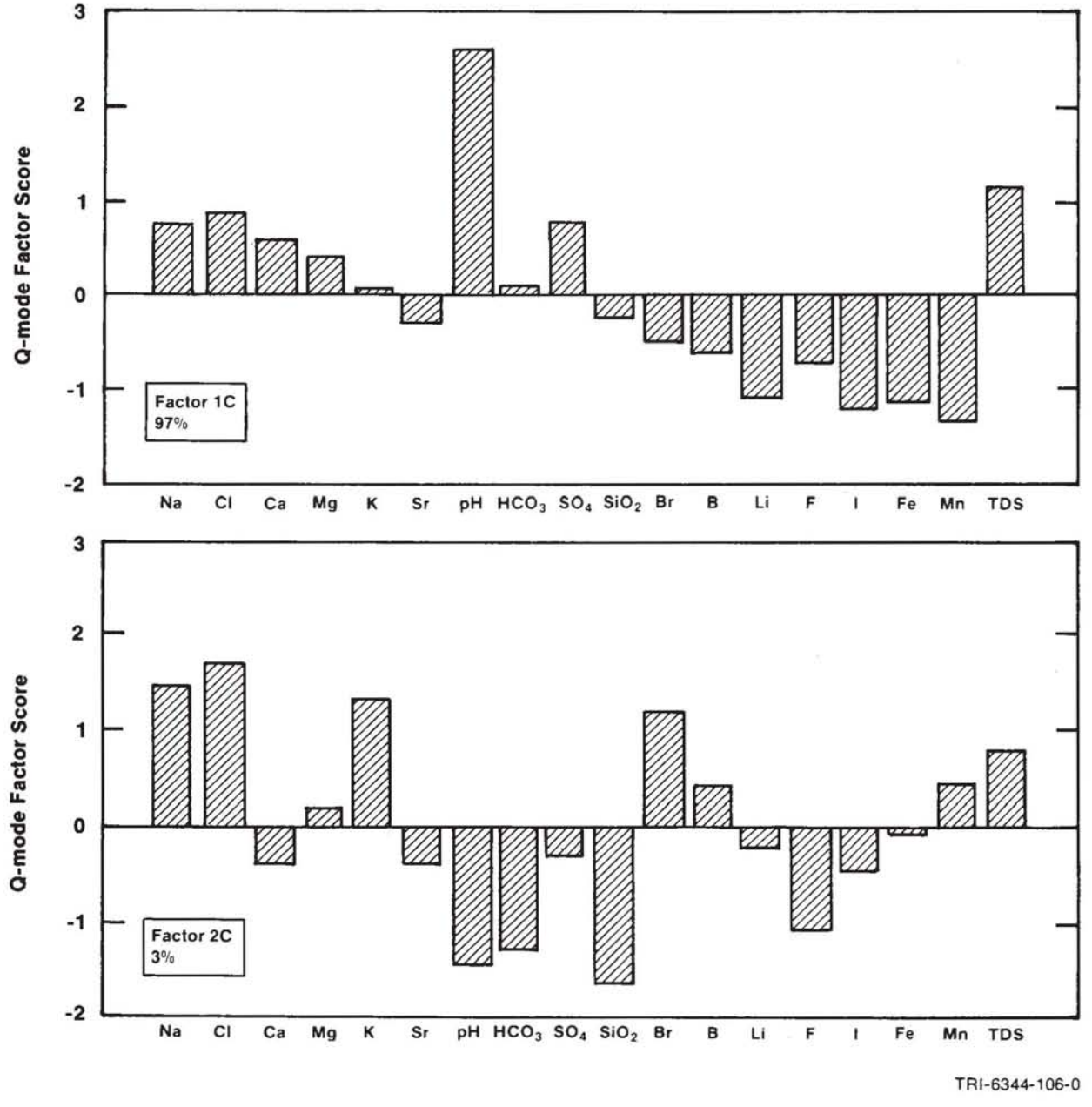

Figure 2D-4. Unrotated Q-mode factor scores for factors 1C and 2C of Rustler, Dewey Lake, and Bell Canyon groundwaters (population 2).

other solutes decrease. The rest of the variation in the sample population can be expressed in terms of factor 2C. Along the factor-2C axis, concentrations of Na, Cl, K, Br, B, Mn, and TDS increase, and the other concentrations decrease. Culebra samples from WIPP-29 and H-8 are the extrema of factor 2C.

Figure 2D-3 also shows that samples from the Dewey Lake are similar to samples from hydrochemical facies zone B of the Culebra. The sample from the Bell Canyon Formation at DOE-2 has the same TDS concentration as the Culebra sample from H-5B (hydrochemical facies zone A); however, Figure 2D-3 shows that it is very different in composition from Culebra samples from zone A.

As discussed in Appendix 2B, a data set is generally considered homogeneous enough for R-mode analysis if two or three Q-mode factors are sufficient to explain all of the population variance. The results shown in Table 2D-3 indicate that population 2 is amenable to R-mode factor analysis.

2D.3.2 Varimax R-Mode Principal Component Analysis

R-mode PCA was carried out on the data in population 2 using the SAS program (Statistical Analysis System Institute, 1982). The correlation matrix of the data (the common logs of the concentrations) is given in Table 2D-4 Several rotations of the factors were examined; only the varimax solution is considered in this discussion. Seven varimax factors were extracted; they account for more than 99% of the variance (see Table 2D-5). At least 93% of the variance of each variable could be explained by these factors. The first five factors account for 91% of the variance. The factor loadings for the first five factors are shown in Figure 2D-5; the factor scores for the first two factors are plotted in Figure 2D-6.

Table 2D-4. Correlation Matrix for Solute Data[1] in Rustler, Dewey Lake, and Bell Canyon Groundwaters (Population 2)

	Ca	Mg	K	Na	Cl	SO_4	B	Fe	Li
Ca	1.000	0.656	0.505	0.690	0.700	0.450	0.621	0.460	0.796
Mg	0.656	1.000	0.897	0.916	0.909	0.785	0.674	0.566	0.820
K	0.505	0.897	1.000	0.947	0.934	0.703	0.761	0.509	0.753
Na	0.690	0.916	0.947	1.000	0.989	0.740	0.849	0.626	0.852
Cl	0.700	0.909	0.934	0.989	1.000	0.675	0.786	0.582	0.821
SO_4	0.450	0.785	0.703	0.740	0.675	1.000	0.679	0.634	0.665
B	0.621	0.674	0.761	0.849	0.786	0.679	1.000	0.638	0.814
Fe	0.460	0.566	0.509	0.626	0.582	0.634	0.638	1.000	0.610
Li	0.796	0.820	0.753	0.852	0.821	0.665	0.814	0.610	1.000
Mn	0.595	0.811	0.750	0.799	0.784	0.609	0.727	0.662	0.819
SiO_2	-0.520	-0.532	-0.583	-0.679	-0.610	-0.511	-0.858	-0.618	-0.831
Br	0.748	0.866	0.831	0.928	0.950	0.538	0.715	0.558	0.826
F	0.122	0.395	0.328	0.290	0.229	0.739	0.308	0.423	0.276
I	0.628	0.561	0.399	0.521	0.503	0.441	0.499	0.454	0.799
Sr	0.957	0.791	0.644	0.808	0.809	0.629	0.694	0.538	0.810
pH	-0.303	-0.592	-0.465	-0.353	-0.394	-0.227	0.030	0.001	-0.316
HCO_3	-0.547	-0.301	-0.315	-0.473	-0.396	-0.469	-0.770	-0.505	-0.594

1. The data are the common logarithms of the solute concentrations in mg/L (except pH).

Table 2D-4. Correlation Matrix for Solute Data[1] in Rustler, Dewey Lake, and Bell Canyon Groundwaters (Population 2) (Continued)

	Mn	SiO_2	Br	F	I	Sr	pH	HCO_3
Ca	0.595	-0.520	0.748	0.122	0.628	0.957	-0.303	-0.547
Mg	0.811	-0.532	0.866	0.395	0.561	0.791	-0.592	-0.301
K	0.750	-0.583	0.831	0.328	0.399	0.644	-0.465	-0.315
Na	0.799	-0.679	0.928	0.290	0.521	0.808	-0.353	-0.473
Cl	0.784	-0.610	0.950	0.229	0.503	0.809	-0.394	-0.396
SO_4	0.609	-0.511	0.538	0.739	0.441	0.629	-0.227	-0.469
B	0.727	-0.858	0.715	0.308	0.499	0.694	0.030	-0.770
Fe	0.662	-0.618	0.558	0.423	0.454	0.538	0.001	-0.505
Li	0.819	-0.831	0.826	0.276	0.799	0.810	-0.316	-0.594
Mn	1.000	-0.640	0.766	0.311	0.588	0.655	-0.391	-0.349
SiO_2	-0.640	1.000	-0.628	-0.214	-0.720	-0.536	-0.132	0.819
Br	0.766	-0.628	1.000	0.042	0.576	0.821	-0.410	-0.406
F	0.311	-0.214	0.042	1.000	0.272	0.266	-0.087	-0.280
I	0.588	-0.720	0.576	0.272	1.000	0.614	-0.188	-0.538
Sr	0.655	-0.536	0.821	0.266	0.614	1.000	-0.341	-0.566
pH	-0.391	-0.132	-0.410	-0.087	-0.188	-0.341	1.000	-0.377
HCO_3	-0.349	0.819	-0.406	-0.280	-0.538	-0.566	-0.377	1.000

1. The data are the common logarithms of the solute concentrations in mg/L (except pH).

Table 2D-5. Varimax R-Mode Factor Loadings (Percent) For Rustler, Dewey Lake, and Bell Canyon Groundwaters (Population 2)

Element	Factor 1D	Factor 2D	Factor 3D	Factor 4D	Factor 5D	Factor 6D	Factor 7D	Communality (h_i^2)
Na	89	31	11	18	18	17	8	99.5
Cl	89	34	4	16	11	17	3	98.2
Ca	37	86	8	28	3	11	10	98.8
Mg	80	32	-18	27	32	15	8	97.1
K	94	11	- 1	13	23	5	13	97.6
Sr	51	79	8	22	18	13	2	99.4
pH	-40	-22	81	-14	- 9	12	-16	93.2
HCO_3	-19	-37	-79	-31	-21	- 5	- 8	95.1
SO_4	55	20	12	14	73	18	0	93.6
SiO_2	-48	-11	-58	-57	- 8	-16	-22	98.1
Br	82	41	1	28	- 9	22	0	97.6
B	67	27	54	18	20	13	30	98.2
Li	61	41	15	55	16	14	24	96.1
F	7	2	4	9	97	11	6	96.2
I	22	31	9	89	15	12	2	98.3
Fe	36	18	24	19	29	80	9	97.8
Mn	61	22	- 5	33	17	36	52	95.9

Table 2D-5. Varimax R-Mode Factor Loadings (Percent) For Rustler, Dewey Lake, and Bell Canyon Groundwaters (Population 2) (Continued)

	Amount and Percent of Variance Explained by Each Factor					
Factor 1D	Factor 2D	Factor 3D	Factor 4D	Factor 5D	Factor 6D	Factor 7D
6.242	2.523	2.073	2.089	1.970	1.058	0.552
38%	15%	13%	13%	12%	6%	3%

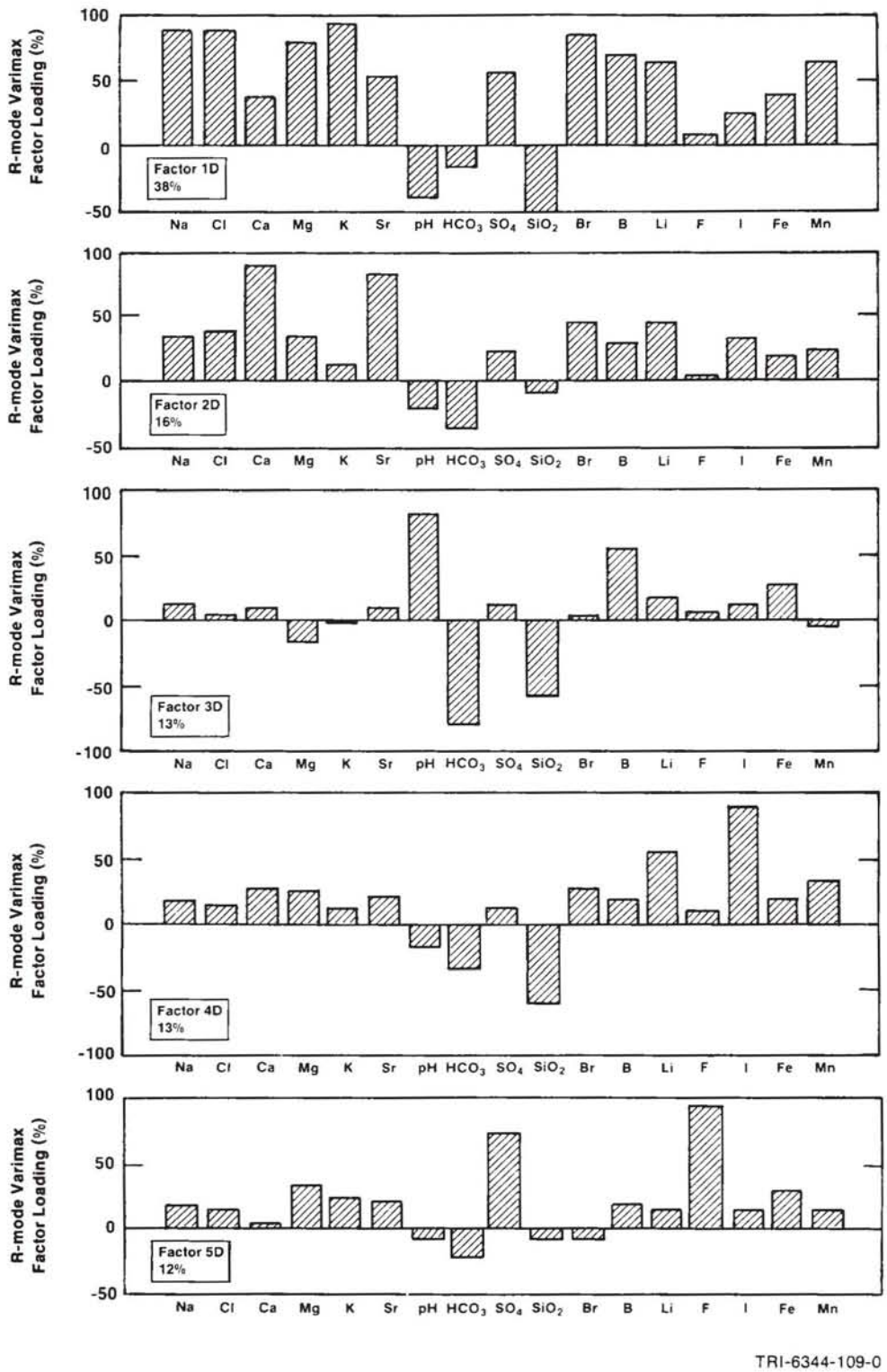

Figure 2D-5. Varimax R-mode factor loadings for factors 1D, 2D, 3D, 4D, and 5D of Rustler, Dewey Lake, and Bell Canyon groundwaters (population 2).

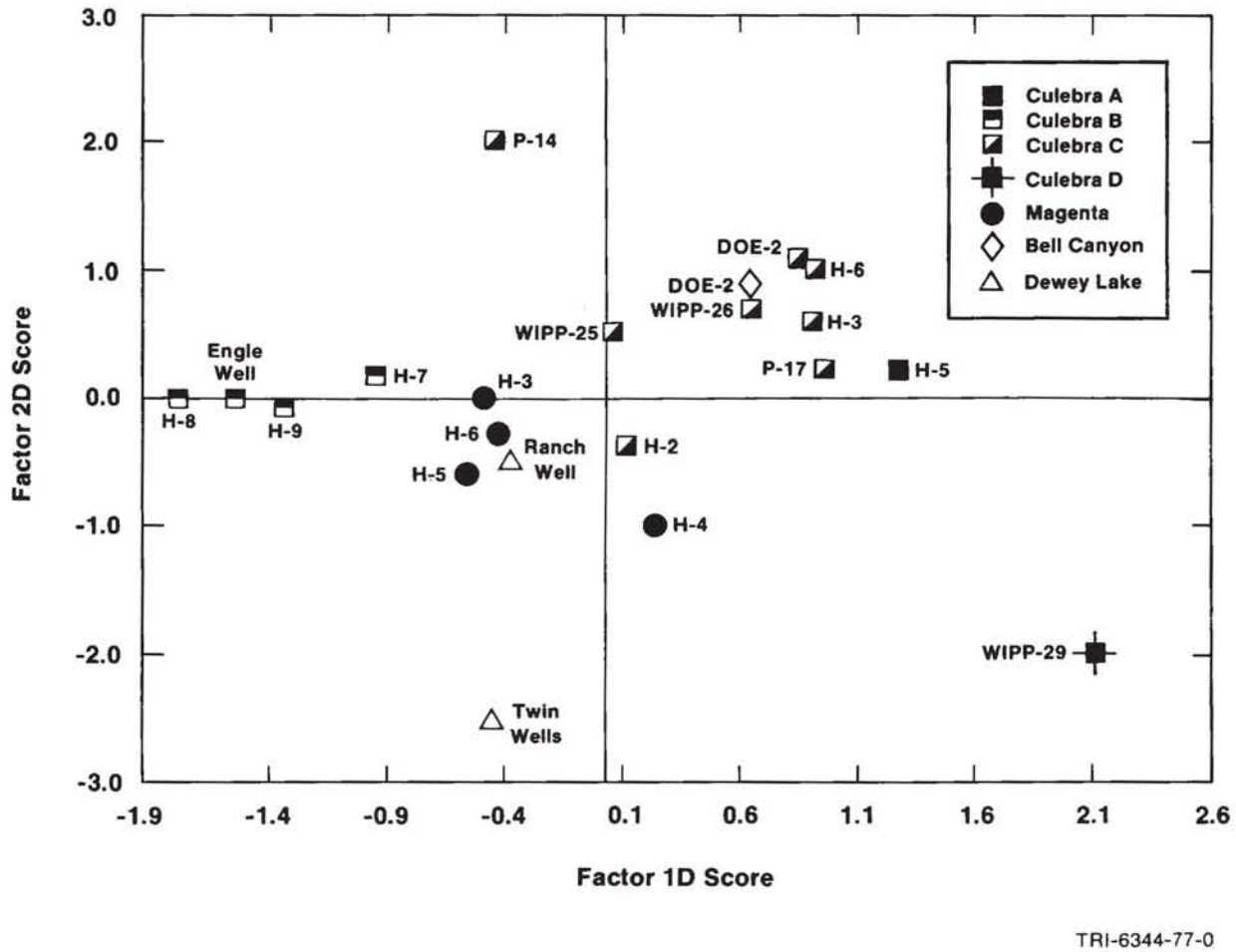

Figure 2D-6. Relationship between varimax R-mode factor scores for factors 1D and 2D of Rustler, Dewey Lake, and Bell Canyon groundwaters (population 2).

"Salinity," "Sulfate," and "Silicate/Bicarbonate" Factors

Most of the chemical variability of the sample population can be correlated with the variance in the concentrations of Na and Cl. Factor 1D, the most important factor produced by the R-mode analysis, is dominated by Na, K, Mg, Br, and Cl. All solutes except for SiO_2, alkalinity, and pH exhibit positive correlations with this factor. Factor 1D is similar to the salinity factor (factor 1A) of population 1 described in Section 2.3.3.4.

The second most important factor, factor 2D, also has a strong Na-Cl influence, but is most strongly influenced by Ca, bicarbonate alkalinity, and Sr. It is similar to the sulfate factor (factor 2A) of population 1. As discussed in Section 2.3.3.4 for the Culebra analysis, several sources of data from the site suggest that these salinity and sulfate factors represent addition of solutes by the dissolution of halite, gypsum, anhydrite, and carbonates.

Factor 3D is similar to the silicate/bicarbonate factor (factor 3A) of population 1. It is strongly influenced by the concentrations of Si, B, Li, and bicarbonate and by the pH. However, the loading of Mg in this factor is different from that in the Culebra factor 3A.

Additional Elements

This R-mode analysis allows an examination of the behavior of several elements that were not included in population 1. Factor 4D of population 2 (see Table 2D-5) is dominated by the behaviors of I, Si, and Li and has no counterpart in the Culebra analysis. The geochemical significance of this factor is unclear. Iodide is concentrated in residual brines and in formation waters. The iodide concentration of the waters in population 2 ranges from a level approximately equal to that of seawater (0.05 mg/L in Culebra samples from H-7B) to 6.4 mg/L in the Bell Canyon sample from DOE-2. Nearly all of the waters are generally enriched in iodide relative to the seawater evaporation curve (cf. Collins, 1975). Potential sources of the excess iodide include dissolution of iodide from evaporite minerals or organic material and desorption from clays.

Iodide is correlated with Na and Cl and inversely correlated with Si on all factors extracted in the R-mode analysis. If high silica contents are assumed to be indicative of effects related to clay diagenesis, then this may indicate that the desorption from clays is not a significant source of iodine. In the Magenta and in hydrochemical facies zone A, zone C, and zone D of the Culebra, the main source of the iodide is probably halite and associated evaporite salts. The high I/Cl ratios and low Cl concentrations in the samples from the Dewey Lake and hydrochemical facies zone B of the Culebra, however, do not support a salt source for the iodide in that area.

Factor 5D is the most significant factor for both F and SO_4 (see Table 2D-5). Fluorine occurs most commonly in fluorite (CaF_2) and sellaite (MgF_2). Sonnenfeld (1984) notes that typically, MgF_2 occurs as an accessory mineral associated with anhydrite, whereas CaF_2 more commonly occurs with carbonates. The association of F, SO_4, and Mg in factor 5D may indicate that MgF_2 in anhydrite or gypsum is the source of fluorine in these waters.

Iron loads primarily onto its own principal component, factor 6D; Mn has an appreciable loading onto this factor also (see Table 2D-5). The lack of correlation between Fe and Mn with other major and minor solutes may be due to random errors in sampling or analyses as discussed in Section 2.2. Manganese also loads strongly onto factor 1D and factor 7D; the geochemical significance of these elemental associations is unclear, but might be related to corrosion of well casing in the borehole.

2D.3.3 Varimax R-Mode Principal Component Analysis With Total Dissolved Solids Partialled Out

A second set of R-mode PCAs was carried out in which the correlation of each element with the TDS concentration was partialled out; the method is described in Appendix B. The resulting factor pattern shows the interelement correlations independent of the effects that may be attributed to halite dissolution.

The factor-loading matrix is shown in Table 2D-6. The first three factors account for 57% of the variance left after the TDS concentration is partialled out (see Figure 2D-7). The results are similar to those obtained from the analysis of the population 1.

The primary factor (factor 1E) contains two groups of inversely correlated elements. Mg, bicarbonate alkalinity, and SiO_2 form one group; and Na, pH, B, and Li form another group. All of these chemical variables are known to be related with dissolution or ion-exchange reactions involving clays (see Section 2.4.3). This pattern of element associations might reflect clay diagenesis or silicate hydrolysis.

The second factor (factor 2E) shows a Ca-Sr-HCO_3-SO_4 association indicative of coprecipitation of Sr and Ca in sulfates and carbonates. Sulfate and fluorine dominate factor 3E and may reflect the occurrence of accessory MgF_2 in $CaSO_4$ as discussed previously.

Table 2D-6. Varimax R-Mode Factor Loadings (Percent) Obtained from Partial-Correlation Matrix with Respect to Total Dissolved Solids for Rustler, Dewey Lake, and Bell Canyon Groundwaters (Population 2)

Element	Factor 1E	Factor 2E	Factor 3E	Factor 4E	Factor 5E	Factor 6E	Factor 7E	Factor 8E	Factor 9E	Communality (h_i^2)
Ca	8	94	-18	3	20	- 2	- 1	-14	8	99.5
Mg	-82	0.1	11	-26	5	- 9	5	37	-21	95.3
K	- 2	-77	- 5	23	-25	-24	-15	-43	- 2	96.5
Na	42	- 9	-19	83	-10	-20	11	- 2	7	97.5
Cl	1	4	-32	92	-12	- 6	- 3	- 8	- 3	98.6
SO_4	8	- 3	86	-16	- 2	-18	19	34	13	96.5
B	97	3	3	0.3	4	6	7	- 3	9	95.1
Fe	23	7	20	7	8	20	92	3	- 0.3	99.4
Li	28	30	-12	-13	82	12	5	- 3	31	98.0
Mn	3	- 3	- 8	-16	16	94	18	1	1	98.0
SiO_2	-74	9	12	8	-61	- 2	-19	- 3	5	98.9
Br	- 8	24	-70	55	18	- 1	11	17	-17	95.5
F	- 1	- 4	93	-21	3	3	12	-11	-19	97.4
I	3	25	5	- 5	92	12	2	5	-18	96.1
Sr	4	97	- 1	11	9	-12	1	0.2	- 8	97.9
pH	85	1	18	30	5	2	14	24	- 5	92.9
HCO_3	-82	-31	-10	8	-29	17	-13	- 6	21	97.1

Table 2D-6. Varimax R-Mode Factor Loadings (Percent) Obtained from Partial-Correlation Matrix with Respect to Total Dissolved Solids for Rustler, Dewey Lake, and Bell Canyon Groundwaters (Population 2) (Continued)

Amount and Percent of Variance Explained by Each Factor								
Factor 1E	Factor 2E	Factor 3E	Factor 4E	Factor 5E	Factor 6E	Factor 7E	Factor 8E	Factor 9E
3.887	2.751	2.398	2.190	2.177	1.141	1.059	0.570	0.328
24%	17%	15%	13%	13%	7%	6%	3%	2%

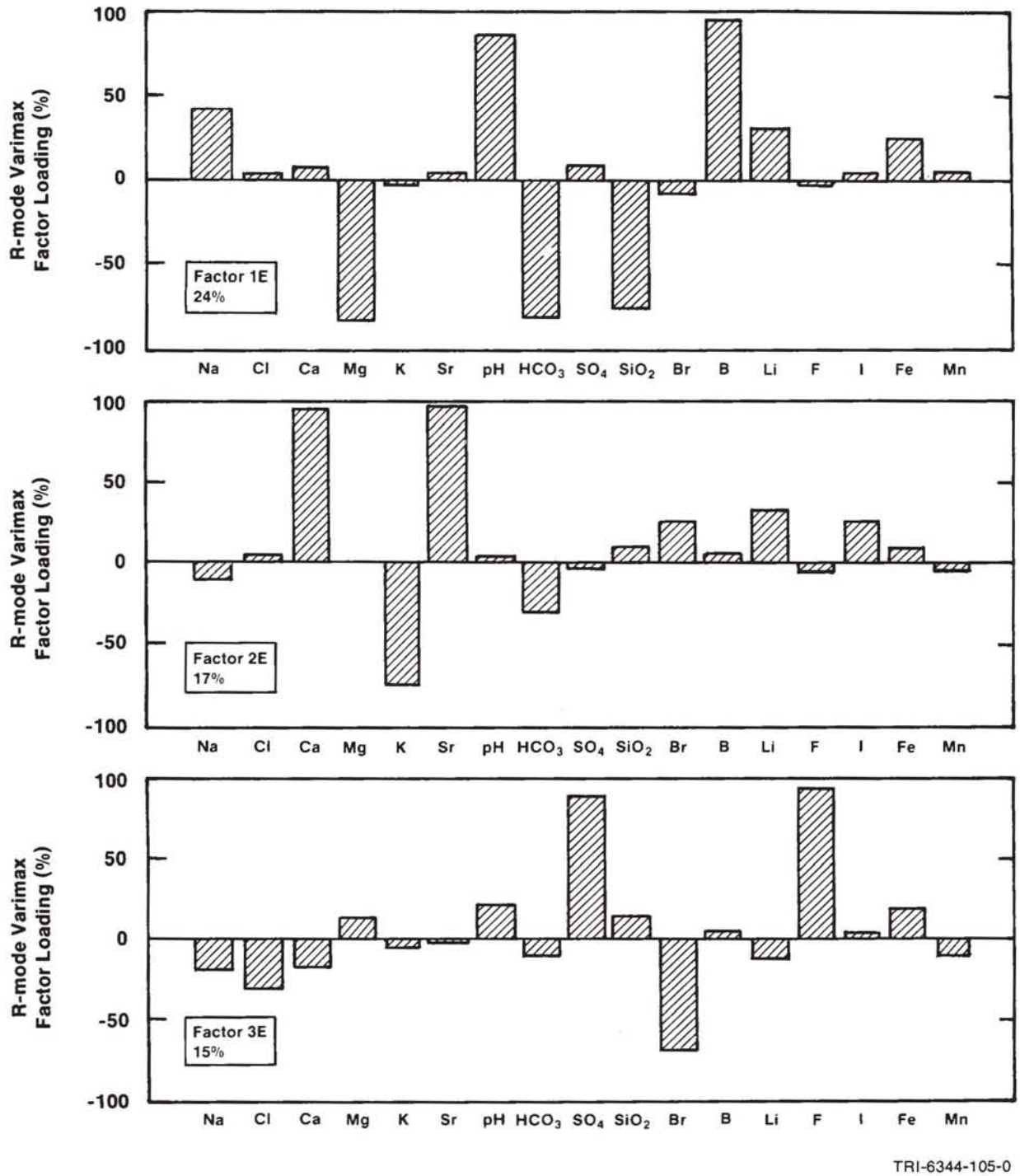

Figure 2D-7. Varimax R-mode factor loadings for factors 1E, 2E, and 3E obtained from partial-correlation matrix with respect to TDS of Rustler, Dewey Lake, and Bell Canyon groundwaters (population 2).